Universitat
de les Illes Balears

Instituto de Física Interdisciplinar y Sistemas Complejos

DOCTORAL THESIS

2016

MAJORANA PHYSICS IN HYBRID NANOWIRES, TOPOLOGICAL PHASES AND TRANSPORT

Javier Osca Cotarelo

Universitat
de les Illes Balears

DOCTORAL THESIS

2016

Doctoral Program of Physics

MAJORANA PHYSICS IN HYBRID NANOWIRES, TOPOLOGICAL PHASES AND TRANSPORT

Javier Osca Cotarelo

Thesis Supervisor: Rosa López Gonzalo

Thesis Supervisor: Llorenç Serra Crespí

Doctor by the Universitat de les Illes Balears

MAJORANA PHYSICS IN HYBRID NANOWIRES, TOPOLOGICAL PHASES AND TRANSPORT

Javier Osca Cotarelo
Tesis realizada en el Instituto de Física Interdisciplinar y Sistemas Complejos (IFISC) y presentada en la Universidad de las Islas Baleares (UIB)

PhD Thesis

Director: Prof. Rosa López Gonzalo
Director: Prof. Llorenç Serra Crespí

Universidad de las Islas Baleares
Palma de Mallorca, Spain

Este documento ha sido compuesto en LaTeX 2_ε
Arte gráfico de la cubierta: Marc Peregrina Parera

Los profesores Rosa López Gonzalo y Llorenç Serra Crespí, Profesores Titulares de la Universidad de las Islas Baleares

HACEN CONSTAR

que esta tesis doctoral ha sido realizada por el Sr. *Javier Osca Cotarelo* bajo su dirección en el Instituto de Física Interdisciplinar y Sistemas Complejos (UIB-CSIC) y, para dar constancia, firman la misma.

Palma, 1 de Junio de 2016

Rosa López Gonzalo

Director

Llorenç Serra Crespí

Director

Javier Osca Cotarelo

Doctorando

A mi padre y a mi madre.

Agradecimientos

En primer lugar quiero agradecer a mis directores de tesis, el Dr. Llorenç Serra y la Dra. Rosa López todo el esfuerzo, tiempo y dedicación que han invertido en hacer que este trabajo sea una realidad. Quisiera agradecer a Llorenç no tan sólo haberme transmitido sus conocimientos sino también haberme enseñado la importancia de la atención al detalle y el rigor científico. Sobre todo quisiera agradecerle su paciencia y el haber tenido siempre tiempo para todas mis preguntas. A Rosa quisiera agradecerle todo su apoyo, muy especialmente a la hora de buscar la financiación necesaria para mi doctorado y por haberme transmitido una parte de su conocimiento, casi enciclopédico, de toda la literatura existente. Tampoco quisiera olvidarme de las secretarias de la UIB por su inestimable guía en los laberintos burocráticos sin la cual esta tesis no habría ni podido empezar. Quiero agradecer también a mi abuela y a mi tío su preocupación por mí y mis estudios. Y para acabar, quisiera dedicar un agradecimiento muy muy especial a mi padre y a mi madre que han estado a mi lado desde el principio (son 34 años ya) apoyándome y ayudándome en todas las decisiones que he tomado fueran sensatas o no.

Agradezco también a la Universidad de las Islas Baleares la beca doctoral que ha financiado este trabajo sin la cual no habría sido posible.

Resum

En general, els Majoranas són un tipus de partícules caracteritzades per ser les seves pròpies antipartícules, per tant dues del mateix tipus juntes s'aniquilen l'una a l'altra. Les partícules de Majorana hereten el seu nom del notable físic italià Ettore Majorana que va postular la seva existència al 1937. Malgrat no s'han trobat partícules fonamentals de Majorana a la natura el concepte ha guanyat una nova vida al regne de la física de la matèria condensada. Es creu que és possible dissenyar dispositius capaços de contenir Majoranas com excitacions col.lectives d'electrons. Aquestes excitacions col.lectives tindrien la propietat fonamental dels Majoranas de ser creades i aniquilades per parelles malgrat no serien fermions com el seus equivalents en física de partícules sinó anyons no abelians. El resultat del seu intercanvi dependria de la orientació i l'ordre en el qual aquest es realitzi, propietat que podria ser utilitzada per construir computadors quàntics.

De les moltes propostes de sistemes que poden contenir Majoranas aquesta tesi es dedica al estudi dels modes de Majorana en nanofils híbrids semiconductors-superconductors. Un nanofil és una construcció 1d o quasi-1d on els Majoranas poden aparèixer si es proveeixen els ingredients apropiats. En el context d'aquest treball aquests ingredients són superconductivitat, acoblament spin orbita i un camp magnètic extern, malgrat aquesta selecció no és única. Hem elegit aquest sistema perquè és simple, això és un avantatge que permet models més realistes i propostes pràctiques que poden dur a la realització de nous experiments.

Els Majoranas varen ser originalment teoritzats en nanofils tancats purament unidimensionals però això pot ser difícil d'aconseguir en sistemes físics reals. A més a més, els Majoranas són molt difícils de detectar experimentalment perquè en aquest context no tenen carrega, spin i són estats d'energia zero. Per aquestes raons, els experiments que sostenen haver detectat Majoranas es basen principalment en les seves propietats de transport. En aquesta tesi ens ocupem d'estendre el model 1d a altres més generals que tenguin en consideració alguns efectes realistes i estudiam també les propietats de transport dels Majoranas en si mateixos. Per fer això fem servir una combinació de diferents mètods numérics i analítics que ens han permès descobrir un nou conjunt de característiques dels Majoranas prèviament desconegudes.

Aquesta tesi està presentada como un compendi de publicacions on cada contribució ha sigut publicada o está en preparació per ser publicada. Primer, dedicam la nostra

atenció a l'estudi d'unions suaus entre un nanofil de Majorana i un cable normal. En aquest estudi les unions estan caracteritzades per les posicions i suavitats dels interfaços de potencial i superconductor i es discuteix com aquestes característiques afecten a la protecció dels modes de Majorana. A continuació, investigam els efectes que la inclinació del camp magnètic té en els estats d'un nanofil purament unidimensional. Particularment, estam interessats en les condicions d'existència dels modes de Majorana. Hem descobert una nova relació analítica que restringeix els valors dels paràmetres en els que una fase de Majorana és possible. En el mateix capítol també s'ha estudiat la física dels Majoranas en nanofils unidimensionals doblegats en forma de L tractats com si fossin nanofils rectes, magnèticament inhomogenis compostos per dos braços homogenis. L'espectre i la localització dels Majoranas en aquests tipus de nanofils es discuteix àmpliament.

Després d'estudiar unions i fils unidimensionals enfocam la nostra atenció a la física dels nanofils plans amb una amplada petita peró finita. Demostram que els Majoranas sobreviuen a inclinacions considerables del camp magnètic en presència de moviments orbitals causats per les components fora del pla d'aquest camp magnètic. A més a més hem descobert un diagrama de fases característic dels Majoranas on calculem en el límit d'efectes orbitals forts les expressions analítiques de les fronteres de les fases. Addicionalment, també obtenim els corrents locals i la secció transversal d'absorbiment electromagnètic per al mateix tipus de nanofil. D'aquesta manera, proposam un mètode alternatiu per la detecció de Majoranas complementari a les mesures de transport. Mostram como la presència de modes de Majorana té una manifestació a l'espectre d'absorbiment quan el camp eletromagnètic incident està polaritzat en la direcció transversal al nanofil. A continuació també discutim la robustesa dels modes de vora de Majorana en la superfície de nanofils quàntics finits de forma cilíndrica. Més específicament, discutim la robustesa dels Majorana per diferents inclinacions del camp magnètic extern. A més a més, investigam com la presència dels modes de Majorana depèn del radi del nanofil cilíndric.

Finalment, usant un model de "*tight binding*" i el formalisme de Keldysh per a funcions de Green derivam les expressions per a las corrents elèctrica i d'energia en un circuit que conté un nanofil de Majorana. El nostre resultat principal informa d'un comportament singular dels Majorana en les admitàncies elèctriques i d'energia.

En el seu conjunt, els treballs publicats que formen aquesta tesi incrementen el nostre coneixement sobre els modes de Majorana en nanofils amb potencials aplicacions en experiments i també donen un nou enteniment de les propietats de transport dels Majorana. Els experiments proposats poden ser implementats amb la tecnologia actual i algunes de les tècniques numèriques poden ser generalitzades a altres problemes.

Resumen

En general, los Majoranas son un tipo de partículas caracterizadas por ser sus propias antipartículas, por tanto dos del mismo tipo juntas se aniquilan la una a la otra. Las partículas de Majorana heredan su nombre del notable físico italiano Ettore Majorana que postuló su existencia en 1937. Aunque no se han encontrado partículas fundamentales de Majorana en la naturaleza el concepto ha ganado una nueva vida en el reino de la física de la materia condensada. Se cree que es posible diseñar dispositivos capaces de contener Majoranas como excitaciones colectivas de electrones. Estas excitaciones colectivas tendrían la propiedad fundamental de los Majoranas de ser creadas y aniquiladas por parejas aunque no serían fermiones como sus equivalentes en física de partículas sino anyones no abelianos. El resultado de su intercambio dependería de la orientación y el orden en que este se realice, propiedad que podría ser usada para construir computadores cuánticos.

De las muchas propuestas capaces de contener Majoranas esta tesis se dedica al estudio de los modos de Majorana en nanohilos híbridos semiconductores-superconductores. Un nanohilo es una construcción 1d o quasi-1d donde los Majoranas pueden aparecer si se proveen los ingredientes apropiados. En el contexto de este trabajo estos ingredientes son superconductividad, acoplamiento spin órbita y un campo magnético externo, aunque esta selección no es única. Hemos elegido este sistema porque es simple, esto es una ventaja que permite modelos más realistas y propuestas prácticas que puedan llevar a la realización de nuevos experimentos.

Los Majoranas fueron originalmente teorizados en nanohilos cerrados puramente unidimensionales pero esto puede ser difícil de conseguir en sistemas físicos reales. Además, los Majoranas son muy difíciles de detectar experimentalmente porque en este contexto no tienen carga, spin y son estados de energía cero. Por estas razones, los experimentos que sostienen haber detectado Majoranas se basan principalmente en sus propiedades de transporte. En esta tesis nos ocupamos de extender el modelo 1d a otros más generales que tomen en consideración algunos efectos realistas y estudiamos también las propiedades de transporte de los Majoranas en si mismas. Para hacer eso usamos una combinación de diferentes métodos numéricos y analíticos que nos han permitido descubrir un nuevo conjunto de características de los Majorana previamente desconocidas.

Esta tesis esta presentada como un compendio de publicaciones donde cada con-

tribución ha sido publicada o está en preparación para ser publicada. Primero, prestamos nuestra atención al estudio de uniones suaves entre un nanohilo de Majorana y un cable normal. En este estudio las uniones están caracterizadas por las posiciones y suavidad de las interfaces de potencial y superconductora y se discute como estas características afectan a la protección de los modos de Majorana. A continuación, investigamos los efectos que la inclinación del campo magnético tiene en los estados de un nanohilo puramente unidimensional. Particularmente, estamos interesados en las condiciones de existencia de los modos de Majorana. Descubrimos una nueva relación analítica que restringe los valores de los parámetros en los que una fase de Majorana es posible. En el mismo capítulo también se estudian la física de los Majoranas en nanohilos unidimensionales doblados en forma de L tratados como si fueran nanohilos rectos magnéticamente inhomogéneos compuestos por dos brazos homogéneos. El espectro y la localización de los Majoranas en este tipo de nanohilos se discute ampliamente.

Después de estudiar uniones e hilos unidimensionales enfocamos nuestra atención en la física de los nanohilos planos con una anchura pequeña pero finita. Demostramos que los Majoranas sobreviven a inclinaciones considerables del campo magnético en presencia de movimientos orbitales causados por las componentes fuera del plano de ese campo magnético. Además hemos descubierto un diagrama de fases característico de los Majoranas donde calculamos en el límite de efectos orbitales fuertes las expresiones analíticas de las fronteras de las fases. Adicionalmente, también obtenemos las corrientes locales y la sección transversal de absorción electromagnética para el mismo tipo de nanohilo. De este modo proponemos un método alternativo para la detección de Majoranas complementario a las medidas de transporte. Mostramos como la presencia de modos de Majorana tiene una manifestación en el espectro de absorción cuando el campo eletromagnético incidente está polarizado en la dirección transversal al nanohilo. A continuación también discutimos la robustez de los modos de borde de Majorana en la superficie de nanohilos cuánticos finitos de forma cilíndrica. Más específicamente, discutimos la robustez de los Majorana para diferentes inclinaciones del campo magnético externo. Además, investigamos como la presencia de los modos de Majorana depende del radio del nanohilo cilíndrico.

Finalmente, usando un modelo de "*tight binding*" y el formalismo de Keldysh para funciones de Green derivamos las expresiones para las corrientes eléctrica y de energía en un circuito que contiene un nanohilo de Majorana. Nuestro resultado principal informa de un comportamiento singular de los Majorana en las admitancias eléctricas y de energía.

En su conjunto, los trabajos publicados que forman esta tesis incrementan nuestro conocimiento sobre los modos de Majorana en nanohilos con potenciales aplicaciones en experimentos y también dan un nuevo entendimiento de las propiedades de transporte de los Majorana. Los experimentos propuestos pueden ser implementados con la tecnología actual y algunas de las técnicas numéricas pueden ser generalizadas a otros problemas.

Abstract

In general, Majoranas are a kind of particles that are their own antiparticles; therefore two of the same kind put together annihilate each other. Majorana particles inherited their name from the notable italian physicist Ettore Majorana who postulated their existence in 1937. Although no Majorana fundamental particles have been found in nature the concept has gained a new life in the realm of condensed matter physics. It is believed that it is possible to engineer devices able to hold Majoranas in the form of collective electronic excitations. These collective excitations would have the fundamental Majorana property of being created and annihilated in equal pairs albeit they would not be fermions like their particle physics equivalents but non-abelian anyons. The result of their interchange depends on the orientation and order of such interchange, a property that could be used to build quantum computers.

From the many theoretical proposals of systems able to hold Majoranas this thesis is devoted to the study of Majorana modes in hybrid semiconductor-superconductor nanowires. A nanowire is a 1d or quasi-1d construct where Majoranas can appear if the proper ingredients are provided. In the context of this work these ingredients are superconductivity, spin orbit coupling and an external magnetic field, although this selection is not unique. We have chosen this system because of its simplicity, an advantage that allows for more realistic models and feasible proposals that can lead to new experiments.

Majoranas were originally theorized for purely 1d closed nanowires but this can not be easily achieved in real physical systems. Furthermore, Majoranas are very difficult to be detected experimentally because in this context they are chargeless, spinless, zero energy states. For this reason, experiments claiming Majorana detection are mainly based on their transport properties. In this thesis we take care of extending the 1d model to more general ones that take into consideration some realistic effects and we also study the Majorana transport properties in themselves. To do this we use a combination of different numerical and analytical methods that have allowed us to uncover a whole new set of Majorana features previously unknown.

This thesis is presented as a compendium of publications where each contribution has been published or is in preparation to be published. First, we will focus on the study of smooth junctions between a Majorana nanowire and a normal lead. In this

study the junctions are characterized by the potential and superconductor interface position and softness and it is discussed how this features affect the protection of the Majorana modes. Next, we investigate the effect that a tilting of the magnetic field has on the states of a purely 1d Majorana nanowire. Particularly, we are interested in the conditions of existence of the Majorana zero modes. We uncover a new analytical relation that restricts the parameter values in which a Majorana phase is possible. In the same chapter, we have also studied the Majorana physics of bent L-shaped 1d nanowires treated as if they were magnetically inhomogeneous straight nanowires composed of two homogeneous arms. The spectrum and the localization of Majoranas in this kind of nanowires are thoroughly discussed.

After studying 1d junctions and wires we move on to the study of Majorana physics of planar nanowires with a small but finite width. We demonstrate that Majoranas survive sizable vertical field tiltings of the external magnetic field in presence of the orbital motion caused by off plane components of this same magnetic field. Furthermore, we uncover a characteristic phase diagram for Majoranas where the analytical expressions of the phase boundaries are calculated for the limit of strong orbital effects. Additionally, we also obtain for the same kind of nanowire the local currents and the electromagnetic absorption cross section. This way we propose an alternative method of Majorana detection but complementary to transport measurements. We show how the presence of Majorana modes have a manifestation in the absorption spectra when the incident electromagnetic field is polarized in a transverse direction to the nanowire. Next, we also discuss the robustness of Majorana edge modes in the surface of finite quantum nanowires of cylindrical shape. More specifically we discuss the Majorana robustness for different external magnetic field tiltings. Furthermore, we investigate how the presence of Majorana modes depends on the radius of the nanowire cylinder.

Finally, using a tight binding model and the Keldysh-Green function formalism we derive the time dependent electrical and energy currents in a circuit that contains a Majorana nanowire. Our main results for the AC transport report a singular behavior of the Majorana for the energy and electrical current admittances.

Taken together, the published works that form this thesis increase our knowledge of the Majorana modes in nanowires with potential applications in experiments and also give a new insight of the Majorana transport properties. The experiments proposed can be implemented with the present technology and some of the numerical techniques can be generalized to non Majorana problems.

List of Publications

This thesis is presented as a compendium of publications where the following articles form its main body.

1. Javier Osca and Llorenç Serra
   Majorana modes in smooth normal-superconductor nanowire junctions
   Phys. Rev. B **88**, 144512
   Published 22 October 2013

2. Javier Osca, Rosa López and Llorenç Serra
   Majorana mode stacking, robustness and size effect in cylindrical nanowires
   Eur. Phys. J. B **87**, 84
   Published 9 April 2014

3. Javier Osca, Daniel Ruiz and Llorenç Serra
   Effects of tilting the magnetic field in one-dimensional Majorana nanowires
   Phys. Rev. B **89**, 245405
   Published 5 June 2014

4. Javier Osca and Llorenç Serra
   Majorana states and magnetic orbital motion in planar hybrid nanowires
   Phys. Rev. B **91**, 235417
   Published 12 June 2015

5. Javier Osca and Llorenç Serra
   Electromagnetic absorption of quasi-1d Majorana nanowires
   Phys. Status Solidi C **12**, No 12, 1409-1411
   Published 31 July 2015

6. Javier Osca and Llorenç Serra
   Quasi-particle current in planar Majorana nanowires
   J. Phys. Conf. Ser. **647** 012063
   Published 13 October 2015

7. Javier Osca, Rosa López and Jong Soo Lim
   Charge and energy transport in a Majorana nanowire
   In preparation.

Contents

Chapter 1

Introduction

1.1 Motivation

In its simpler definition a Majorana is a particle that is its own antiparticle. We can find the origin of this term in the realm of particle physics when in 1937 italian physicist Ettore Majorana discovered real solutions of Dirac equation for relativistic electrons and positrons [1]. This discovery implied the theoretical prediction of neutral particles that are their own antiparticles. In particular, Ettore Majorana proposed this model for neutrinos. Many particles have been discovered since Majorana's breakthrough, although none has been found to obey Majorana physics up to the present date, although the debate on neutrinos and other yet undiscovered particles is still open. However, the possibility of Majorana modes as new emergent quantum states in condensed matter systems has drawn broad interest in the Physics community. Majorana modes theorized in condensed matter devices arise as collective excitations caused by many body electronic interactions. Furthermore, in this context they are not fermions but chargeless, spinless, zero energy quasi-particles that exist as topological states in superconductors [2–4]. A consequence of the Majorana's topological nature is their resilience to local sources of noise. This is caused by the energy separation between the topological Majorana states and the bulk ones and the impossibility to lift the Majorana states from zero energy because of their symmetry protection. In general, topological states are zero-temperature states that appear localized in the limits of their corresponding physical system [5,6]. This kind of states also represent ordered phases of matter that can not be characterized by local order parameters because their orderings are global system properties.

Majoranas non-abelian statistics and their inherent robustness to noise makes them ideal candidates for quantum computation. Two Majoranas circulating around each other will acquire a non trivial phase that depends on the circulation direction. However, the non-abelian nature of Majoranas is not violating the spin-statistics theorem because the theorem is restricted to localized particles not attached to a domain wall. The non commuting interchanges of Majoranas allows to perform quantum computation and store quantum information by braiding them; i.e., manipulating

the Majoranas space-time trajectories. The available operations and algorithms can be found in knot theory [5]. Despite braiding requires a 2d system it can also be performed in networks of more simple 1d nanowires as proposed in Ref. [7].

The fact that Majoranas can be engineered in relatively cheap solid state devices offers the opportunity to study new physics traditionally reserved to expensive radiotelescopes and particle accelerators. Currently, there are several theoretical proposals for solid state devices able to support Majorana modes but their spinless and chargeless nature hinders their detection. For example, Majoranas have been predicted to appear in 2d Abrikosov vortices created in the surface of topological insulators in contact with thin superconductor layers [8]. However, 1d systems have the advantage to be the simplest ones that can hold Majoranas thus leading to more feasible experimental setups. In this direction there are various theoretical proposals to engineer Majoranas, like using the edges of topological insulators [9, 10], nanowires made of 3D topological insulator inside and external magnetic field [11], helical spin chains [12] and semiconductor quantum wires proximity coupled with a superconductor [3, 4]. In fact, various experimental groups already claimed to have detected Majorana modes using different experimental setups [13–24]. However, in spite of the compelling evidence in favor of Majoranas, experimental results are not yet conclusive.

Of the many proposals able to hold Majoranas, this thesis is devoted to the study of Majorana modes in hybrid 1d and quasi-1d semiconductor-superconductor nanowires. We have chosen these systems because, even though Majoranas are in general exotic states, this kind of devices uses more common experimentally available ingredients and there already exist experimental realizations [13–15, 17, 18]. These ingredients are superconductivity [25], spin orbit interaction [26] (Rashba effect) and an external magnetic field [27,28] (Zeeman effect). In those devices the experimental signature of the Majorana is a peak in the conductance at zero bias named Zero Bias Peak (ZBP). Although the obtained results are qualitatively consistent with a Majorana mode there are alternative explanations to the ZBP that do not involve Majoranas. To overcome this uncertainty, theoretical and experimental advances are needed. From a experimental point of view, new more controlled experiments are being performed [24]. On the other hand, a better theoretical knowledge is also needed about the Majorana phases and their transport properties.

As explained below there is a gap of knowledge between the purely 1d closed-system models and the real experimental setups. With the aim to fill this gap this thesis is devoted to the theoretical study of Majorana nanowires with non-ideal normal-superconductor NS junctions, quasi-1d planar and cylindrical nanowire geometries and also to the study of different experimental setups, like the AC response of a Majorana nanowire or its optical absorption properties. In the following subsections the Majorana basic concepts, properties and applications will be introduced.

1.2 Majoranas in solid state physics

It is widely accepted that nature is built up of two fundamental kinds of particles, bosons and fermions, obeying two different kinds of statistics [29,30]. On one hand, bosons are integer spin particles that fulfill the commutation relation

$$\left[d_i\,,d_j^\dagger\right]=\delta_{ij}\,, \tag{1.1}$$

where $d_i^\dagger$, d_i are the boson creation and annihilation operators in second quantization formalism, respectively. This commutation relation requires a symmetric wavefunction and, as a consequence, there is no upper limit in the number of bosons that can be stacked in one particular quantum state. On the other hand, fermions are fractionary spin particles that fulfill the anti-commutation relation

$$\left\{c_i\,,c_j^\dagger\right\}=\delta_{ij}\,, \tag{1.2}$$

where $c_i^\dagger$, c_i are the corresponding fermion creation and annihilation operators. The anti-commutation relation requires the fermion wavefunction to be anti-symmetric, therefore not more than one fermion can be found in the same quantum state. However, quasi-particles present in low-dimensional nanostructures are not fundamental particles and they are not bound by these two options.

Indeed, Majoranas in solid state physics devices emerge as quasi-particles that fulfill a new anti-commutation relation

$$\{\gamma_i\,,\gamma_j\}=2\delta_{ij}\,, \tag{1.3}$$

where γ_i is simultaneously the Majorana creation and annihilation operator in second quantization. This new anti-commutation relation makes Majoranas different from fermions and bosons reflecting the Majorana status as a particle that is its own antiparticle. It is possible to stack as many Majoranas in the same quantum state like bosons but they annihilate each other in pairs. As a consequence, we can find only zero or one Majorana at a definite quantum state, like fermions. This fact has important implications in the nature of the Majorana wavefunction. First, two Majoranas can coexist only if they are completely uncoupled, any overlapping or interaction between two Majoranas will result in their mutual annihilation. Second, the spin statistical connection in low dimensional states is broken, in fact the Majorana state that we study in this thesis is effectively spinless. We will discuss a bit more about these statements in the section *Majorana properties* that can be found below. For the moment we will be satisfied to understand how Majorana fermions arise in mesoscopic devices made of many electrons.

As reasoned in Ref. [6], in general one can perform a canonical transformation in a way that any system of electrons can be formally recast in terms of Majorana fermion states,

$$|\gamma_1\rangle = \frac{1}{\sqrt{2}}\left(\,|E\rangle+|-E\rangle\,\right)\,, \tag{1.4}$$

$$|\gamma_2\rangle = \frac{i}{\sqrt{2}}\left(\,|E\rangle-|-E\rangle\,\right)\,, \tag{1.5}$$

where $|\gamma_1\rangle$ and $|\gamma_2\rangle$ are two Majorana states while $|E\rangle$ and $|-E\rangle$ are two fermionic states at energies E and $-E$, respectively. The positive energy state is a particle state while the negative energy one is a hole state. This occurs in many body electron devices because two electrons can not be in the same state as imposed by the Fermi exclusion principle. Therefore, electrons pile up in different states until they reach the Fermi energy level that we label as our origin of energies by convenience. Positive energy levels are excited states that arise from the addition of an electron while negative energy ones arise from an electron removal from the Fermi sea. In general, the transformations implied by Eqs. (1.4) and (1.5) only represent a change in the point of view and usually is not even helpful in the analysis of a system behavior. The physical reason is that Majorana states can only be stationary states at zero energy. In general the Majorana wavefunctions overlap in space and there is no advantage in a separate description. However, in certain devices Majoranas are possible at zero energy and appear as two physically separated non-overlapping topological solutions. In the particular case of 1d Majorana nanowires one Majorana appears on each end of the nanowire. In those cases, the Majorana basis is the most natural base and the one that better reflects the physics of the device.

1.3 Majorana properties

The implementation of a Majorana nanowire requires the use of superconductivity. This is hinted in Eqs. (1.4) and (1.5), whereby Majoranas are created by means of a coherent superposition of electron and hole degrees of freedom. Majorana modes can appear as device eigenstates due to the superconductor coupling; hence, Majorana modes are protected by particle hole symmetry (PHS). In general, topological states are symmetry protected and can be classified by their symmetries [5, 31, 32]. Symmetries are non-local properties, each one related to its own non-local operator. In particular, PHS imposes a restriction in the superconductor spectrum, requiring that every positive-energy E particle state has a negative energy $-E$ anti-state. As a consequence, Majorana states are very robust against local noise and decoherence because they appear at the middle of the superconductor energy gap and can not be lifted from zero energy due to the PHS. As mentioned above, their robustness to noise and their particular statistics are specially useful for topological quantum computation schemes [5, 7, 33].

Devices in strict 1d with PHS have only two possible phases, the trivial and the topological one [32]. Therefore, in a purely 1d nanowire it is not possible to have more than one Majorana at each nanowire end. Two Majoranas on the same end of the nanowire would result in their mutual annihilation. This is the reason why Majoranas exist only in spinless or effectively spinless nanowires. Spin degeneracy would lead to the creation of two Majoranas on the same end that would destroy each other becoming a fermion.

Taken together, the above characteristics of Majoranas as topological states are a mixture of properties, some of them general to all topological states and others particular to Majorana states only. For the sake of clarity of exposition we now list

and summarize these properties:

1. *Majoranas are edge states.* By definition, topological states arise on a device physical limits or are associated to imperfections and impurities. This must not be confused with Anderson localized states where the localization is caused by the cumulative effect of extended disorder. In 1d or quasi-1d nanowires Majoranas appear on the nanowire ends.

2. *Majoranas are zero energy states.* In any particle-hole symmetric system each state at positive energy has its anti-state at negative energy. Therefore, in order to have Majoranas that are particles identical with their own antiparticles they must exist at zero energy.

3. *Majorana modes are spinless states.* Majoranas are spatially separated and attached to different edges of the device, provided there is no spin degeneracy. If spin degeneracy is present then two identical Majoranas would appear at the same edge, with an overlapping wavefunction. This way, the formation of two Majoranas is prevented as they would become fermion states with their energy lifted from zero.

4. *Majoranas appear inside a gap.* This is a common feature to all topological states. It arises from the practical need to maintain an energy separation of the topological states from the non-topological ones. Differently from the topological states, local noise introduces uncontrolled dynamics in a device bulk states above the gap. Furthermore, for large enough levels of noise, a topological device can jump from its topological ground state to a non topological bulk state out of the energy gap. Hence, to avoid this situation it is required to have the Majoranas states isolated inside a gap as large as possible.

5. *Majoranas appear in pairs.* Single unpaired Majoranas can live only in semi-infinite systems. In general, it is assumed that the second Majorana of the pair is attached to a second edge lying at infinite distance from the first one. On the other hand, in systems of finite size Majoranas appear in pairs, each one located on a different edge.

6. *Majoranas have non-abelian statistics.* The exchange of two Majoranas gives as a result a fractional complex phase. Furthermore, this phase depends on the Majoranas interchange direction. This feature can be profited to perform topological quantum computation and quantum storage of information.

In order to engineer a Majorana 1d or quasi-1d nanowire we will need superconductivity and a mechanism to avoid the inherent spin degeneracy of real electronic devices. In this thesis the mechanism considered is the simultaneous use of an external magnetic field (Zeeman effect) in combination with the effective magnetic field caused by the intrinsic spin orbit interaction (Rashba effect). Superconductivity, Zeeman and Rashba effects are next presented in more detail.

1.4 Bogoliubov-deGennes equations and superconductivity

In this thesis we work with an effective single quasiparticle model having a superconductive term that couples particle and hole degrees of freedom. The mixing between them allows for the existence of a neutral Majorana quasiparticle. In general, superconducting materials are metals where electrons feel an effective attractive force between them [34]. Furthermore, if the temperature is low enough this force is strong enough to pair the electrons into Cooper pairs causing the superconducting behavior to appear. Below the critical temperature the superconducting phase exists while above this temperature a superconductor behaves like a normal metal [35,36]. The superconducting behavior is characterized by zero resistivity [36, 37] and zero magnetic field inside the superconductor [38, 39] among other properties. More importantly for us, in superconductors the density of states has an energy gap at the Fermi level. This gap is important to grant the Majorana mode robustness against noise.

There are several superconducting mechanism of different physical origin but we will focus on s-wave superconductivity. The reason is that s-wave superconductivity was the first kind of superconductivity discovered, therefore, it is the one that can be found in the more common superconductors like Al, Nb, Pb, Sn. As a consequence, s-wave superconductivity is easy to be achieved in a laboratory and is better known than more exotic p-wave or d-wave high temperature superconductors. S-wave superconductivity arises from a phonon assisted attractive force between electrons [25]. In more plain words, we can model a superconductor as a free electron gas like in metals plus an electron-electron interaction caused by the atomic network vibration. That is,

$$\mathcal{H} = \sum_{k,\sigma} \epsilon_k \, c^\dagger_{k,\sigma} c_{k,\sigma} + \sum_{k,k',\sigma,\sigma',q} V_{\mathit{eff}}(q) \, c^\dagger_{k+q,\sigma} c^{+}_{k'-q,\sigma'} c_{k',\sigma'} c_{k,\sigma} \,, \tag{1.6}$$

where $c^\dagger_{k,\sigma}$ and $c_{k,\sigma}$ are the electron creation and annihilation operators in second quantization, $\epsilon_k = \hbar k^2/2m$ is the kinetic energy of a normal metal, k and k' are the electron wavenumbers, q is the atomic network phonon momentum, m is the effective electron mass and V_{eff} is the effective attractive phonon-mediated interaction between electrons. $V_{\mathit{eff}}(q)$ is an attractive potential for low q values while it is repulsive for higher q. This attractive potential causes the electron pairing into Cooper pairs. $V_{\mathit{eff}}(q)$ can be calculated with a microscopic model, however its exact dependence with q is not necessary to understand the essentials of superconductivity.

In the BCS model of superconductivity a series of approximations are done for superconductors of weak coupling, weak shielding and weak interaction potential. Essentially, we restrict ourselves to lattice vibration energies under a particular value where the potential is attractive and then we approximate the potential as a constant for those energies. This way the potential is greatly simplified and becomes manageable analytically. Furthermore, we consider only interactions between electrons with opposite momentum and spin because Cooper pairs total momentum has been theorized to be zero and no macroscopic magnetization has been observed in a

superconductor [34]. As a consequence, Cooper pairs are singlet states. With these approximations the Hamiltonian is simplified into

$$\mathcal{H} = \sum_{k,\sigma} \epsilon_k \, c^\dagger_{k\sigma} c_{k\sigma} - V_0 \sum_{k,k'} c^\dagger_{k'\uparrow} c^\dagger_{-k'\downarrow} c_{-k\downarrow} c_{k\uparrow} \,, \tag{1.7}$$

where V_0 is the ideal constant magnitude of the attractive potential in this model.

At this point, the Hamiltonian in Eq. (1.7) can be further simplified using a mean field approximation into

$$\mathcal{H} = \sum_{k\sigma} \epsilon_k \, c^\dagger_{k\sigma} c_{k\sigma} + \sum_{k} \left(\Delta^* \, c_{-k\downarrow} c_{k\uparrow} + \Delta \, c^\dagger_{-k\uparrow} c^\dagger_{k\downarrow} \right) \,, \tag{1.8}$$

with

$$\Delta \equiv -V_0 \sum_{k'} \langle c_{-k'\downarrow} c_{k'\uparrow} \rangle = V_0 \sum_{k''} \langle c_{-k''\uparrow} c_{k''\downarrow} \rangle \,, \tag{1.9}$$

where $\uparrow$ and $\downarrow$ indicate the spin up and down degrees of freedom. The rest of the symbols have the same meaning of the Hamiltonian in Eq. (1.7). In this approximation the two-body interaction is reduced to a single body self-interaction, like an external field. Eq. (1.8) Hamiltonian is given referred to a ground state of Cooper pairs presented below. The propagating bands of this Hamiltonian are shown in Fig. 1.1. They can be interpreted physically as the excitation energies of the quasiparticles not bounded to a Cooper pair (where Δ is the Cooper pair breaking energy). These quasiparticles have simultaneous nonzero components of the particle and hole degrees of freedom. An electron-like quasiparticle has a greater electronic component while in a hole-like one is the other way around. No propagating states are found inside the gap because in non-topological superconductors no quasiparticle excitations can be found for energies lower than the Cooper pair binding energy. Superconductivity in combination with the Rashba and Zeeman effects will make the superconductor topological allowing a perfect mixture of both degrees of freedom at zero energy. In this manner, the Majorana neutral quasiparticle can be obtained. The kind of Hamiltonian presented in Eq. (1.8) is called Bogoliubov-deGennes Hamiltonian. Here, it is written using second quantization notation although it is equivalent up to a basis change to the more familiar version shown below in Eq. (1.12).

As stated above, in BCS formalism the Hamiltonian is expressed in relation of a reference state of Cooper pairs. This reference state is postulated under the same arguments and approximations used above to derive the Hamiltonian in Eq. (1.8). Cooper pairs are assumed to be singlet states of definite momentum independent of each other. This approximation is fairly good because of the good localization of the states in momentum space. On the other hand, if we consider each pair independently then each one is subjected to the same mean field . Therefore, the overall wavefunction of the BCS reference state $|\psi_{BCS}\rangle$ can be rewritten as a multiplication of every independent pair

$$|\psi_{BCS}\rangle = \prod_{k} \left(u_k + v_k \, c^\dagger_{k\uparrow} c^\dagger_{-k\downarrow} \right) |0\rangle \,, \tag{1.10}$$

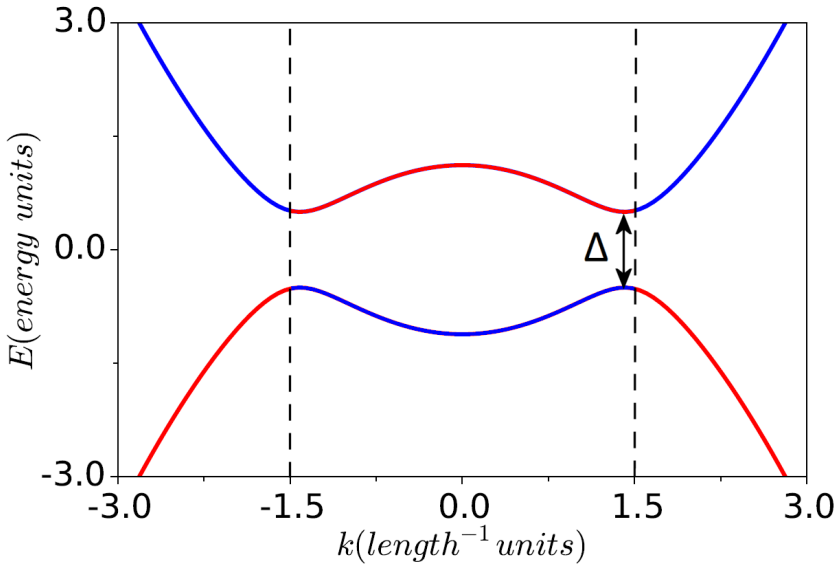

Figure 1.1: Schematic of the propagating bands of a 1d s-wave superconductor modeled by the Hamiltonian in Eq. (1.8) for a particular case where $\mu/\Delta > 1$. Excitation energies of electron-like quasiparticles are shown in blue while the energies of hole-like ones are shown in red. The superconductor gap Δ separates the two bands. The particular choice of the chemical potential μ has been based in aesthetic reasons with the intention to ease the distinction between electron and hole-like excitations in the schematic.

where u_k is the amplitude of probability to have and empty Cooper pair state while v_k is the amplitude of probability to have this same state occupied. This expression is equivalent to

$$|\psi_{BCS}\rangle = \sum_N \lambda_N |\Psi_N\rangle \,, \tag{1.11}$$

where $|\Psi_N\rangle$ is a reference state made of N Cooper pairs. In general, the ground state of Eq. (1.8) has an undefined number of zero energy Cooper pairs.

As an alternative to the above formulation, it is possible to write the Hamiltonian of Eq. (1.8) without second quantization notation. Making the projection of Eq. (1.8) in the basis of spatial degrees of freedom the Hamiltonian is written as

$$\mathcal{H}_{BdG} = \left(\frac{p_x^2}{2m} - \mu \right) \tau_z + \Delta \, \tau_x, \tag{1.12}$$

where $p_x = -i\hbar\partial_x$, μ is the nanowire chemical potential and Δ is the constant s-wave superconductor coupling introduced above. It is usual to work with an abbreviated notation that makes use of the Pauli matrices τ_x, τ_y and τ_z for the isospin (particle and hole) degrees of freedom. Note also that we take the superconductor coupling Δ as a real number. The superconductor phase is not relevant in single superconductor or normal-superconductor interface problems. Phase is only relevant in superconductor-superconductor interfaces not discussed in this thesis.

To obtain the eigenenergies and eigenstates of the Bogoliubov-deGennes Hamilto-

nian (Eq. (1.12)) we solve the corresponding energy eigenstate equation $\mathcal{H}_{BdG}\Psi(x) = E\Psi(x)$ where $\Psi(x) = (f(x), g(x))$. This equation has the same mathematical form and can be solved in the same ways than a Schrödinger equation but here the energy E does not represent the system absolute energy but its excitation energy instead. The same equation can be written as the two more familiar coupled Bogoliubov-deGennes equations. Each one of these equations are functions of the spatially varying electron and hole degrees of freedom $f(x)$ and $g(x)$,

$$+ \quad \left(-\frac{\hbar^2\nabla^2}{2m} - \mu\right) f(x) + \Delta\, g(x) = Ef\,, \tag{1.13}$$

$$- \quad \left(-\frac{\hbar^2\nabla^2}{2m} - \mu\right) g(x) + \Delta\, f(x) = Eg\,, \tag{1.14}$$

where μ is the nanowire chemical potential and Δ is the constant s-wave superconductor coupling introduced above.

As explained below, the Majorana nanowires are not made of a superconducting material themselves but superconductivity is achieved by means of the proximity effect [40]. When a superconductor is placed in close contact with a thin layer of a normal non-superconductor material the latter becomes also a superconductor. This is called the proximity effect or the Holm-Meissner effect and it is caused by the leaking of Cooper pairs from the superconductor into the normal material. If the normal material thickness is smaller than the Cooper pairs coherence length then this leakage is enough to change its nature into a superconductive one. Independently of the origin of the superconductivity, the resulting hybrid system is modeled with a superconductor coupling of the kind present in Eq. (1.12).

1.5 Zeeman effect

The theoretical justification of the spin as an actual degree of freedom can be found in the four component vector solutions of the Dirac equation. In these solutions each of the components are labeled by a two valued spin and isospin quantum numbers [41]. However, the spin was known even before Dirac equation was theorized. For example, in 1922 Stern and Gerlach carried out an experiment devised by Stern the year before [30, 42–44] where it was demonstrated that the spatial orientation of the angular momentum is quantized. The experiment consisted in sending silver atoms through a non-homogeneous magnetic field which deflected their straight trajectories before impacting in a detector screen. The main point is that the silver atom electrons are known to have a zero orbital angular momentum. Furthermore, the number of electrons of silver is 47, an odd number, therefore the total angular momentum of the whole atom is roughly the intrinsic angular momentum of one electron. The working principle of this experiment is the coupling of the magnetic field with the spin of the electron to separate silver atoms in two beams of opposite $1/2$ and $-1/2$ values of their spin projection. This coupling is postulated to be

$$\mathcal{H}_Z = \Delta_B\, \vec{n} \cdot \vec{S}\,, \tag{1.15}$$

where $\Delta_B = g\mu_B B$, $\vec{S} = \frac{1}{2}\vec{\sigma}$ and $\vec{n}$ is the direction of the magnetic field created by the magnet. At the same time, in these expressions g is the gyromagnetic factor of the electron, $\mu_B = e\hbar/2m_e$ is the Bohr magneton, e is the electron charge and m_e is the electron bare mass.

The Hamiltonian in Eq. (1.15) is called Zeeman term after the famous physicist who explained the splitting of the spectral lines of the hydrogen atom using an interaction of this kind [27]. In this thesis, we will not study such atomic systems but 1d and quasi-1d hybrid nanowires where we use this term to model the coupling between the magnetic field and the spin degrees of freedom. As stated above the coupling depends on the gyromagnetic factor g. The coupling between the magnetic field and the spin lead to an effective material dependent value of g different from vacuum conditions. For instance, it takes the values 0.44 (GaAs), 15 (InAs), 52 (InSb) [45]. As explained in the next section, in order to have have Majorana the magnetic coupling must be comparable with the Rashba coupling. For this reason we will consider hybrid semiconductor-superconductor nanowires with metallic-like behavior made of high g materials like InSb or InAs.

In a metallic-like material all the atoms share the conduction bands, therefore electrons move in the same way as in a free electron gas where the electron dispersion relation is parabolic. We consider nanowires much longer than wide or high, thus quasiparticle motion is almost free along the longitudinal axis of the nanowire but is quantized in the transversal directions. On a first approximation, the transversal confinement energies become constants that we can ignore by a proper tuning of the chemical potential. Therefore, we can devise a purely 1d model of a nanowire inside an external magnetic field devoid of any geometric consideration,

$$\mathcal{H} = \left(\frac{p_x^2}{2m} - \mu\right)\tau_z + \Delta_B\,\vec{n}\cdot\vec{\sigma}\,, \tag{1.16}$$

where $\vec{\sigma}$ is the vector of Pauli matrices $\vec{\sigma} = (\sigma_x, \sigma_y, \sigma_z)$ and the rest of the symbols have the same meaning as in previous equations.

Equation (1.16) is a Hamiltonian of a 1d system, hence there are no terms related with the transversal motion of quasiparticles. In some parts of the thesis we will consider not only 1d wires but also quasi-1d planar nanowires with some width. In quasi-1d nanowires it is also possible the coupling of the magnetic field with the spatial degrees of freedom of the electron. This coupling is introduced in the Hamiltonian by means of the substitution

$$\vec{p} \to \vec{p} - \frac{e}{c}\vec{A}(r,t)\,, \tag{1.17}$$

as indicated, e.g., in Ref. [30], where e is the electron charge, c is the velocity of light and $\vec{A}(r,t)$ is the magnetic field vector potential. If we consider Eq. (1.17) substitution in the kinetic energy of a free electron we obtain

$$-\frac{\hbar^2}{2m}\nabla^2\Psi \to -\frac{\hbar^2}{2m}\nabla^2\Psi - \frac{ie\hbar}{mc}\,\vec{A}\cdot\nabla\Psi + \frac{e^2}{2mc^2}\,A^2\Psi\,. \tag{1.18}$$

For the same physical problem the vector potential can be written in many different ways depending on the gauge choice. In our case, we will usually turn to the Landau

gauge with the origin at the center of the nanowire, because it is the one that is better adapted to the geometry of our problem

$$\vec{A} = (0, -B_z y, 0) \ , \tag{1.19}$$

where B_z is the out-of-plane component in a planar Majorana nanowire. In this gauge the Hamiltonian terms in Eq. (1.18) become

$$\mathcal{H}_{orb} = -\frac{\hbar^2}{2m}\nabla^2 + \frac{\hbar^2}{2ml_z^4}\, y^2 - \frac{\hbar}{ml_z^2}\, y p_x \ . \tag{1.20}$$

where $l_z^2 = \hbar c/eB_z$. The first term is the usual kinetic energy term while the second one has the mathematical form of an effective quantum oscillator potential. The remaining term is also a Zeeman term that couples the magnetic field with the orbital motion. As a side note, in spherical or cylindrical systems this last term becomes proportional to the angular momentum $\vec{L}$ and takes a mathematical form similar to Eq. (1.15).

1.6 Rashba effect

The spin orbit interaction is the coupling between the electron spin and its own momentum in presence of an external electric field [30]. Although its physical origin must be searched in the series expansion of the electron relativistic energy, it can also be reasoned physically. The Hamiltonian of spin orbit interaction (SOI) is a Zeeman like term caused by the presence of an effective magnetic field B_{eff}. This magnetic field is the one that an electron perceives in its own frame of motion when it is moving inside an external electric field (see Fig. 1.2a). It can be written as

$$\mathcal{H}_{SOI} \propto \vec{\sigma} \cdot \vec{B}_{\mathit{eff}}(\vec{k}\,) \, , \tag{1.21}$$

where $\vec{\sigma}$ is a vector of Pauli matrices (as in the preceding section). The magnetic field can be expressed as

$$\vec{B}_{\mathit{eff}} = -\frac{1}{c^2}(\vec{v} \times \vec{\mathcal{E}}\,) \, , \tag{1.22}$$

where c is the light velocity, $\vec{v}$ is the electron velocity and $\vec{\mathcal{E}}$ is the electric field. The Rashba effect is the momentum dependent splitting of the spin bands in a low dimensional condensed matter system due to this spin orbit interaction [46] (see Fig. 1.2b). Rigorously, in condensed matter systems Rashba spin orbit interaction emerges from an approximation to a more complicated Kane Hamiltonian for crystalline solids [45]. In this case, the spin orbit interaction arises by an asymmetry in the growth direction of the semiconductor. In other words, an electric field appears because there is an asymmetry in the confining potential that gives rise to an electric field $\vec{\mathcal{E}} = -\nabla V(\vec{r}\,)$.

Making the substitution of the effective magnetic field of Eq. (1.22) in the Hamiltonian of Eq. (1.21) we obtain the electric field dependent expression for the Hamiltonian Rashba term

$$\mathcal{H}_{SOI} \propto \vec{\sigma} \cdot \left(\vec{\mathcal{E}} \times \vec{p}\right) \ , \tag{1.23}$$

where $\vec{p}$ is the electron momentum and the rest of the symbols have the same meaning as in Eq. (1.22).

The Rashba effect is closely related to the Dresselhaus effect [47]. In the Dresselhaus effect the asymmetry is found in the semiconductor crystal structure that does not have an space inversion center. Depending on the selected semiconductor material it is possible to find the dominance of one effect (Rashba or Dresselhaus) over the other, or the coexistence between the two. In our particular case, we are going to consider materials where the Rashba effect dominates over the Dresselhaus one, in such a way that the Dresselhaus effect becomes negligible. This is justified for the choice of InSb semiconductor as the building material of Majorana nanowires in the experiments of Refs. [13, 24]. On the other hand, we want to stress that the choice of InSb and similar materials is motivated by its simultaneously large gyromagnetic factor and spin orbit coupling strength. That does not mean that from a theoretical point of view the Dresselhaus effect is not suited to obtain Majorana zero modes. Dresshelhaus and Rashba Hamiltonians are equivalent in 1d models although the Majorana phase will appear for a different range of values of the magnetic field orientation. Furthermore, theoretical predictions of Majorana modes making use of the Dresselhaus effect in 2d devices have also been claimed [48].

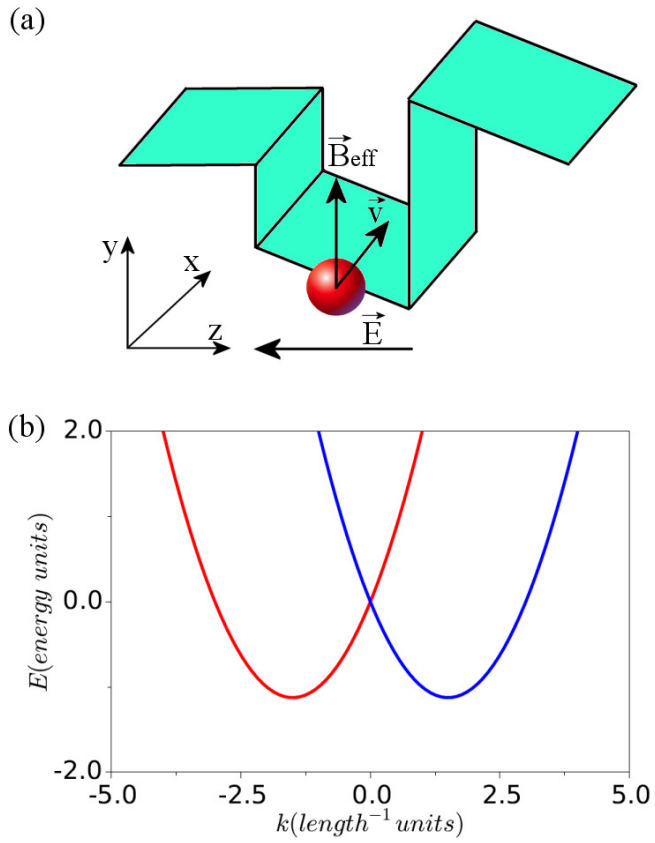

Figure 1.2: a) Diagram of the forces, velocities and fields involved in the Rasba spin orbit coupling. b) Schematic of the propagating bands of a 1d Rashba semiconductor. The two colors (red and blue) indicate different spin components.

After some algebraic manipulation the Rashba term can be written as

$$H_R = \frac{\alpha}{\hbar}(\vec{\sigma} \times \vec{p}) \cdot \hat{z}\,, \tag{1.24}$$

where

$$\alpha \propto \mathcal{E}_0\,, \tag{1.25}$$

is the spin orbit coupling strength and $\mathcal{E}_0 = |\vec{\mathcal{E}}|$ the electric field magnitude. We have assumed here that $\hat{z}$ is the growth direction where the confinement asymmetry is present. In a 2d system this model leads to a coordinate dependent expression,

$$\mathcal{H}_R = -\frac{\alpha}{\hbar}\left(p_x\sigma_y - p_y\sigma_x\right), \tag{1.26}$$

where p_x and p_y are the $\hat{x}$ and $\hat{y}$ components of the momentum and σ_x and σ_y the corresponding Pauli matrices. Equation (1.26) is the sum of the one dimensional Rashba term ($\approx p_x\sigma_y$) and the Rashba mixing term ($\approx p_y\sigma_x$). The one dimensional Rashba term is the only one to appear in a purely 1d system. This term is the responsible of the splitting of the one dimensional semiconductor dispersion equation into two spin dependent parabolas, one for spin up and one for spin down (see Fig. 1.2b). Furthermore, the momentum dependent Rashba coupling in combination with an external Zeeman field leads to a spatial spin precession in the Hamiltonian eigenstates. In this manner, different spatial positions of the same eigenstate will have a different spin projection because the spin acquires an spatial helicity, this way the eigenstate becomes effectively spinless. On the other hand, the Rashba mixing term $\alpha p_y\sigma_x$ is called this way because it couples the quantized nanowire transverse modes and it only appears in 2d or quasi-1d models. Its role in the Majorana formation will be further discussed below in Chap. 4.

1.7 Experimental setups

Although Majoranas can be found in different systems, those in 1d have the advantage to be the simplest able to hold Majorana modes. In this thesis we focus on the hybrid semiconductor-superconductor quantum wires because they can be built using the already known technological background developed for the implementation of electronic semiconductor devices. The use of hybrid semiconductor-superconductor 1d nanowires was initially proposed in Refs. [3, 4] and finally experimentally tested in Ref. [13] and later on in Refs. [14–18, 24].

A semiconductor with strong spin orbit coupling (like InSb or InAs) is deposited on the surface of an s-wave superconductor becoming a hybrid semi-superconductor. As explained above in Sec. 1.4, from an experimental point of view it is preferable the use of well known s-wave superconductivity than an exotic p-wave topological superconductor. Superconductivity is achieved in the semiconductor by means of the proximity effect that is the tunneling of Cooper pairs from a superconductor to a close semiconductor device. If the height of the semiconductor device is smaller than the coherence length of the Cooper pairs the semiconductor becomes an effective

superconductor metal. However, the presence of spin in a superconductor causes all bands to be double degenerate thus preventing the formation of an uncoupled Majorana mode. Nevertheless, a hybrid semiconductor-superconductor nanowire retains the strong spin orbit coupling strength characteristic of the semiconductor material. An external magnetic field breaks the time reversal symmetry and in combination with the spin orbit coupling the Hamiltonian eigenstates acquire a spin precession, this way becoming effectively spinless states. This is the kind of hybrid system modeled by the Bogoliubov-deGennes Hamiltonian

$$\mathcal{H}_{BdG} = \left(\frac{p_x^2}{2m} + V(x) - \mu \right) \tau_z + \Delta_B \, \sigma_x + \Delta \, \tau_x + \frac{\alpha}{\hbar} \, p_x \sigma_y \tau_z \ , \tag{1.27}$$

where the combination of s-wave superconductivity, Rashba and Zeeman effecs in a 1d ballistic nanowire makes possible the existence of Majorana states.

The nanowire is in a Majorana topological phase when the magnetic field strength Δ_B exceeds a particular limit, $\Delta_B > \sqrt{\Delta^2 + \mu^2}$, determined by the superconductor coupling Δ and the chemical potential μ [4]. The constant α characterizes the spin orbit strength and the potential $V(x)$ models the nanowire edges where Majoranas need to be located. In general, we will find a Majorana edge state in a finite or semi-infinite nanowire if its corresponding (i.e., same Hamiltonian except for the confinement) infinite edgeless nanowire is in a topological phase, this is called the bulk to edge correspondence principle. The Hamiltonian of Eq. (1.27) has been proposed as a model for very thin semiconductor nanowires in the mesoscopic scale, proximity coupled to a metallic superconductor.

Currently, the greatest progress in Majorana detection in solid state devices has been achieved in hybrid nanowires. The biggest challenge in Majorana detection is that Majoranas are zero energy, chargeless, spinless modes, therefore no experiment relying on those properties can be performed. With the intention of detecting Majorana states, in the experiment of Ref. [13] a Majorana nanowire is attached to a normal reservoir with the objective of detecting a zero bias peak (ZBP) in the electrical conductance, $g(V) = dI/dV$ (see Figs. 1.3a and 1.3b). A Majorana mode transport signature is a conductance peak at zero energy due to Andreev reflection like the one of Fig. 1.3c. As shown in Fig. 1.3b, a gate is used to create a tunnel barrier between the normal and superconductor contacts. The barrier is important not only to provide an edge where the Majorana can arise, but also to observe the Majorana transport properties. In a normal-superconductor junction electrons are reflected into holes naturally by Andreev reflection, therefore the barrier also takes the role of frustrate all the Andreev reflection of non-Majorana origin. The external magnetic fields applied here are of the order 100 mT while the nanowire length is of the order of various μm.

In our opinion, there is a gap of knowledge between the purely 1d closed models and real experimental setups. Actual mesoscopic semiconductor wires are not really one dimensional but, at most, they are quasi-1d. These nanowires width and height may be orders of magnitude smaller than their length, but still finite. Furthermore, they can be manufactured with different geometries, in the particular case of the experiment of Ref. [13] it was used an approximately cylindrical nanowire. Therefore,

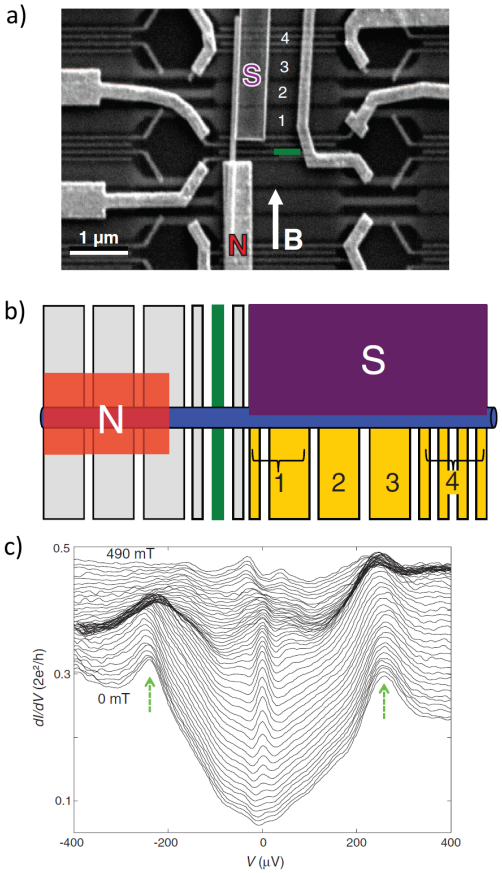

Figure 1.3: a) Implemented version of the theoretical proposals. Scanning electron microscope image of the device with normal (N) and superconducting (S) contacts. The S contact only covers the right part of the nanowire. The underlying gates, numbered 1 to 4, are covered with a dielectric. b) Schematic of the device. The green rectangle indicates the tunnel barrier separating the normal part of the nanowire on the left from the wire section with induced superconducting gap Δ. An external voltage V applied between N and S drops across the tunnel barrier. Only the left Majorana is probed in this experiment. Figure and caption taken from Ref. [13].

there is the possibility that some theoretical predictions for 1d wires may or may not be fulfilled in quasi-1d nanowires or even if they are qualitatively fulfilled, important changes in the phase diagram boundaries may arise. On the other hand, real wire junctions are not perfect either, the smoothness of the potential and deviations from ideal behaviors at the superconductor interfaces may affect the junction behavior.

Furthermore, although the ZBP detection has been reproduced by several groups, it has been noted that ZBP's can be obtained in superconductor systems in the same experimental conditions by other non Majorana sources. Disorder or trapped magnetic impurities are some of the other plausible explanations given to the same experimental results. In order to discard some of these alternative explanations Ref. [24] experiment reproduces the results of Ref. [13] using a cleaner nanowire and more controlled experimental conditions. An special effort is done to demonstrate the absence of disorder in the nanowire. In general, nanowire experiments reproduce

qualitatively well the behavior expected by a Majorana zero mode. A ZBP arises when particular magnetic field magnitudes are achieved and disappears when the orientation of the magnetic field is perpendicular to the nanowire. Nevertheless, in order to be sure of the relation of the peak with a Majorana phase a better knowledge of the phase boundaries is also needed.

This thesis focuses on many of the above issues from a theoretical point of view, like non ideal junctions, quasi-1d nanowires or geometry considerations to cite a few. Different experimental setups, like the AC response of Majorana nanowires or their optical absorption properties, are also studied. We will take too a closer look to the influence of the orbital motion of the electrons caused by the external magnetic field in arbitrary orientation.

1.8 Outline of this thesis

This thesis is presented as a compendium of publications where each work has been published independently; with the exception of Chap. 8 that is in preparation for publication. Each article is grounded in the conclusions of the previous ones, creating as a whole an homogeneous and consistent set of knowledge. Furthermore, each article will be preceded by an introductory text that will include a divulgative description of the objectives and results obtained in each article, a brief description of the methodology and occasionally some clarifications, remarks or discussions not suited for an article but useful in their reading.

First, we will study different Majorana properties in general and their phase diagram in particular with the aim to generate knowledge potentially useful in the identification of Majorana modes. We will be mainly concerned on how certain realistic effects change the Majorana phase boundaries. Later on, we will study the Majorana transport properties themselves and the optical absorption spectra of a Majorana nanowire. A more detailed chapter-oriented outline is:

- In Chap. 2, junctions between a Majorana nanowire and a normal lead are studied in detail. We consider non-ideal junctions with a certain distance between the two different interfaces, the potential interface and the superconductor interface. Both interfaces are considered to be soft with a smooth transition between their minimum and maximum values.
- In Chap. 3, the robustness of a Majorana mode to the tilting of the magnetic field with respect to the nanowire direction is investigated. This study is performed in a purely 1d nanowire. In the same chapter L-shaped 1d nanowires are modeled as magnetically inhomogeneous straight nanowires. Different issues related to this nanowire geometry are addressed, of particular interest is how a Majorana gets delocalized when one arm does not fulfill all the Majorana conditions while at the same time the other arm does.
- In Chap. 4, the Majorana phase diagram is determined for planar quasi-1d hybrid nanowires where the motion of quasiparticles is modified by orbital effects

caused by off plane magnetic field components. This calculation is performed using a novel efficient and accurate numerical method. A new method is also used to calculate the Majorana wavefunction with unprecedented spatial resolution.

- In Chap. 5, quasi-particle local currents are obtained using the high resolution Majorana wavefunction calculated in Chap. 4. It is demonstrated that different flows of local currents appear in presence or absence of perpendicular components of the magnetic field.

- In Chap. 6, the electromagnetic absorption cross section is calculated on the same kind of the quasi-1d nanowires of Chaps. 4 and 5. The dipole absorption cross section is computed taking into account quasi-particle transitions from negative to positive energy eigenstates of the Bogoliubov-deGennes Hamiltonian. The presence of a Majorana mode can be observed in the absorption spectra for particular polarizations of the external electromagnetic field.

- In Chap. 7, the robustness of Majorana edge modes are discussed for a finite quantum nanowire of cylindrical shape in presence of orbital effects. The Hamiltonian is numerically diagonalized to obtain the spectra for different experimental configurations. The robustness of the Majorana modes are discussed for these configurations and, in particular, their dependence with varying orientations of the external magnetic field.

- In Chap. 8, time dependent electrical and energy current expressions are obtained for a Majorana nanowire connected to one or two reservoirs using a tight binding 1d model. We use the Keldysh-Green function formalism to study the response of a nanowire to an AC driving potential applied to one reservoir whereas the Majorana nanowire is kept grounded. We give an analysis of the DC and AC current responses depending on the voltage drop configuration in the leads.

- In Chap. 9, the last chapter, the concluding remarks are presented. The main results of this thesis are summarized and related with each other. Finally, some future work proposals are presented and possible investigation directions on Majorana modes are discussed.

Bibliography

[1] E. Majorana, "Teoria simmetrica dell'elettrone e del positrone," *Nuovo Cimento*, vol. 14, pp. 171–184, 1937.

[2] A. Y. Kitaev, "Unpaired majorana fermions in quantum wires," *Physics-Uspekhi*, vol. 44, no. 10S, pp. 131–136, 2001.

[3] R. M. Lutchyn, J. D. Sau, and S. Das Sarma, "Majorana fermions and a topological phase transition in semiconductor-superconductor heterostructures," *Phys. Rev. Lett.*, vol. 105, p. 077001, 2010.

[4] Y. Oreg, G. Refael, and F. von Oppen, "Helical liquids and majorana bound states in quantum wires," *Phys. Rev. Lett.*, vol. 105, p. 177002, 2010.

[5] C. Nayak, S. H. Simon, A. Stern, M. Freedman, and S. Das Sarma, "Non-abelian anyons and topological quantum computation," *Rev. Mod. Phys.*, vol. 80, pp. 1083–1159, 2008.

[6] S. R. Elliott and M. Franz, "*Colloquium* : Majorana fermions in nuclear, particle, and solid-state physics," *Rev. Mod. Phys.*, vol. 87, pp. 137–163, 2015.

[7] J. Alicea, Y. Oreg, G. Refael, F. von Oppen, and M. Fisher, "Non-abelian statistics and topological quantum information processing in 1d wire networks," *Nat Phys*, vol. 7, pp. 131–136, 2011.

[8] L. Fu and C. L. Kane, "Superconducting proximity effect and majorana fermions at the surface of a topological insulator," *Phys. Rev. Lett.*, vol. 100, p. 096407, 2008.

[9] X.-L. Qi and S.-C. Zhang, "Topological insulators and superconductors," *Rev. Mod. Phys.*, vol. 83, pp. 1057–1110, 2011.

[10] M. Franz and L. Molenkamp, *Topological Insulators, 1st Edition.* Elsevier, 2013.

[11] A. Cook and M. Franz, "Majorana fermions in a topological-insulator nanowire proximity-coupled to an *s*-wave superconductor," *Phys. Rev. B*, vol. 84, p. 201105, 2011.

[12] J. Klinovaja, P. Stano, A. Yazdani, and D. Loss, "Topological superconductivity and majorana fermions in rkky systems," *Phys. Rev. Lett.*, vol. 111, p. 186805, 2013.

[13] V. Mourik, K. Zuo, S. M. Frolov, S. R. Plissard, E. P. A. M. Bakkers, and L. P. Kouwenhoven, "Signatures of majorana fermions in hybrid superconductor-semiconductor nanowire devices," *Science*, vol. 336, no. 6084, pp. 1003–1007, 2012.

[14] H. O. H. Churchill, V. Fatemi, K. Grove-Rasmussen, M. T. Deng, P. Caroff, H. Q. Xu, and C. M. Marcus, "Superconductor-nanowire devices from tunneling to the multichannel regime: Zero-bias oscillations and magnetoconductance crossover," *Phys. Rev. B*, vol. 87, p. 241401, 2013.

[15] M. T. Deng, C. L. Yu, G. Y. Huang, M. Larsson, P. Caroff, and H. Q. Xu, "Anomalous zero-bias conductance peak in a Nb-InSb Nanowire-Nb hybrid device," *Nano Letters*, vol. 12, no. 12, pp. 6414–6419, 2012.

[16] L. P. Rokhinson, X. Liu, and J. K. Furdyna, "Observation of the fractional ac josephson effect: the signature of majorana particles," *Nat. Phys.*, vol. 8, p. 795, 2012.

[17] A. Das, Y. Ronen, Y. Most, Y. Oreg, M. Heiblum, and H. Shtrikman, "Zero-bias peaks and splitting in an AlInAs nanowire topological superconductor as a signature of majorana fermions," *Nat. Phys.*, vol. 8, pp. 887–895, 2012.

[18] A. D. K. Finck, D. J. Van Harlingen, P. K. Mohseni, K. Jung, and X. Li, "Anomalous modulation of a zero-bias peak in a hybrid nanowire-superconductor device," *Phys. Rev. Lett.*, vol. 110, p. 126406, 2013.

[19] J. D. Sau, S. Tewari, and S. Das Sarma, "Experimental and materials considerations for the topological superconducting state in electron- and hole-doped semiconductors: Searching for non-abelian majorana modes in 1d nanowires and 2d heterostructures," *Phys. Rev. B*, vol. 85, p. 064512, 2012.

[20] S. Nadj-Perge, I. K. Drozdov, J. Li, H. Chen, S. Jeon, J. Seo, A. H. MacDonald, B. A. Bernevig, and A. Yazdani, "Observation of majorana fermions in ferromagnetic atomic chains on a superconductor," *Science*, vol. 346, no. 6209, pp. 602–607, 2014.

[21] J. R. Williams and D. Goldhaber-Gordon, "Majorana fermions: Doubling down on Majorana," *Nat. Phys.*, vol. 8, pp. 778–779, 2014.

[22] S. Cho, B. Dellabetta, A. Yang, J. Schneeloch, Z. Xu, T. Valla, G. Gu, M. J. Gilbert, and N. Mason, "Symmetry protected josephson supercurrents in three-dimensional topological insulators," *Nat. Commun.*, vol. 4, p. 1689, 2014.

[23] Y. Xu, L. Mao, B. Wu, and C. Zhang, "Dark solitons with majorana fermions in spin-orbit-coupled fermi gases," *Phys. Rev. Lett.*, vol. 113, p. 130404, 2014.

[24] H. Zhang, Ö. Gül, S. Conesa-Boj, K. Zuo, V. Mourik, F. K. de Vries, J. van Veen, D. J. van Woerkom, M. P. Nowak, M. Wimmer, D. Car, S. Plissard, E. P. A. M. Bakkers, M. Quintero-Pérez, S. Goswami, K. Watanabe, T. Taniguchi, and L. P. Kouwenhoven, "Ballistic Majorana nanowire devices," *ArXiv e-prints*, 2016.

[25] J. Bardeen, L. N. Cooper, and J. R. Schrieffer, "Theory of superconductivity," *Phys. Rev.*, vol. 108, pp. 1175–1204, 1957.

[26] E. Rashba, "Properties of semiconductors with an extremum loop," *Sov. Phys. Solid State*, vol. 3, p. 1109, 1960.

[27] P. Zeeman, "On the influencce of magnetism on the naure of the light emitted by a substance," *Phil. Mag.*, vol. 43, p. 226, 1897.

[28] D. J. Griffiths, *Introduction to Quantum Mechanics (2nd ed.).* Prentice Hall, 2004.

[29] R. K. Pathria and P. D. Beale, *Statistical Mechanics, third edition.* Elsevier, 2011.

[30] J. J. Sakurai and S. F. Tuan, *Modern Quantum Mechanics, Revised edition.* Prentice Hall, 1993.

[31] A. Kitaev, "Periodic table for topological insulators and superconductors," *AIP Conference Proceedings*, vol. 1134, no. 1, pp. 22–30, 2009.

[32] A. Altland and M. R. Zirnbauer, "Nonstandard symmetry classes in mesoscopic normal-superconducting hybrid structures," *Phys. Rev. B*, vol. 55, pp. 1142–1161, 1997.

[33] J. K. Pachos, *Introduction to Topological Quantum Computation.* Cambridge University Press, 2012.

[34] L. N. Cooper, "Bound electron pairs in a degenerate fermi gas," *Phys. Rev.*, vol. 104, pp. 1189–1190, 1956.

[35] V. Ginzburg and L. Landau, "On the theory of superconductivity," *Zh. Eksp. Teor. Fiz.*, vol. 20, p. 1064, 1950.

[36] M. Tinkham, *Introduction to Superconductivity (2nd ed.).* McGraw-Hill, 1996.

[37] H. K. Onnes, "The resistance of pure mercury at helium temperatures," *Commun. Phys. Lab. Univ. Leiden*, vol. 12, p. 120, 1911.

[38] W. Meissner and R. Ochsenfeld, "Ein neuer effekt bei eintritt der supraleitfähigkeit," *Naturwissenschaften*, vol. 21, pp. 787–788, 1933.

[39] F. London and H. London, "The electromagnetic equations of the supraconductor," *Proceedings of the Royal Society of London A: Mathematical, Physical and Engineering Sciences*, vol. 149, no. 866, pp. 71–88, 1935.

[40] R. Holm and W. Meissner, "Messungen mit hilfe von flüssigem helium. xiii," *Z. Phys*, vol. 74, p. 715, 1932.

[41] P. A. M. Dirac, "The quantum theory of the electron," *Proceedings of the Royal Society of London A: Mathematical, Physical and Engineering Sciences*, vol. 117, no. 778, pp. 610–624, 1928.

[42] W. Gerlach and O. Stern, "Der experimentelle nachweis der richtungsquantelung im magnetfeld," *Zeitschrift für Physik*, vol. 9, no. 1, pp. 349–352, 1922.

[43] W. Gerlach and O. Stern, "Das magnetische moment des silberatoms," *Zeitschrift für Physik*, vol. 9, no. 1, pp. 353–355, 1922.

[44] W. Gerlach and O. Stern, "Der experimentelle nachweis des magnetischen moments des silberatoms," *Zeitschrift für Physik*, vol. 8, no. 1, pp. 110–111, 1922.

[45] R. Winkler, *Spin-Orbit coupling effects in two-dimensional electron and hole systems.* Springer, 2003.

[46] E. I. Rashba, "A method of experimental examination of possibility of introduction of universal surface recombination rate during investigation of the photoelectric processes kimnetics," *Sov. Phys. Solid State*, vol. 2, p. 1109, 1960.

[47] G. Dresselhaus, "Spin-orbit coupling effects in zinc blende structures," *Phys. Rev.*, vol. 100, pp. 580–586, 1955.

[48] J. You, C. H. Oh, and V. Vedral, "Majorana fermions in s-wave noncentrosymmetric superconductor with dresselhaus (110) spin-orbit coupling," *Phys. Rev. B*, vol. 87, p. 054501, 2013.

Chapter 2

Majorana modes in smooth normal-superconductor nanowire junctions

Javier Osca and Llorenç Serra
Phys. Rev. B **88**, 144512. Published 22 October 2013

2.1 Objectives

It is well known that Majoranas localize on the two ends of a finite nanowire [13,14]. In a semi-infinite nanowire, however, we consider a single edge (left) where a Majorana state is located. It is assumed that a second Majorana will be located on the second edge (right) at infinity. The left edge is usually modeled as a perfect abrupt interface while some softness in the potential is likely to be found in real physical devices.

At the same time, it is also usually assumed that superconductivity terminates abruptly at the end of the nanowire. In nanowires superconductivity is induced by proximity; therefore a superconductor soft interface is also something likely to be found. Furthermore, in a normal superconductor junction the potential edge may be located far away from the place where superconductivity starts to decrease (i.e., the superconductor interface). The objective of this chapter is to clarify the junction physics and its effects on the Majorana robustness. With this purpose, the potential and superconductor softness interfaces and distance between them are parametrized and the resulting junctions are classified in different categories. The junction is modeled as a system of equations that is solved for each case, then the energy spectrum of the junction and the Majorana density function are both analyzed.

2.2 Methodology

The used methodology requires the numerical resolution of large and sparse linear systems of equations. The junction is spatially discretized in a grid and in each grid point we impose either the Bogoliubov-deGennes equation or the asymptotic boundary behavior. The energy is treated as a parameter and the wavefunction components at each grid site are the unknowns of the linear system. The resulting set of equations can be written in the mathematical form $A\vec{\Psi} = \vec{b}$ for each of the grid points, where $\vec{\Psi}$ represents the unknown column vector and A is a sparse matrix (in our particular case it is $\vec{b} = 0$). In this work, we have used the Harwell library [39] to solve large systems of equations encoded in sparse matrices. The equations are solved by the routine library using a back substitution algorithm in a triangular matrix. The computational order of this method is $O(n^2)$ that represents and advantage over the direct numerical diagonalization methods of order $O(n^3)$ where n is the number of grid points. Furthermore, we solve the system of equations using infinite homogeneous regions as open boundaries therefore we do not restrict ourselves to closed nanowires.

The first part of the article focuses on the characteristic modes of the junction when no open incident propagating modes are considered. In this case, the trivial empty $\vec{\Psi} = \vec{0}$ solution is a solution that has to be avoided. Therefore, an extra mechanism is needed to obtain a nonzero solution from the devised numerical method. We choose an arbitrary spin and isospin component of an arbitrary point and impose a non-zero condition for this component instead of the corresponding BdG equation. This is equivalent to a normalization condition of the wavefunction. The removal of an equation implies that we need to check afterwards the obtained solution. This check is on the continuity at the point and component forced to be non-zero. As a consequence, the resulting wavefunction will be only a physical solution if the wavefunction and its derivatives are continuous at that point.

The second part of the article is focused on the behavior of the junction when external open channels are active. In other words, if there is a propagating incident mode in one of the homogeneous boundaries. An open incident channel set to a non-zero value is already a normalization component, thus no additional mechanism is needed to avoid the trivial solution in presence of open channels.

In order to work with a numerical algorithm we use dimensionless units. In 1d nanowires the only possible characteristic length is given by the length of spin precession. This length may be difficult to calculate and is not used directly, however it is set indirectly by the Rashba spin orbit coupling strength α. Furthermore, as demonstrated in Ref. [23] a high Rashba strength enhances the Majorana localization. The length and energy units of this work depend on α and on the effective mass of the electron for the considered materials. In InAs and InSb based nanowires the Rashba coupling is $\alpha \approx 30\,\text{meVnm}$ while the electron effective masses are respectively $0.033m_e$ and $0.015m_e$, where m_e is the bare electron mass. That makes the length and energy units to be $L_{so} = 77\,\text{nm}$ and $E_{so} = 0.39$ meV for InAs; and $L_{so} = 170\,\text{nm}$ and $E_{so} = 0.18\,\text{meV}$ for InSb. Therefore, the typical values of the superconductor gap (typically $\Delta \approx$ meV) in dimensionless units are smaller or equal

to $\Delta = 0.25E_{so}$. Although we do not mention any particular superconductor material this value for the superconductivity is realistic for many s-wave superconductors at finite temperature. Furthermore, the proximity contact of the superconductor with the semiconductor nanowire changes the superconductor gap in the bulk of the nanowire with respect to the pure isolated superconductor energy gap.

2.3 Conclusions and remarks

With this method we first confirm the appearance of Majorana modes at the nanowire edge when a critical magnetic field is surpassed. Only two topological phases are found, trivial (where no Majorana is found) and topological (where a Majorana is found) as expected for a class D nanowire. In the periodic table for topological insulators and superconductors a device is classified into class D if it has particle hole symmetry but not time reversal and chiral symmetries [41].

Second, we determine that if there is enough distance between the potential and the superconductor interfaces, Andreev resonant states can be formed in this region. The protection of the Majorana regarding these states is affected by the distance between the two interfaces and by their softness.

On the other hand, we need to overcome a critical potential value in order to have an edge where the Majorana can be localized. The appearance of the Majorana peak with the potential is an abrupt phenomenon. Any infinitesimal deviation below the critical value of the potential will not lead to a Majorana.

As an additional comment on the paper, the potential and chemical potential take an analogous role to the Majorana mass in the Kitaev chain model where Majoranas are localized at the points where the mass changes sign. Note that the critical value of the potential imposes some constraints in the design of a braiding scheme. No matter how slow you approach the potential critical point a Majorana will not exist until the critical value is reached. Then this critical value will represent a singular point in the evolution if we want to split a nanowire o create a new couple of Majoranas. In short, manipulating Majoranas may be done adiabatically but their creation or destruction manipulating the barrier height will be a non adiabatic process.

2.4 Published paper

PHYSICAL REVIEW B **88**, 144512 (2013)

Majorana modes in smooth normal-superconductor nanowire junctions

Javier Osca[1,*] and Llorenç Serra[1,2]

[1]*Institut de Física Interdisciplinària i de Sistemes Complexos IFISC (CSIC-UIB), E-07122 Palma de Mallorca, Spain*

[2]*Departament de Física, Universitat de les Illes Balears, E-07122 Palma de Mallorca, Spain*

(Received 18 August 2013; revised manuscript received 23 September 2013; published 22 October 2013)

A numerical method to obtain the spectrum of smooth normal-superconductor junctions in nanowires, able to host Majorana zero modes, is presented. Softness in the potential and superconductor interfaces yields opposite effects on the protection of Majorana modes. While a soft potential is a hindrance for protection, a soft superconductor gap transition greatly favors it. Our method also points out the possibility of extended Majorana states when propagating modes are active far from the junction, although this requires equal incident fluxes in all open channels.

DOI: 10.1103/PhysRevB.88.144512 PACS number(s): 74.45.+c, 73.63.Nm

I. INTRODUCTION

In 1936, Ettore Majorana theorized the existence of elementary particles, now called Majorana fermions, that coincide with their own antiparticles.[1] The implementation of quasiparticle excitations having a similar property, called Majorana states, is currently attracting much interest in condensed matter systems in general,[2–12] and in nanowires in particular.[13–26] Interest has been further fueled by recent experimental evidences of these Majorana states in quantum wires.[27–31] They are also known as Majorana zero modes (MZM) and, in essence, they are topological zero-energy states living close to the system edges or interfaces. The existence of an energy gap between the MZM and nearby excitations protects the former from decoherence. These properties make MZM's interesting not only for their exotic fundamental physics but also for their potential use in future topological quantum-computing applications.[32,33]

Majorana modes can be implemented in a superconductor wire by the combined action of superconductivity, Rashba spin-orbit coupling, and Zeeman magnetic effect. In a superconductor, nanowire electrons play the role of particles, while holes of opposite charge and spin perform the role of antiparticles. Superconductivity leads to a charge symmetry breaking and allows quasiparticles without a good isospin number. On the other hand, the Rashba effect is a direct result of an inversion asymmetry caused by an electric field in a direction perpendicular to the propagation while the Zeeman magnetic field breaks the spin rotation symmetry of the system. The combined action of both couplings can create effective spinless Majorana states.

It is known that in semiconductor nanowires having a region of induced superconductivity, Majorana edge states are formed in the junction between the superconductor and the normal side of the nanowire. This work addresses the physics of soft-edge junctions, where both superconductivity and potential barrier characterizing the edge vary smoothly as one moves from the normal to the superconductor side. The inset in Fig. 1 sketches the physical system we have in mind. As suggested in the figure, the potential smoothness could be electrically manipulated by gates while the induced superconductivity crossover might be controlled by spatially modulating the distance between nanowire and underlying superconductor. This latter effect is represented by an intermediate wedge of insulating material. It is worth mentioning that our model could also represent an intrinsic smoothness due to uncontrolled effects in the device fabrication, such as, e.g., shape distortions or impurity migration.

Previous works on nanowire Majorana physics assumed abrupt transitions, with a few exceptions. In Refs. 34 and 35, smooth 1D models were considered, emphasizing how smooth edge potentials possess eigenstates at very low (but finite) energies that, in practice, imply a loss of protection for the MZM. Similar conclusions were found with 2D models of tight-binding chains in Refs. 36 and 37. Our work generalizes those studies by focusing on the role of a diffuse superconductivity edge placed either at the same or at different position of the potential barrier. We find a strong influence of the superconductivity smoothness on the finite-energy Andreev states occurring in between potential and superconductivity edges. This is relevant for the protection of MZM's as it is affected in opposite ways by the smoothness in potential and superconductivity: protection is hindered by a smooth potential (also discussed in Ref. 35) and, remarkably, it is favored by a smooth superconductivity.

This work is divided in six sections. In Sec. II, the physical system is introduced, and in Sec. III, the numerical method is explained. Section IV contains different results for bound and resonant states in different kinds of junctions, in absence of any input flux. Section V is devoted to an extension for junctions under an input flux, demonstrating that in this case extended MZM's are possible, as opposed to the localized ones of preceding sections. The conclusions are drawn in Sec. IV.

II. PHYSICAL SYSTEM

We consider a purely 1D nanowire model with spin-orbit interaction inside a homogenous Zeeman magnetic field as in Ref. 38. The system is described by a Hamiltonian of the Bogoliubov-deGennes kind,

$$\mathcal{H}_{\mathrm{BdG}} = \left(\frac{p_x^2}{2m} + V(x) - \mu\right)\tau_z + \Delta_B\,\vec{\sigma}\cdot\hat{n} + \Delta(x)\,\tau_x + \frac{\alpha}{h}\,p_x\sigma_y\tau_z, \tag{1}$$

where the Pauli operator for spin is represented by $\vec{\sigma}$, while the operator for isospin (electron/hole charge) is represented

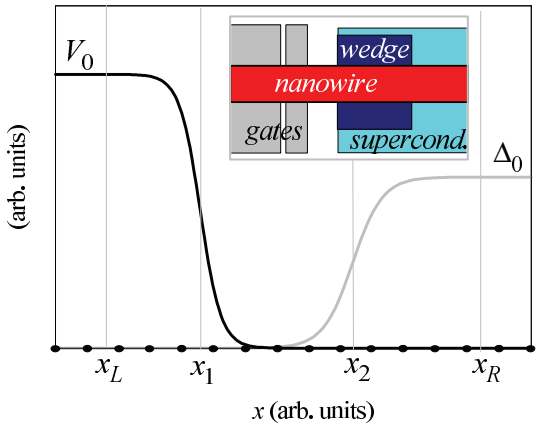

FIG. 1. (Color online) NS junction of an infinite nanowire. The black curve is the nanowire potential $V(x)$ created by nearby gates, while the gray curve is the superconductor gap induced by proximity with an s-wave superconductor. The inset sketches the physical system. The normal contact ($x < x_L$) is characterized by a potential V_0 and the superconducting one ($x > x_R$) by a gap Δ_0. A smooth variation of $V(x)$ and $\Delta(x)$ occurs at transition points x_1 and x_2, respectively. A Zeeman magnetic field is applied homogenously along the entire nanowire pointing in x direction, while the Rashba SOI effective magnetic field points perpendicularly in y direction. The numerical method uses a grid as indicated schematically by the dots on the x axis.

by $\vec{\tau}$. The successive energy contributions in Eq. (1) are the following (in left to right order): kinetic, electric potential, chemical potential, Zeeman, superconduction, and the Rashba term. The latter arises from the self-interaction between an electron (or hole) spin with its own motion due to the presence of a transverse electric field, perceived as an effective magnetic field in the rest frame of the quasiparticle. On the other hand, the Zeeman effect is the band splitting caused by the application of an external magnetic field. Rashba spin-orbit and Zeeman effects depend on the parameters α and Δ_B, respectively. Since we consider a nanowire made of a homogenous material inside a constant magnetic field, these parameters are assumed homogenous. The magnetic field points in the $\hat{x}$ direction, parallel to the propagation direction and perpendicular to the spin-orbit effective magnetic field direction $\hat{y}$. The superconduction term arises from a mean-field approximation over the phonon assisted attractive interaction between electrons. This leads to the coupling of the opposite states of charge of the base and the creation of Cooper pairs whose breaking energy is the energy gap $\Delta(x)$. The remaining terms in Eq. (1) are the potential term $V(x)$ created by the presence of a metallic gate over the nanowire and the chemical potential term μ.

The nanowire smooth junction is sketched in Fig. 1, with left ($x < x_L$) and right ($x > x_R$) contacts corresponding to the normal and superconductive sides, respectively. The normal contact is characterized by a bulk potential V_0 and the superconducting one by a gap Δ_0. Superconduction in a semiconductor nanowire region is achieved by maintaining that region in contact with a 3D superconductor. In the junction region between the two asymptotic behaviors, $x_L < x < x_R$, a smooth transition is described by the potential $V(x)$ and gap $\Delta(x)$ functions of the position x.

The transitions between bulk values in $V(x)$ and $\Delta(x)$ are modeled with two soft Fermi functions centered at x_1 and x_2, respectively. Their softness is controlled with parameters s_1 and s_2. A zero softness means a step interface, while a high value implies a smooth one. These two functions read

$$V(x) = \frac{V_0}{1 + e^{(x-x_1)/s_1}}, \tag{2}$$

$$\Delta(x) = \Delta_0 \left[1 - \frac{1}{1 + e^{(x-x_2)/s_2}} \right]. \tag{3}$$

III. NUMERICAL METHOD

The energy eigenstates fulfill the time independent Schrödinger equation with the Bolgoliubov-deGennes Hamiltonian,

$$(\mathcal{H}_{\mathrm{BdG}} - E)\, \Psi(x, \eta_\sigma, \eta_\tau) = 0, \tag{4}$$

where the wave function variables are the spatial coordinate $x \in (-\infty, \infty)$, the spin $\eta_\sigma \in \{\uparrow, \downarrow\}$, and the isospin $\eta_\tau \in \{\Uparrow, \Downarrow\}$. The basis projection for spin and isospin is taken in $\hat{z}$ orientation, with isospin up and down representing electron and hole quasiparticles, respectively. We expand next the wave function in spin and isospin spinors,

$$\Psi(x, \eta_\sigma, \eta_\tau) = \sum_{s_\sigma s_\tau} \Psi_{s_\sigma s_\tau}(x)\, \chi_{s_\sigma}(\eta_\sigma)\, \chi_{s_\tau}(\eta_\tau), \tag{5}$$

with the quantum numbers $s_\sigma = \pm$ and $s_\tau = \pm$. The spin and isospin states fulfill

$$\vec{\sigma} \cdot \hat{n}\, \chi_{s_\sigma}(\eta_\sigma) = s_\sigma\, \chi_{s_\sigma}(\eta_\sigma), \tag{6}$$

$$\tau_z\, \chi_{s_\sigma}(\eta_\sigma) = s_\tau\, \chi_{s_\tau}(\eta_\tau). \tag{7}$$

We numerically obtain the wave function amplitudes $\Psi_{s_\sigma s_\tau}(x)$ on the set of N grid points, qualitatively sketched in Fig. 1 (N is actually much larger than shown in the figure). In our approach, the energy E is given, and we determine whether a physical solution exists or not for that energy. In particular, MZM's will be found for values of E equal to zero. Using n-point finite difference formulas for the x derivatives, Eq. (4) transforms on the grid into a matrix linear equation of homogenous type.

The solution must be compatible with the bulk boundary conditions for grid points in the normal ($x < x_L$) and superconductor contacts ($x > x_R$). In these asymptotic regions, the solutions, at the desired energy E, are given by a linear combination of bulk eigensolutions $\Phi_k^{(c)}(x, \eta_\sigma, \eta_\tau)$, each one characterized by a wave number k and $c = L, R$ being a generic label for the contact,

$$\Psi(x, \eta_\sigma, \eta_\tau) = \sum_k C_k^{(c)}\, \Phi_k^{(c)}(x, \eta_\sigma, \eta_\tau). \tag{8}$$

The bulk eigensolutions are expressed in terms of exponentials:

$$\Phi_k^{(c)}(x, \eta_\sigma, \eta_\tau) = \sum_{s_\sigma s_\tau} \Phi_{k s_\sigma s_\tau}^{(c)}\, e^{ik(x-x_c)} \chi_{s_\sigma}(\eta_\sigma) \chi_{s_\tau}(\eta_\tau). \tag{9}$$

The set of wave numbers and state coefficients $\{k, \Phi_{k s_\sigma s_\tau}^{(c)}\}$ characterizing the solutions in contact c must be known in advance in order to proceed with the numerical calculations. These coefficients can be obtained for the homogenous and

infinite problem either analytically or by means of additional numerical methods.[14,38] Equation (8) must be fulfilled in replacement of Eq. (4) for grid points in the asymptotic regions. Notice that they are local relations in x and, therefore do not involve wave function amplitudes on points located further to the left or right of the grid ends.

Due to symmetries, there are always four bulk wave numbers per contact in *outward* direction. By outward direction we mean either exponentially decaying from the junction, in case of evanescent modes, or moving away from it, in case of propagating modes. Notice that for propagating modes, the flux direction is parallel and antiparallel to the corresponding real k for quasiparticles of electron and hole type, respectively. A closed linear system for the set of $4N+4+4$ unknowns $\{\Psi_{s_\sigma s_\tau}(x), C_k^{(L)}, C_k^{(R)}\}$ is easily obtained from Eqs. (4) and (8). A final complication, however, is found in the homogenous character of this linear system mathematically admitting the trivial solution of all unknowns equal to zero.

We discard the trivial solution by introducing an arbitrary matching point x_m as well as a specific pair of spin-isospin components (s,t). Assuming $\Psi_{st}(x_m)$ does not identically vanish, we can arbitrarily impose

$$\Psi_{st}(x_m) = 1, \tag{10}$$

$$\left(\frac{d^{(L)}}{dx} - \frac{d^{(R)}}{dx}\right)\Psi_{s_\sigma s_\tau}(x_m) = 0, \quad (s_\sigma, s_\tau) \neq (s,t). \tag{11}$$

Equations (10) and (11) are four equations that we require at x_m in place of the Bogoliubov-deGennes one. Thanks to Eq. (10) the resulting system is no longer homogenous. In Eq. (11), $d^{(L)}/dx$ and $d^{(R)}/dx$ indicate grid derivatives using only left or right grid neighbors. Crossing the matching point is actually avoided using noncentered finite difference formulas. With this substitution of one equation the resulting linear system admits a nontrivial solution, robust with respect to changes in the arbitrary choices: x_m, (s,t).

By means of Eq. (11) our algorithm ensures the continuity at the matching point of the first derivative for all spin-isospin components, with the exception of the arbitrarily chosen (s,t). This relaxation of one condition makes the algorithm numerically robust and free from singularities. The mathematical solutions can be discriminated by defining the physical *measure*

$$\mathcal{F} = \left|\left(\frac{d^{(L)}}{dx} - \frac{d^{(R)}}{dx}\right)\Psi_{st}(x_m)\right|^2. \tag{12}$$

Only those results with $\mathcal{F} = 0$ are true physical solutions but this can be tested afterwards, at the end of the algorithm. Varying the energy E or the Hamiltonian parameters the method allows the exploration of the topological phases.

The resulting system of equations is solved with a sparse-matrix linear algebra package.[39] As in Refs. 14 and 38, the numerical algorithm works in adimensional units, using the Rashba spin-orbit interaction (SOI) as a reference. The corresponding length and energy units read

$$L_{\rm so} = \frac{\hbar^2}{\alpha m}, \tag{13}$$

$$E_{\rm so} = \frac{\alpha^2 m}{\hbar^2}. \tag{14}$$

Assuming, for instance, an InAs-based nanowire with $m = 0.033 m_e$ and $\alpha = 30$ meVnm, the physical units are $L_{\rm so} = 77$ nm and $E_{\rm so} = 0.39$ meV. For an InSb nanowire with $m = 0.015 m_e$ and the same α, the corresponding values would be $L_{\rm so} = 170$ nm and $E_{\rm so} = 0.18$ meV. In the rest of this work, all results will be referred to this material-dependent units.

The strict 1D character of our model represents the low-energy limit of laterally confined additional dimensions, when only the lowest transverse mode is allowed. A generalization of the present numerical method to a multimode situation is possible with the use of the higher-dimensional complex band structure, discussed in Ref. 38 for 2D. Notice, however, that this generalization would also require modifying the present matching algorithm and it would be computationally much more demanding.

IV. RESULTS WITHOUT INPUT FLUX

We study first the physics of the junction in absence of any input fluxes. Physically, this situation occurs when propagating modes in both contacts are either not active or, at most, they carry flux only in outwards direction from the junction. This behavior is expected in presence of purely absorbing (reflectionless) contacts. It is well known that in absence of propagating modes bounded MZM's may exist in some cases. The allowed asymptotic wave numbers have an imaginary component causing the wave functions to decay away from the junction. As a consequence, the main characteristic of these bounded MZM's is that they are confined in a particular region of space. We will first check our method comparing with the analytical limits of Klinovaja and Loss,[23] extending later the analysis to other results not obtainable analytically. These results range from the formation of Majorana modes in soft edge junctions of different kinds, to the influence of the edge on the MZM localization and protection.

A. Comparison with analytical expressions

Reference 23 provides analytical expressions for MZM's in a sharp NS junction, in a semi-infinite system. They are approximations valid deep into the topological phase $\Delta_B \gg \sqrt{\Delta_o^2 + \mu^2}$. The approximations are done for both strong SOI ($E_{\rm so} \gg \Delta_B$) and weak SOI ($E_{\rm so} \ll \Delta_B$) regimes. In the strong SOI regime, the Rashba spin-orbit effect is the dominating term while the magnetic field and the superconductivity are treated as small perturbations. On the other hand, in the weak SOI regime, the magnetic field term dominates. In Fig. 2, density distributions for NS junctions in a semi-infinite nanowire are shown for the strong and weak SOI regimes, as well as for an intermediate situation. The strong- and weak-regime numerical solutions (in dark blue) are compared with their analytical counterparts (in light green). The exclusion effect on the hard edge on the left is achieved in the numerical method by putting a very high sharp potential step at $x = -L$, while the sharp superconductor interface is located at $x = 0$.

The strong SOI Majorana density function is characterized by the combination of an oscillatory behavior modulated by exponential bounds in the normal side of the junction while, on the other hand, the weak SOI density is characterized

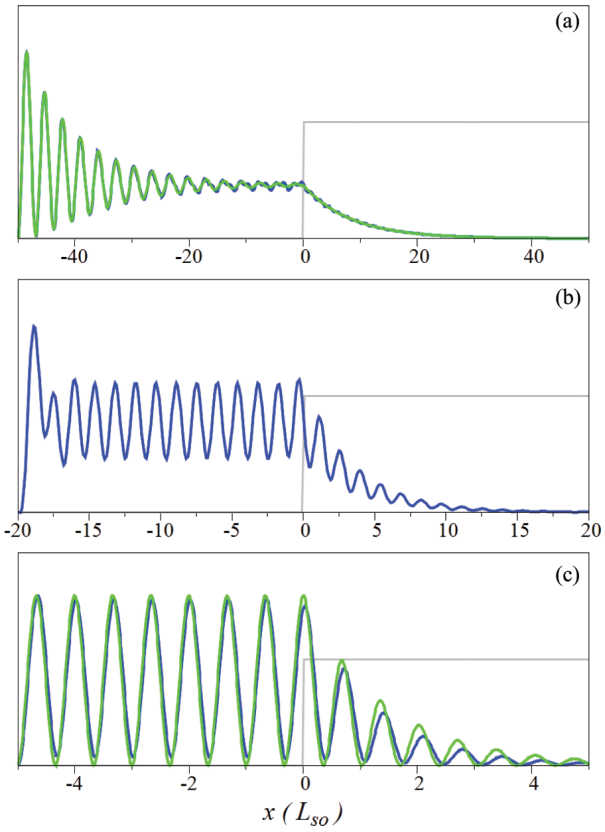

FIG. 2. (Color online) Density distributions of MZM's obtained with our numerical method (dark gray or blue) and with analytical approximations (light gray or green).[23] (a) Strong SOI regime $E_{so} \gg \Delta_B$: $\Delta_B = 0.09E_{so}$, $\Delta_0 = 0.06E_{so}$, and $L = 50L_{so}$. (b) Intermediate regime $E_{so} = \Delta_B$: $\Delta_0 = 0.2E_{so}$, $L = 20L_{so}$. In this case, the analytical result is not known. (c) Weak SOI regime $E_{so} \ll \Delta_B$: $\Delta_B = 10E_{so}$, $\Delta_0 = 4E_{so}$, and $L = 5L_{so}$.

by constant oscillations up to the NS interface. Entering the superconductor contact both densities decay, although in a more oscillatory way for the weak SOI. Note also that the intermediate regime $E_{so} \approx \Delta_B$ represents a sort of mixed situation with a first density peak near the $x = -L$ edge followed by regular oscillations of constant amplitude up to the NS junction. The theoretical and numerical results agree well in their corresponding regimes (but for some fine effects). However, the analytical solutions are not applicable out of their regimes of approximation. Therefore a numerical approach is potentially very useful in order to predict MZM's density distributions in many realistic physical realizations that can be out of the strong and weak regimes in a varying degree.

B. Soft edge junction results

Assume now the normal side contains a soft potential step characterized by a finite V_0, allowing some penetration. As can be seen in Fig. 3, this implies the appearance of a maximum in the density distribution near the potential edge followed by regular oscillations of decreasing amplitude. The density starts decaying exponentially in the superconductor interface until it vanishes well inside the superconductor side of the system.

The present method allows us to obtain the solutions not only for $E = 0$ but for any arbitrary value of E. Figure 4

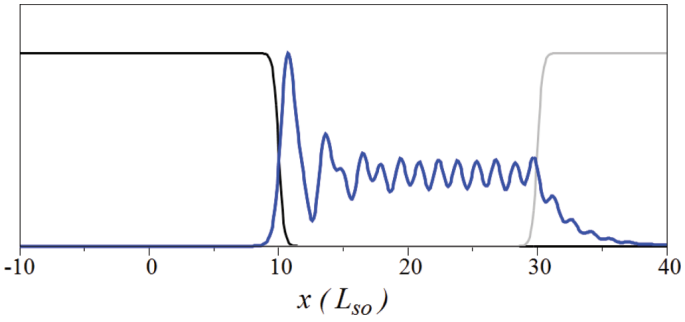

FIG. 3. (Color online) MZM density (thick curve) in arbitrary scale when the potential interface is located at $x_1 = 10L_{so}$ with a softness parameter $s_1 = 0.2L_{so}$ and the superconductor gap interface is located at $x_2 = 30L_{so}$ with softness $s_2 = 0.2L_{so}$. The rest of parameters are $V_o = 2E_{so}$, $\Delta_o = 0.25E_{so}$, $\Delta_B = 0.4E_{so}$, and $\mu = 0.1E_{so}$. The position dependent potential and superconductor gap are shown by the thin black and gray curves, respectively.

shows the location of the eigenstates in a Δ_B-E plane. They are signaled by the zeros of the function $\mathcal{F}$ [cf. Eq. (12)], represented here in a color (gray scale) plot. Black and white curves in Fig. 4 inform us on the presence of propagating modes in the superconductor and normal sides, respectively. That is, for energies above the curve, propagating modes are possible in the superconductor (black) and normal (white) contacts. When propagating modes become possible asymptotically, the zeros of $\mathcal{F}$ no longer represent bounded states, but purely outgoing resonances created by the junction.

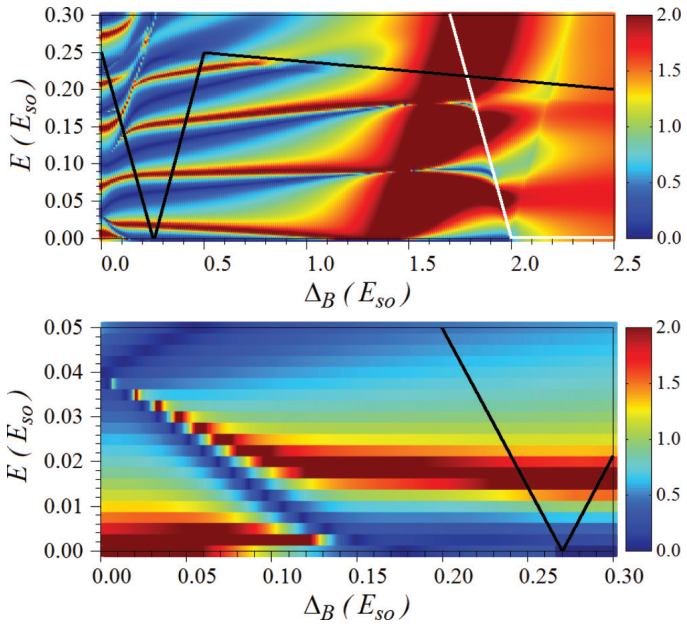

FIG. 4. (Color online) (a) Junction spectrum for different values of the magnetic field. The same parameters of Fig. 3 have been used. The colors represent the values of the function $\mathcal{F}$. Note that a solution exists when $\mathcal{F} = 0$ (in dark blue). Above the black line, propagating modes exist in the superconductor side of the junction, while above the white line, the propagating modes exist in the normal side. (b) Zoom of the spectrum showing the formation of the Majorana zero mode when the magnetic field becomes high enough for the system to perform a transition to the topological phase. $\Delta_B = 0.27E_{so}$ is the topological critical value of the Zeeman field.

In this case, there is no violation of charge conservation since outgoing electron and hole equal fluxes imply zero currents.

For Zeeman energies lower than the critical value $\Delta_B^{(c)} \equiv \sqrt{\Delta_0^2 + \mu^2}$ no MZM exists but, instead, finite energy subgap fermions may be found. Only those at positive energies are shown in Fig. 4, but the spectrum is exactly symmetrical for negative energies. When the magnetic field energy equals $\Delta_B^{(c)}$ the gap closes in the superconductor side. This is hinted in Fig. 4 by the presence of propagating modes in the superconductor side of the junction even at zero energies for this specific magnetic field. For higher fields, the gap immediately reopens in the supercoductor region and the junction enters the topological phase with an $E = 0$ solution, a MZM. In this phase, finite-energy resonant Andreev states can be found as well. The energy difference between the MZM and the finite-energy states is a measure of the protection of the MZM. The greater the energy difference the greater the protection of the Majorana. Increasing further the magnetic field the MZM is finally destroyed due to the closing of the gap in the normal side of the junction. This is signaled by the appearance of propagating modes in this side of the junction even at zero energy. When the state at zero energy becomes propagating the bounded Majorana zero modes can not exist. All these results are in agreement with the present knowledge on MZM's and represent a further check on our numerical method.

C. Softness effects

This section is devoted to the study of effects that changes in the softness parameter of the potential and superconductor interfaces cause on the Majorana density function and on the junction spectrum. In general, the shape of the density function is robust to moderate changes in the softness of the superconductor gap interface [see Fig. 5(a)]. If we replace the sharp superconductor interface by a region of a gradually increasing superconductivity, the Majorana wave function is not greatly affected. However, if we assume a very soft (almost linear) increase in superconductivity, it is possible to see how the density tail of the MZM adapts to the appearance of the superconductivity [see Fig. 5(b)].

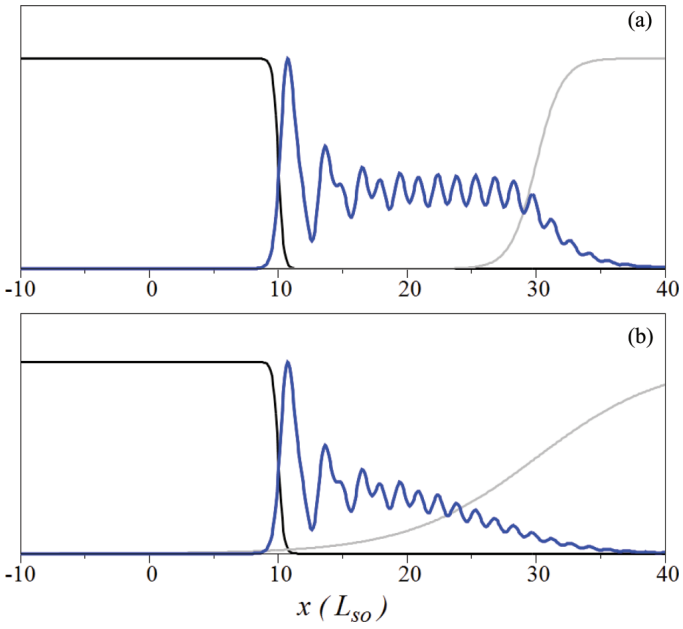

FIG. 5. (Color online) (a) Same as in Fig. 3 but with a softer superconductivity interface $s_2 = L_{so}$. (b) Same as in Fig. 2 and (a) but with an even softer, almost linear, superconductivity interface $s_2 = 5L_{so}$.

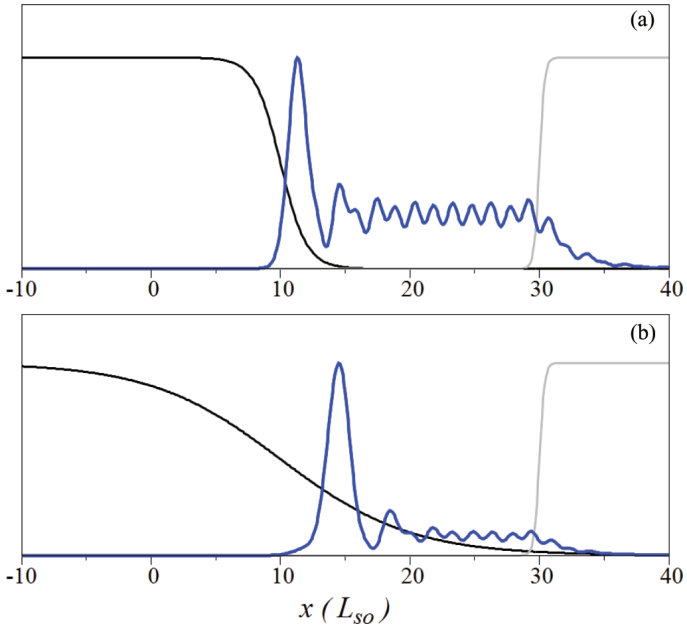

FIG. 6. (Color online) (a) Same as in Fig. 3 but with a potential softness parameter $s_1 = L_{so}$ while the superconductor gap interface has a softness parameter $s_2 = 0.2L_{so}$. (b) Same as (a) but with a potential softness parameter $s_1 = 5L_{so}$.

The MZM is also robust with changes of the potential interface softness [see Fig. 6(a)]. Again, only with an almost linear decrease of the junction potential a sizable reduction of the density tail towards the supercoductor side can be seen with respect to the result for an abrupt potential. We also notice a slight increase in the width of the density peak as well as a change in the peak position [see Fig. 6(b)]. Combining the two effects, if the softness of both potential and superconducting interfaces is high enough, an MZM with a well localized density peak is found [see Fig. 7(a)].

A similar robustness against softness is found in the junction energy spectrum. Figure 8(a) shows the spectrum of eigenenergies, containing the MZM at zero energy and its closest excited bound and resonant states at finite energies. As before, the location of the eigenenergies is signaled by the zeros of the function $\mathcal{F}$ (in black). Note that although the function $\mathcal{F}$ is not symmetrical with respect to $E = 0$, the position of the zeros indeed is. The particular shape of $\mathcal{F}$ is actually irrelevant and only the position of its zeros bears a physical meaning. The blue staircase curve informs us about the number of propagating modes in the superconductor side of the junction. The protection of the MZM, proportional to the energy gap with its nearby eigenenergies, does not change significantly for moderate values of the softness of the superconductor and potential interfaces. On the other hand, for high enough values of the softness, interesting results arise.

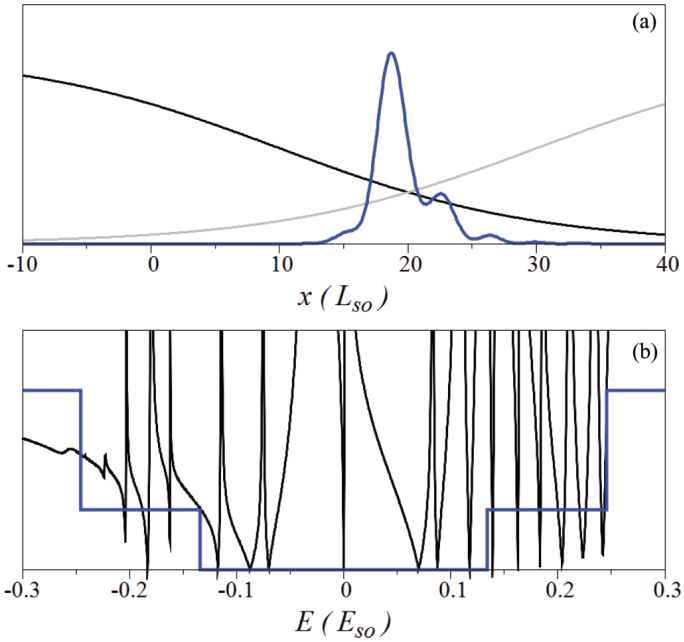

FIG. 7. (Color online) (a) MZM density when the potential interface is located at $x_1 = 10L_{so}$ while the superconductor interface is located at $x_2 = 30L_{so}$, both with a softness parameter $s_1 = s_2 = 10L_{so}$. The rest of parameters are $V_o = 2E_{so}$, $\Delta_o = 0.25E_{so}$, $\Delta_B = 0.4E_{so}$, and $\mu = 0.1E_{so}$. (b) Energy spectrum of the junction in (a). As before the function $\mathcal{F}$ is shown in black, while the number of propagating modes in the superconductor side of the junction is shown in blue gray. Zeros in $\mathcal{F}$ indicate the existence of a solution with the corresponding energy E.

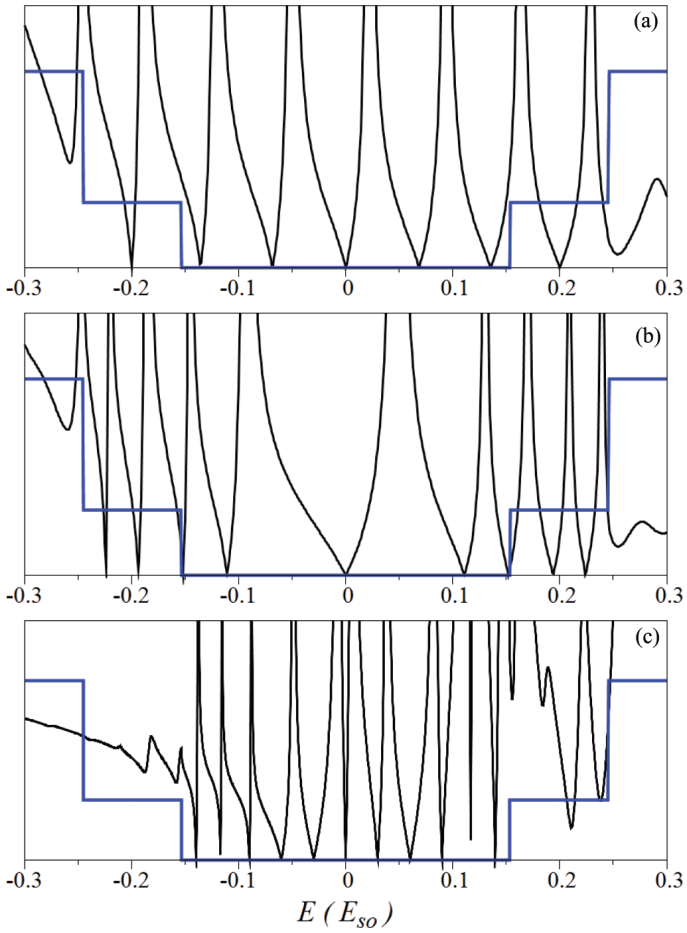

FIG. 8. (Color online) (a) Junction spectrum when the potential interface is located at $x_1 = 10L_{so}$ while the superconductor gap interface is located at $x_2 = 30L_{so}$ both with softness parameters $s_1 = s_2 = 0.2L_{so}$. The rest of parameters are $V_0 = 2E_{so}$, $\Delta_o = 0.25E_{so}$, $\Delta_B = 0.4E_{so}$, and $\mu = 0$. The function $\mathcal{F}$ is shown in black, while the number of propagating modes in the superconductor side of the junction is shown in blue gray. Each step corresponds to the activation of a propagating mode. The zeros of $\mathcal{F}$ indicate the existence of a solution with the corresponding energy E. (b) Same as (a) but with a superconductor gap interface softness $s_2 = 10L_{so}$ while the potential softness is $s_1 = 0.2L_{so}$. (c) Same as (a) and (b) but this time with a potential interface softness $s_1 = 10L_{so}$ and a superconductor gap interface softness $s_2 = 0.2L_{so}$.

For high values of the superconductor interface softness, shown in Fig. 8(b), the protection of the MZM is increased since its neighboring eigenenergies are repelled from zero. In this case, the finite energy modes get closer to the activation energy of the propagating modes, i.e., to the energy gap on the superconductor side of the junction. On the contrary, the increase of the potential softness introduces more excited states inside the superconductor energy gap, thus getting closer to the MZM energy [see Fig. 8(c)]. The appearance of low-energy states in a soft potential interface is in agreement with the results of Ref. 35. The characteristic features of these low-energy states in tunneling conductance experiments were discussed in Ref. 40.

When both interfaces are made soft the two effects on the spectrum we have just discussed compete. That is, the higher softness of the potential introduces more bound states inside the superconductor energy gap, while the softness of the superconducting interface tries to push them apart from the MZM. The result is that many excited states get densely packed near the superconducting gap energy [see Fig. 7(b)].

D. MZM's in different kinds of junctions

Up to this point, it has been assumed that the position of the potential interface x_1 and the superconduction interface x_2 are such that $x_1 < x_2$, i.e., they do not overlap. In this subsection we consider a more general situation, defining two kind of junctions: type I junctions without overlapping region ($x_1 < x_2$) and type II junctions in the opposite case ($x_1 > x_2$).

Figure 9 shows a comparison between both types, as well as the limiting intermediate situation. In type I junctions, the MZM density behaves as in previous sections, with a density peak localized on the potential edge followed by regular oscillations and a decaying behavior inside the superconductor region. On the other hand, type II junctions just show an oscillatory density whose amplitude decays as the function penetrates the superconductor region. The limiting case $x_1 = x_2$ behaves similarly to the type II junction.

We also notice from Fig. 9 that the density peak is always found close to the potential interface. That is, the MZM is located on the potential step and not on the superconductivity interface. Superconductivity is a necessary ingredient for the formation of the MZM but, in practice, its maximum probability can be located quite far from the superconductor interface.

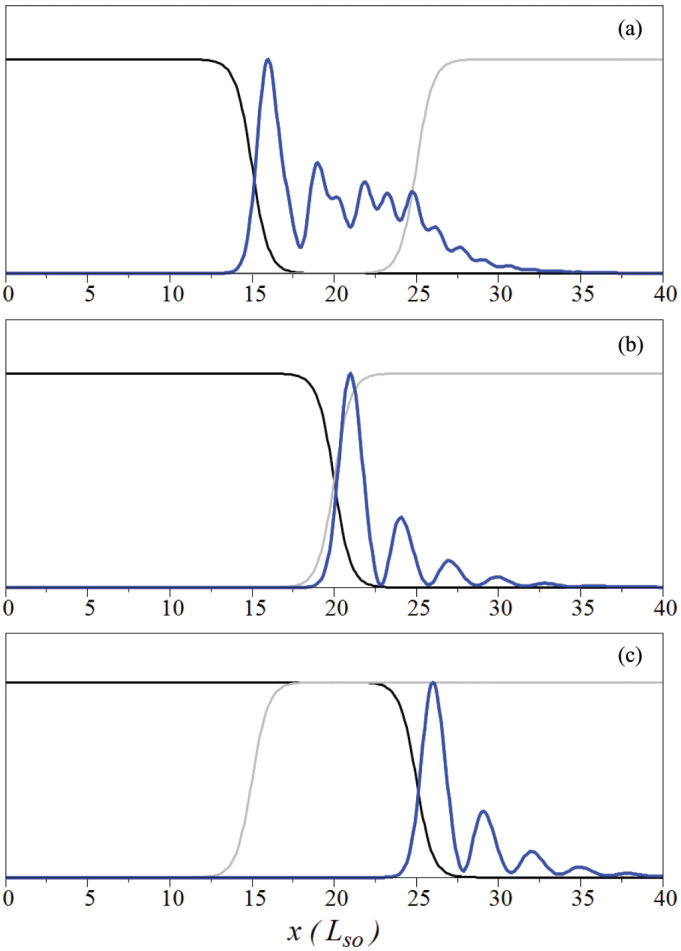

FIG. 9. (Color online) Different kinds of soft NS junctions in an infinite nanowire. The used parameters are $V_o = 2E_{so}$, $\Delta_o = 0.25E_{so}$, $\Delta_B = 0.4E_{so}$, and $\mu = 0.1E_{so}$. (a) Type I junction, with nonoverlapping high-potential and superconductivity regions. (c) For a type II junction, it is just the opposite. (b) This is the limiting case between the two when the potential and superconductor interfaces are located at the same point.

As shown in Fig. 8(a), bounded states are found in type I junctions at energies different from zero. We believe these states are Andreev resonant states formed in the region between the two interfaces. This statement is confirmed by means of a change in the superconductor bulk value Δ_0. As shown in Fig. 10, out of the topological regime, the MZM splits into two subgap fermionic states but the Andreev resonant states remain almost with the same eigenenergies. Notice also that the number of Andreev states is larger and their energies are closer to zero in type I junctions with a large nonoverlapping region, i.e., large $d = x_2 - x_1$ [see Fig. 11(a)]. On the contrary, if d is diminished the number of Andreev resonant states diminishes and their energies fall apart from zero. In the limiting case when d is zero, the Andreev resonant states disappear and the protection of the MZM is determined by the amplitude of the gap on the superconductor side of the junction as shown in Fig. 11(b). The same happens for type II junctions with $d < 0$. Furthermore, in this case ($d \leqslant 0$), the junction spectrum is even more resilient to changes in the softness of the interfaces, being almost insensitive to them.

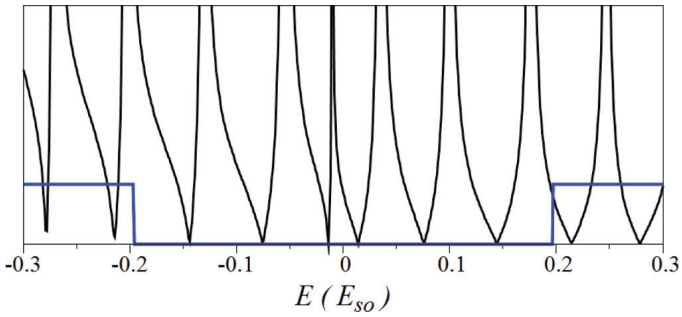

FIG. 10. (Color online) Junction spectrum out of the topological phase. In this regime, the MZM is split into two subgap fermions. The used parameters are $V_o = 2E_{so}$, $\Delta_o = 0.6E_{so}$, $\Delta_B = 0.4E_{so}$, and $\mu = 0$.

The distinction between genuine MZM's and split fermionic states out of the topological regime can be experimentally very challenging for type I junctions. As can be seen in the lower panel of Fig. 4, for values of the magnetic field $\Delta_B > 0.15E_{so}$, the first eigenvalue quickly moves near zero energy as the magnetic field increases. If the experimental resolution is not high enough, these two states (recall that the spectrum is symmetric for negative energies) could be perceived as a single one and their sudden displacement near zero energy misinterpreted as a topological transition; the actual transition being for $\Delta_B > 0.27E_{so}$. This effect of proximity to zero energy of fermionic states out of the topological phase is exclusive of $d > 0$ (type I) junctions. In $d \leqslant 0$ (type II) junctions, these states do not get close to zero energy until the true topological transition.

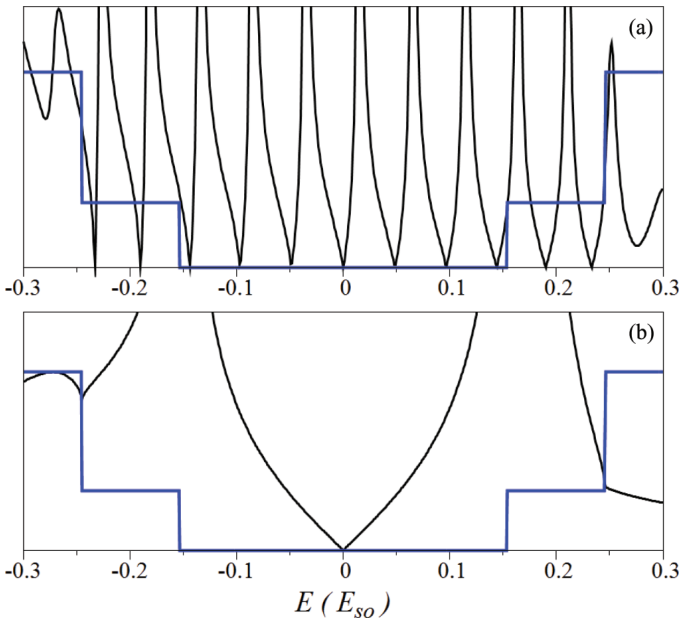

FIG. 11. (Color online) Spectra for different kinds of junctions. The used parameters are $V_o = 2E_{so}$, $\Delta_o = 0.25E_{so}$, $\Delta_B = 0.4E_{so}$, and $\mu = 0$. (a) Type I junction with a long separation between potential and superconductor interfaces ($d = 30L_{so}$), while (b) corresponds to the limiting case between type I and type II junctions when both interfaces are located on the same position ($d = 0$). Like in preceding figures, the zeros of $\mathcal{F}$ indicate the existence of a solution with the corresponding energy E.

V. RESULTS WITH INPUT FLUX

Decreasing the potential V_0, for a fixed Δ_B, Δ_0, and zero energy, wave functions characterized by real wave numbers arise in the bulk normal side of the junction. When this occurs, bounded MZM's no longer exist due to their coupling with propagating modes. In the preceding section, we assumed that if propagating modes were present, they only carried outgoing flux. In this section, we explore the influence of incident fluxes on the junction. The same numerical method explained above can be used here, disregarding the use of the matching point and just fixing the coefficients C_k of the input modes as this already yields a nonhomogenous linear system. We only consider input modes from the normal side of the junction, given by electron states of positive k and hole states of negative k. Furthermore, it is also assumed that all propagating input modes impinge on the junction with exactly the same flux.

Following the sequence from high to low values of V_0, the system evolves from no propagating modes at high V_0 to four input modes (with two different k's) for moderately low values of the potential V_0. In this case, the resulting zero-mode density is characterized by a beating pattern of a large wavelength modulated by a smaller one [see Fig. 12(b)]. For $\Delta_0 = 0.25E_{\rm so}$ and $\Delta_B = 0.4E_{\rm so}$, this regime ranges from $V_0 = 0.68E_{\rm so}$, where the propagating modes arise, down to $V_0 = 0.50E_{\rm so}$. Above $V_0 = 0.68E_{\rm so}$, only evanescent modes are possible [see Fig. 12(a)]. The zero-mode solution obtained in this range does not represent a MZM since its wave function components do not fulfill the requirement

$$\Psi_{s_\sigma s_\tau}(x) = (-1)^{\frac{s_\sigma - s_\tau}{2}}\, \Psi^*_{-s_\sigma - s_\tau}(x). \tag{15}$$

For $V_0 < 0.50E_{\rm so}$, half of the normal side allowed wave numbers become purely imaginary, thus leading to an evanescent contribution to the boundary condition. As a consequence, there are only two modes (with the same k) and the resulting density has a single period of oscillation [see Fig. 13(b)]. In this case, the wave function represents an MZM since it fulfills Eq. (15). This example of extended MZM's demonstrates that their existence is not limited to bounded states.

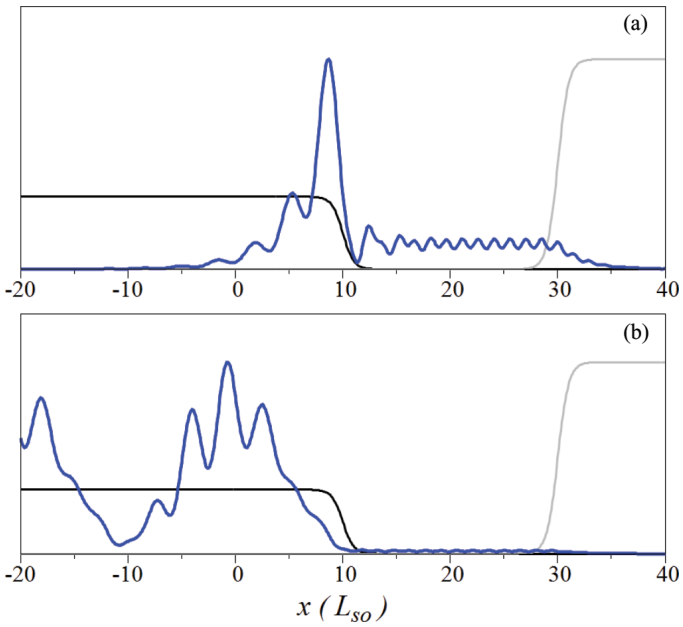

FIG. 12. (Color online) (a) Majorana bounded state found for $V_o = 0.69E_{\rm so}$, $\Delta_o = 0.25E_{\rm so}$, $\Delta_B = 0.4E_{\rm so}$, and $\mu = 0.1E_{\rm so}$. Potential and superconductor interfaces are located at $x_1 = 10L_{\rm so}$ and $x_2 = 30L_{\rm so}$, respectively, and their softness parameters are $s_1 = s_2 = 0.5L_{\rm so}$. (b) Zero-energy non-Majorana extended state. The figure is shown for the same parameters as in (a) but with $V_0 = 0.67E_{\rm so}$.

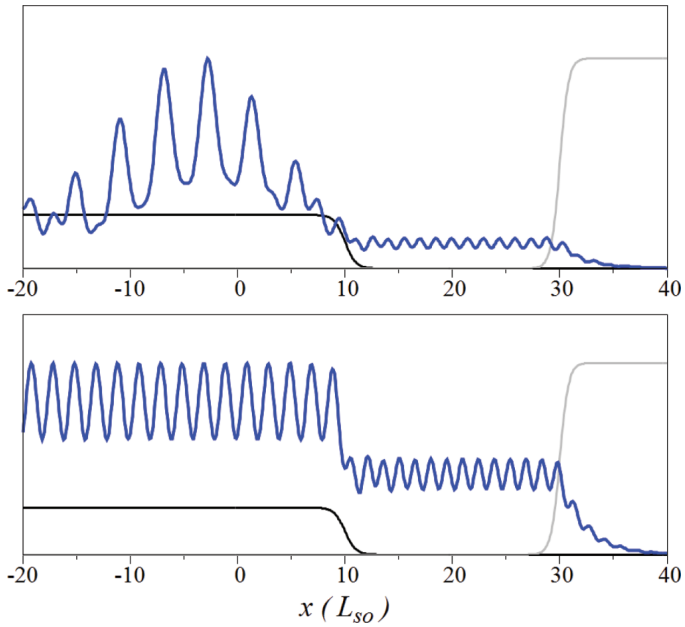

FIG. 13. (Color online) (a) Non-Majorana bounded state found for $V_0 = 0.51E_{\rm so}$, $\Delta_o = 0.25E_{\rm so}$, $\Delta_B = 0.4E_{\rm so}$, and $\mu = 0.1E_{\rm so}$. Excluding V_0 these are the same parameters as in Figs. 12(a) and 12(b). (b) Density for an MZM extended state. The figure is shown for the same parameters as in (a) but with $V_0 = 0.49E_{\rm so}$.

Physically, the distinction between extended and bounded MZM's is that the former require input fluxes from the asymptotic contacts to the junction, while the latter do not. This definition has no ambiguity when junction and contacts are properly defined. For these extended states the assumption of equal incident flux in electron and hole channels is crucial. If the input is prepared in a specific electron or hole state of a given spin, the MZM condition Eq. (15) is lost for low values of the bulk potential. Therefore extended MZM's are possible albeit for a particular superposition of input states only.

VI. CONCLUSIONS

A numerical method to calculate the wave function of MZM's in presence of a soft normal-superconductor junction has been developed. This method is able to detect whether a particular energy E is an eigenenergy or not of the junction and, when it is the case, obtain the corresponding wave function. The junction is described by smooth functions of position in a 1D nanowire with the Rashba spin-orbit interaction, the Zeeman magnetic field, and superconductivity. It has been applied to a semi-infinite abrupt nanowire junction in order to compare its results with those obtained analytically, as well as to infinite soft junctions in order to study the dependence to different parameters of the MZM density and its protection from energetically alike excited states.

We have proven the resilience of the MZM density to the softness parameters and studied the dependence of its

localization with the potential interface position. This latter feature hints the possibility of manipulating the position of the Majorana modes in order to perform topological quantum operations. We have found the remarkable result of an increase in the protection of the MZM for high values of the softness of the superconductor gap interface, while high values of the softness of the potential interface have an opposite effect. Finally, we have shown the existence of extended MZM's, albeit limited to feed the junction with a particular set of propagating input states. This result demonstrates that MZM's are not always restricted to bounded states.

The verification of our predictions would require experimental manipulation of the junction smoothness. Qualitatively, it has been suggested that this could be accomplished with gates for the electrical potential and with an insulating wedge for the induced superconductivity, modulating the distance to the nearby superconductor. Our model could also represent an intrinsic smoothness due to uncontrolled effects in the device fabrication. Extending the present analysis to multimode nanowires might reveal interesting effects from the combination of junction smoothness and mode-mode competition.[15,24]

ACKNOWLEDGMENTS

This work was funded by MINECO-Spain (Grant FIS2011-23526), CAIB-Spain (Conselleria d'Educació, Cultura i Universitats), and FEDER. Discussions with R. López are gratefully acknowledged.

*javier@ifisc.uib-csic.es

[1] E. Majorana, Nuovo Cimento **14**, 171 (1937).
[2] A. Y. Kitaev, Phys. Usp. **44**, 131 (2001).
[3] F. Wilceck, Nat. Phys. **5**, 614 (2009).
[4] J. Alicea, Rep. Prog. Phys. **75**, 076501 (2012).
[5] X. L. Qi and S. C. Zhang, Rev. Mod. Phys. **83**, 1057 (2011).
[6] M. Leijnse and K. Flensberg, Semicond. Sci. Technol. **27**, 124003 (2012).
[7] C. W. J. Beenakker, Annu. Rev. Condens. Matter Phys. **4**, 113 (2013).
[8] T. D. Stanescu and S. Tewari, J. Phys. Condens. Matter **25**, 233201 (2013).
[9] L. Fu and C. L. Kane, Phys. Rev. Lett. **100**, 096407 (2008).
[10] A. R. Akhmerov, J. Nilsson, and C. W. J. Beenakker, Phys. Rev. Lett. **102**, 216404 (2009).
[11] Y. Tanaka, T. Yokoyama, and N. Nagaosa, Phys. Rev. Lett. **103**, 107002 (2009).
[12] K. T. Law, P. A. Lee, and T. K. Ng, Phys. Rev. Lett. **103**, 237001 (2009).
[13] R. M. Lutchyn, J. D. Sau, and S. Das Sarma, Phys. Rev. Lett. **105**, 077001 (2010).
[14] Y. Oreg, G. Refael, and F. von Oppen, Phys. Rev. Lett. **105**, 177002 (2010).
[15] T. D. Stanescu, R. M. Lutchyn, and S. Das Sarma, Phys. Rev. B **84**, 144522 (2011).
[16] K. Flensberg, Phys. Rev. B **82**, 180516 (2010).
[17] A. C. Potter and P. A. Lee, Phys. Rev. Lett. **105**, 227003 (2010).
[18] A. C. Potter and P. A. Lee, Phys. Rev. B **83**, 094525 (2011).
[19] S. Gangadharaiah, B. Braunecker, P. Simon, and D. Loss, Phys. Rev. Lett. **107**, 036801 (2011).
[20] R. Egger, A. Zazunov, and A. L. Yeyati, Phys. Rev. Lett. **105**, 136403 (2010).
[21] A. Zazunov, A. L. Yeyati, and R. Egger, Phys. Rev. B **84**, 165440 (2011).
[22] J. Klinovaja, S. Gangadharaiah, and D. Loss, Phys. Rev. Lett. **108**, 196804 (2012).
[23] J. Klinovaja and D. Loss, Phys. Rev. B **86**, 085408 (2012).
[24] J. S. Lim, L. Serra, R. Lopez, and R. Aguado, Phys. Rev. B **86**, 121103 (2012).
[25] J. S. Lim, R. Lopez, and L. Serra, New J. Phys. **14**, 083020 (2012).
[26] J. S. Lim, R. Lopez, and L. Serra, Europhys. Lett. **103**, 37004 (2013).
[27] V. Mourik, K. Zuo, S. Frolov, S. Plissard, E. Bakkers, and L. Kouwenhoven, Science **336**, 1003 (2012).
[28] M. T. Deng, C. L. Yu, G. Y. Huan, M. Larsson, and P. Caroff, Nano Lett. **12**, 6414 (2012).
[29] L. P. Rokhinson, X. Liu, and J. K. Furdyna, Nat. Phys. **8**, 795 (2012).
[30] A. Das, Y. Ronen, Y. Most, Y. Oreg, M. Heiblum, and H. Shtrikman, Nat. Phys. **8**, 887 (2012).
[31] A. D. K. Finck, D. J. Van Harlingen, P. K. Mohseni, K. Jung, and X. Li, Phys. Rev. Lett. **110**, 126406 (2013).
[32] J. K. Pachos, *Introduction to Topological Quantum Computation* (Cambridge University Press, Cambridge, UK, 2012).
[33] C. Nayak, S. H. Simon, A. Stern, M. Freedman, and S. Das Sarma, Rev. Mod. Phys. **80**, 1083 (2008).
[34] E. Prada, P. San-Jose, and R. Aguado, Phys. Rev. B **86**, 180503(R) (2012).
[35] G. Kells, D. Meidan, and P. W. Brouwer, Phys. Rev. B **86**, 100503(R) (2012).
[36] D. Rainis, L. Trifunovic, J. Klinovaja, and D. Loss, Phys. Rev. B **87**, 024515 (2013).
[37] D. Roy, N. Bondyopadhaya, and S. Tewari, Phys. Rev. B **88**, 020502(R) (2013).
[38] L. Serra, Phys. Rev. B **87**, 075440 (2013).
[39] HSL (2013). A collection of FORTRAN codes for large scale scientific computation. http://www.hsl.rl.ac.uk.
[40] T. D. Stanescu and S. Tewari, Phys. Rev. B **87**, 140504 (2013).

2.5 Additional bibliography

[41] Alexander Altland and Martin R. Zirnbauer, Phys. Rev. **B** 55, 1142 (1997)

Chapter 3

Effects of tilting the magnetic field in 1d Majorana nanowires

Javier Osca, Daniel Ruiz and Llorenç Serra
Phys. Rev. B **89**, 245405. Published 5 June 2014

3.1 Objectives

As discussed in Chap. 1, to find Majorana modes in a 1d nanowire we need the simultaneous action of s-wave superconductivity, Rashba spin orbit interaction and an external magnetic field. In the literature it is usual to consider the external magnetic field pointing either along the longitudinal direction of the nanowire or in a perpendicular direction to the nanowire and to the effective spin orbit magnetic field. No spin precession can be achieved if both magnetic fields (the external and the spin orbit effective one) point in the same direction because in that case there is a privileged direction of spin quantization. However, it remained unanswered what is the critical tilting angle separating a Majorana from a non Majorana phase of a nanowire.

The article of this chapter is divided into two parts, with two different objectives. In the first part the objective is to study the effect of the magnetic field tilting on the spectrum and the Majorana phase of a straight 1d nanowire. In other words, we search for the critical angle mentioned above and we give an analytical expression for it. On the other hand, the second part of the article is focused on L-shaped nanowires inside an homogeneous magnetic field. They are modeled as straight nanowires inside an inhomogeneous magnetic field. Here, we focus on the question of what happens if half of a nanowire fulfills all the Majorana conditions and the other half does not. At this point it is important to remark that a wavefunction can not be separated in Majorana and non Majorana regions. The property of being a Majorana is a topological feature and therefore it is a global property fulfilled for the Majorana wavefunction globally, at every point of space.

3.2 Methodology

In the first part of the paper we use the complex band structure of the quantum wire to determine the Majorana phase diagram in a parameter space. This parameter space includes the magnetic field strength Δ_B, its tilting (θ, ϕ) (see Fig. 1 of the article) with respect to the nanowire longitudinal direction and the superconductor gap Δ_s. A mathematical relationship is established between the complex band structure of an infinite nanowire with the Majorana physics that arises if we introduce an edge on the same nanowire. In other words, to have a Majorana in a semi-infinite nanowire the equivalent infinite homogeneous nanowire (with the edges removed) must not have any real wavenumber. Furthermore the equation $\Psi(x_e) = 0$, where x_e is the edge position, must have a nontrivial solution. The main point here is that this equation may be expressed as a linear combination of the homogeneous nanowire solutions. These conditions are an explicit mathematical formulation of the more general bulk-to-edge correspondence principle, ensuring that edge states will appear in the limits of any physical system if the bulk is in a topological phase.

To check phase boundary predictions and with the objective of study L-shaped nanowires we also make use of a direct numerical diagonalization method. First, we discretize the nanowire into a grid. The Hamiltonian is then defined for each site and each component of spin and isospin. This results in a large and sparse Hamiltonian matrix to be diagonalized. This is done using again a Harwell library module, like in Chap. 2. In this case it calculates n real eigenvalues of the equation $A\vec{\Psi} = E\vec{\Psi}$, where $\vec{\Psi}$ is a vector of unknowns, E is now the eigenvalue to be determined and A is a large real and symmetric matrix. The method yields the n real eigenvalues closer to a given reference value, in our case zero. We use a real diagonalization procedure to obtain the eigenvalues of a complex set of equations, the eigensolutions are separated in real and imaginary parts and the number of Hamiltonian equations for each of the lattice sites are doubled. This results in a larger but solvable matrix A.

3.3 Conclusions and remarks

In this chapter we have determined that in straight nanowires the Majorana phase is restricted by two independent rules and we can relate them with properties of the bulk nanowire. Only one of these rules was already known while the other one has been reported for the first time. First, to be in a Majorana phase the magnetic field must overcome a critical value,

$$\Delta_B > \sqrt{\Delta_s^2 + \mu^2}\,, \tag{3.1}$$

where Δ_B is the magnetic field magnitude, Δ_s the superconductor gap and μ the chemical potential. Although this expression was already known in itself we would like to claim here a generalization and, therefore, a certain degree of novelty. In previous works the magnetic field was not considered in arbitrary directions. That is, to have a Majorana the magnetic field was studied in the longitudinal direction ($\hat{x}$ direction for us) or in a direction perpendicular to the the nanowire and to the

spin orbit coupling effective magnetic field ($\hat{z}$ direction for us). In this context, Eq. (3.1) was assumed equivalent to $\Delta_{Bx,Bz} > \sqrt{\Delta_s^2 + \mu^2}$ where only one component of the magnetic field is present (either $\hat{x}$ or $\hat{z}$). In our opinion, it was not clear which component or components of the magnetic field were going to be involved in the calculation of the critical magnetic field for an arbitrary orientation of the same field. In Eq. (3.1) it is clarified that the relevant magnitude is the modulus of the magnetic field, the orientation of the magnetic field being irrelevant for this rule in particular.

In order to know how the magnetic field orientation affects the Majorana phase it is necessary to take into consideration a second rule that we named the projection rule. In this work we demonstrate that the external magnetic field component in the direction of the spin orbit effective field ($\Delta_{By} = \Delta_B \sin\theta \, \sin\phi$) can not exceed the value of the superconductor gap,

$$|\Delta_B \sin\theta \, \sin\phi| < \Delta_s \, . \tag{3.2}$$

Note that we assume without loss of generality that the effective spin orbit magnetic field points in $\hat{y}$ direction. The absolute value in this expression generalizes the paper projection rule inequality where ϕ was assumed not to exceed 180°.

In the second part of the paper we deal with L-shaped nanowires, modeled as inhomogeneous magnetic fields. Although strictly speaking some additional terms should be added to the Hamiltonian, they are negligible at the mesoscopic scale. Here, we have determined that the Majorana can be delocalized if half of the nanowire fulfills all the Majorana conditions while the other half does not fulfill them. However, the resulting wavefunction continues to be the one of a Majorana state. Finally, we also study how the relative position of the magnetic orientation interface with respect to the nanowire edges affects the localization of the Majorana state.

3.4 Published paper

PHYSICAL REVIEW B **89**, 245405 (2014)

Effects of tilting the magnetic field in one-dimensional Majorana nanowires

Javier Osca,[1,*] Daniel Ruiz,[1] and Llorenç Serra[1,2]

[1]*Institut de Física Interdisciplinària i de Sistemes Complexos IFISC (CSIC-UIB), E-07122 Palma de Mallorca, Spain*

[2]*Departament de Física, Universitat de les Illes Balears, E-07122 Palma de Mallorca, Spain*

(Received 14 March 2014; revised manuscript received 23 May 2014; published 5 June 2014)

We investigate the effects that a tilting of the magnetic field from the parallel direction has on the states of a one-dimensional Majorana nanowire. Particularly, we focus on the conditions for the existence of Majorana zero modes, uncovering an analytical relation (the projection rule) between the field orientation relative to the wire, its magnitude, and the superconducting parameter of the material. The study is then extended to junctions of nanowires, treated as magnetically inhomogeneous straight nanowires composed of two homogeneous arms. It is shown that their spectrum can be explained in terms of the spectra of two independent arms. Finally, we investigate how the localization of the Majorana mode is transferred from the magnetic interface at the corner of the junction to the end of the nanowire when increasing the arm length.

DOI: 10.1103/PhysRevB.89.245405 PACS number(s): 73.63.Nm, 74.45.+c

I. INTRODUCTION

In 2003, Kitaev pointed out the usefulness of topological states for quantum computing operations [1]. Essentially, topological states are quantum states with a hidden internal symmetry [2]. They are usually localized close to the system edges or interfaces and their nonlocal nature gives them a certain degree of immunity against local sources of noise. A subset of this kind of states called Majorana edge states is attracting much interest in condensed matter physics [3–13]. Majorana states are effectively chargeless zero-energy states that behave as localized non-Abelian anyons. It is theorized that nontrivial phases arise from their mutual interchange, caused by their nonlocal properties [14,15]. Furthermore, these states have the property of being their own antistates, giving rise to statistical behavior that is neither fermionic nor bosonic. Instead, the creation of two Majorana quasiparticle excitations in the same state returns the system to its equilibrium state. This kind of quasiparticle inherits its name from Majorana who theorized the existence of fundamental particles with similar statistical properties [16].

Majorana states have been theoretically predicted in many different systems, and some of them have been realized experimentally. In particular, evidences of their formation at the ends of semiconductor quantum wires inside a magnetic field with strong spin-orbit interaction and in close proximity to a superconductor have been seen in Refs. [17–21]. Superconductivity breaks the charge symmetry creating quasiparticle states without a defined charge that are a mixture of electron and hole excitations. On the other hand, the spin-orbit Rashba effect is caused by an electric field perpendicular to the propagation direction that breaks the inversion symmetry of the system while the external magnetic field breaks the spin-rotation symmetry of the nanowire. The combined action of both effects makes the resulting state effectively spinless and, including superconductivity, also effectively chargeless and energyless [22–41].

This work addresses the physics of one-dimensional (1D) nanowires with varying relative orientations between the external magnetic field and the nanowire (see Fig. 1). This physics is of relevance, e.g., for the exchange of Majoranas on networks of 1D wires, where it has been suggested that Majoranas can be braided by manipulating the wire shapes and orientations [42–44]. The Hamiltonian of the system is expressed in the continuum and the analysis is performed using two complementary approaches: the complex band structure of the homogeneous wire and the numerical diagonalization for finite systems. The complex band structure allows a precise characterization of the parameter regions of the semi-infinite wire where Majoranas, if present, are not distorted by finite-size effects. On the contrary, numerical diagonalizations of finite systems, even though reflecting the same underlying physics, yield smoothened transitions between different physical regions of parameter space.

For the semi-infinite system, we uncover an analytical law limiting the existence of Majorana modes below critical values of the angles between the magnetic field and the nanowire. This law, referred to in this paper as the projection rule, is shown to be approximately valid in finite systems too. We find a correspondence of the finite-system spectrum with its infinite wire counterpart, explaining this way its distinctive features and regimes in simplest terms. Our work is related to Ref. [31], which proved the influence of a transverse component of the field to be consistent with the experimental observations of Ref. [17].

The results for the homogeneous nanowire are subsequently used to explain the spectrum of a junction of two nanowires with arbitrary angle. The junction is modeled as a nonhomogeneous straight nanowire with two regions characterized by different magnetic field orientations [see Fig. 1(b)]. While the magnetic field remains parallel to the nanowire in one arm, we study the spectrum variation when changing the magnetic field angles in the other. Similarities between the homogeneous and inhomogeneous nanowire spectra allow us to explain many of the features of the latter in terms of those of the former. Finally, we investigate the dependence with the distance of the magnetic interface (the corner of the junction) to the end of the nanowire, finding a transfer phenomenon where the Majoranas change localization from the interface for a short arm to the nanowire end as the arm length is increased.

*javier@ifisc.uib-csic.es

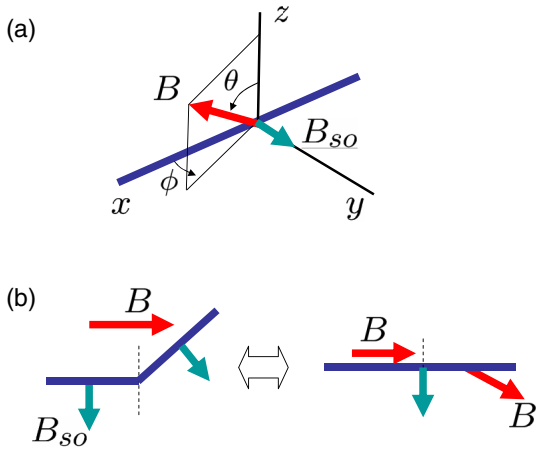

FIG. 1. (Color online) Sketches of the physical systems considered in this work. (a) Straight nanowire on the x axis in a homogeneous magnetic field characterized by spherical angles θ and ϕ. (b) Junction of two nanowires in a uniform magnetic field (left) represented as a straight nanowire with a magnetic inhomogeneity (right).

This work is organized as follows. In Sec. II, the physical model is introduced and Sec. III presents the above-mentioned projection rule. In Sec. IV, we discuss the spectrum of excited states of a homogeneous nanowire, while in Sec. V we address an inhomogeneous system representing a nanowire junction. We study changes in the spectrum due to the tilting (Sec. V A) and stretching (Sec. V B) of one of the junction arms. Finally, the conclusions of the work can be found in Sec. VI.

II. PHYSICAL MODEL

We assume a one-dimensional model of a semiconductor nanowire as a low-energy representation of a higher-dimensional wire with lateral extension, when only the first transverse mode is active. The system is described by a Hamiltonian of the Bogoliubov–de Gennes kind

$$\begin{aligned}\mathcal{H}_{\mathrm{BdG}} = &\left(\frac{p_x^2}{2m} + V(x) - \mu\right)\tau_z \\ &+ \Delta_B\,(\sin\theta\cos\phi\,\sigma_x + \sin\theta\sin\phi\,\sigma_y + \cos\theta\,\sigma_z) \\ &+ \Delta_s\,\tau_x + \frac{\alpha}{h}\,p_x\sigma_y\tau_z, \end{aligned} \tag{1}$$

where the different terms are, in left to right order, kinetic, electric, and chemical potential, Zeeman, superconducting, and Rashba spin-orbit terms. The Pauli operators for spin are represented by $\sigma_{x,y,z}$ while those for isospin are given by $\tau_{x,y,z}$. Superconductivity is modeled as an s-wave superconductive term that couples different states of charge.

The superconductor term in Eq. (1) is an effective mean field approximation to a more complicated phonon-assisted attractive interaction between electrons. This interaction leads to the formation of Cooper pairs with breakup energy Δ_s. Experimentally, superconductivity can be achieved by close proximity between the semiconductor nanowire and a metal superconductor. The semiconductor wire becomes superconducting when its width is smaller than the coherence length of the Cooper pairs. On the other hand, the Rashba spin-orbit term arises from the self-interaction between an electron (or hole) spin with its own motion. This self-interaction is due to the presence of a transverse electric field that is perceived as an effective magnetic field in the rest frame of the quasiparticle. This electric field can be induced externally but, usually, is a by-product of an internal asymmetry of the nanostructure. In the Hamiltonian (1), we have taken $\hat{x}$ as the orientation of the 1D nanowire while an effective spin-orbit magnetic field $\vec{B}_{\mathrm{so}}$ pointing along $\hat{y}$ may be defined due to the coupling of the Rashba term with the y component of the spin.

We consider the nanowire in an external magnetic field, giving spin splittings through the Zeeman term in Eq. (1). In this paper, we assume the magnetic field in arbitrary direction, including the possibility of being inhomogeneous in space for some setups. The direction of the magnetic field is parametrized by the spherical polar and azimuthal angles θ and ϕ. These two angles are constant for a homogeneous wire [Fig. 1(a)] and they change smoothly from one to the other arm in a nanowire junction [Fig. 1(b)].

Summarizing, superconductor, Rashba spin-orbit, and Zeeman effects are parametrized in Eq. (1) by Δ_s, α, and Δ_B, respectively. These parameters are taken constant because the nanowire is considered to be made of a homogeneous material. The only inhomogeneity allowed in certain cases is a change in the magnetic field direction at a single magnetic interface between two homogeneous regions.

Along this work the Hamiltonian of Eq. (1) is solved for homogeneous parameters in the infinite, semi-infinite, and finite wires, as well as for the inhomogeneous finite case, using different approaches. When a direct diagonalization of the Hamiltonian for a finite system is performed, soft potential edges and magnetic interface are used. The shape of the potential edges is modeled as Fermi-type functions centered on those edges. High potential is imposed outside the nanowire while low potential (usually zero) is assumed inside. When a magnetic interface is present, a smooth variation in the field angles is modeled in the same way. Specifically, those smooth functions read as

$$V(x) = V_0[1 + \mathcal{F}(x;x_L,s_v) - \mathcal{F}(x;x_R,s_v)], \tag{2}$$

$$\theta(x) = \theta_L + (\theta_R - \theta_L)[1 - \mathcal{F}(x;x_m,s_m)], \tag{3}$$

$$\phi(x) = \phi_L + (\phi_R - \phi_L)[1 - \mathcal{F}(x;x_m,s_m)] \tag{4}$$

for the potential and the field polar and azimuthal angles, respectively. The Fermi function $\mathcal{F}$ is defined as

$$\mathcal{F}(x;x_0,s) = \frac{1}{1 + e^{(x-x_0)/s}}. \tag{5}$$

In Eq. (2) V_0 is the value of the potential outside the nanowire, while $\theta_{L/R}$ and $\phi_{L/R}$ are the field angles at left and right of the magnetic interface. The potential left and right edges are centered on x_L and x_R and the magnetic interface is centered on x_m. Their softness is controlled by the parameters s_v and s_m, where zero softness means a steep interface and a high value implies a smooth one.

The numerical results of this work are presented in special units obtained by taking $\hbar$, m, and the Rashba spin-orbit

interaction α as reference values. That is, our length and energy units are

$$L_{\rm so} = \frac{\hbar^2}{\alpha m}, \tag{6}$$

$$E_{\rm so} = \frac{\alpha^2 m}{\hbar^2}. \tag{7}$$

III. A PROJECTION RULE

Let us consider a nanowire in a uniform magnetic field with $\theta = 90^\circ$ and an arbitrary ϕ [see Fig. 1(a)]. A direct diagonalization of Eq. (1) for a finite length of the wire and $\phi = 15^\circ$ yields the spectrum depicted in Fig. 2 as a function of the magnetic field intensity. A main feature of this figure is the existence of a Majorana mode, lying very near zero energy, but only for a particular range of values of the magnetic field. For the parameters of the figure, the Majorana mode is created around $\Delta_B = 0.3E_{\rm so}$ and destroyed in a rather abrupt way around $\Delta_B = E_{\rm so}$.

It is well known that Majorana wave functions decay to zero towards the nanowire interior. We can therefore analyze the creation and destruction of Majoranas in the semi-infinite system and use those results to understand the physics of Majoranas in a finite system. In this approach, we eliminate from the analysis the finite-size effects caused by the overlapping of the Majorana wave functions at both ends of a finite nanowire. Although it is obvious that for long enough wires the size effect becomes negligible, disentangling finite-size behavior from intrinsic Majorana physics using calculations of only finite systems is much less obvious.

Majorana mode creation has been understood as a phase transition of the lowest-excited state, signaled by the closing and reopening of a gap in the infinite nanowire band spectrum [23], as shown in Figs. 3(a) and 3(b). The phase transition follows in this case a well-known law, requiring high-enough fields for Majoranas to exist:

$$\Delta_B \geqslant \sqrt{\Delta_s^2 + \mu^2}. \tag{8}$$

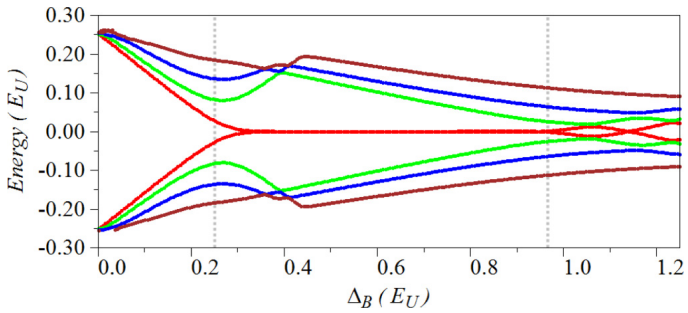

FIG. 2. (Color online) Spectrum of a finite-length nanowire with $L = 50L_{\rm so}$ as a function of the external magnetic field magnitude Δ_B. Other nanowire parameters are $\Delta_s = 0.25E_{\rm so}$ and $\mu = 0$. The magnetic field angles are $\theta = 90^\circ$ and $\phi = 15^\circ$. Only the eight states lying closer to zero energy are displayed. Note that a zero-energy Majorana mode is created at around $\Delta_B = 0.3E_{\rm so}$ and destroyed for values of Δ_B near one unit. The vertical lines (dots) indicate the onset and destruction of the Majorana mode as predicted by Eqs. (8) and (13), respectively.

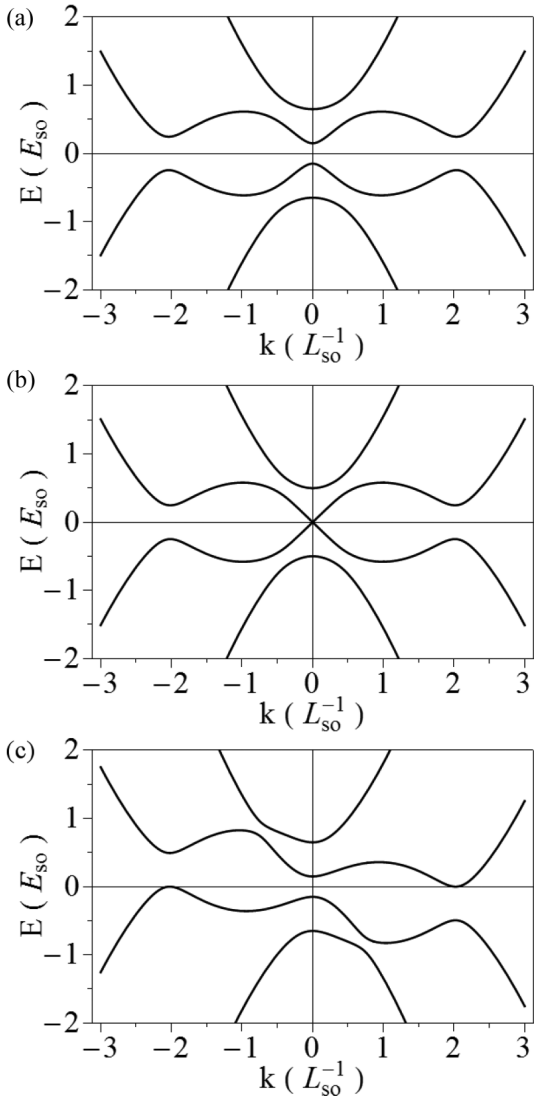

FIG. 3. Band structure of the infinite homogeneous nanowire with $\Delta_s = 0.25E_{\rm so}$ and $\mu = 0$ for (a) parallel field $(\theta,\phi) = (90^\circ,0^\circ)$ with $\Delta_B = 0.4E_{\rm so}$, (b) the same as (a) but on the phase transition point $\Delta_B = 0.25E_{\rm so}$, (c) tilted field $(\theta,\phi) = (90^\circ,38.68^\circ)$ with $\Delta_B = 0.4E_{\rm so}$.

Notice that, as mentioned, for the equality in Eq. (8) a gap closes for $k = 0$ in Fig. 3(b). It is also worth stressing that Eq. (8) depends on the full Zeeman energy Δ_B and not just the partial contribution due to the parallel field $\Delta_B \sin\theta\cos\phi$, as one might naively assume.

In Ref. [38], Eq. (8) was derived, in an alternative way, from the analysis of the complex-k solutions compatible with the boundary condition of a semi-infinite nanowire in a parallel field. This approach relies on the property that the complex band structure (allowing an imaginary part in k) of the homogeneous wire contains all the information about all possible eigenstates of any piecewise homogeneous wire. In general, an eigenstate of the infinite homogeneous wire with a given arbitrary k can be expressed as

$$\Psi^{(k)}(x,\eta_\sigma,\eta_\tau) = \sum_{s_\sigma,s_\tau} \Psi^{(k)}_{s_\sigma s_\tau}\, e^{ikx}\, \chi_{s_\sigma}(\eta_\sigma)\chi_{s_\tau}(\eta_\tau), \tag{9}$$

where $\Psi^{(k)}_{s_\sigma s_\tau}$ are state amplitudes and the quantum numbers are $s_\sigma = \pm$ and $s_\tau = \pm$. In Eq. (9), $\eta = \uparrow, \downarrow$ indicate bivalued variables for spin (η_σ) and isospin (η_τ). The corresponding spinors are denoted by $\chi(\eta)$ [38]. It is worth stressing here that analytical treatments in the limits of very weak and very strong Rashba couplings were discussed in Refs. [34,45]. We follow a general approach, at the price of being numerical.

The sharp semi-infinite wire with $x > 0$ is obviously piecewise homogeneous, implying that the Majorana solution allowed by the existence of an edge at $x = 0$ must be a linear superposition of the homogeneous nanowire eigenstates of complex wave number with $\mathrm{Im}(k) > 0$, otherwise, it could not be a localized state. The resulting restriction is

$$\sum_{k,\,\mathrm{Im}(k)>0} C_k \Psi^{(k)}_{s_\sigma s_\tau} = 0, \tag{10}$$

where the C_k's are complex numbers characterizing the superposition of state amplitudes. The allowed wave numbers are calculated solving the determinant

$$\det\{H_{s_\sigma s_\tau, s'_\sigma s'_\tau}(k) - E\,\mathbb{1}\} = 0, \tag{11}$$

for $E = 0$. In fact, the allowed k's can be calculated for any energy, but we are interested in particular in those at zero energy corresponding to Majorana solutions.

The wave-number dependence on magnetic field is depicted in Fig. 4(a) for a selected case. For a fixed energy E, there are always eight possible wave numbers, but only those with $\mathrm{Im}(k) > 0$ are displayed in Fig. 4(a). In this representation, the closing of the $k = 0$ gap in Fig. 3(b) corresponds to a node of

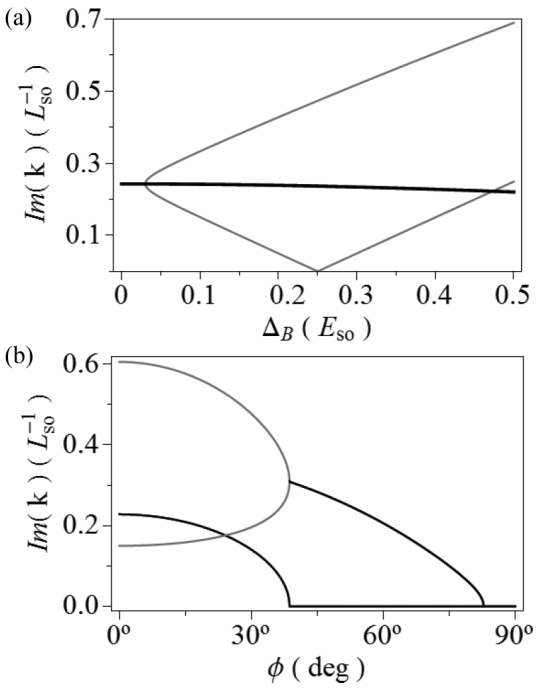

FIG. 4. Imaginary parts of the wave numbers (only positive ones) in an infinite homogeneous nanowire with $\Delta_s = 0.25E_{so}$ and $\mu = 0$ as function of (a) the value of the longitudinally oriented magnetic field, (b) the azimuthal angle ϕ of a magnetic field with $\Delta_B = 0.4E_{so}$ and polar angle $\theta = 90^\circ$. Gray color is used for nondegenerate modes while black is indicating degeneracy with two or more modes actually having the same $\mathrm{Im}(k)$.

$\mathrm{Im}(k)$ in Fig. 4(a). In order to be able to hold a Majorana, a semi-infinite nanowire has to fulfill two simultaneous requirements. First, the nanowire must have four complex wave numbers with $\mathrm{Im}(k) > 0$ allowed at zero energy; and second, a solution different from zero (nontrivial) must be possible for the C_k's in Eq. (10). That is, interpreting the state amplitudes $\Psi^{(k)}_{s_\sigma s_\tau}$ as a 4×4 matrix where the four k's correspond for instance to rows and the four spin-isospin values $\{++, +-, -+, --\}$ to columns, the condition for a nontrivial solution is

$$\det\left\{\Psi^{(k)}_{s_\sigma s_\tau}\right\} = 0. \tag{12}$$

In a parallel field, this condition is fulfilled only above a critical value of the magnetic field $\Delta_B^{(c)} = \sqrt{\Delta^2 + \mu^2}$, but not under this quantity, thus leading to Eq. (8). Further details on the methodology can be found in Ref. [38]. Here, we want to use this approach to determine whether a similar condition on the field orientation, with critical values of the angles, exists or not.

Figure 4(b) shows the evolution of the wave numbers when increasing ϕ while maintaining $\theta = 90^\circ$, i.e., maintaining the magnetic field in the plane formed by the nanowire direction and the effective spin-orbit magnetic field direction $\vec{B}_{so}$. This means that for $\phi = 0^\circ$, the magnetic field is aligned with the nanowire, while for $\phi = 90^\circ$ it is completely perpendicular to it and parallel to $\vec{B}_{so}$. In Fig. 4(b), care has been taken to choose a value of Δ_B that fulfills the Majorana condition for the parallel $\phi = 0$ orientation Eq. (8). We can see that for $\phi = 40.1^\circ$ two of the complex wave numbers become real, thus destroying the Majorana mode for azimuthal angles above this value.

The physical behavior implied by Fig. 4(b) is a sudden loss of the Majorana mode as the tilting angle ϕ exceeds a critical value, due to the system no longer having the required four evanescent modes with $\mathrm{Im}(k) > 0$. The evanescent modes are lost because of the closing of the gap between states of opposite wave numbers [$k \approx \pm 2L_{so}^{-1}$ for the particular case shown in Fig. 3(c)]. We characterize next the dependence of the critical angle on Δ_B and Δ_s. In Fig. 5(a), we can see a contour plot of $\mathrm{Im}(k)$ as a function of ϕ and the ratio Δ_s/Δ_B for an external branch wave number [34], corresponding to the lower black line of Fig. 4(b). The values where $\mathrm{Im}(k)$ vanish separate the plot into two regions: the lower one where the Majorana is allowed and the upper (white) where no Majorana can exist. Although Eq. (11) can be solved analytically, the angles where $\mathrm{Im}\left[k(\phi, \Delta_s/\Delta_B)\right]$ vanishes can be obtained only numerically because ϕ appears as argument of sine and cosine functions and no isolation is possible. As a consequence, the values of ϕ where the wave number first reaches zero have been found numerically and are plotted in Fig. 5(c) against the test function $\arcsin(\Delta_s/\Delta_B)$. The perfect coincidence between the two results within computer precision demonstrates that a Majorana can not exist for angles such that $\sin\phi > \Delta_s/\Delta_B$, provided $\theta = 90^\circ$.

Figure 5(b) shows a contour plot of $\mathrm{Im}(k)$ for an internal branch wave number [34], corresponding to the upper mode in Fig. 4(b). In this plot, the ϕ roots of $\mathrm{Im}(k)$ lie inside an upper and lower bounded region around $0.95E_{so} < \Delta_B < E_{so}$. In fact, two of the wave numbers become real in the white region of the contour plot. Note that this region lies

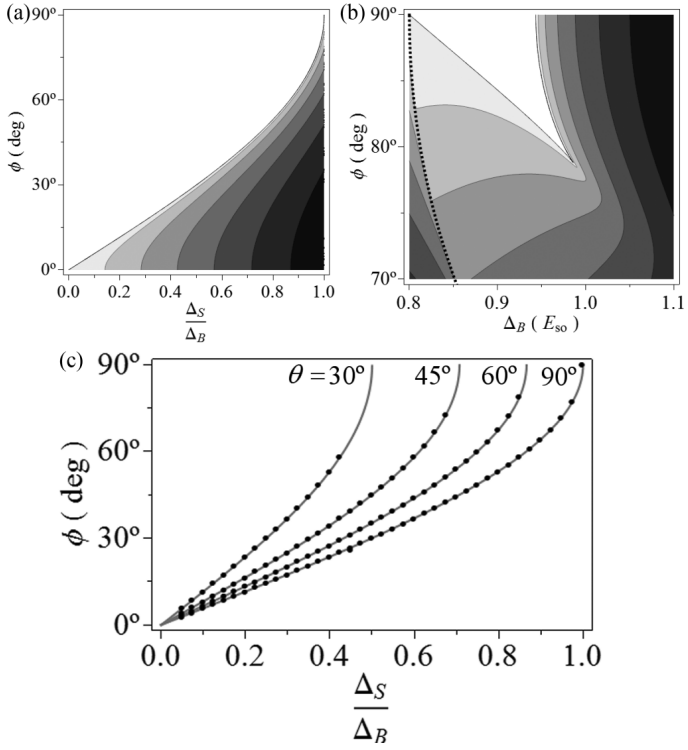

FIG. 5. (a) Contour plot of Im(k) for the external branch of the nanowire propagating bands. The horizontal axis contains the ratio Δ_s/Δ_B and the vertical one the azimuthal angle ϕ. The polar angle is fixed to $\theta = 90°$ and $\mu = 0$. (b) Contour plot of Im(k) for the internal branch of the nanowire propagating bands. The horizontal axis shows Δ_B and the vertical one the azimuthal angle ϕ. The polar angle is fixed to $\theta = 90°$, $\Delta_s = 0.8E_{so}$, and $\mu = 0$. (c) Plot of the azimuthal critical angle where Im(k) vanishes in the upper left panel as function of Δ_s/Δ_B (points) checked against the projection-rule prediction (13). Aside from the $\theta = 90°$ case of the upper left panel, the figure also contains the comparison for other values of θ. The value of the chemical potential can be taken arbitrarily since it is irrelevant for this comparison.

in the non-Majorana sector, above the transition discussed in Fig. 5(a) which is now signaled by the dotted line. Theoretically, the existence of this region determines two different fermionic regimes: one where a fermion mode at zero energy is constructed of plane waves with two complex and two real wave numbers and another one made of a full set of real wave numbers. Since we assume bound states in order to extrapolate the results to finite systems, these cases have no relevance to us. Nevertheless, the underlying causes for the existence of this region will be relevant in the study of the excited states of the finite nanowire. This will be further developed in Sec. IV.

Repeating the analysis for different polar angles θ, as shown in Fig. 5(c), we conclude that the angular restriction for the existence of Majoranas is

$$\Delta_B \sin\theta \sin\phi < \Delta_s. \tag{13}$$

In other words, the projection of the magnetic field energy parameter into the spin-orbit effective magnetic field $\vec{B}_{so}$ needs to be smaller than the superconductor gap energy in order to have Majoranas in a semi-infinite wire. We refer to this condition as the projection rule. Notice that Eq. (13) is not a generalization of Eq. (8), but an additional law. Both Eqs. (8) and (13) have to be simultaneously met for the existence of a Majorana mode in a semi-infinite wire. Finding this projection rule using a complex band-structure approach is the main result of this work.

In general, the projection rule (13) yields an extra bound to be considered when identifying regions of Majoranas in parameter space. For instance, assuming fixed angles (θ,ϕ) and varying Δ_B, there is a lower bound on Δ_B from Eq. (8) and an upper bound from the projection rule. Analogously, if for a fixed Δ_B the Majorana is allowed by Eq. (8) at $\phi = 0°$ and and we increase ϕ, the projection rule yields an upper bound on ϕ. Therefore, as explained, both equations must be met simultaneously to obtain a Majorana mode. Furthermore, after some parameter testing we have determined that the projection rule is not affected by the value of the chemical potential μ. This means that the overall dependence on μ for the existence of Majorana modes in the semi-infinite nanowire is completely covered by Eq. (8).

The disappearance of the Majorana when increasing ϕ is not a phase transition in the sense that no imaginary part of a mode wave number crosses zero in-between two regions with non-null values. As shown in Fig. 4(b) for the polar angle $\theta = 90°$, above the critical ϕ the value of Im(k) remains stuck at zero value. The main difference between the phase transition law in Eq. (8) and the projection rule (13) lies in the different type of gap closing for both cases. As shown in Fig. 3(b), the phase transition delimited by Eq. (8) is caused by a gap closing and reopening on a single wave number $k = 0$ (labeled as interior branches of the spectrum). In the language of semiconductor band-structure physics, we may call this the closing of a direct gap. Oppositely, the projection rule is caused by the closing of an indirect gap for $k \approx \pm k_f$ (labeled as exterior branches of the spectrum), as shown in Fig. 3(c) for a selected case. This indirect gap remains closed if ϕ is further increased beyond a critical value [Fig. 4(b)], a sign of the metallic character of the new phase.

We have checked these laws against the direct numerical diagonalization for a finite nanowire, finding a reasonable agreement as shown in Figs. 2 and 6. In Fig. 2, the magnetic field orientation is kept fixed to a tilted orientation while the field magnitude is changed and in Fig. 6 the magnitude is fixed while the orientation is changed. The main difference between the precise laws for the semi-infinite model and the finite-system results is in the smoothness of the spectrum evolution around the transition points. While in the semi-infinite model the transition between fermionic modes to Majorana modes and vice versa happens at a single point in the parameter space, in the finite system we can see these transitions smoothed. This occurs due to the finite-size effects, i.e., the little overlap of Majoranas on opposite ends of the nanowire. Furthermore, while Majoranas lie at exactly zero energy in the semi-infinite model, this small interaction makes the finite system Majoranas to have a finite small energy ϵ.

A close inspection of the projection rule (13) reveals that there exist critical values for θ and ϕ such that if they are not surpassed, a Majorana is always allowed, independently of the value of the other angle [provided Eq. (8) is fulfilled], that is, below the critical angle a projection into $\vec{B}_{so}$ is never high

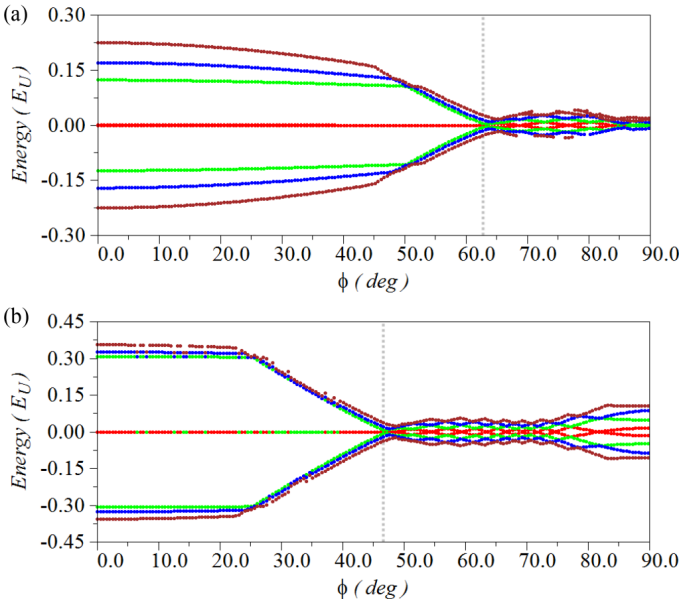

FIG. 6. (Color online) (a) Spectrum of a nanowire of length $L = 50L_{so}$ with $\Delta_s = 0.8E_{so}$ and $\mu = 0$ as a function of ϕ with a fixed $\theta = 90^\circ$ and $\Delta_B = 0.9E_{so}$. Note the spectrum change at the angle predicted by the projection rule (dotted line) as well as the spectrum collapse for values of ϕ close to 90°. For values of ϕ above 90°, the spectrum is given by the mirror image of the shown values. (b) The same as (a) but for a fixed magnetic field value $\Delta_B = 1.1E_{so}$. Note that for values of ϕ close to 90°, now the two modes closer to zero are fermionic modes separated from each other by an energy gap.

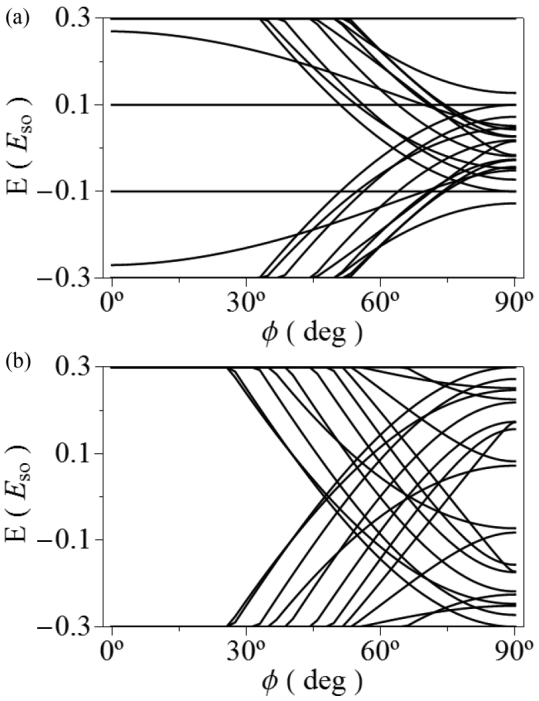

FIG. 7. Spectrum obtained from the homogeneous nanowire band energies at selected wave numbers, displayed as tracers as a function of ϕ. Panel (a) corresponds to the same parameters of Fig. 6(a). Note that qualitatively similar regions occur for increasing angles in both figures. In particular, the spectrum nearly collapses for values of ϕ close to 90°. Panel (b) shows the same as (a) but for the parameters of Fig. 6(b). Note that for values of ϕ close to 90°, the two lower states (closer to zero energy) are fermionic modes separated by a gap as in Fig. 6(b).

enough to break the Majorana. In practice, if the Majorana is allowed by Eq. (8), it will survive for any ϕ provided $\theta < \theta_c$ or, alternatively, for any θ provided $\phi < \phi_c$. These critical angles are

$$\theta_c = \phi_c = \arcsin\left(\frac{\Delta_s}{\Delta_B}\right). \tag{14}$$

Tilting the magnetic field has been investigated in the experiment of Ref. [17], where the variation of differential conductance when rotating the magnetic field in the xz and yz planes (with the definitions of Fig. 1) has been followed in detail. A transition angle from presence to absence of zero bias anomaly is observed for yz rotation, while no transition is found for xz rotation. This is fully consistent with the projection rule [31], but the observed transition angle for yz rotation seems to be smaller by a factor ≈2 with respect to the theoretical prediction (14). We think this may be due to differences between our closed nanowire and the necessarily open experimental one, as well as to temperature effects [31]. In any case, an experimental confirmation of the critical angles in the sense of Eq. (14) would lend additional support to the Majorana scenario.

IV. EXCITED STATES

While in the preceding section we focused on the physics of the Majoranas at zero energy, comparing semi-infinite and finite nanowires, in this section we address the spectrum of excited states. The main effect of the boundary conditions is to allow only a discrete set of wave numbers instead of a continuous one. What we have done is sketch the finite nanowire spectrum by selecting wave numbers at regular intervals and tracking the evolution of their energy levels with an increasing angle ϕ. For these examples, we maintain the polar angle $\theta = 90^\circ$ because this is the most physically interesting configuration due to the possibility of aligning external and spin-orbit magnetic fields; nevertheless, analogous plots can be done for different values of θ. The resulting spectrum, shown in Fig. 7, explains the main features of the numerical diagonalization results of Fig. 6 for the same parameters.

In principle, we could also set the boundary conditions exactly as we did in Eq. (10), but we have found this approach impossible to follow on a practical level. The resulting set of equations reads as

$$\begin{aligned} \sum_k C_k^{(L)} \Psi_{s_\sigma s_\tau}^{(k)} e^{-ikL/2} &= 0, \\ \sum_k C_k^{(R)} \Psi_{s_\sigma s_\tau}^{(k)} e^{ikL/2} &= 0, \end{aligned} \tag{15}$$

where $C_k^{(L)}$ and $C_k^{(R)}$ are the coefficients at the left and right nanowire ends, respectively. Basically, the resulting matrix from Eq. (15) is ill defined since it contains very large and very small matrix elements.

The spectra of both panels of Fig. 7 can be divided into three different regions depending on the angle ϕ. First, for low values of ϕ there is a region where a Majorana mode exists

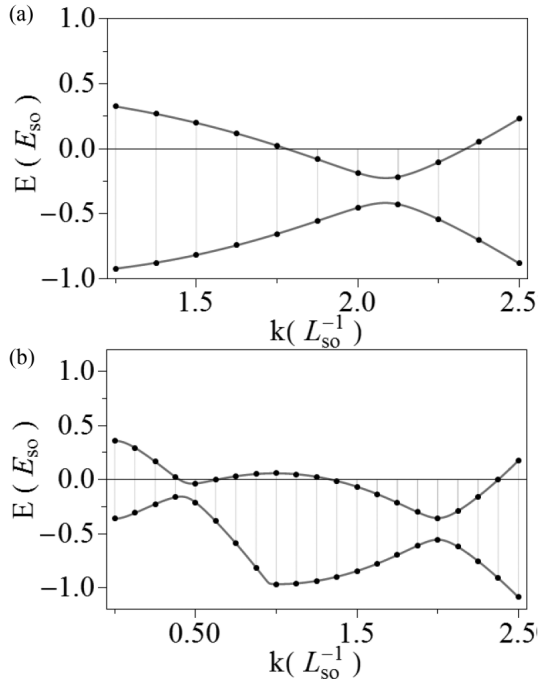

FIG. 8. Approximate spectrum of a finite nanowire in a particular configuration of the external magnetic field. (a) With only two positive real wave numbers. (b) With four positive real wave numbers.

and is topologically protected. In Fig. 7, the Majorana is not seen since only excited states of real wave number are shown, but we can see the corresponding gap. For values of ϕ above those determined by the projection rule, the Majorana mode is destroyed and we can see a region of many level crossings. This behavior of the spectrum is explained by the gap closing of the external branches of the conduction band noticing that in the finite model only some discrete values are allowed, as sketched in Fig. 8. Finally, for higher angular values, the region of zero crossings finishes and a third region arises with two possible behaviors.

As shown in Figs. 6 and 7 for high ϕ angles (near 90°), depending on the parameters the spectrum either opens a gap or collapses near zero energy. The behavior depends on the way the internal branches of the band cross the zero-energy value for those angles. The internal branches of the band can cross the zero-energy level for high angles in one $k > 0$ point, like in Fig. 8(a), thus leading (jointly with the external branch crossing point) to four real and four complex wave numbers or, alternatively, the interior branch can cross zero energy in more than one $k > 0$ point, like in Fig. 8(b), leading to wave functions characterized by eight real wave numbers. In the latter case, there is a wave-number range where the band spectrum lies very close to zero energy, yielding this way a collapse of the finite wire spectrum. The particular set of parameters where one or the other situation happens depends on the behavior of the internal branches of the band structure and it is not as easily predictable as the behavior of the external branches that led to the projection rule. The region of values where this collapse arises coincides with the region where the allowed solutions at zero energy are made of real wave numbers only and it was already presented in Fig. 5(a) for the $\mu = 0$ case.

V. MAGNETIC INHOMOGENEITY MODELS

In this section, we explore the physics of a junction of two straight nanowires with a certain angle in presence of a homogeneous magnetic field parallel to one of the arms, as sketched in Fig. 1(b). We assume a representation of the system as a single straight 1D nanowire containing a magnetic interface. The inhomogeneity separates two homogeneous regions with different directions (but the same magnitude) of the external magnetic field. The system is solved by numerical diagonalization, assuming a soft magnetic interface, interpreting the results by comparing with the homogeneous nanowire discussed in the preceding section. We focus on two specific effects: tilting and stretching of one of the two junction arms. Other nanowire junction properties have been discussed in Refs. [39,46,47].

A. Arm tilting

The magnetic field is aligned with the left arm and the spectrum of the nanowire is computed for varying orientations of the field in the the right arm (see Fig. 9). As mentioned, this model represents under certain approximations a bent nanowire in a homogeneous magnetic field. It was shown in Ref. [48] that bent nanowires can be approximated by 1D models with a potential well simulating the effect of the bending. Here, we have only considered the magnetic field change of direction as the main inhomogeneity source, disregarding the electrical potential effects of the bending.

The spectrum of the inhomogeneous nanowire can be explained in terms of the homogeneous one for a tilted magnetic field. Figure 9 compares the inhomogeneous (upper)

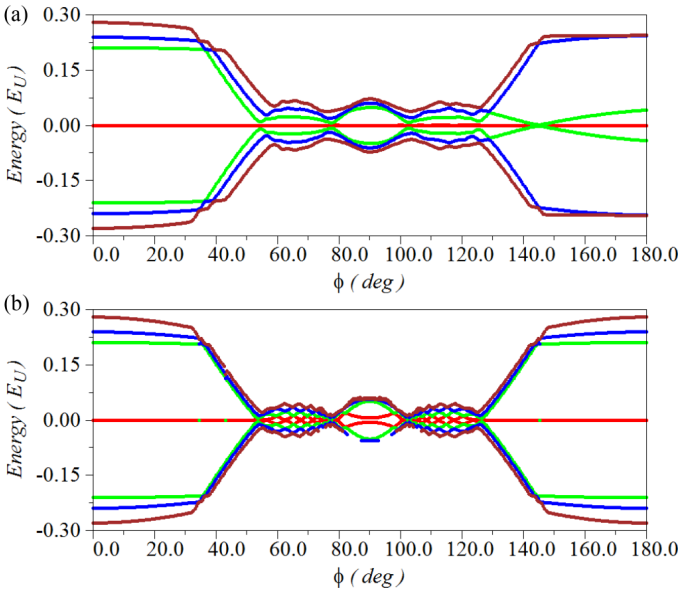

FIG. 9. (Color online) (a) Nanowire spectrum for $\Delta_s = 0.8E_{so}$ and $\mu = 0$ with a magnetic inhomogeneity at its center as a function of the tilting angle ϕ. On the left side of the nanowire the magnetic field is parallel, while on the right side its angles are $(\theta = 90°, \phi)$. The magnetic field strength is constant in both sides and equal to $\Delta_B = E_{so}$. (b) Spectrum of a nanowire in a homogeneous magnetic field with angles $(\theta = 90°, \phi)$ and with the rest of parameters as in (a).

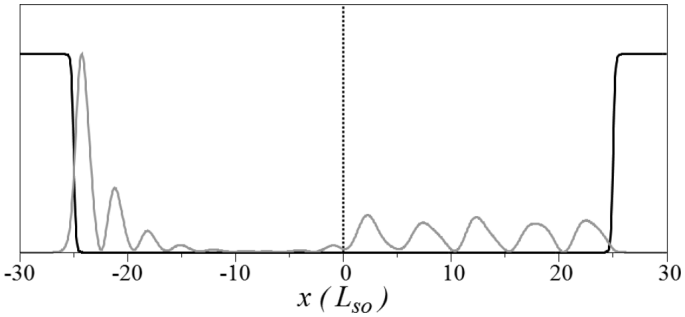

FIG. 10. Majorana density function of an inhomogeneous nanowire similar to the one described in Fig. 9(a). The magnetic field azimuthal angles in the two arms are $\phi_L = 0^\circ$ and $\phi_R = 90^\circ$, while all along the nanowire it is $\theta = 90^\circ$. Other parameters are $\Delta_B = 0.4$, $\Delta_s = 0.25$.

with the homogeneous (lower) nanowire spectrum for the same set of parameters, showing that both results share the same essential features. More precisely, three ϕ regions can be found in both cases, but with two main differences. First, while for the homogeneous nanowire increasing ϕ leads to the destruction of the Majoranas on both ends, for the inhomogeneous nanowire only the localization of the right side Majorana is destroyed, leading to a spread state (Fig. 10). This spread state retains characteristic Majorana properties such as a nearly zero eigenenergy [Fig. 9(a)] and the typical relation of wave-function components. As a consequence, the bent junction holds only one localized Majorana mode in the left side of the inhomogeneity. The density of the Majorana for the inhomogeneous nanowire is shown in Figs. 10 and 11 for selected values of the parameters.

A second difference between upper and lower panels of Fig. 9 is that the spectrum for the inhomogeneous nanowire is not symmetric with respect to $\phi = 90^\circ$, in contrast with the homogeneous nanowire. A zero-energy crossing localized in the inhomogeneity interface arises at $\phi = 145^\circ$ for the selected parameters in Figs. 9(a) and 11. The corresponding bound state originates in the second excited state of the system and it is not Majorana in nature. Furthermore, this localized state is caused completely by the magnetic inhomogeneity and has no relationship with the localized states found in the bending region in Ref. [48] because we have disregarded those effects.

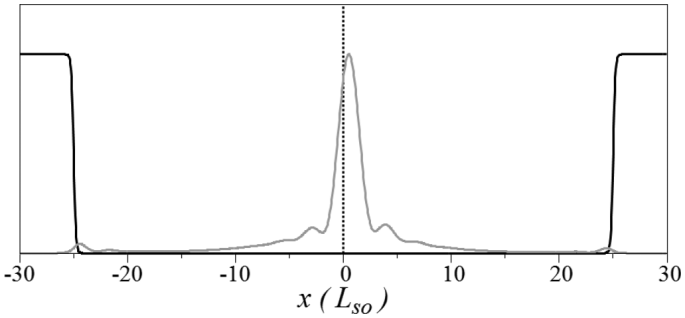

FIG. 11. Density function of the first excited state of the inhomogeneous nanowire of Fig. 9(a). This state becomes localized at the magnetic inhomogeneity for an azimuthal angle $\phi = 145^\circ$ (and polar angle $\theta = 90^\circ$).

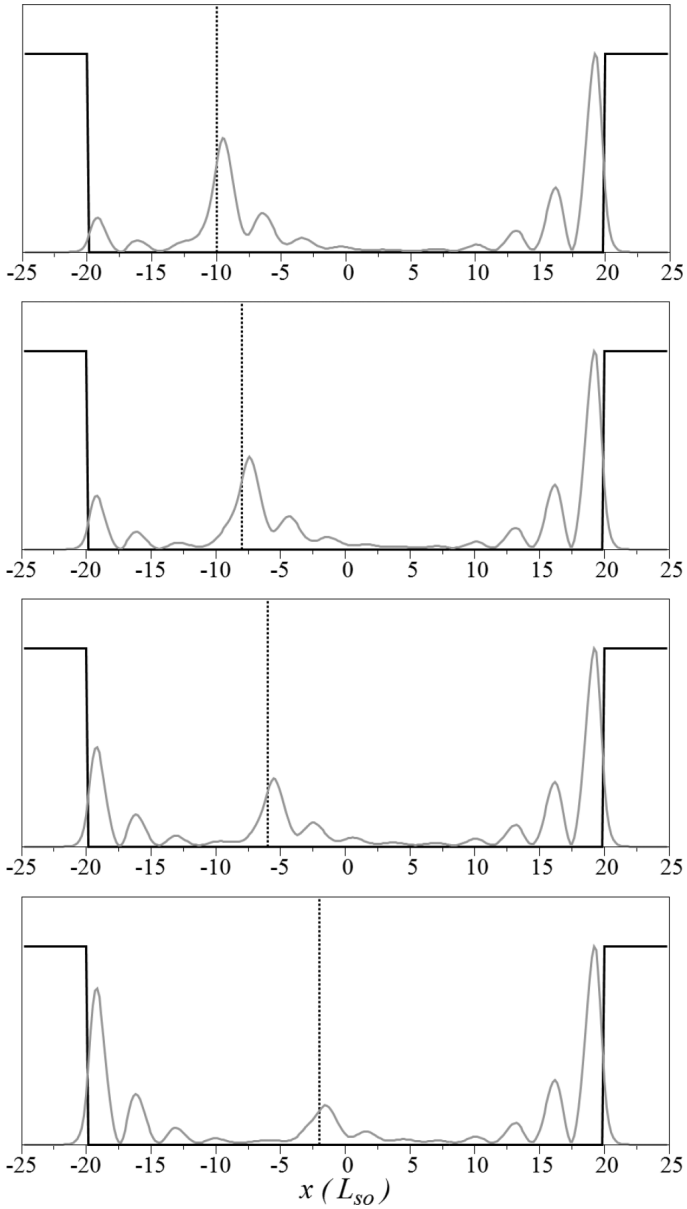

FIG. 12. Density distributions of the Majorana mode in a finite nanowire with a magnetic inhomogeneity. We used $\Delta_s = 0.25E_{so}$, $\mu = 0$, and a magnetic field of magnitude $\Delta_B = 0.4E_{so}$ oriented parallel in the left side of the magnetic interface and antiparallel in the right side. In each panel, the potential well and the position of the magnetic interface are shown. The latter corresponds to a Fermi-type function whose position shifts to the right following the sequence from upper to lower panels.

Although we know these states are related with the magnetic inhomogeneity, a deep understanding of their causes and the particular set of parameters leading to their enhancement or quenching is yet to be understood.

B. Arm stretching

We study now the behavior of the Majorana modes in the nanowire as a function of the inhomogeneity distance to the nanowire end. The magnetic field directions are fixed at $\theta = 90^\circ, \phi = 0^\circ$ on the left end and $\theta = 90^\circ, \phi = 180^\circ$ on the right end of the nanowire. This is a particularly interesting

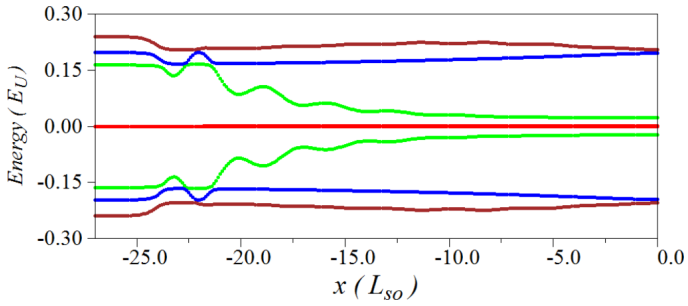

FIG. 13. (Color online) Spectrum of the nanowire described in the caption of Fig. 12 as a function the magnetic interface position.

configuration as it is the only setup where both ends lie inside a longitudinal magnetic field, apart from the homogeneous case. This way, all the observed effects must be caused by the inhomogeneity and its distance with respect to the left nanowire end.

Figure 12 shows the probability densities of the zero-energy state at different positions of the magnetic interface with respect to the left side of the nanowire. From upper to lower panels of Fig. 12 we may follow the evolution as the distance of the magnetic interface to the left end of the system is increased. Most remarkably, for short distance, the left Majorana is not peaked on the left end, but remains stuck on the magnetic interface (upper panels). If the distance is increased, however, the Majorana is eventually transferred to the left nanowire end after some critical distance (lower panels). This transfer is seen as a smooth decrease of the density maximum at the magnetic interface accompanied by an increase at the left end. Finally, when the interface is on the middle point of the nanowire, both Majoranas are located at their corresponding ends. It is also worth noticing that this Majorana transfer does not imply a departure of the mode from zero energy because the Majorana on the other end of the nanowire is not affected (see Fig. 13). Additionally, the transfer phenomenon is not caused by finite-size effects since we have checked that it happens for the same characteristic distance when the right end is further displaced to the right.

VI. CONCLUSIONS

In this work, we have studied the spectra of 1D nanowires for arbitrary orientation of the magnetic field, focusing in particular on the conditions leading to a Majorana mode. This study has been realized from different perspectives and methods in an effort to explain the variety of observed phenomena. We have combined the complex band-structure techniques of infinite homogeneous nanowires with numerical diagonalizations of finite systems.

We have demonstrated an additional condition, aside from the well-known topological transition law, that needs to be taken into account in order to predict the regimes of existence of Majorana modes with tilted fields. We have named this additional condition the projection rule. The projection rule predicts an upper bound on the magnetic field at which Majoranas are to be found in a 1D wire with tilted field. We have stressed that the topological transition law with tilted fields depends on the full-field Zeeman energy and not just on the contribution of the magnetic field component parallel to the wire. When the topological law is fulfilled, the projection rule leads to critical values of the field angles θ_c and ϕ_c, such that a Majorana mode is always found for any ϕ provided $\theta < \theta_c$ or, alternatively, for any θ provided $\phi < \phi_c$.

We have extended our analysis to nanowire junctions with an arbitrary angle, modeled as magnetically inhomogeneous nanowires, explaining most of their properties in terms of the behavior of its homogeneous parts. We have focused, particularly, on the role of tilting and stretching of one of the junction arms. We also reported the existence of a bound non-Majorana state located on the magnetic inhomogeneity. Finally, we have studied the Majorana transfer phenomenon as the distance of the magnetic inhomogeneity to the nanowire end is increased. Testing these predictions would require experiments of nanowires in inhomogeneous magnetic fields. Alternatively, it has been suggested in this work that a bent nanowire in a homogeneous field should display similar phenomena, while being more feasible in practice. As an interesting continuation of this work we are presently analyzing the validity of the projection rule in higher-dimensional nanowires, where the transverse degrees of freedom require a multimode description of the electronic states.

ACKNOWLEDGMENT

This work was funded by MINECO-Spain (Grant No. FIS2011-23526), CAIB-Spain (Conselleria d'Educació, Cultura i Universitats), and FEDER.

[1] A. Y. Kitaev, Ann. Phys. (NY) **303**, 2 (2003).
[2] I. Affleck, T. Kennedy, E. H. Lieb, and H. Tasaki, Phys. Rev. Lett. **59**, 799 (1987).
[3] F. Wilceck, Nat. Phys. **5**, 614 (2009).
[4] X. L. Qi and S. C. Zhang, Rev. Mod. Phys. **83**, 1057 (2011).
[5] J. Alicea, Rep. Prog. Phys. **75**, 076501 (2012).
[6] M. Leijnse and K. Flensberg, Semicond. Sci. Technol. **27**, 124003 (2012).
[7] C. W. J. Beenakker, Annu. Rev. Condens. Matter Phys. **4**, 113 (2013).
[8] T. D. Stanescu and S. Tewari, J. Phys.: Condens. Matter **25**, 233201 (2013).
[9] M. Franz, Nat. Nanotechnol. **8**, 149 (2013).
[10] L. Fu and C. L. Kane, Phys. Rev. Lett. **100**, 096407 (2008).
[11] A. R. Akhmerov, J. Nilsson, and C. W. J. Beenakker, Phys. Rev. Lett. **102**, 216404 (2009).
[12] Y. Tanaka, T. Yokoyama, and N. Nagaosa, Phys. Rev. Lett. **103**, 107002 (2009).
[13] K. T. Law, P. A. Lee, and T. K. Ng, Phys. Rev. Lett. **103**, 237001 (2009).
[14] C. Nayak, S. H. Simon, A. Stern, M. Freedman, and S. Das Sarma, Rev. Mod. Phys. **80**, 1083 (2008).
[15] J. K. Pachos, *Introduction to Topological Quantum Computation* (Cambridge University Press, Cambridge, UK, 2012).

[16] E. Majorana, Nuovo Cimento **14**, 171 (1937).
[17] V. Mourik, K. Zuo, S. Frolov, S. Plissard, E. Bakkers, and L. Kouwenhoven, Science **336**, 1003 (2012).
[18] M. T. Deng, C. L. Yu, G. Y. Huan, M. Larsson, and P. Caroff, Nano Lett. **12**, 6414 (2012).
[19] L. P. Rokhinson, X. Liu, and J. K. Furdyna, Nat. Phys. **8**, 795 (2012).
[20] A. Das, Y. Ronen, Y. Most, Y. Oreg, M. Heiblum, and H. Shtrikman, Nat. Phys. **8**, 887 (2012).
[21] A. D. K. Finck, D. J. Van Harlingen, P. K. Mohseni, K. Jung, and X. Li, Phys. Rev. Lett. **110**, 126406 (2013).
[22] R. M. Lutchyn, J. D. Sau, and S. Das Sarma, Phys. Rev. Lett. **105**, 077001 (2010).
[23] Y. Oreg, G. Refael, and F. von Oppen, Phys. Rev. Lett. **105**, 177002 (2010).
[24] T. D. Stanescu, R. M. Lutchyn, and S. Das Sarma, Phys. Rev. B **84**, 144522 (2011).
[25] K. Flensberg, Phys. Rev. B **82**, 180516 (2010).
[26] A. C. Potter and P. A. Lee, Phys. Rev. Lett. **105**, 227003 (2010).
[27] A. C. Potter and P. A. Lee, Phys. Rev. B **83**, 094525 (2011).
[28] S. Gangadharaiah, B. Braunecker, P. Simon, and D. Loss, Phys. Rev. Lett. **107**, 036801 (2011).
[29] R. Egger, A. Zazunov, and A. L. Yeyati, Phys. Rev. Lett. **105**, 136403 (2010).
[30] A. Zazunov, A. L. Yeyati, and R. Egger, Phys. Rev. B **84**, 165440 (2011).
[31] C.-H. Lin, J. D. Sau, and S. Das Sarma, Phys. Rev. B **86**, 224511 (2012).
[32] E. Prada, P. San-José, and R. Aguado, Phys. Rev. B **86**, 180503(R) (2012).
[33] J. Klinovaja, S. Gangadharaiah, and D. Loss, Phys. Rev. Lett. **108**, 196804 (2012).
[34] J. Klinovaja and D. Loss, Phys. Rev. B **86**, 085408 (2012).
[35] J. S. Lim, L. Serra, R. Lopez, and R. Aguado, Phys. Rev. B **86**, 121103 (2012).
[36] J. S. Lim, R. Lopez, and L. Serra, New J. Phys. **14**, 083020 (2012).
[37] J. S. Lim, R. Lopez, and L. Serra, Europhys. Lett. **103**, 37004 (2013).
[38] L. Serra, Phys. Rev. B **87**, 075440 (2013).
[39] J. Osca and L. Serra, Phys. Rev. B **88**, 144512 (2013).
[40] X.-J. Liu and A. M. Lobos, Phys. Rev. B **87**, 060504 (2013).
[41] M. Lee, H. Khim, and M.-S. Choi, Phys. Rev. B **89**, 035309 (2014).
[42] J. Alicea, G. Refael, F. von Oppen, and M. P. A. Fisher, Nat. Phys. **7**, 412 (2011).
[43] J. D. Sau, D. J. Clarke, and S. Tewari, Phys. Rev. B **84**, 094505 (2011).
[44] B. I. Halperin, Y. Oreg, A. Stern, G. Refael, J. Alicea, and F. von Oppen, Phys. Rev. B **85**, 144501 (2012).
[45] J. Klinovaja, P. Stano, and D. Loss, Phys. Rev. Lett. **109**, 236801 (2012).
[46] F. Pientka, L. Jiang, D. Pekker, J. Alicea, G. Refael, Y. Oreg, and F. von Oppen, New J. Phys. **15**, 115001 (2013).
[47] L. Jiang, D. Pekker, J. Alicea, G. Refael, Y. Oreg, A. Brataas, and F. von Oppen, Phys. Rev. B **87**, 075438 (2013).
[48] H. Wu, D. W. L. Sprung, and J. Martorell, Phys. Rev. B **45**, 11960 (1992).

Chapter 4

Majorana states and magnetic orbital motion in planar hybrid nanowires

Javier Osca and Llorenç Serra
Phys. Rev. B **91**, 235417. Published 12 June 2015.

4.1 Objectives

In the preceding chapters we have analyzed different aspects of 1d Majorana nanowires. In this chapter we introduce for the first time in this thesis a nanowire with a finite width. In the context of mesoscopic semiconductor devices, 1d nanowires are simplified approximations to real nanowires of finite non-zero dimensions. The objective of this chapter is then analyzing more realistic nanowires by introducing a finite transverse dimension. With this objective in mind we obtain the phase diagram of planar quasi-1d nanowires. We consider planar nanowires of rectangular shape, but they are still much longer than wider. No experiments have been done yet with this kind of geometry but, instead, with a hexagonal and cylindrical 3d geometries. Nevertheless, we think it is an interesting proposal because it is the simpler non 1d geometry that can be devised and it already contains a new set of physical effects.

A finite width not only introduces the physics arising from the transverse confinement, but also the orbital motion of quasiparticles due to the perpendicular component of the magnetic field. Hence, the Hamiltonian will contain additional terms coupling the magnetic field with the spatial degrees of freedom of the Majorana wavefunction. In the Landau gauge these terms are

$$\mathcal{H}_{orb} = \frac{\hbar^2}{2ml_z^4}\, y^2\tau_z - \frac{\hbar}{ml_z^2}\, yp_x \ , \tag{4.1}$$

plus a Rashba orbital term,

$$\mathcal{H}_{R,orb} = -\frac{\alpha}{l_z^2}\, y\sigma_y \ , \tag{4.2}$$

where $l_z^2 \equiv \hbar c/eB_z$ is the magnetic length and τ_z is the Pauli matrix for the isospin (particle and hole) degrees of freedom. Here, B_z is the component of the magnetic field perpendicular to the nanowire plane, c is the speed of light and e is the charge of the electron. The two new terms in Eq. (4.1) arise from the substitution $\vec{p} \to \vec{p} - e\vec{A}/c$ in the kinetic energy, while the Rashba orbital term given in Eq. (4.2) arises from the same substitution in the Rashba term. In this work we show how this three terms modify the Majorana phase diagram in characteristic ways and discuss their effect on the Majorana density function.

4.2 Methodology and clarifications

In order to uncover the Majorana phase diagram of a planar nanowire we use the combination of two main methods. The first one is the complex band analysis already introduced in Chap. 2 while the second one is the generalization to 2d of the computer efficient method to solve 1d Hamiltonians given in Chap. 3.

As discussed in Chap. 3, a Majorana requires the presence of an edge. However, the complex band analysis of the equivalent homogeneous infinite nanowire provides all the information needed to determine if the nanowire is in a topological or in a trivial phase. In plain words, we know that in pure 1d nanowires the closing and reopening at $k = 0$ of the infinite nanowire propagating bands signal the phase transition [8]. It can be reasoned that the additional terms from the increase in dimensions do not change the Majorana topological mechanism. In fact, we will make this reasoning in the remarks section below. However, the article of this chapter does not take this result for granted. In the article we first assume, as a working hypothesis, that the closing and reopening of the Majorana nanowire energy gap at $k = 0$ signals the Majorana phase boundaries also in a quasi-1d nanowire. With this hypothesis we generate the Majorana phase diagram and in the second part of the article we check the validity of our assumption solving the Hamiltonian for particular values, in two different ways. We develop a numerically precise and computer efficient method for semi-infinite nanowires, and a less precise but well known direct diagonalization method for finite length nanowires.

The avid reader may be questioning himself/herself where topology intervenes in this problem and about the fundamental reasons for the closing and reopening of the gap at $k = 0$. In general, by means of the bulk to boundary correspondence principle we need a non trivial change of the propagating bands in the corresponding infinite nanowire in order to enter a topological phase. This change must necessarily imply a closing and reopening of the gap at some point because a smooth transformation of a system spectrum does not imply a topological transition. A well known method (but not the only one) is to calculate the so-called topological invariant by means of the calculation of the Pfaffian in highly symmetric points [37]. For example, in topological insulators with time reversal symmetry these points are called Time

Reversal Invariant Momenta points or TRIM. The Pfaffian can be calculated in these points because the Hamiltonian becomes anti-symmetric on them [37]. However, in continuous nanowires with particle hole symmetry but without time reversal symmetry the only point where the Hamiltonian becomes antisymmetric is $k = 0$. The Pfaffian at this point gives us the topological invariant and the closing and reopening of the gap will signal the phase transition. Therefore, obtaining the change of the topological invariant and the gap closing at $k = 0$ are equivalent approaches. We want to stress at this point that this link between them makes unnecessary the actual calculation of the topological invariant unless the study is focused on its particular properties. On a practical basis, our objective here is to calculate the Majorana phase diagram in an hybrid nanowire in presence of orbital effects and we propose a numerically efficient method to do it tracking the closings and reopenings of the gap.

The main technical point of the paper is that direct diagonalization of a finite nanowire is an ineffective method to calculate the overall Majorana phase diagram, in the whole space of parameters. This is because of the following drawbacks of the finite system diagonalization method:

1. It is imprecise. Providing different values of the parameters to a numerical diagonalization method and checking whether a zero mode appears or not is imprecise. In a finite nanowire Majoranas have associated an hybridization energy caused by a little overlapping between them in the middle of the nanowire. This makes difficult to determine the phase boundaries with high precision because the Majorana energy in finite nanowires is never exactly zero and it is difficult to pinpoint the exact transition value (although it can be done with some error).

2. It is resource inefficient. We do not need to know any finite portion of the nanowire spectrum. All the information we need is encoded around wavenumber zero. Therefore, it is not necessary to calculate and store parts of the spectrum and their corresponding eigensolutions.

3. It is time consuming. The full Hamiltonian diagonalization for a particular set of parameter is time consuming even for a coarse spatial discretization of the nanowire. That makes this method simply impractical to calculate the phase diagram over a wide region of the space of parameters.

From complex band analysis we know than in a semi-infinite nanowire the Majorana solution will be a linear combination of the equivalent infinite nanowire eigensolutions

$$\Psi(x, y, \eta_\sigma, \eta_\tau) = \sum_k C_k \, \Psi_k(x, y, \eta_\sigma, \eta_\tau) \, , \tag{4.3}$$

where Ψ_k is an homogeneous nanowire eigensolution and C_k is its corresponding probability amplitude. Each one of the infinite nanowire solutions has a wavenumber k as a good quantum number. By means of the separation of variables the longitudinal and transverse dependences of Ψ_k can be written as a product of a

plane wave in x and a transverse function,

$$\Psi_k(x, y, \eta_\sigma, \eta_\tau) = \sum_{s_\sigma s_\tau} \Psi^{(k)}_{s_\sigma s_\tau}(y)\, e^{ikx}\, \chi_{s_\sigma}(\eta_\sigma)\, \chi_{s_\tau}(\eta_\tau)\ , \tag{4.4}$$

where $\Psi^{(k)}_{s_\sigma s_\tau}(y)$ is now the transverse component of the homogeneous nanowire eigensolution and $\chi_{s_\sigma}(\eta_\sigma)$ and $\chi_{s_\tau}(\eta_\tau)$ are the basis spinors for spin and isospin ($s_\sigma = \pm$, $s_\tau = \pm$). Using this separation of variables the infinite nanowire eigenvalue equation for each k reads

$$(h - E) \sum_{s_\sigma s_\tau} \Psi^{(k)}_{s_\sigma s_\tau}(y)\, \chi_{s_\sigma}(\eta_\sigma)\, \chi_{s_\tau}(\eta_\tau) = 0\ , \tag{4.5}$$

where

$$\begin{aligned} h \;\; = \;\; & \left(\frac{\hbar^2 k^2}{2m} + \frac{p_y^2}{2m} + V(y) - \mu \right) \tau_z + \Delta_s\, \tau_x - i\alpha k \sigma_y \tau_z - \frac{\alpha}{\hbar}\, p_y \sigma_x \tau_z \\ & + \Delta_B\, \hat{\sigma} \cdot \hat{n} + \frac{\hbar^2}{2m l_z^4} y^2 \tau_z - \frac{\alpha}{l_z^2} y \sigma_y\ , \end{aligned} \tag{4.6}$$

and the different symbols have the same meaning as in Chap. 1. As stated above, a topological transition occurs for certain parameters when the gap closes and reopens at zero energy and wavenumber. When this condition is met Eq. (4.5) will have a solution for $E = 0$ and $k = 0$. A key point is that Eq. (4.5) is a 1d equation that only depends on the y coordinate. Therefore, a dimensional reduction of the problem has been achieved and we need to solve this new equation only at zero energy and wave number. The solution of this equation can be obtained using the matching method already presented in Chap. 2.

The continuity of the derivatives of the solution at zero energy and wavenumber at the matching point will signal when a particular solution of Eq. (4.5) is physical or not. As explained in Chap. 2 this continuity is measured by the function $\mathcal{F}$. Therefore, when $\mathcal{F}$ is zero then Eq. (4.5) has a physical solution and that means that the gap of the overall two dimensional Hamiltonian is closed at $k = 0$ and the system is in a phase transition point. The overall method is computer efficient since a simple sweep of parameter will give us the phase diagram in a time efficient way.

The same approach can be used to obtain the complex wave numbers at a given energy ($E = 0$) of the homogeneous nanowire. Once we have enough of them we can solve the equation $\Psi(0, y, \eta_\sigma, \eta_\tau) = 0$ to obtain the set of values of C_k's. With this information the Majorana wavefunction is then calculated using Eq. (4.3). Note that the obtained solution will be an approximation because of the truncation of the solution to a finite number of wavenumbers. However, this is a very good approximation if we take first the wavenumbers with the smallest imaginary part. The homogeneous nanowire eigensolutions with big imaginary wavenumbers are highly evanescent and therefore they will have a small contribution to the Majorana edge state wavefunction. This method is used to check the phase diagram predictions. We only have Majorana solutions in the parameter regions pointed by the phase diagram.

This method has the advantage, as compared with direct diagonalization methods, to provide wavefunctions with very high resolutions. While direct diagonalization

methods are able to solve spatial grids of 100×100 points at most, with this method the transverse resolution can be of various thousands of points. Furthermore, the semi-analytic nature of the solution provides an arbitrary resolution in the longitudinal direction.

Finally, the phase diagram is also checked against direct diagonalization of a finite nanowire for selected values. The direct diagonalization method performs poorly in time, even at low spatial resolutions, but is a well known and widely accepted method, and thus useful for checking purposes. The diagonalization method used here is the same of Chap. 2, but for a 2d wavefunction implies a larger number of components.

To use the different numerical algorithms we use the nanowire width as the unit length, this also determines the energy scale

$$L_U \equiv l_y \,, \tag{4.7}$$
$$E_U \equiv \hbar^2/m l_y^2 \,. \tag{4.8}$$

This is a better choice of units for this particular kind of nanowire than the more usual selection based on the Rashba spin orbit coupling strength (as in Chaps. 2 and 3). In 1d nanowires the only characteristic dimension of the problem is the Rashba length $l_\alpha = \hbar^2/m\alpha$. Length units based on α are then used for nanowires of higher dimensions to make an easy comparison. However, as proven in this work, the phase diagrams depends on one hand on the relationship between the Rashba length l_α and the nanowire width l_y while, on the other hand, it also depends on the relationship between the nanowire width and the magnetic length l_z. The nanowire width l_y will be key to the scaling reasonings and therefore is the more useful selection of units for this case.

A realistic nanowire 150 nm wide made of InAs will have a Rashba spin orbit coupling strength of $\alpha = 30$ meVnm, in characteristic units this is about $\alpha \approx 2\ E_U L_U$. As shown in the article, this corresponds to an almost ideal phase diagram behavior depicted in Fig. 2b. In this context ideal means that the phase boundaries closely follow the analytical expression of the limits. Phase diagrams are drawn for a Zeeman energy between $0E_U$ and $25E_U$, that for this nanowire correspond to values between 0 and 6 Tesla. Therefore, we can find Majorana phases for values of the magnetic field in the range of the current technology. Finally we have also used a superconductor gap $\Delta = 3E_U$ that for this particular nanowire is equivalent to 0.3 meV. In the same vein of previous chapters, this does not precisely correspond to the bulk value of any particular superconductor material but we believe it is a value within a realistic range.

4.3 Conclusions and remarks

In this chapter we obtain the phase diagram for a planar nanowire of finite width in presence of orbital effects and we check the validity of such diagram. Majorana phases are located as a function of the magnitude and orientation of the external

magnetic field for different values of the Rashba spin orbit strength. If we restrict ourselves to in-plane magnetic fields, the Majorana phase boundaries are determined by critical magnetic field strengths. However, magnetic fields with out-plane components, in presence of orbital effects, change the Majorana phase boundaries into critical angles. Analytical expressions for the critical magnetic fields and angles can be given for some particular limits. The Rashba coupling strength has a role adding further corrections that modify the phase diagram away from the ideal analytical conditions.

Physically, adding a second dimension introduces six new terms in the nanowire Hamiltonian with respect the 1d one used in previous chapters. The first two ones are the p_y dependent kinetic energy and the transverse component of the confinement

$$\mathcal{H}_{2d} = \frac{p_y^2}{2m} + V(y) \, . \tag{4.9}$$

These two terms are responsible for the quantization of the nanowire in the transverse direction creating many transverse modes. In absence of a Rashba mixing term these transverse modes would behave like independent 1d nanowires, each one with its own Majorana critical field. The different transverse modes get coupled by the Rashba mixing term, that is also responsible of the alternation of the Majorana and trivial phases. This happens because two Majoranas annihilate each other in pairs becoming a fermion and lifting their energy away from zero. This in agreement with Ref. [38] discussion for class D systems that do not fulfill time reversal symmetry. The Rashba mixing term,

$$\mathcal{H}_{R,m} = -\frac{\alpha}{\hbar} \, p_y \sigma_x \tau_z \, , \tag{4.10}$$

has the same origin of the 1d Rashba term. α is the same spin orbit coupling strength, p_y is the momentum on the $\hat{y}$ direction and τ_z is a Pauli matrix for the isospin degrees of freedom.

Finally, the last new three terms are the orbital ones already given in Eqs. (4.1) and (4.2), these are the terms whose physical effect are analyzed in detail in the article that follows. In general, the two first orbital terms, Eq. (4.1), provide an additional effective parabolic confinement that depends on the magnetic field strength. These terms introduce critical angles in the phase diagram. On the other hand, the Rashba orbital term presented in Eq. (4.2) only becomes non-negligible when the Rashba coupling is very strong. It has the mathematical form of an inhomogeneous magnetic field effectively reducing the magnetic field tilting. This effective reduction leads to a change in the Majorana phase diagram.

In short, the Rashba mixing term couples different transverse bands allowing only one Majorana at each edge and the orbital terms behave as an effective transverse confinement, or as an inhomogeneous magnetic field, changing the phase boundaries but none of them produces a non-trivial change in the propagating bands of the quasi-1d homogeneous nanowire. This means that the quasi-1d nanowire is topologically equivalent to the 1d nanowire. Therefore, as stated above the closing and reopening of the gap at zero wavenumber signals the Majorana phase transition in the same way as in a 1d nanowire.

As a final side note, see that in this work the typical values for InAs imply $\alpha/E_U L_U = L_y/L_{so} = 2$, therefore our result lie in a regime where $L_y > L_{so}$. In this paper we take the width of the nanowire as length unit $L_y = L_U$ by the reasons given above. Nevertheless, to diminish L_y would be equivalent to diminish α. Trivially, at $\alpha = 0$ all the transverse bands get decoupled but Majoranas get delocalized to a point in which they does not exist anymore. Remember that the greater α the more localized Majoranas become. In fact for $\alpha = 0$ there is no gap in the parameter regions able to hold Majoranas because $\Delta_B > \Delta_o$. Increasing, α will restore again the Majoranas for the appropriate regions of the phase diagram but also the repulsion between Majoranas in the non Majorana phases. Strictly speaking, in the terms presented in this work this repulsion grows progressively. However, it has been noted that it remains small if $L_y << L_{so}$ [39]. In this case it can be considered that increasing the magnetic field from zero will add up, in an approximate way, a new Majorana mode for each phase boundary crossed. This approximation may be not noticeable in finite nanowires if the repulsion energy is of the order of the hybridization one but strictly speaking topological differences can be found between this limit case and semi-infinite devices having multiple modes exactly at zero energy (a so-called Z topological invariant).

4.4 Published paper

PHYSICAL REVIEW B **91**, 235417 (2015)

Majorana states and magnetic orbital motion in planar hybrid nanowires

Javier Osca[1,*] and Llorenç Serra[1,2]

[1]*Institut de Física Interdisciplinària i de Sistemes Complexos IFISC (CSIC-UIB), E-07122 Palma de Mallorca, Spain*

[2]*Departament de Física, Universitat de les Illes Balears, E-07122 Palma de Mallorca, Spain*

(Received 28 January 2015; revised manuscript received 27 May 2015; published 12 June 2015)

The Majorana phase boundaries in planar 2D hybrid (semiconductor-superconductor) nanowires are modified by orbital effects due to off plane magnetic components. We show that Majorana zero modes survive sizable vertical field tiltings, uncovering a remarkable phase diagram. Analytical expressions of the phase boundaries are given for the strong orbital limit. These phase boundaries can be fulfilled with attainable setups, such as an InAs nanowire of 150 nm in transverse width.

DOI: 10.1103/PhysRevB.91.235417 PACS number(s): 73.63.Nm, 74.45.+c

I. INTRODUCTION

The physics of 2D electron gases in magnetic fields has proved invaluable for the condensed matter field with, e.g., the celebrated quantum Hall effect [1] as well as with many devices based on quantum wells, wires, and dots [2]. On the other hand, Majorana zero modes in quasi-1D wires have recently attracted strong interest, both as exotic quasiparticles and as candidates for topological quantum computing [3–6]. In this article we relate 2D-gas properties and Majorana physics, showing the remarkable role of the orbital motions characteristic of 2D systems in magnetic fields.

Majorana modes in quasi-1D wires are effectively chargeless, zero-energy quasiparticles. They arise from the splitting, through a phase transition, of bulk electronic states into pairs of quasiparticles on the wire ends, each one being its own antiparticle [7–18]. An important feature of the Majorana mode is that it appears only when a critical value of the external magnetic field, a phase-transition threshold, has been surpassed. Several experiments with hybrid superconductor-semiconductor nanowires using tunneling spectroscopy from a normal conductor to the nanowire have observed a zero bias peak consistent with a Majorana state [19–22]. The observed peak height is, however, an order of magnitude lower than the quantized value $2e^2/h$. This discrepancy is not yet well understood, as it might be due to effects ranging from finite temperature, experimental, and tunneling resolutions to other low-energy subgap states and possible inelastic and renormalization processes [23,24].

In practice, distinguishing zero-bias peaks due to Majorana modes from other potential sources relies on the detailed knowledge of the phase diagram in each particular physical realization. Therefore, it is highly relevant knowing how Majorana physics is affected by the extra dimension in 2D, with respect to 1D. This question has been addressed with quasi-1D *multiband* wires [25–28], modeling transverse modes as mutually coupled 1D wires. This leads to essentially the 1D physics with only one Majorana mode at each nanowire end when an odd number of transverse modes are above their critical magnetic field. However, the role of the magnetic orbital motion has been usually disregarded. Addressing Majorana physics in 2D systems with orbital motion is therefore relevant as a way to discard alternative scenarios that have been suggested, such as attributing the observations to Kondo-like interaction effects [28]. We want to clarify too that the above mentioned experiments [19–22] used cylindrical nanowires, for which the orbital effects may be different from those discussed here.

In this article we show that in a planar nanowire the orbital motion strongly affects the phase transition boundaries. We show how the Majorana phase survives sizable vertical field tiltings (Fig. 1), even reaching the purely perpendicular orientation in some cases. This is not an intuitive result since the electronic orbital motion might lead to a gap closing, allowing edge propagating solutions, or it might totally change the character of the topological states. In this sense we note that the s-wave nanowires inside a magnetic field have an associated directionality with their Majoranas located at the left and right edges (Fig. 1), while a 2D p-wave nanowire has their edge states located all along the 1D perimeter.

In the strong orbital limit, the phase transitions occur for critical values of the polar angle, following a simple analytical law that does not depend on sample details. With parallel (x) field orientation the transition law is also analytical, while for intermediate regimes the phase transitions are obtained numerically. We assess the consistency between the phase diagram and direct calculations of the Majorana modes in semi-infinite and finite 2D wires, emphasizing the importance of covariant grid discretizations for the latter [29,30].

The work is organized as follows. Section II introduces the physical system in detail, while Sec. III contains the algorithm used to determine the phase-transition boundaries. In Sec. IV we discuss the phase diagrams for out-of-plane tiltings of the magnetic field with different strengths of the spin-orbit coupling. Sections V and VI deal with the actual Majorana solutions in semi-infinite and finite 2D Majorana nanowires, respectively. Section VII contains the conclusions of the work.

II. PHYSICAL MODEL

The combination of s-wave superconductivity, Rashba interaction, and an external magnetic field is a well known source of Majorana fermions [7]. We consider electronic motion restricted to the $\hat{x}$ (longitudinal) and $\hat{y}$ (transverse) directions in the presence of these three effects. The homogeneous magnetic field points in an arbitrary direction and the edges are

*javier@ifisc.uib-csic.es

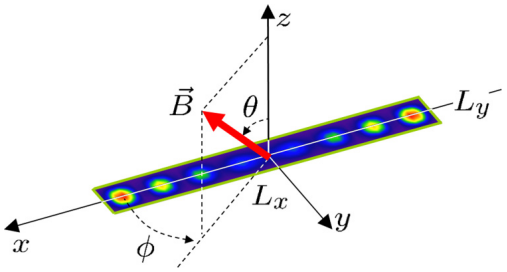

FIG. 1. (Color online) Schematic of a 2D planar nanowire showing the axis definitions. A magnetic field in a tilted direction is included. The density distribution of Majorana modes on the wire ends is qualitatively shown.

modeled as infinite square well potentials in the longitudinal and transverse directions (Fig. 1).

The nanowire physics is described by a Hamiltonian of the Bogoliubov–de Gennes kind, split in the following way:

$$\mathcal{H}_{\rm BdG} = \mathcal{H}_0 + \mathcal{H}_Z + \mathcal{H}_R + \mathcal{H}_{\rm orb}. \tag{1}$$

The successive contributions to Eq. (1) are the zero-field and superconducting energies

$$\mathcal{H}_0 = \left(\frac{p_x^2 + p_y^2}{2m} + V(x,y) - \mu\right)\tau_z + \Delta_s \tau_x, \tag{2}$$

the Zeeman term

$$\mathcal{H}_Z = \Delta_B(\sin\theta\ \cos\phi\,\sigma_x + \sin\theta\ \sin\phi\,\sigma_y + \cos\theta\,\sigma_z), \tag{3}$$

the Rashba coupling term

$$\mathcal{H}_R = \frac{\alpha}{\hbar}(p_x\sigma_y - p_y\sigma_x)\tau_z, \tag{4}$$

and, finally, the magnetic orbital terms

$$\mathcal{H}_{\rm orb} = \frac{\hbar^2}{2ml_z^4}y^2\tau_z - \frac{\hbar}{ml_z^2}yp_x - \frac{\alpha}{l_z^2}y\sigma_y. \tag{5}$$

In Eqs. (2)–(5) we used the following Nambu-spinor convention, relating discrete components with spin ($\uparrow\downarrow$) and isospin ($\Uparrow\Downarrow$) as $\Psi \equiv (\Psi_{\uparrow\Uparrow}, \Psi_{\downarrow\Uparrow}, \Psi_{\downarrow\Downarrow}, -\Psi_{\uparrow\Downarrow})^T$.

The contributions in Eq. (2) are, in left to right order, the kinetic, electrical potential V, chemical potential μ, and superconducting Δ_s energies. The Pauli operators for isospin (particle-hole) are represented by $\tau_{x,y,z}$, while those for spin are $\sigma_{x,y,z}$. The superconductor term represents an effective mean field approximation to more complicated interactions with a nearby s-wave superconductor. The Zeeman term, Eq. (3), depends on parameter Δ_B and models the coupling of the spin with a magnetic field of arbitrary polar and azimuthal angles $(\theta,\phi) \equiv \hat{n}$.

The Rashba coupling Eq. (4) is the result of the self-interaction between the quasiparticle spin with its own motion. This interaction is due to the presence of a transverse electric field representing an internal asymmetry in the confinement along z that may be either intrinsic or externally induced. The first Rashba contribution, depending on $p_x\sigma_y$, is called the 1D Rashba term while the second one, $p_y\sigma_x$, is the Rashba mixing term.

The joint effects of superconductivity, Zeeman, and 1D Rashba terms give rise to independent Majorana states, one from each transverse band like in the 1D model. Each one of the modes has a different critical magnetic field $\Delta_{B,n}^{(c)} = [(\mu - \epsilon_n)^2 + \Delta_s^2]^{1/2}$, with $n = 1,2,\ldots$, and ϵ_n the transverse mode energies. Adding the Rashba mixing term to this scenario changes the critical fields due to the coupling between different transverse bands. It effectively allows only one Majorana zero mode in parameter regions where the 1D Rashba term would yield an odd number of them (even-odd effect) [27,31]. This is further discussed in the Appendix as a particular analytical limit of the most general case presented below. Besides, in 1D wires the effect of tilting the magnetic field implies the additional requirement of the so-called projection rule $\Delta_B \sin\theta\ \sin\phi < \Delta_s$ [32,33]. This is due to the indirect gap closing of the infinite wire energy bands at $\pm k_c$ due to the tilted field, where k_c is a nonvanishing wave number. As discussed in Sec. IV, in 2D nanowires we find strong modifications of the critical magnetic fields, but the projection rule still applies.

In a planar nanowire the perpendicular component of the magnetic field induces orbital motions of the nanowire quasiparticles. The magnetic orbital terms, Eq. (5), describe this motion and their effect on the Majorana states is the central point of this article. These terms depend on the magnetic length l_z, defined as $l_z^2 = \hbar c/eB_z$, and they stem from the kinetic and Rashba energies with the magnetic substitution $p_x \to p_x - \hbar y/l_z^2$ and adding the required Pauli matrix τ_z for proper particle-hole symmetry. In Eq. (5) we assumed the Landau gauge centered on $y_c = 0$, although our results are independent on this choice as discussed below.

All parameters of the complete Hamiltonian are constant inside the nanowire, modeled as a perfectly confining box with $L_x \gg L_y$. The numerical results of this work are presented in characteristic units of the problem obtained by taking $\hbar$, m and the width of the nanowire L_y as reference values. That is, our length and energy units are, respectively, $L_U \equiv L_y$ and $E_U \equiv \hbar^2/mL_y^2$. A spin-orbit length L_{so} is usually defined as $L_{so} = \hbar^2/m\alpha$ but, as explained below, the Hamiltonian orbital terms will introduce an effective transversal confinement. Therefore, the comparison between its characteristic length and the one of the nanowire real confinement is relevant. We notice that, in our convention, the numerical value of α is precisely the ratio of transverse and spin-orbit lengths, $\alpha/E_U L_U = L_y/L_{so}$.

III. MATCHING METHOD

In topological systems it is in general possible to relate the states of the bulk with those at the boundaries, a consequence of the bulk-to-edge correspondence principle. In our particular case this means that the semi-infinite Majorana solution Ψ will be expressed as a linear superposition of the infinite-nanowire eigensolutions $\Psi^{(k)}$ (i.e., for the same Hamiltonian but disregarding the left and right edges),

$$\Psi(x,y,\eta_\sigma,\eta_\tau) = \sum_k C_k \Psi^{(k)}(x,y,\eta_\sigma,\eta_\tau), \tag{6}$$

where spin and isospin variables are indicated with η_σ and η_τ, respectively. Notice that the infinite-nanowire solutions $\Psi^{(k)}$ are characterized by a wave number k that, accounting for evanescent waves, may be a complex quantity. In a given spin-isospin basis, $\chi_{s_\sigma}(\eta_\sigma)$ and $\chi_{s_\tau}(\eta_\tau)$, with $s_\sigma = \pm$ and $s_\tau = \pm$,

the infinite-wire solutions read

$$\Psi^{(k)}(x,y,\eta_\sigma,\eta_\tau)=\sum_{s_\sigma s_\tau}\Psi^{(k)}_{s_\sigma s_\tau}(y)e^{ikx}\chi_{s_\sigma}(\eta_\sigma)\chi_{s_\tau}(\eta_\tau), \quad (7)$$

where $\Psi^{(k)}_{s_\sigma s_\tau}(y)$ is a 1D four-component spinor characteristic of the infinite-wire solution with wave number k.

It has been demonstrated that a Majorana phase transition occurs in a semi-infinite nanowire when the propagating bands for the corresponding infinite nanowire perform a gap closing and reopening when increasing the magnetic field, at vanishing energy and wave number [8,32]. Therefore, to determine the phase boundaries we only need to investigate the band structure at $k=0$ and $E=0$. However, a full determination of the band spectrum for every set of Hamiltonian parameters by diagonalization is time consuming and computationally ineffective. In accordance with this, it has been pointed out that in spite of the nonlocality of the topological states a full knowledge of the band spectrum is not necessary in general to determine the phase of a topological system, but the only relevant regions are those near the Dirac cones that appear at the phase transitions [34]. In our case, this implies searching the solutions of

$$\sum_{s'_\sigma s'_\tau}\langle s_\sigma s_\tau|h|s'_\sigma s'_\tau\rangle\Psi^{(0)}_{s'_\sigma s'_\tau}(y)=0, \quad (8)$$

where h is obtained neglecting all p_x-dependent terms in Eq. (1),

$$h=\left(\frac{p_y^2}{2m}+V(y)-\mu\right)\tau_z+\Delta_s\tau_x-\frac{\alpha}{h}p_y\sigma_x\tau_z + \Delta_B\hat{\sigma}\cdot\hat{n}+\frac{\hbar^2}{2ml_z^4}y^2\tau_z-\frac{\alpha}{l_z^2}y\sigma_y. \quad (9)$$

Notice that with Eq. (8) we achieved a reduction to an effective 1D problem.

We can use the algorithm devised in Refs. [31,35] to study the solutions of Eq. (8). The particular parameter sets allowing such a solution will signal the gap closing of the original 2D Hamiltonian of Eq. (1) and thus the phase transition we are looking for. The algorithm consists in solving Eq. (8) in a 1D grid as a linear system, assuming vanishing boundary conditions at $y=0$ and $y=L_y$. However, due to the homogeneous character of this linear system the trivial solution $\Psi^{(0)}_{s_\sigma s_\tau}(y)=0$ is always possible. The algorithm discards the trivial solution by means of a matching point y_m, where for an arbitrary pair of components $(s_\sigma s_\tau)=(st)$ a nonvanishing wave function is imposed. In addition, continuity of the first derivative at the matching point is also imposed for the components other than (st),

$$\Psi^{(0)}_{st}(y_m)=1, \quad (10)$$

$$\left(\frac{d^{(U)}}{dy}-\frac{d^{(L)}}{dy}\right)\Psi^{(0)}_{s_\sigma s_\tau}(y_m)=0, \quad (s_\sigma,s_\tau)\neq(s,t), \quad (11)$$

where $d^{(U,L)}/dy$ denote grid derivatives using only upper (U) or lower (L) y-grid neighbors.

Equations (10) and (11) are used at y_m in place of the Bogoliubov–de Gennes ones. In particular, Eq. (10) makes the system no longer homogenous and such that it always admits a solution. The algorithm does not ensure the first-derivative continuity for the component (st) at the matching point. Therefore, this condition is used to distinguish the physical from the nonphysical solutions with the continuity *measure*

$$\mathcal{F}=\left|\left(\frac{d^{(U)}}{dy}-\frac{d^{(L)}}{dy}\right)\Psi^{(0)}_{st}(y_m)\right|^2. \quad (12)$$

As mentioned, the $\mathcal{F}$ zeros will signal the desired gap closing boundaries of Eq. (1). Further details about the algorithm can be found in Ref. [35].

IV. PHASE DIAGRAMS

Figure 2(b) shows the phase transition boundaries obtained with the matching method for an $L_y=150$ nm nanowire with material parameters typical of InAs and a magnetic field strength between 0 and 6 T ($\Delta_B=0$–$25E_U$). Phase boundaries are signaled by zero values of $\mathcal{F}$ (red lines). Only $\mathcal{F}=0$ values represented by red lines have physical sense and the color scale is only indicating the measure deviation from zero. As mentioned, the energy unit scales as L_y^{-2}, such that in a 300 nm wire $25E_U$ would correspond to 1.5 T. The other panels of Fig. 2 correspond to lower [2(a)] and higher [2(c),2(d)] values of the Rashba coupling strength. We will explicitly calculate the zero modes for particular sets of parameters below. Here, let us anticipate that the orbital terms do not change the even-odd effect of multiband nanowires [25–28].

The phases in Fig. 2 contain either no Majoranas or at most one Majorana mode in regions labeled with an M. The main result of this article is that orbital effects do not destroy Majoranas into other phases. However, they do lead to characteristic phase maps where the Majorana states survive sizable vertical tiltings [even up to $\theta=0$ in Fig. 2(d)]. The change in transition boundaries is caused by two reasons. First, by the change in the effective transversal confinement due the first two terms of Eq. (5). Note that the first contribution leads to a harmonic confining. Second, the third term of Eq. (5) can be understood as an effective inhomogeneous magnetic field pointing in y direction due to the combination of Rashba and orbital effect.

It is possible to give analytical expressions of the phase boundaries in particular limits (see the Appendix). For $\theta=90^\circ$ and $\phi=0$ the critical magnetic fields read

$$\Delta^{(c)}_{B,n}=\sqrt{\left(\mu-\epsilon_n+\frac{m\alpha^2}{2\hbar^2}\right)^2+\Delta_s^2}, \quad (13)$$

where $n=1,2,\ldots$ and ϵ_n are the (transverse) square well eigenenergies. This analytical result extends recent findings from other authors [25,28] who assumed that the contribution in parentheses in Eq. (13) is an effective chemical potential from subband n, without specifying its detailed α dependence. Analogously, in the strong orbital limit $\Delta_B >> (\hbar^2/mL_y^2, m\alpha^2/\hbar^2, \Delta_s, \mu)$ the critical angles are

$$\theta^{(c)}_n=\arccos\left(\frac{gm^*}{4\left(n-\frac{1}{2}\right)}\right), \quad (14)$$

where g is the gyromagnetic factor and $m^*=m/m_e$ the ratio between the electron effective and bare masses (m and

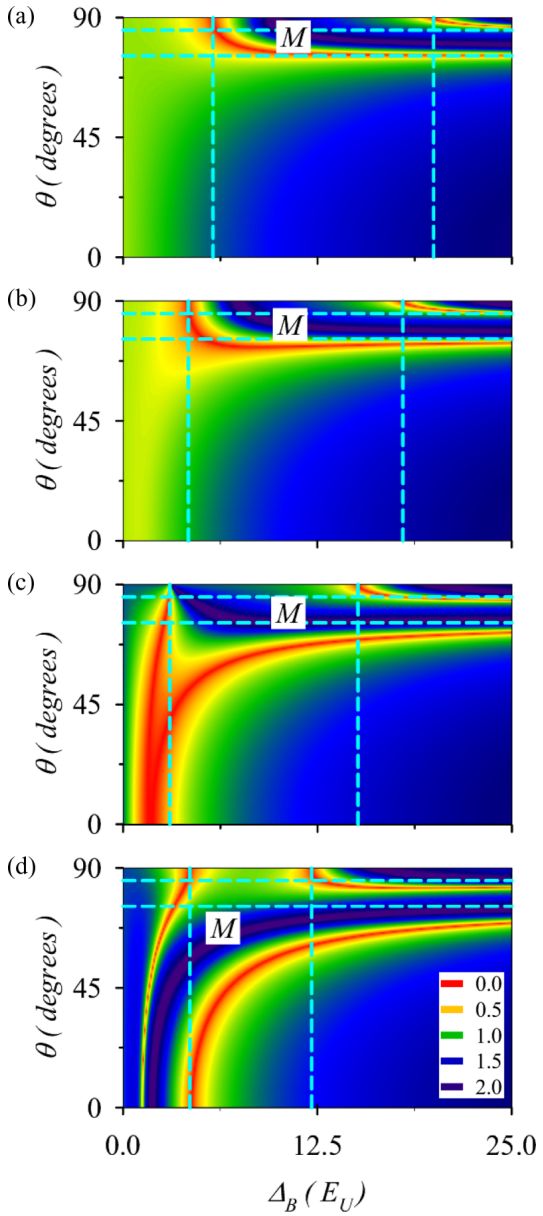

FIG. 2. (Color online) $\mathcal{F}$ measure in a color (gray) scale as a function of Δ_B and polar angle θ. The azimuthal angle remains $\phi = 0$. Zero values of $\mathcal{F}$ (red) signal the phase transition boundaries. Phases with a Majorana mode are labeled with an M. From top to bottom the panels correspond to $\alpha = 0.1 E_U L_U$ (a), $2 E_U L_U$ (b), $\pi E_U L_U$ (c), and $4 E_U L_U$ (d). Dashed lines indicate the analytical limits. We have assumed $\Delta_s = 3 E_U$ and typical InAs parameters $g = 15, m^* = 0.033$. Panel (b) corrresponds to an InAs nanowire with $\alpha = 30$ meV nm, $\Delta_s = 0.3$ meV, and $L_y = 150$ nm in a magnetic field range from zero to 6 T.

m_e, respectively). In this limit quasiparticles are confined by the effective Δ_B-dependent harmonic potential caused by the first and second terms of Eq. (5), independent of the real nanowire transversal boundaries. Quite remarkably, Eq. (14) is independent of the magnetic field, Rashba, and superconductivity strengths, as well as on the specific wire width L_y. In this sense, the critical angles are rather universal. The values of Eqs. (13) and (14) for the particular parameters used in Fig. 2 are overprinted as vertical and horizontal dashed lines, respectively. As shown, the numerical values match the analytical ones in their corresponding limits. In Figs. 2(a) and 2(b) the transitions boundaries do not deviate substantially from the analytical laws in all the plot, while Figs. 2(c) and 2(d) show large differences for intermediate values of the parameters.

TABLE I. Numerical values in effective units of the inequalities, Eq. (11) of the paper, corresponding to the four panels in Fig. 2 of the paper.

Panel	$\Delta_{B,1}^{(c)} \cos\theta_1^{(c)}$	$\frac{gm^*}{4E_U}$	$\frac{gm^*\alpha^2}{4E_U^2 L_U^2}$	$\frac{gm^*\Delta_s}{4}$
(a)	1.43	0.12	0.001	0.36
(b)	1.03	0.12	0.48	0.36
(c)	0.74	0.12	1.22	0.36
(d)	1.06	0.12	1.98	0.36

The structure of the phase transitions in Fig. 2(a) is typical for cases when the kinetic orbital effects already dominate around the first transition boundary with increasing Δ_B. The phase boundaries just bend from a vertical to a horizontal line due to the effective change of the transversal confinement in the nanowire, from square well to a Δ_B-dependent harmonic confinement [Eq. (5)]. Assuming $\mu \approx 0$, the conditions for this simpler phase diagram (l_z shortest scale) can be written as a triple inequality

$$\Delta_{B,1}^{(c)} \cos\theta_1^{(c)} \gg \frac{gm^*}{4}\left(E_U, \frac{\alpha^2}{E_U L_U^2}, \Delta_s\right). \qquad (15)$$

Figure 2(b) (InAs with $L_y = 150$ nm) still presents a phase diagram qualitatively similar to Fig. 2(a) although the second inequality of Eq. (15) is not well satisfied (see Table I in the Appendix). On the other hand, Figs. 2(c) and 2(d) show the modifications of the phase diagram as α increases in effective units. As anticipated, the deviations can even allow a Majorana state in perpendicular field ($\theta = 0$) in Fig. 2(d). However, so large spin orbit strengths give rise to complicated phase maps that strongly deviate from the analytical limits.

The strong-α effects seen in the lower panels of Fig. 2 are caused by the term $-\alpha y \sigma_y / l_z^2$ of Eq. (5). Indeed, this term effectively adds a component along y to the magnetic field. Therefore, the effective angle θ_e is such that $\theta_e > \theta$, thus explaining the downwards shift of the lower phase transition boundary in Figs. 2(c) and 2(d). Figures 2(a) and 2(b) do not change with other azimuthal angles, while in the strong-α diagrams [Figs. 2(c) and 2(d)] ϕ modifies the precise boundary positions for $\theta = 90^\circ$ (vertical lines), but not the horizontal asymptotes and the overall qualitative behavior. Note that, as mentioned in Sec. II, with $\phi \neq 0$ there is an additional requirement for the existence of Majorana modes, the projection rule $\Delta_B \sin\theta \sin\phi < \Delta_s$ [32,33]. However, the effective tilting of the magnetic field towards y caused by the term $-\alpha y \sigma_y / l_z^2$ does not modify the projection rule because this effective tilting is in opposite directions for positive and negative y's, while the projection rule applies only to homogeneous magnetic fields.

V. SEMI-INFINITE NANOWIRES

Explicit zero-energy eigenstates can be obtained in semi-infinite and finite nanowires in order to confirm the above phase diagrams. We have checked that either one or no Majoranas are obtained in the corresponding regions of Fig. 2. In the semi-infinite system exact zero-energy solutions can be studied with the complex band structure method of Refs. [31,32]. The calculation is carried out solving the boundary condition

$$\sum_k C_k \Psi^{(k)}_{s_\sigma, s_\tau}(y) = 0, \tag{16}$$

where the allowed complex wave numbers $\{k\}$ and the $\Psi^{(k)}_{s_\sigma s_\tau}(y)$ functions are obtained with the matching method discussed previously in Sec. III, with the only difference that k now is not vanishing.

Equation (16) can be reworked into

$$\sum_k \mathcal{M}_{k'k} C_k = 0, \tag{17}$$

with the matrix

$$\mathcal{M}_{k'k} = \sum_{s_\sigma, s_\tau} \int dy\, \Psi^{(k')*}_{s_\sigma, s_\tau}(y) \Psi^{(k)}_{s_\sigma, s_\tau}(y). \tag{18}$$

Equation (17) shows that, when enough wave numbers are included, each Majorana state is represented by a null-space eigenvector of matrix $\mathcal{M}$. In Fig. 3(a) we can see the convergence of the $\mathcal{M}$ eigenvalues with the cutoff in wave number for a particular point of Fig. 2(c). Clearly, the lower eigenvalue vanishes asymptotically indicating that for this point of the phase diagram a Majorana mode is present as expected. In Fig. 3(b) we can see the corresponding density function, confirming the edge character of the mode, as also expected for a Majorana.

Decay lengths

Within our complex-band-structure approach to the semi-infinite nanowire we can estimate the length of the Majorana decay tail from the imaginary part of the allowed wave numbers. The lower the imaginary part, the longer the Majorana decay tail (and thus the required length of the nanowire to contain it without distortion). Figure 4 shows

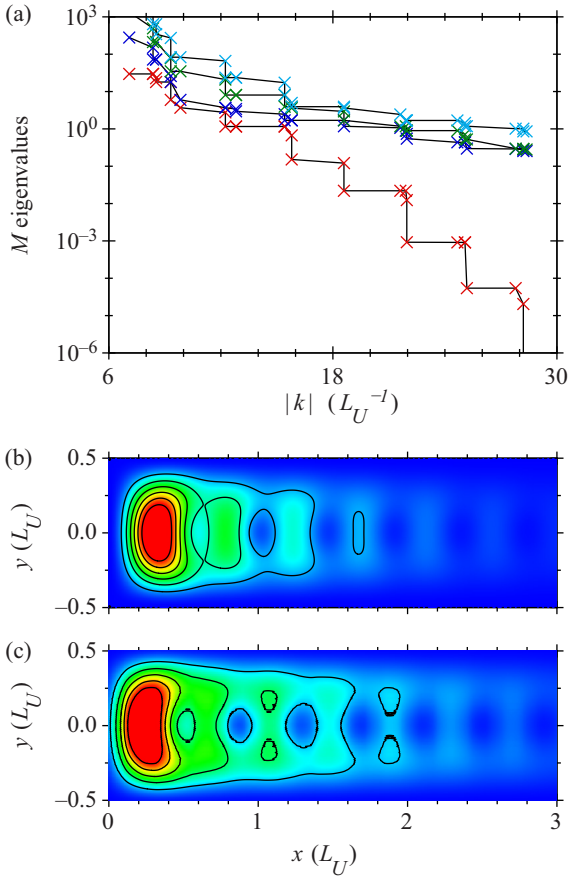

FIG. 3. (Color online) (a) Evolution of the lower eigenvalues of matrix $\mathcal{M}$ when increasing the number of evanescent modes, as given by a cutoff $|k|$. (b) Majorana density function in a semi-infinite nanowire for the null eigenvector of $\mathcal{M}$. (c) Majorana density function in a finite nanowire with $L_x = 20L_U$ calculated by direct diagonalization of the Hamiltonian using covariant derivative discretization. The three panels correspond to $\Delta_B = 10E_U$, $\theta = 75^\circ$ and the rest of the parameters as in Fig. 2(c).

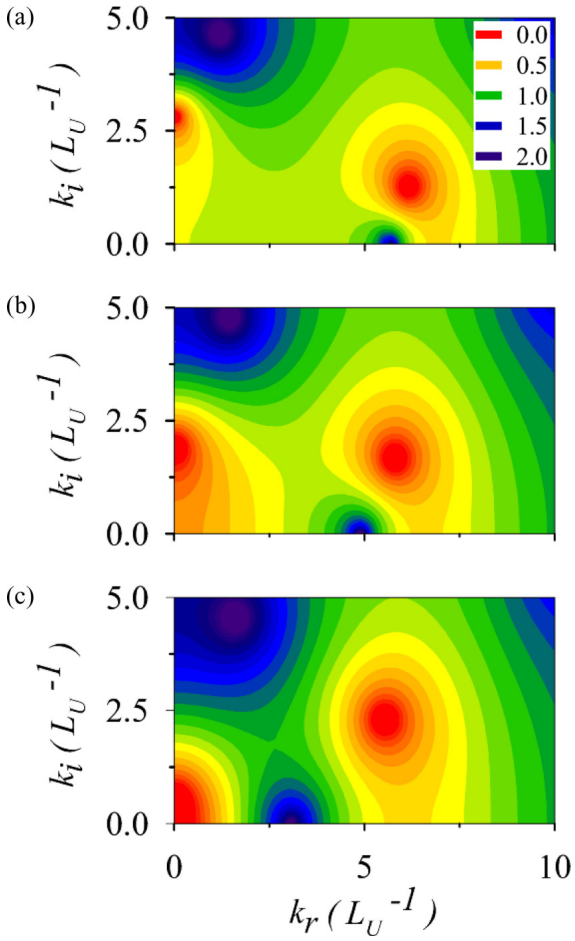

FIG. 4. (Color online) $\mathcal{F}$ measure in a color (gray) scale showing the position of the allowed wave numbers as zeros (red islands). The parameters used are $g = 15$, $m^* = 0.033$, $\alpha = \pi E_U L_U$, $\Delta_s = 3E_U$, and $\Delta_B = 10E_U$. Panels from top to bottom are for different polar angles: $\theta = 68^\circ$ (a), $\theta = 67^\circ$ (b), and $\theta = 66^\circ$ (c).

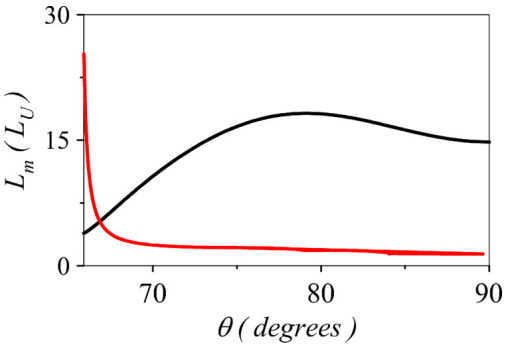

FIG. 5. (Color online) Mode lengths L_m (defined in Sec. V A) for the two wave numbers shown in Fig. 4. Note that the required nanowire length at each θ is the higher of both curves.

a typical evolution of the wave numbers (red islands) in the complex plane as the polar angle is approaching the critical value. In the sequence from upper to lower panels, one of the wave numbers moves along the imaginary axis towards the origin; the phase transition being signaled by one mode touching the origin (lower panel).

We calculate the required nanowire length with the smallest imaginary wave number of the set of all allowed wave numbers $\{k^{(m)}\}$. However, as shown in Fig. 4 the smallest imaginary part $\mathrm{Im}(k^{(m)}) \equiv k_i^{(m)}$ changes from an approximately fixed mode to the one touching the origin when approaching the phase transition. We define the mode length L_m as two times the length needed for the wave function to drop to one percent of its maximum, that is $e^{-k_i^{(m)} L_m/2} = 0.01$. An estimate of the nanowire length for undistorted Majoranas is simply the maximum of all mode lengths.

In Fig. 5 we show the mode lengths of the two allowed wave numbers of Fig. 4. As we decrease the polar angle from 90°, the needed nanowire length (the higher of the two curves) remains more or less stable until θ approaches the critical value. A few degrees before the transition the Majorana contracts before diverging to infinity at the phase transition angle.

VI. FINITE NANOWIRES

The phase diagram can also be checked with full diagonalizations of nanowires with large, but finite, L_x. Though more realistic, this approach is conceptually more qualitative, since finite-nanowire Majoranas are not exact zero modes but small energy modes (the smaller the energy the larger L_x). Equivalently, the phase boundaries become blurred due to the finite size effect. Figure 3(c) shows the density of the finite nanowire Majorana corresponding to the semi-infinite one of Fig. 3(b). Differences are small, just a slight distortion and a somewhat longer decay tail of the finite-nanowire density.

In the finite nanowire diagonalization with orbital terms we have found it crucial to use a covariant grid discretization [29,30]. Otherwise, numerical artificial biases wrongly suggest that Majoranas are always destroyed by orbital terms [36], in clear contradiction with the phase diagram (Fig. 2) and the semi-infinite wire analysis. In essence, the covariant discretization amounts to expressing the canonical momentum components as symmetrylike transformations. For instance,

$$\Pi_x \equiv -i\hbar\frac{\partial}{\partial x} - \hbar\frac{y}{l_z^2} = e^{iyx/l_z^2}\left(-i\hbar\frac{\partial}{\partial x}\right)e^{-iyx/l_z^2}. \qquad (19)$$

Although these two representations of the canonical operator are equivalent in the continuous limit, they are not on a discrete grid.

As demonstrated in Ref. [30] the covariant derivative preserves by construction the gauge invariance of the solutions, while a noncovariant treatment only does that for extremely fine discretizations, unfeasible in our case. Changing the gauge origin usually constitutes a severe difficulty for numerical discretizations not using covariant derivative formulations. In our case, we can introduce an arbitrary gauge center y_c for the canonical momentum, generalizing Eq. (19) to

$$\Pi_x = e^{i(y-s_\tau y_c)x/l_z^2}\left(-i\hbar\frac{\partial}{\partial x}\right)e^{-i(y-s_\tau y_c)x/l_z^2}, \qquad (20)$$

where the isospin sign $s_\tau = \pm$ is introduced in order to preserve the particle-hole symmetry of the Bogoliubov–de Gennes equation. We have checked that our numerical results for the finite nanowire diagonalization as, e.g., in the lower panel of Fig. 3, do not depend on the choice of y_c, thus proving the gauge invariance of the finite system results. We have also obtained good agreement of the finite nanowire diagonalizations and the results of the semi-infinite system regarding the existence or absence of a zero mode in the different regions of the phase diagrams (Fig. 2), again proving the reliability of the method. Notice that the semi-infinite solution, being purely 1D, can be obtained in very dense y grids, while the finite system 2D diagonalization requires much coarser xy grids.

VII. CONCLUSIONS

In this work we have shown that the orbital motions caused by perpendicular components of the magnetic field in planar 2D nanowires give rise to a rich phase diagram, with regions containing Majoranas for sizable vertical tilting of the magnetic field. In fact, with proper parameters, it is possible to find Majoranas in a fully perpendicular field. We have developed a general numerical method to obtain the Majorana phases in nanowires in a computer efficient way and we have checked this method against alternative calculations for semi-infinite and finite nanowires. Analytical expressions of the transition boundaries in asymptotic regions have been found. For realistic parameter values (weak α) these analytical expressions are a good approximation in general and not only asymptotically. In the strong orbital limit the critical angles are independent of sample details. Finally, the relevance of the covariant grid discretization for the finite nanowire diagonalization has been pointed out.

ACKNOWLEDGMENTS

We acknowledge useful discussions with R. López and D. Sánchez. This work was funded by MINECO-Spain (Grant No. FIS2011-23526), CAIB-Spain (Conselleria d'Educació, Cultura i Universitats), and FEDER.

APPENDIX: ANALYTICAL LIMITS

1. Longitudinal magnetic field

When the magnetic field is along x (see axis orientations in Fig. 1) the phase transition law is fully analytical. As discussed in Sec. III, finding the phase transition implies searching for the zero energy eigenstates of the simplified Hamiltonian h given in Eq. (9). For an x-oriented field $l_z^{-2} = 0$ and all orbital terms vanish. Assuming also a vanishing bottom potential for $V(y)$ we have

$$h = \left(\frac{p_y^2}{2m} - \mu\right)\tau_z + \Delta_s\tau_x + \left(\Delta_B - \frac{\alpha}{\hbar}p_y\tau_z\right)\sigma_x. \quad \text{(A1)}$$

The eigenstates of Eq. (A1) can be obtained analytically noticing that the linear p_y term from the Rashba interaction can be absorbed in the kinetic term

$$h = \left(\frac{\tilde{p}_y^2}{2m} - \frac{m\alpha^2}{2\hbar^2} - \mu\right)\tau_z + \Delta_s\tau_x + \Delta_B\sigma_x, \quad \text{(A2)}$$

where $\tilde{p}_y = p_y - m\alpha\sigma_x/\hbar$. Using a basis of square-well eigenstates of energies $\epsilon_n = \hbar^2\pi^2n^2/(2mL_y^2)$, the matrix to diagonalize is

$$h \equiv \begin{pmatrix} \epsilon_n - \mu - \frac{m\alpha^2}{2\hbar^2} & \Delta_s \\ \Delta_s & -\left(\epsilon_n - \mu - \frac{m\alpha^2}{2\hbar^2}\right) \end{pmatrix}. \quad \text{(A3)}$$

The diagonalization of this simplified Hamiltonian yields the eigenenergies

$$E_{ns_1s_2} = s_1\Delta_B + s_2\sqrt{\left(\mu - \epsilon_n + \frac{m\alpha^2}{2\hbar^2}\right)^2 + \Delta_s^2}, \quad \text{(A4)}$$

with $n = 1,2,\ldots, s_1 = \pm 1$, and $s_2 = \pm 1$. Of the four eigenenergies only the two with opposite s_1 and s_2 can lead to a zero energy solution at the critical values

$$\Delta_{B,n}^{(c)} = \sqrt{\left(\mu - \epsilon_n + \frac{m\alpha^2}{2\hbar^2}\right)^2 + \Delta_s^2}. \quad \text{(A5)}$$

Equation (A5) with $n = 1,2,\ldots$ gives the critical Zeeman parameter of phase transitions for a two dimensional nanowire in parallel magnetic field. Notice that in Eq. (A5) n has to be interpreted simply as an ordering index of the successive transitions, and not as a label of independent transverse modes. These latter interpretations would be wrong, since different transverse modes are coupled through the Rashba mixing term and one cannot associate a particular transverse mode with a particular transition point. Shaded regions in Fig. 6 contain one Majorana mode, while white regions have none. There are no regions with multiple Majoranas due to the energy splittings induced by the Rashba mixing in planar nanowires [27,31].

2. Strong orbital limit

When the kinetic orbital effect overcomes both the confinement by the transverse square well and the Rashba term, the magnetic length $l_z \equiv \sqrt{\hbar c/eB_z}$ is smaller than l_y (here we define $l_y = L_y$ of Fig. 1) and also smaller than the Rashba length $l_\alpha \equiv \hbar^2/m\alpha$. In the limit $l_z \ll (l_y, l_\alpha)$ it is possible to derive an analytical expression of the transition boundaries.

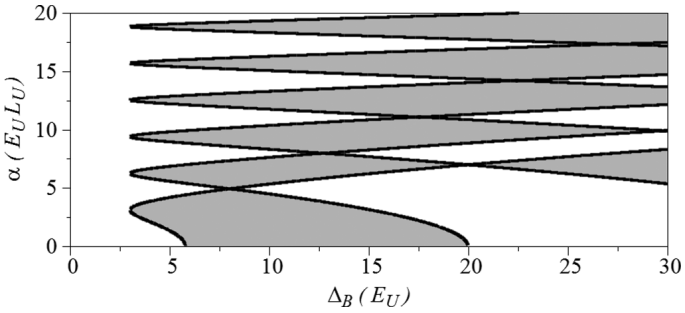

FIG. 6. Phase transition boundaries for a 2D planar nanowire with a longitudinal (x) magnetic field. We have assumed $\Delta_s = 3E_U$ and $\mu = 0$. The shaded regions correspond to topological phases with a Majorana zero mode.

Neglecting the square well $V(y)$ and the Rashba terms in Eq. (9) we find

$$h = \left(\frac{p_y^2}{2m} + \frac{\hbar^2}{2ml_z^4}y^2 - \mu\right)\tau_z + \Delta_B\vec{\sigma}\cdot\hat{n} + \Delta_s\tau_x. \quad \text{(A6)}$$

The eigenvalues of Eq. (A6) are straightforward in a basis $|ns_\sigma s_\tau\rangle$, where $n = 1,2,\ldots$ represent now harmonic oscillator eigenstates, $s_\sigma = \pm$ indicates spin eigenstates in direction $\hat{n}$, while $s_\tau = \pm$ indicates isospin in direction z. Since the h matrix is diagonal in spin, we can diagonalize each subspace independently. For instance, the matrix for $s_\sigma = +$ reads

$$\begin{pmatrix} \epsilon_n^{(ho)} - \mu + \Delta_B & \Delta_s \\ \Delta_s & -\left(\epsilon_n^{(ho)} - \mu\right) + \Delta_B \end{pmatrix}, \quad \text{(A7)}$$

with $\epsilon_n^{(ho)} = (n - 1/2)\hbar^2/ml_z^2$. The eigenvalues of Eq. (A7) are easily found, as well as those of the analogous matrix for spin $s_\sigma = -$.

The null-eigenvalue condition for h is now

$$\Delta_B = \sqrt{\left[(n - 1/2)\frac{\hbar^2}{ml_z^2} - \mu\right]^2 + \Delta_s^2}, \quad \text{(A8)}$$

that looks similar to Eq. (A5). An essential difference, however, is that the right-hand side in Eq. (A8) depends itself on the Zeeman parameter Δ_B through l_z. It is

$$\frac{\hbar^2}{ml_z^2} = \frac{4}{gm^*}\Delta_B\cos\theta, \quad \text{(A9)}$$

where m^* is the ratio of effective to bare mass, $m = m^*m_e$, while g is the gyromagnetic factor defined from the Zeeman parameter by $\Delta_B \equiv g\mu_B B/2$. From Eq. (A8) we finally arrive at the following relation:

$$\cos\theta = \frac{gm^*}{4}\frac{\sqrt{\Delta_B^2 - \Delta_s^2} + \mu}{\left(n - \frac{1}{2}\right)\Delta_B}. \quad \text{(A10)}$$

For large enough Δ_B, as compared to Δ_s and μ, this leads to the prediction of field-independent critical angles

$$\cos\theta_n^{(c)} = \frac{gm^*}{4\left(n - \frac{1}{2}\right)}, \quad \text{(A11)}$$

as given in Eq. (14).

The triple inequality $l_z \ll (l_y, l_\alpha, l_s)$, where we define $l_s \equiv \sqrt{\hbar^2/m\Delta_s}$, leads, when written in effective units, to Eq. (15). In this situation the phase diagram does not deviate much from the straight lines of the analytical limits, Eqs. (A5) and (A11). Table I contains the numerical values of the inequality sides for the four panels in Fig. 2. While panel (a) fulfills all conditions, for the rest of the panels the second inequality degrades as α increases from panel (b) to (d). This explains the deviations in those panels from the analytical limits.

[1] T. Chakraborty and P. Pietiläinen, *The Quantum Hall Effects* (Springer, New York, 1995).
[2] T. Ihn, *Semiconductor Nanostructures* (Oxford University Press, Oxford, 2010).
[3] J. Alicea, Rep. Prog. Phys. **75**, 076501 (2012).
[4] C. W. J. Beenakker, Annu. Rev. Condens. Matter Phys. **4**, 113 (2013).
[5] T. D. Stanescu and S. Tewari, J. Phys.: Condens. Matter **25**, 233201 (2013).
[6] M. Franz, Nat. Nanotechnol. **8**, 149 (2013).
[7] R. M. Lutchyn, J. D. Sau, and S. Das Sarma, Phys. Rev. Lett. **105**, 077001 (2010).
[8] Y. Oreg, G. Refael, and F. von Oppen, Phys. Rev. Lett. **105**, 177002 (2010).
[9] T. D. Stanescu, R. M. Lutchyn, and S. Das Sarma, Phys. Rev. B **84**, 144522 (2011).
[10] K. Flensberg, Phys. Rev. B **82**, 180516 (2010).
[11] S. Gangadharaiah, B. Braunecker, P. Simon, and D. Loss, Phys. Rev. Lett. **107**, 036801 (2011).
[12] C.-H. Lin, J. D. Sau, and S. Das Sarma, Phys. Rev. B **86**, 224511 (2012).
[13] J. Klinovaja and D. Loss, Phys. Rev. B **86**, 085408 (2012).
[14] D. Sticlet, C. Bena, and P. Simon, Phys. Rev. Lett. **108**, 096802 (2012).
[15] X.-J. Liu and A. M. Lobos, Phys. Rev. B **87**, 060504 (2013).
[16] L. Jiang, D. Pekker, J. Alicea, G. Refael, Y. Oreg, A. Brataas, and F. von Oppen, Phys. Rev. B **87**, 075438 (2013).
[17] F. Pientka, L. Jiang, D. Pekker, J. Alicea, G. Refael, Y. Oreg, and F. von Oppen, New J. Phys. **15**, 115001 (2013).
[18] P. San-Jose, E. Prada, and R. Aguado, Phys. Rev. Lett. **108**, 257001 (2012).
[19] V. Mourik, K. Zuo, S. Frolov, S. Plissard, E. Bakkers, and L. Kouwenhoven, Science **336**, 1003 (2012).
[20] M. T. Deng, C. L. Yu, G. Y. Huang, M. Larsson, P. Caroff, and H. Q. Xu, Nano Lett. **12**, 6414 (2012).
[21] A. Das, Y. Ronen, Y. Most, Y. Oreg, M. Heiblum, and H. Shtrikman, Nat. Phys. **8**, 887 (2012).
[22] A. D. K. Finck, D. J. Van Harlingen, P. K. Mohseni, K. Jung, and X. Li, Phys. Rev. Lett. **110**, 126406 (2013).
[23] Y. Peng, F. Pientka, L. I. Glazman, and F. von Oppen, Phys. Rev. Lett. **114**, 106801 (2015).
[24] S. D. Sarma, H.-Y. Hui, P. M. R. Brydon, and J. D. Sau, arXiv:1503.00594v1.
[25] R. M. Lutchyn, T. D. Stanescu, and S. Das Sarma, Phys. Rev. Lett. **106**, 127001 (2011).
[26] A. C. Potter and P. A. Lee, Phys. Rev. Lett. **105**, 227003 (2010).
[27] A. C. Potter and P. A. Lee, Phys. Rev. B **83**, 094525 (2011).
[28] P. San-Jose, E. Prada, and R. Aguado, Phys. Rev. Lett. **112**, 137001 (2014).
[29] M. Governale and C. Ungarelli, Phys. Rev. B **58**, 7816 (1998).
[30] S. Janecek and E. Krotscheck, Phys. Rev. B **77**, 245115 (2008).
[31] L. Serra, Phys. Rev. B **87**, 075440 (2013).
[32] J. Osca, D. Ruiz, and L. Serra, Phys. Rev. B **89**, 245405 (2014).
[33] S. Rex and A. Sudbø, Phys. Rev. B **90**, 115429 (2014).
[34] A. R. Akhmerov, J. P. Dahlhaus, F. Hassler, M. Wimmer, and C. W. J. Beenakker, Phys. Rev. Lett. **106**, 057001 (2011).
[35] J. Osca and L. Serra, Phys. Rev. B **88**, 144512 (2013).
[36] J. S. Lim, L. Serra, R. Lopez, and R. Aguado, Phys. Rev. B **86**, 121103 (2012).

4.5 Additional bibliography

[37] Qi y Zhang, Rev. Mod. Phys. **83**, 1057–1110 (2011)
[38] Wakatsuki et al, Phys. Rev. B **89**, 174514 (2014)
[39] M. Diez, J. P. Dahlhaus, M. Wimmer, and C. W. J. Beenakker Phys. Rev. B **86**, 094501 (2012)

Chapter 5

Quasi-particle current in planar Majorana nanowires

Javier Osca and Llorenç Serra
J. Phys.: Conf. Ser. **647**, 012063. Published 13 October 2015.

5.1 Objectives

In the preceding chapter we presented a computer efficient method to calculate the Majorana wavefunction with unprecedented spatial resolution. In this chapter we want to profit this high resolution to calculate the local currents of a planar hybrid Majorana nanowire.

It is well known that the local current density for a ballistic conductor is given in terms of the wavefunction by

$$\vec{j}(x,y) = \Re\left[\Psi^*(x,y)\left(-i\frac{\hbar}{m}\vec{\nabla}\right)\Psi(x,y)\right], \tag{5.1}$$

where $\Re$ is used for the real part of a complex number. In this chapter we generalize this expression to consider superconductors with Rashba spin orbit interaction inside an external magnetic field. The objective of this calculation is determining whether these currents are altered, and in what ways, in presence of vertical components of the magnetic field. Although these currents are difficult to measure in the closed nanowires considered in this work, ours is a prospective study with the aim to ease the path towards the understanding of more complicated open nanowires.

5.2 Methodology

We use the same methodology already presented in Chap. 4 to calculate the Majorana wavefunction. The only information needed to calculate the local currents is

the mentioned Majorana wavefunction and the Hamiltonian parameters. The local current new expression is obtained from the quasi-particle continuity equation,

$$\frac{\partial \rho}{\partial t} = -\nabla \cdot \vec{j} \,, \tag{5.2}$$

where $\rho \equiv |\Psi|^2$ is the Majorana probability density and $\vec{j}$ is the quasi-particle current. The physical ground of this equation is the conservation of probability, implying conservation of the number of quasi-particles.

5.3 Conclusion and remarks

We show how the pattern of local currents in a Majorana nanowire changes in absence or presence of vertical components of the magnetic field. In absence of vertical components of the magnetic field the current flows in closed paths without a preferred sense of circulation, forming alternatively clockwise and anticlockwise quasiparticle current vortices. On the other hand, if there is vertical component of the magnetic field the quasiparticle current circulates in an anticlockwise fashion only, the position of each vortex corresponding to a density maxima of the Majorana state.

5.4 Future work

As stated above, this is a prospective work made as previous step to the study of more complicated open nanowires. Differently from semi-infinite nanowires that end in a hard edge the open nanowires end with an interface to a normal region. Therefore, the systems of equations that arises from the edge condition $\Psi(0) = 0$ must be substituted for a new set of matching equations between the normal side and the Majorana nanowire. In this case the normalization condition will be given by the amplitude of the incident mode.

In addition, it would be useful to calculate the charge and spin currents. For example, an electron or hole moving in a left to right direction represent the same quasiparticle current but opposite charge current because they are opposite charge carrying quasiparticles. Therefore,

$$\vec{j_c}\,(x,y) = -e\Re\left[\Psi^*(x,y)\left(-i\frac{\hbar}{m}\vec{\nabla}\right)\tau_z\Psi(x,y)\right] , \tag{5.3}$$

$$\vec{j_s}\,(x,y) = \Re\left[\Psi^*(x,y)\left(-i\frac{\hbar}{m}\vec{\nabla}\right)\sigma_z\Psi(x,y)\right] , \tag{5.4}$$

where $\vec{j_c}$ is the charge current, $\vec{j_s}$ is the spin current and τ_z and σ_z are the corresponding Pauli matrices for spin and isospin degrees of freedom. The rest of the symbols have the same meaning as above.

In Fig. 5.1 we can see some preliminary results for the case of an open nanowire with a junction in $x = 0$. On the right side of the junction there is a Majorana nanowire while on the left side we can find out a normal lead. The Rashba coupling and the external magnetic field are considered to be constant all along the nanowire at both sides of the junction. This way we model a semiconductor nanowire with a section in proximity contact with a superconductor inside an homogeneous magnetic field. In Fig. 5.1a we can see the probability density and quasiparticle current while in Fig. 5.1b the charge density and current are shown.

From this result we derive two conclusions in relation with the proceedings article. First, the quasiparticle density and current in the Majorana side ($x > 0$) hold essentially the same features than the ones found in the close semi-infinite nanowire but they are perturbed in order to allow the coupling through the barrier. This coupling is summarized as an incident stream of electrons at $y > 0$ in the normal side of the nanowire reflected into and outgoing flow of holes at $y < 0$. Second, this two flows combine to create a flow of charge also in the normal side with a maximum in the center. Note that the maximum flow of charge coincides with a minimum flow of quasiparticles because it is the place where electron and hole flows cancel each other. Furthermore, there is zero charge at the position of the peak of Majorana probability density because a Majorana quasiparticle is neutral.

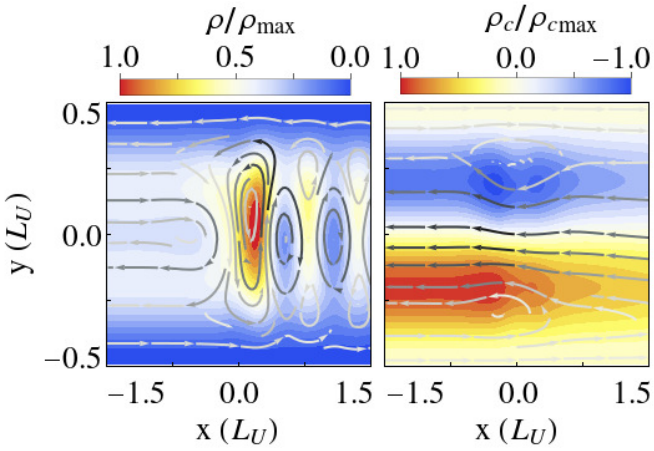

Figure 5.1: Quasiparticle current stream lines a) and charge current stream-lines b) for a normal-Majorana nanowire junction inside a titled magnetic field. The background in panel a) shows the probability density, while b) shows the charge density. In each case the fields are normalized to their respective maximum values. The junction is located at $x = 0$. From $x = -0.15L_U$ to $x = 0.15L_U$ a potential barrier is present with height $V = 5E_U$. The Rashba coupling $\alpha = 2E_U L_U$ has a value compatible with an InAs nanowire of 150 nm width. The magnetic field strength $\Delta_B = 12E_U$ and its polar and azimuthal angles are $\theta = 80°$ and $\phi = 0°$, respectively. The superconductor gap at the right side of the junction ($x > 0$) is $\Delta_s = 3E_U$.

5.5 Published paper

EDISON'19 IOP Publishing
Journal of Physics: Conference Series **647** (2015) 012063 doi:10.1088/1742-6596/647/1/012063

Quasi-particle current in planar Majorana nanowires

Javier Osca and Llorenç Serra

Institut de Física Interdisciplinària i de Sistemes Complexos IFISC (CSIC-UIB), E-07122 Palma de Mallorca, Spain
Departament de Física, Universitat de les Illes Balears, E-07122 Palma de Mallorca, Spain

E-mail: javier@ifisc.uib-csic.es

Abstract. We calculate the local quasi-particle current of a Majorana state in a planar hybrid (superconductor-semiconductor) nanowire. In absence of perpendicular components of the magnetic field the current flows in circular trajectories without a preferred orientation. On the other hand, when a perpendicular component of the magnetic field is present the quasi-particle current circulates surrounding the Majorana density peak with an orientation established by the magnetic field.

1. Introduction

Majorana modes appear in quasi-1D wires as effectively charge-less, zero-energy eigensolutions. They arise from the splitting, through a phase transition, of bulk electronic states into pairs of quasi-particles on the wire ends, each one being its own antiparticle [1, 2, 3, 4]. These phase transitions are known to occur at particular values of the magnetic field [5] giving rise to characteristic phase diagrams. Recently, we have investigated the role of the magnetic orbital motion on the physics of Majorana states. In Ref. [6] it is shown that in a planar nanowire the main effect of the orbital motion is to change the Majorana phase boundaries. In general, stationary Majorana states can sustain non-vanishing local quasi-particle currents. Furthermore, these currents are altered by the kinetic orbital motion caused by the off plane components of the magnetic field. In this proceedings article we extend the work of Ref. [6] studying the quasi-particle current present in planar Majorana nanowires with and without components of the magnetic field perpendicular to the nanowire surface.

2. Physical model

Majoranas can be obtained in nanowires due the combined effects of s-wave superconductivity, Rashba interaction and an external magnetic field. We consider a nanowire where the electronic motion is restricted to the $\hat{x}$ (longitudinal) and $\hat{y}$ (transverse) directions in presence of these three effects. The homogeneous magnetic field points in an arbitrary direction and the edges are modeled as infinite square well potentials in the longitudinal and transverse directions (see Fig. 1a). Therefore the nanowire physics is described by a Hamiltonian of the Bogoliubov-de Gennes kind

$$\mathcal{H}_{BdG} = \left(\frac{p_x^2 + p_y^2}{2m} + V(x,y) - \mu \right) \tau_z + \Delta_s \, \tau_x + \frac{\alpha}{\hbar} \left(p_x \sigma_y - p_y \sigma_x \right) \tau_z + \Delta_B \left(\sin\theta \cos\phi \, \sigma_x + \sin\theta \sin\phi \, \sigma_y + \cos\theta \, \sigma_z \right) , \tag{1}$$

EDISON'19 IOP Publishing
Journal of Physics: Conference Series **647** (2015) 012063 doi:10.1088/1742-6596/647/1/012063

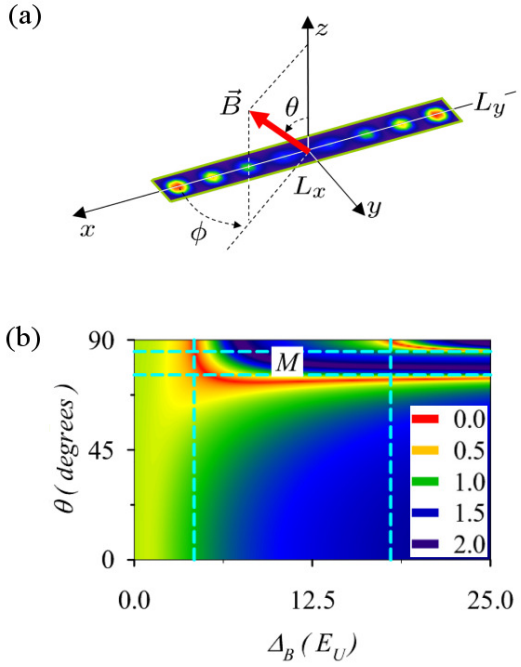

Figure 1. a) Schematic of a 2D planar nanowire showing the axis definitions. The density distribution of Majorana modes on the wire ends is qualitatively shown. b) Phase transition proximity measure with phase transitions (at zero value) in red, as a function of Δ_B and polar angle θ. The azimuthal angle remains $\phi = 0$. The results correspond to an InAs nanowire with $\alpha = 30\,\text{meVnm}$, $\Delta_s = 0.3\,\text{meV}$, gyro-magnetic factor $g = 15$, effective mass ratio $m^* = 0.033$, and $L_y = 150\,\text{nm}$ in a magnetic field range from zero to 6 T. Both figures taken from Ref. [6].

where the different terms are, in left to right order: kinetic energy, electrical potential V, chemical potential μ, the superconductor term with strength Δ_s, the Rashba spin orbit interaction term with coupling strength α and finally, the Zeeman term of a magnetic field of magnitude Δ_B and arbitrary polar and azimuthal angles $(\theta, \phi) \equiv \hat{n}$. The Pauli operators for isospin (particle-hole) are represented by $\tau_{x,y,z}$ while those for spin are $\sigma_{x,y,z}$. In a planar nanowire the perpendicular component of the magnetic field induces orbital motions of the nanowire quasi-particles through the substitution $\vec{p} \to \vec{p} + \frac{e}{c}\vec{A}(x,y)$ in the kinetic and Rashba terms (using the $e > 0$ convention). The additional orbital terms obtained with this substitution in Eq. (1) are given in Ref. [6].

The semi-infinite nanowire exact zero-energy solution can be obtained by means of the complex band structure method of Refs. [6, 7]. More specifically, the infinite nanowire eigensolutions are obtained numerically from the effective one dimensional Hamiltonian. Imposing the boundary condition to a superposition of infinite-nanowire solutions with different wave numbers yields the Majorana edge state. This method has the advantage of being computationally effective in comparison with direct diagonalization methods, even with fine spatial grids, and can also be used to obtain the phase diagram of a Majorana nanowire inside a tilted magnetic field as shown in Fig. 1b. In particular, a phase transition proximity measure is displayed where phase boundaries (zero values) appear as red lines, and the regions with a Majorana mode are labeled with an M while regions without a Majorana are not labeled. Dashed lines indicate the phase transition analytical limits

$$\Delta_{B,n}^{(c)} = \sqrt{\left(\mu - \epsilon_n + \frac{m\alpha^2}{2\hbar^2}\right)^2 + \Delta_s^2}\,, \tag{2}$$

and

$$\theta_n^{(c)} = \arccos\left(\frac{gm^*}{4(n-\frac{1}{2})}\right)\,, \tag{3}$$

where $n = 1, 2, 3, \ldots$. We refer to Ref. [6] for further details. The results are presented in characteristic units of the problem obtained by taking $\hbar$, m and the width of the nanowire

EDISON'19 IOP Publishing
Journal of Physics: Conference Series **647** (2015) 012063 doi:10.1088/1742-6596/647/1/012063

L_y as reference values. That is, our length and energy units are, respectively, $L_U \equiv L_y$ and $E_U \equiv \hbar^2/mL_y^2$.

3. Quasiparticle current

The quasi-particle continuity equation for the Hamiltonian of Eq. (1),

$$\frac{\partial \rho(x,y)}{\partial t} = -\nabla \cdot \vec{j}(x,y) \ , \tag{4}$$

is obtained from the Majorana probability density $\rho(x,y) = \Psi(x,y)\Psi^*(x,y)$ and the time dependent Schrödinger equation $i\hbar\partial_t\Psi(x,y) = \mathcal{H}_{BdG}\Psi(x,y)$, where $\Psi(x,y)$ is defined as the four-component spinor $\Psi \equiv (\psi_{++}, \psi_{-+}, \psi_{+-}, \psi_{--})^T$ in spin and isospin space. The rate of change of the Majorana density depends on the divergence of the quasi-particle current

$$\vec{j}(x,y) = \Re\left[\, \Psi^*(x,y)\, \hat{v}\, \Psi(x,y) \,\right] \ , \tag{5}$$

that is directly proportional to the real part of the velocity operator $\hat{v} \equiv (\hat{v}_x, \hat{v}_y)$, where $\hat{v}_x = \partial\mathcal{H}/\partial p_x$ and $\hat{v}_y = \partial\mathcal{H}/\partial p_y$, in the same way as in Ref. [8]. For our particular Hamiltonian the x and y components of the velocity operator read

$$\hat{v}_x = -i\frac{\hbar}{m}\partial_x\tau_z + \frac{e}{mc}A_x(x,y) + \frac{\alpha}{\hbar}\sigma_y\tau_z \ , \tag{6}$$

$$\hat{v}_y = -i\frac{\hbar}{m}\partial_y\tau_z + \frac{e}{mc}A_y(x,y) - \frac{\alpha}{\hbar}\sigma_x\tau_z \ . \tag{7}$$

As the density is constant in time, the resulting current has zero divergence, $\nabla \cdot \vec{j} = 0$. Equation (5) can be rewritten as the sum of a familiar quasi-particle current for non Rashba superconducting devices [9, 10], plus a Rashba current $\vec{j}_{so}$

$$\vec{j}(x,y) = \frac{\hbar}{m}\Im\left[\, \Psi^*(x,y)\, \nabla\tau_z\, \Psi(x,y) \,\right] + \frac{e}{mc}\,\rho(x,y)\,\vec{A}(x,y) + \vec{j}_{so}(x,y) \ , \tag{8}$$

where

$$\vec{j}_{so}(x,y) = \frac{\alpha}{\hbar}\Re\left[\, \Psi^*(x,y)\, (\sigma_y\hat{x} - \sigma_x\hat{y})\tau_z\, \Psi(x,y) \,\right] \ . \tag{9}$$

In this form it is possible to recover the usual expression for the current in absence of Rashba and superconductivity [9, 10] making the Rashba strength α zero and removing τ_z.

4. Results

We can see in Figs. 2a and 2b the quasi-particle current streamlines with the Majorana density $\rho(x,y)$ in the background, for two cases. In the first one (Fig. 2a) the magnetic field points along the longitudinal direction of the nanowire ($\theta = 90°$) while in the second one (Fig. 2b) the magnetic field has a component perpendicular to the surface of the nanowire ($\theta = 75°$). We notice that the current field is modified by the electronic orbital motion in the second case.

The main effect of the Majorana, in terms of quasi-particle transport, is to create circulating currents. For the longitudinally oriented magnetic field there is no preferred circulation orientation. As shown in Fig. 2c, the (z-component) rotational of the current has a maximum near the Majorana density peak and a minimum between the main and the secondary Majorana peaks. In the second case, with a perpendicular component of the magnetic field, a circulation orientation is enhanced over the other. We can see a strong current circulation around the Majorana density peak (see Fig. 2d) creating a maximum in the rotational near that point. This has similarities to what happens to the current near vortices in p-wave superconductors. On the other hand, the region of high circulating current around the Majorana peak is surrounded by regions of low or no current near the edges of the nanowire. This gives rise to minima in the value of the rotational.

EDISON'19 IOP Publishing
Journal of Physics: Conference Series **647** (2015) 012063 doi:10.1088/1742-6596/647/1/012063

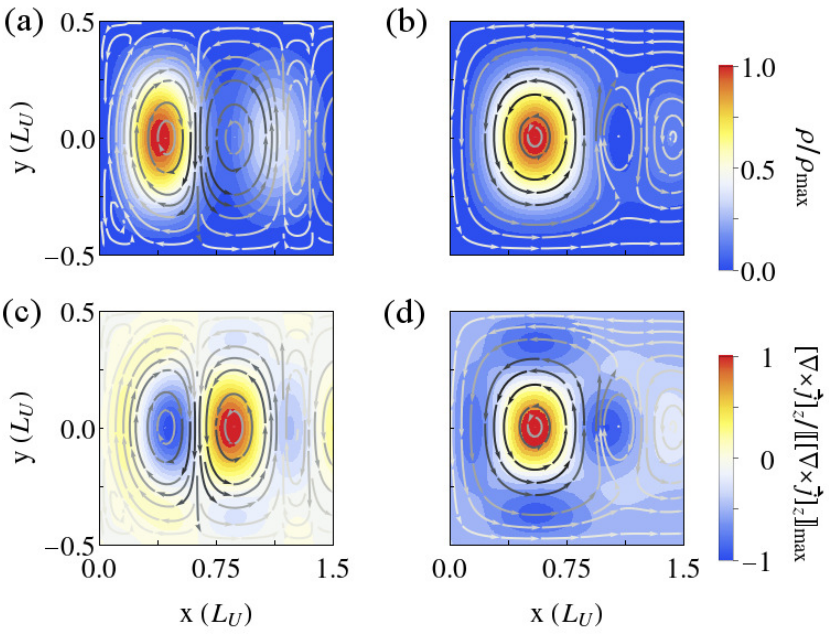

Figure 2. Current ($\vec{j}$) streamlines for longitudinal (a, c) and tilted field (b, d). The background in panels (a, b) shows the density, while in (c, d) it shows the z-component of the rotational $[\nabla \times \vec{j}]_z$. In each case the fields are normalized to their respective maximum values. The parameters are the same of Fig. 1. The streamlines are colored in a gray scale to show the regions of maximum current in black and the regions of zero current in white.

5. Conclusions

We have extended the study of Ref. [6] by calculating the local current associated with the Majorana state. We have shown that the main effect is the emergence of circulating currents. These currents follow closed trajectories without a preferred direction of circulation, in absence of a perpendicular component of the magnetic field. On the other hand, when a perpendicular component is present a quasi-particle current circulates around the Majorana peak in a vortex-like scenario. These quasi-particle currents may be difficult to measure experimentally in closed nanowires. However, in future work we will address the study of how these quasi-particle currents may change in open Majorana nanowires where they give a contribution to the nanowire conductance.

6. Acknowledgments

This work was funded by MINECO-Spain (grant FIS2011-23526), CAIB-Spain (Conselleria d'Educació, Cultura i Universitats) and FEDER. We hereby acknowledge the PhD grant provided by the University of the Balearic Islands.

References

[1] Alicea J 2012 *Rep. Prog. Phys.* **75** 076501
[2] Beenakker C W J 2013 *Annu. Rev. Condens. Matter Phys.* **4** 113
[3] Stanescu T D and Tewari S 2013 *J. Phys. Condens. Matter* **25** 233201
[4] Franz M 2013 *Nature Nanotechnology* **8** 149
[5] Lutchyn R M, Stanescu T D and Das Sarma S 2011 *Phys. Rev. Lett.* **106**(12) 127001
[6] Osca J and Serra L 2015 *Phys. Rev. B* **91**(23) 235417
[7] Serra L 2013 *Phys. Rev. B* **87** 075440
[8] Molenkamp L W, Schmidt G and Bauer G E W 2001 *Phys. Rev. B* **64**(12) 121202
[9] Vignale G and Rasolt M 1988 *Phys. Rev. B* **37**(18) 10685–10696
[10] Beenakker C 1992 *Low-Dimensional Electronic Systems* (*Springer Series in Solid-State Sciences* vol 111) ed Bauer G, Kuchar F and Heinrich H (Springer Berlin Heidelberg) pp 78–82 ISBN 978-3-642-84859-9

Chapter 6

Electromagnetic absorption of quasi-1d Majorana nanowires

Javier Osca and Llorenç Serra
Phys. Status Solidi C **12**, No. 12, 1409-1411. Published 31 July 2015.

6.1 Objectives

Present Majorana detection experiments are heavily based on their transport properties. As discussed in Chap. 1, these experiments aim at detecting a peak of conductance at zero energy. However, it has been pointed out that other mechanisms can be responsible for that peak. The previous chapters where we calculate the Majorana phase diagram are intended to provide some help in this issue. However, here we take a different approach. The main objective of this chapter is to study the feasibility of using the Majorana optical absorption properties as a possible detection method. This chapter in particular is an extension of Ref. [13], of which the author of this thesis is also co-author. In this chapter we want to calculate the optical absorption of Majorana nanowires in the quasi-1d limit of very long and narrow nanowires.

6.2 Methodology

The methodology used here requires two steps. First the Hamiltonian is numerically diagonalized using similar techniques to those of the preceding chapters. However, the main difference from those chapters is the use of a mixed-basis approach. Instead of spatially discretizing the nanowire in the longitudinal and transversal directions, the nanowire is discretized only in the longitudinal direction. The transverse degree of freedom is described in a basis of square well eigenstates. Therefore our basis depends on the position x, the quantum number n of the transverse square well

and the spin and isospin degrees of freedom. Once we have calculated the nanowire spectrum the absorption cross section is calculated for a classical electromagnetic field in the dipole approximation.

A question that may arise is how this model takes into consideration the protection against noise between topological states. This is a question not covered in this proceedings article but it was answered in Ref. [13]. First, we should clarify which states are protected from what in which conditions. Topological states form a degenerate set of states living at zero energy protected one from another in a way that only nontrivial changes in the device (i.e. braiding) will lead to a transition from one to another. From a strict topological point of view it is said that no local operator can couple two topological states $\langle 1|O(x)|2\rangle = 0$. Where $|1\rangle$ and $|2\rangle$ are two topological states and $O(x)$ is an arbitrary local operator. In this sense, two topological states are protected from each other against the presence of an external electromagnetic field but this does not happen with two non topological states, neither between topological and non topological states. This protection is achieved thanks to the gap that separates the two kind of states and that protection will be as big as the gap itself.

Therefore, in presence of an external electromagnetic field we will find two kind of transitions. Transitions of type I between states out of the gap and transitions of type II between a Majorana state and out of the gap states. However, we will not find transitions between Majorana states. Note that, transitions of type II will arise even if the electromagnetic field excites only certain section of the nanowire in a local way. Nevertheless, this is not in contradiction with the known Majorana physics because topological states will remain protected between themselves. On the other hand, to obtain signatures of absorption the amplitude of the external electromagnetic field must be big enough to overcome the gap width. In this sense we are assuming a model that considers the external electromagnetic field as a controlled element of the experiment and not like random noise.

In a simple nanowire model two energy degenerated topological states arise at zero energy. In Ref. [13] is demonstrated that in this particular model the protection of these states is guaranteed by means of the particle hole symmetry. Essentially, the absorption amplitude in the dipole approximation is proportional to the matrix element of the momentum operator. Here, the main point is that this matrix element between particle-hole conjugate states is zero

$$\langle \Psi_E | \, \vec{p} \, | \Psi_{-E} \rangle = \langle \Psi_E | \, \vec{p} \Theta \, | \Psi_E \rangle = 0 \, . \tag{6.1}$$

Therefore no transition is possible between the two conjugate Majorana states and the protection between them is guaranteed. To see signatures of Majoranas in the absorption spectrum we need to use a radiation amplitude high enough to excite type II transitions from Majorana states to states out of the gap.

6.3 Conclusions and remarks

The main conclusion of this work is that there are clear Majorana signatures in the absorption spectrum of the nanowire, provided that we use light polarized in the nanowire transverse direction. The typical nanowire dimensions and materials are the same considered in Chaps. 4 and 5. For these typical values of the Majorana nanowire the absorbed light would have a frequency of around 100 GHz. This frequency is in the microwave region and is experimentally feasible with the current technology.

6.4 Published paper

Phys. Status Solidi C **12**, No. 12, 1409–1411 (2015) / **DOI**10.1002/pssc.201510131

Electromagnetic absorption of quasi-1D Majorana nanowires

Javier Osca[*,1] **and Llorenç Serra**[1,2]

[1] Institut de Física Interdisciplinària i de Sistemes Complexos IFISC (CSIC-UIB), 07122 Palma de Mallorca, Spain
[2] Departament de Física, Universitat de les Illes Balears, 07122 Palma de Mallorca, Spain

Received 22 June 2015, accepted 12 July 2015
Published online 31 July 2015

Keywords Majorana modes, semiconductor wires, electromagnetic absorption

[*] Corresponding author: e-mail javier.osca@uib.es, Phone: +34-971259880, Fax: +34-971173248

We calculate the electromagnetic absorption cross section of long and narrow nanowires, in the so-called quasi-1D limit. We consider only two transverse bands and compute the dipole absorption cross section taking into account quasiparticle transitions from negative to positive energy eigenstates of the Bogoliubov-de Gennes Hamiltonian. The presence of the zero energy (Majorana) state manifests in the different absorption spectra for x (parallel) and y (transverse) polarizations of the electromagnetic field. In the y-polarized case, the Majorana state causes a low energy absorption plateau extending from mid-gap up to full-gap energy. Increasing further the energy, the plateau is followed by a region of enhanced absorption due to transitions across the full gap. For x polarization the low energy absorption plateau is not observed.

1 Introduction The physics of Majorana states in semiconductor nanowires has been attracting much attention in recent years [1–4]. There is a fundamental motivation, as they are a novel realization of the physics envisioned by Majorana for a class of elementary particles already in 1937 [5]. Majorana states in semiconductor nanowires are also interesting from the point of view of technological applications. Indeed, it has been suggested that their character of nonabelian anyons with topological protection could be exploited for implementing quantum computation in practice [6].

Several electrical transport experiments with semiconductor nanowires have observed a zero bias peak for a certain range of magnetic fields, consistent with a zero energy Majorana state [7–10]. The observed peak height is, however, an order of magnitude lower than the quantized value $2e^2/h$. This discrepancy is not yet well understood, as it might be due to effects ranging from finite temperature, experimental and tunneling resolutions to other low-energy subgap states and possible inelastic and renormalization processes [11, 12]. It is, therefore, important to characterize the Majorana mode and its role in different experimental signals in order to ascertain the existence of such peculiar states.

In Ref. [13] we investigated the role of the Majorana state on the optical absorption of 2D semiconductor nanowires. It was suggested that the Majorana causes a low energy absorption feature, observed when the polarization of the electromagnetic (EM) field is in transverse direction to the nanowire (Fig. 1). We used a grid approach, whereby the xy plane was discretized in a mesh of points and the Bogoliubov-de Gennes eigenvalue equation was trans-

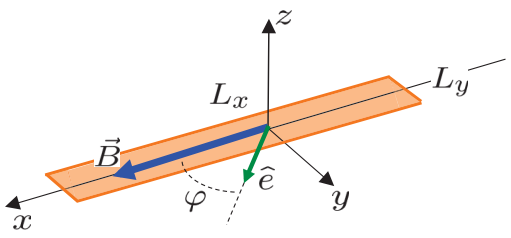

Figure 1 Sketch of the system.

physica status solidi c

formed into a matrix diagonalization problem using finite differences on the grid. A shortcoming of that method is the high computational cost for fine grids, that aggravates when a large number of Hamiltonian eigenstates need to be obtained. Indeed, the absorption cross section is the result of many quasiparticle transitions from occupied to empty eigenstates (see Fig. 2).

In this work we extend the analysis of Ref. [13] by focussing on the quasi-1D limit of very long and narrow nanowires. We use a mixed grid-basis approach, discretizing the longitudinal x coordinate in a grid and describing the transverse y degree of freedom in a basis of square well eigenstates (Fig. 1 contains the axis definitions). As we are interested in the case of narrow wires, we will restrict to only two transverse states. This technique is computationally less demanding and it will allow us the calculation of large numbers of eigenstates, thus better characterizing the absorption cross section.

2 Model and linear absorption formalism We use the model and notation already described in Ref. [13], to which the reader is addressed for the details. The Hamiltonian reads

$$\mathcal{H}_{BdG} = \left[\frac{p_x^2+p_y^2}{2m} + V(x,y) - \mu\right]\tau_z + \Delta_B\,\sigma_x + \Delta_0\,\tau_x + \frac{\alpha}{\hbar}(p_x\sigma_y - p_y\sigma_x)\tau_z\ , \quad (1)$$

where the potential $V(x,y)$ is a hard wall confinement to a rectangle of lengths L_x and L_y, with $L_y << L_x$. Equation (1) contains the three mechanisms giving Majorana physics with semiconductor nanowires. Namely, these are the Zeeman (Δ_B), superconductivity (Δ_0) and Rashba spin-orbit (α) interactions. As a consequence of particle-hole symmetry the eigenstates of $\mathcal{H}_{BdG}$ always come in pairs of energy $\pm E_i$, with $i = 1, 2, \ldots$. When a critical value of the Zeeman parameter is surpassed the system presents a pair of solutions at very small energies $E_1 = \pm\epsilon$, which is signaling the Majorana phase transition (Fig. 2).

We present the results in effective length (L_U) and energy ($E_U = \hbar^2/mL_U^2$) units. For definiteness, we take $L_U = 150\,\mathrm{nm}$ and $E_U = 0.1\,\mathrm{meV}$. We also assume $m = 0.033\,m_e$ and $\alpha = 47\,\mathrm{meVnm}$, typical values for InAs nanowires. With a gyromagnetic factor of $g = 15$ the maximum Zeeman energy in Fig. 2 ($20\,E_U$) corresponds to $\approx 4.4\,\mathrm{T}$.

The dipole absorption cross section, in the limit of weak EM field, is given by the eigenstate transitions,

$$\sigma(\omega) \approx \sum_{k,s} \frac{|\langle k|\mathbf{p}\cdot\hat{e}|s\rangle|^2}{\omega_{ks}}\,\delta(\omega-\omega_{ks})\,f_s\,(1-f_k)\ , \quad (2)$$

where $f_{s,k}$ are the occupations of levels s, k as given by Fermi functions with a given temperature T, and $\hat{e}$ is a unitary vector giving the polarization direction of the EM field. Below, we will restrict for simplicity to the limit of vanishing temperature where only transitions from negative to positive energy eigenstates contribute to Eq. (2), as sketched in Fig. 2.

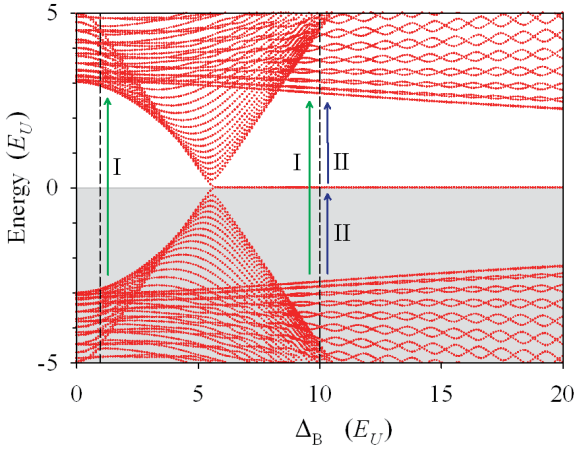

Figure 2 Evolution of the quasiparticle energy levels with the Zeeman energy. A zero energy mode is seen for $\Delta_B > 5E_U$. The vertical dashed lines signal two values of Δ_B for which the cross section is shown in Fig. 3. The shaded region is the Dirac sea of occupied quasiparticles with negative energies. The arrows indicate the transitions across the full gap (I) and across the mid gap (II). The latter are possible only in presence of the Majorana state. Parameters: $\Delta_0 = 3\,E_U$, $\alpha = 3.1\,E_U L_U$, $\mu = 20\,E_U$, $L_y = 0.5\,L_U$, $L_x = 30\,L_U$.

The eigenstates of $\mathcal{H}_{BdG}$ are obtained in a mixed representation, using a space grid in x and a set of square well eigenstates $\phi_n(y)$ in the transverse direction,

$$\Psi \equiv \sum_{n=1,2,\,s_\sigma,s_\tau=\pm} \psi_{ns_\sigma s_\tau}(x)\,\phi_n(y)\,\chi_{s_\sigma}(\eta_\sigma)\,\chi_{s_\tau}(\eta_\tau)\ . \quad (3)$$

The unknown functions $\psi_{ns_\sigma s_\tau}(x)$ are found on the grid by matrix diagonalization. We are interested in the limit of narrow wires and will thus restrict to only two transverse modes $n = 1, 2$. This is the minimum needed in order to account for the possibility of dipole excitations in transverse polarization, i.e., with a p_y operator in Eq. (2).

3 Results Figure 2 displays the energy eigenstates as a function of the Zeeman parameter for a selected case. The Majorana phase transition is clearly seen. For vanishing field the spectrum has a gap of $\approx 2\Delta_0$ ($6\,E_U$); this is followed by an intermediate region without a clear gap and, at large-enough fields, the gap is approximately restored with the qualitative difference of the Majorana pair of eigenstates lying right in the middle of the main gap. Of this particular pair, one state is infinitesimally below zero while the other is infinitesimally above. We may thus expect mid-gap transitions, labelled as II in Fig. 2. We notice here that dipole transitions between the two states of a given pair are forbidden because of particle-hole symmetry [13].

Contributed Article

Phys. Status Solidi C **12**, No. 12 (2015) 1411

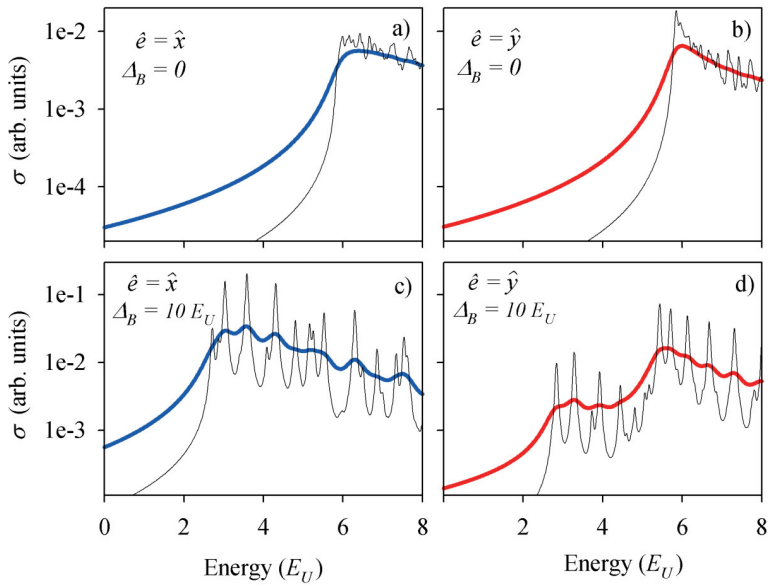

Figure 3 Absorption cross sections for the spectra of Fig. 2, corresponding to the Zeeman values indicated by dashed lines in that figure. Left and right panels are for $\hat{x}$ and $\hat{y}$ polarizations, respectively. In each panel, thin lines resolve individual peaks while thick lines are the smoothened absorptions obtained with larger averaging widths of the Lorentzian peaks. A lower absorption plateau starting around mid gap energy ($\approx 3\,E_U$), caused by the Majorana state, is clearly seen in panel d).

The dipole cross sections corresponding to the eigenstates of Fig. 2 for two selected values of Δ_B are shown in Fig. 3. The delta peaks of Eq. (2) have been replaced by Lorentzian functions of width Γ that could represent the experimental resolution of the apparatus. We show both the result for a low Γ, resolving the individual transitions, and for a high Γ, yielding a smoothened absorption profile. As expected, for vanishing magnetic field absorption occurs only above the full gap ($\approx 6\,E_U$) and there is no significant difference between x and y polarizations (upper panels).

The emergence of the Majorana state causes two remarkable modifications (lower panels in Fig. 3). First, absorption starts at mid-gap energy $\approx 3\,E_U$ due to transitions of type II from and to the Majorana pair of states. Second, there is a qualitative difference between x and y polarizations. For x polarization there is a rather featureless smooth absorption once the mid-gap threshold is overcome. For y polarization, however, there is a lower absorption plateau extending from mid-gap to full-gap energies, followed by an enhanced absorption once the full-gap energy is exceeded. The differences between x and y polarization in presence of a Majorana state were already suggested in Ref. [13]. However, in that work the number of eigenstates was truncated to lower values and thus the absorption for higher energies was less converged than in this work.

4 Conclusions We have improved the analysis of Ref. [13] of the EM absorption of Majorana wires in the quasi-1D limit by considering larger sets of eigenstates. We confirm that the differences between x and y polarized absorptions are an important signature of the presence of the Majorana state. In particular, with y polarization the Majorana mode causes a low-energy absorption plateau, from mid-gap to full-gap energies, followed by an enhanced absorption once the full-gap energy is exceeded. The present method can be easily extended to consider the effect of optical masks covering parts of the nanowire or other quasi-1D geometries like L-junctions.

Acknowledgements This work was funded by MINECO-Spain (grant FIS2011-23526), CAIB-Spain (Conselleria d'Educació, Cultura i Universitats) and FEDER. We hereby acknowledge the PhD grant provided by the University of the Balearic Islands.

References

[1] J. Alicea, Rep. Prog. Phys. **75**, 076501 (2012).
[2] C. W. J. Beenakker, Annu. Rev. Condens. Matter Phys. **4**, 113 (2013).
[3] T. D. Stanescu and S. Tewari, J. Phys.: Condens. Matter **25**, 233201 (2013).
[4] M. Franz, Nature Nanotechnol. **8**, 149 (2013).
[5] E. Majorana, Nuovo Cimento **14**, 171–184 (1937).
[6] C. Nayak, S. H. Simon, A. Stern, M. Freedman, and S. Das Sarma, Rev. Mod. Phys. **80**, 1083 (2008).
[7] V. Mourik, K. Zuo, S. Frolov, S. Plissard, E. Bakkers, and L. Kouwenhoven, Science **336**, 1003–1007 (2012).
[8] M. T. Deng, C. L. Yu, G. Y. Huang, M. Larsson, P. Caroff, and H. Q. Xu, Nano Lett. **12**(12), 6414–6419 (2012), PMID: 23181691.
[9] A. Das, Y. Ronen, Y. Most, Y. Oreg, M. Heiblum, and H. Shtrikman, Nature Phys. **8**, 887 (2012).
[10] A. D. K. Finck, D. J. Van Harlingen, P. K. Mohseni, K. Jung, and X. Li, Phys. Rev. Lett. **110**, 126406 (2013).
[11] Y. Peng, F. Pientka, L. I. Glazman, and F. von Oppen, Phys. Rev. Lett. **114**, 106801 (2015).
[12] S. D. Sarma, H. Y. Hui, P. M. R. Brydon, and J. D. Sau, arXiv:1503.00594v1 (2015).
[13] D. Ruiz, J. Osca, and L. Serra, J. Phys.: Condens. Matter **27**(12), 125302 (2015).

Chapter 7

Majorana mode stacking, robustness and size effect in cylindrical nanowires

Javier Osca, Rosa López and Llorenç Serra
Eur. Phys. J. B **87**, 84. Published 9 April 2014.

7.1 Objectives

In previous chapters we have dealt with the physics of 1d and quasi-1d nanowires. However, as mentioned in Chaps. 1 and 4, real 3d nanowires such as those of Ref. [22] and other similar experiments are approximately cylindrical. In Ref. [20] it was already addressed the question whether a cylindrical nanowire could or could not hold a Majorana state. The proposed model, that is also used in this chapter, is a 2d closed cylindrical shell. This model is grounded in the layer structure of the semiconductor materials of the nanowire as well as on the metallic-like behavior of the proximity induced superconductor that forces the electronic motion in the nanowire to be confined at the surface. Furthermore, this same metallic behavior leads to an orbital motion of the quasi-particles in presence of components of the magnetic field perpendicular to the surface. In this particular case the orbital terms are different of those presented in Chap. 4 because of the different geometry.

In Ref. [20] it was also shown that no Majoranas are possible when the electric field responsible for the Rashba term points in the radial direction of the nanowire. A priori, this might seem the most natural choice for a cylindrical geometry because, experimentally, it is the direction of growth of the nanowire semiconductor layers. In that reference, however, it was proposed to consider an externally induced electric field perpendicular to the nanowire in order to produce Majorana states. This electric field has a fixed spatial direction and may originate in the background materials on which the nanowire is deposited. In this new configuration it was discovered the *stacking effect*, an anti-intuitive result that for high values of the external magnetic field it is possible to find out more than one Majorana on the same edge. More de-

tailed physical explanation or further study about the robustness of these Majoranas was left for future work.

The work presented in this chapter is a direct continuation of Ref. [20]. The main objective of the article presented below is the determination of the Majorana mode robustness for different tiltings of the magnetic field in cylindrical shells. Furthermore, the robustness against variation of other parameters is also checked, specially in those cases that imply a change in the number of Majorana modes active in each end. Finally, the wavefunctions of the different Majorana modes are calculated to uncover the reason of the stacking effect allowing many Majorana modes to coexist in the same edge without annihilating in pairs.

7.2 Methodology

The main method used here is the diagonalization of the Hamiltonian using the eigenstates of the confinement as a basis. In other words, we use the basis of states $|nms_\sigma s_\tau\rangle$, where n is the quantization number of the infinite square well in the longitudinal direction of the nanowire (z direction), m is the eigenvalue of the angular momentum in the same direction L_z, while s_σ and s_τ are, like in preceding chapters, the spin and isospin labels.

The numerical algorithm works in dimensionless units. In this case, we use the cylinder radius as length unit by the same kind of reasoning as was given in Chap. 4. This choice also determines the energy scale with our usual convention of enforcing $\hbar = 1$ and $m^* = 1$ in effective units; that is

$$L_U = \rho\,, \tag{7.1}$$

$$E_U = \frac{\hbar^2}{m^*\rho^2}\,, \tag{7.2}$$

where L_U and E_U represent the length and energy effective units, ρ is the cylinder radius and m^* is the electron effective mass in the nanowire. A realistic nanowire of $\rho = 150$ nm made of InSb will have a Rashba coupling strength parameter of around $\alpha = 0.2\,E_U$. On the other hand, we use a superconductor gap $\Delta = 0.2\,E_U$, equivalent to $\Delta \approx 0.25\,\text{meV}$ in physical (not scaled) units. Again, in the same way of preceding chapters this value does not correspond to any particular bulk superconductor gap but it is a value within a realistic range.

In this work, we study the robustness of the Majorana modes in front of changes on the external magnetic field, the Rashba spin orbit coupling strength and the radius of the considered nanowire. Note that, in the last case we choose a typical value of the nanowire radius as a reference length and then we study the behavior of the Majorana modes in nanowires of different dimensions referred to the original one. We proceed in this way to allow the comparison between nanowires of different diameters, with a different choice each nanowire would be referred to its own units.

7.3 Conclusions and remarks

In this chapter, we have studied the robustness of the Majorana modes in a cylindrical nanowire inside an external magnetic field. It has been established that a perpendicular electrical field is also needed to have Majorana modes. The role of this electric field is to break the azimuthal symmetry of the nanowire. The electric field is perceived by the quasiparticles as an effective magnetic field. In this work we have demonstrated that the Majorana modes are robust to tiltings of the external magnetic field, provided the field is not tilted in the direction of the spin orbit effective magnetic field. This behavior is analogous and appears by the same reason than the limits in the tilts of 1d and quasi-1d Majorana nanowires. If the external magnetic field points in the same direction of the spin orbit effective magnetic field then there is a privileged direction of quantization that prevents any spin precession. As explained in Chap. 1, spin precession of the Majorana modes is needed to avoid the problem of spin degeneracy. However, as shown below, in spite of the analogy with the 1d case the precise formulation of the projection rule is not respected. In this sense, we have also shown that a strong spin-orbit coupling is needed in order to have Majoranas but, at the same time, the orbital terms affect the role of the spin-orbit coupling.

On the other hand, we confirm the stacking behavior by which several Majorana modes can appear on the same edge (by different causes than spin degeneracy). This is a novelty in comparison with 1d and quasi-1d models. It is possible because the Majorana wavefunctions take complementary, in the sense of non overlapping, positions in space. Therefore, it is as if we had various independent or poorly interconnected nanowires. Furthermore, the number of Majorana modes increases with the radius and the strength of the Rashba coupling allowing to a certain degree the tuning of this phenomenon. Note that the origin of this coexistence it is not due the relationship between the width or perimeter of the cylinder and the spin orbit length differently from the considerations done in Chap. 4. In this chapter it was discussed that in very narrow planar nanowires a sort of approximated cohexistence between Majoranas arise when the gap is near to be closed due to the lack of spin coupling. However, here the phenomenon works in an opposite way. The bigger the perimeter of the nanowire due to a greater radius more Majoranas are piled up. Furthermore, there is a complicated interplay between the Rashba and orbital terms that affect the way the Majoranas are piled up.

It is an object of future work to determine the origin of this coexistence. However, we have stated that Majorana coexistence in 2d cylindrical surfaces is different than in quasi-1d planar nanowires explained in Chap. 4. It is the opinion of this author that the periodicity of the space along the azimuthal direction plays a major role in this change, this is something not discussed in Ref. [38] of Chap 4.

7.4 Published paper

Eur. Phys. J. B (2014) 87: 84
DOI: 10.1140/epjb/e2014-41091-8

THE EUROPEAN PHYSICAL JOURNAL B

Regular Article

Majorana mode stacking, robustness and size effect in cylindrical nanowires

Javier Osca[1], Rosa López[1], and Llorenç Serra[1,2,a]

[1] Institut de Física Interdisciplinària i de Sistemes Complexos IFISC (CSIC-UIB), 07122 Palma de Mallorca, Spain
[2] Departament de Física, Universitat de les Illes Balears, 07122 Palma de Mallorca, Spain

Received 19 December 2013 / Received in final form 4 February 2014
Published online 9 April 2014 – © EDP Sciences, Società Italiana di Fisica, Springer-Verlag 2014

Abstract. We discuss the robustness of Majorana edge modes in a finite quantum nanowire of cylindrical shape. The nanowire is modeled as a bidimensional cylindrical shell of semiconductor material with proximity-induced superconductivity and an intrinsic Rashba spin-orbit interaction. The latter is characterized by effective electric and magnetic fields in transverse direction of the nanowire. An applied external magnetic field pointing in an arbitrary orientation is also assumed. The numerical diagonalization of the Hamiltonian allows us to study the spectrum of the nanowire for different experimental configurations. The Majorana modes prove robust against tilting of the magnetic field away from the cylinder longitudinal axis, if the tilt direction is perpendicular to the effective spin-orbit magnetic field, but fragile otherwise. On the other hand, we find an increasing number of Majorana modes in the same cylinder edge for increasing values of the nanowire radius. We refer to this phenomenon as "stacking effect" and it occurs due to the orthogonality between Majorana mode wave functions. In this manner, different Majoranas take complementary positions on the nanowire surface.

1 Introduction

The discovery of topological states of matter was a major milestone in the condensed matter field [1–3]. These states behave as localized non abelian anyons, meaning that a nontrivial phase modification is obtained after the interchange of a pair of them [4]. It has been argued that in addition to new yet to discover physics, their peculiar statistics has the potential of making these states the basic units for quantum processing and opens the possibility of achieving topological quantum computation [5]. The nonlocal properties of these topological quasiparticles gives them a certain degree of immunity against local sources of noise. A particular set of these kind of excitations are the nowadays called Majorana modes. These quasiparticle excitations are identical to their own antiparticles. They inherit their name from the famous physicist Ettore Majorana who proposed a modification of the Dirac equation in order to describe fermionic particles that are their own antiparticles [6].

It has been theorized that Majorana states are formed at the ends of superconductor wires as a consequence of the combined action of superconductivity, Rashba spin-orbit coupling and Zeeman magnetic effect [7–21]. In a superconductor nanowire electrons play the role of particles while holes of opposite charge and spin perform the role of antiparticles. These kinds of systems are modeled as quantum gases with the mentioned interactions and their Majorana modes can only exist at zero energy because antiparticle states have an opposite energy that their particle counterparts. Superconductivity leads to a charge symmetry breaking and allows quasiparticles without a good isospin number to exist. On the other hand, the Rashba effect is a direct result of an inversion asymmetry caused by an electric field in a direction perpendicular to the electron motion while the Zeeman magnetic field breaks the spin rotation symmetry of the system. The combined action of the Rashba and Zeeman effects are needed to create states with a space precessing spin necessary to obtain effective spin less Majorana states at zero energy.

In a finite nanowire Majorana physics necessarily manifests in an approximate way. This is because of the unavoidable interference between the states on the two opposite ends of the finite nanowire. These states never lie exactly at zero energy and their wave functions always overlap to some degree. In long enough nanowires, however, Majorana behavior is seen as energy eigenvalues very close to zero, protected by a sizable energy gap from the rest of eigenvalues and with exponentially small overlap of their wave functions. We can, of course, interpret those near-zero-energy states as the finite-system Majoranas and consider how their Majorana character is increased or decreased when some system parameters are varied. That is, we can investigate whether the scenario of

[a] e-mail: llorens.serra@uib.es

protected near-zero-energy states is better achieved or not after a particular variation. This approach to Majorana physics is realistic since the experiments are always done with finite systems.

Very recently, Mourik et al. [22] have reported the detection of such Majoranas in long InSb nanowires ($L = 2\ \mu$m). Superconductivity is induced by contact with an NbTiN metallic superconductor caused by the leakage of Cooper pairs into the semiconductor. Superconductivity is maintained all along the few nanometer width of the nanowire, shorter than the coherence distance of the Cooper pairs. The large g factor of the InSb semiconductor allows the existence of a noticeable Zeeman effect in presence of a moderate magnetic field while at the same time it maintains a strong enough spin-orbit interaction. Finally the nanowire is connected to two electrodes, one in each end, and the current is measured. The Majorana mode evidence is a peak at zero voltage in the tunneling differential conductance called zero bias anomaly (ZBA). Similar experiments based on the detection of the zero voltage peak have been carried out by different research groups [23–26].

The ZBA only appears in presence of the three required ingredients (superconductivity, Rashba and Zeeman effects) when the system is driven into the topological phase. From the theoretical point of view several authors dealt with one dimensional or two dimensional planar models [18,27,28]. However, the cylindrical geometry of the nanowire motivated the study made by Lim et al. [20]. In the proposed configuration the spin-orbit electric field $\mathcal{E}_{so}$ points perpendicularly to the nanowire (see Fig. 1) while the possibility of Majoranas with a radial electric field was discarded in that work for any configuration of the remaining parameters. It is reasonable to expect a weaker total spin-orbit effect if the field is radial simply because of the compensation for opposite angles. On the other hand, a fixed direction $\mathcal{E}_{so}$ can originate in the asymmetry induced by the superconductor substrate on which the nanowire is deposited.

In reference [20] the effects of magnetic fields pointing into the three Cartesian directions were considered, for different values of its magnitude. It was concluded that only a magnetic field pointing along the nanowire axis (z) is suited to the creation of the Majoranas, but no discussion about the robustness of this particular configuration was made. The present work addresses this issue, studying the robustness of the Majorana modes to different tiltings of the magnetic field and it also investigates the dependence of the nanowire eigenstates with other parameters, such as the cylinder radius and the spin-orbit strength.

We show that Majorana modes are robust to the tilting of the magnetic field only in a particular direction, while these modes are easily destroyed for tiltings in any other directions. This is relevant to avoid possible non Majorana experimental set-ups, but also as possible procedures to verify the Majorana origin of the ZBA checking its robustness against the theoretical predictions. Remarkably, when increasing the nanowire radius and/or the spin-orbit strength we find that more and more Majoranas coexist on the same end, a phenomenon we name "stacking" of Majoranas. These coexisting Majoranas tend to occupy complementary spatial positions on the cylinder edge.

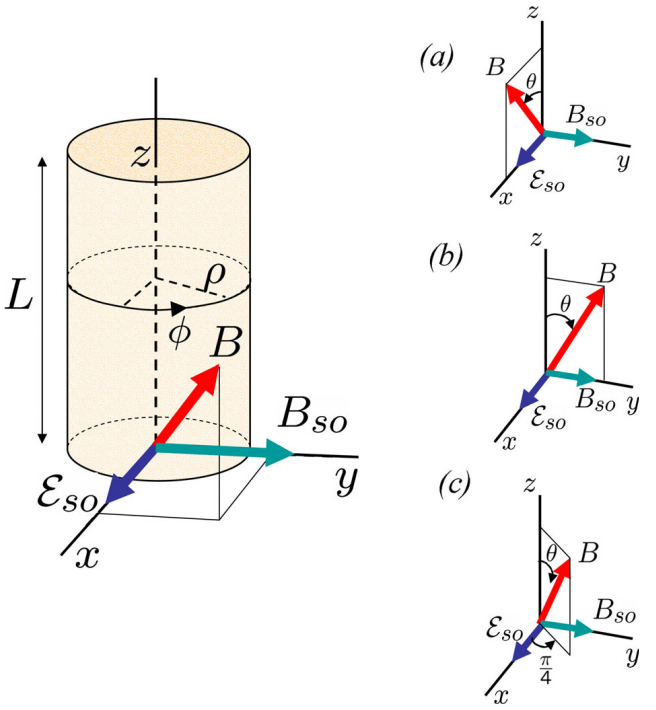

Fig. 1. Hollow semiconductor nanowire of length L with cylindrical geometry. Cylindrical coordinates and unit vectors are indicated. A magnetic field $\boldsymbol{B}$ is applied in an arbitrary direction. The orientation of the Rashba electric and magnetic fields, $\boldsymbol{\mathcal{E}}_{so}$ and $\boldsymbol{B}_{so}$, are also indicated. The three field tiltings discussed in Section 3 are indicated in (a–c).

In Section 2 the physical system is introduced while Section 3 studies the nanowire spectrum for different tilting directions of the magnetic field. Section 4 is devoted to study the spectrum changes when varying the cylinder radius and the spin-orbit strength. Finally, the conclusions can be found in Section 5.

2 Physical model

The nanowire is modeled as a finite two dimensional semiconductor cylindrical shell with spin-orbit interaction and induced superconductivity, inside an homogeneous Zeeman magnetic field, as shown in Figure 1. We assume that due to the superconductive character of the nanowire the quasiparticles move only on the cylinder surface. Experimentally, this type of tubular systems have been produced either as rolled-up quantum wells (e.g. in Ref. [29]) or by epitaxial growth of core/shell nanowires (e.g. in Ref. [30]).

The system is described by a Hamiltonian of Bogoliubov-de Gennes kind [20],

$$\mathcal{H} = \mathcal{H}_{kin} + \mathcal{H}_R + \mathcal{H}_Z + \mathcal{H}_S, \tag{1}$$

where the successive contributions are kinetic, Rashba spin-orbit, Zeeman and superconductivity term. In this

Eur. Phys. J. B (2014) 87: 84

manner, the three ingredients needed to obtain Majorana modes are present in the model: superconductivity, spin-orbit interaction and a Zeeman magnetic field. The kinetic term depends on the canonical momentum $\boldsymbol{\Pi} = \boldsymbol{p} + \frac{e}{c}\boldsymbol{A}$, where $\boldsymbol{p}$ is the usual momentum operator in three dimensions and $\boldsymbol{A}$ is the vector potential. The vector potential models the orbital effects of the magnetic field on the electron trajectories. Therefore, the kinetic term for electrons is $\boldsymbol{\Pi}^2/2m^* - \mu$, where μ is the chemical potential. Since the system has cylindrical symmetry it is convenient to write the Hamiltonian in the cylindrical coordinate system indicated in Figure 1. Being a two dimensional problem the cylindrical coordinates will allow us to express the Hamiltonians as function of two coordinates (z and ϕ, note that the radius ρ is fixed). Furthermore, the kinetic term can be split into a non-magnetic

$$\mathcal{H}_{kin}^{(0)} = \left[\frac{p_\phi^2 + p_z^2}{2m^*} - \mu\right]\tau_z, \tag{2}$$

and a magnetic term

$$\begin{aligned}\mathcal{H}_{kin}^{(1)} = \frac{\hbar^2}{2m^*}\Bigg[&\frac{\rho}{l_z^2}\frac{p_\phi}{\hbar}\tau_z + \frac{\rho^2}{4l_z^2}\tau_z + 2\frac{\rho}{l_x^2}\sin\phi\,\frac{p_z}{\hbar}\tau_z \\ &-2\frac{\rho}{l_y^2}\cos\phi\,\frac{p_z}{\hbar} + \frac{\rho^2}{l_x^4}\sin^2\phi\,\tau_z + \frac{\rho^2}{l_y^4}\cos^2\phi\,\tau_z \\ &-2\frac{\rho^2}{l_x^2 l_y^2}\sin\phi\cos\phi\Bigg],\end{aligned} \tag{3}$$

where the electron and holes degrees of freedom are represented with the Pauli matrices $\tau_{x,y,z}$ acting on the isospin space and the magnetic lengths along direction $i \equiv x, y, x$ are $l_i = \sqrt{\hbar c/eB_i}$. Trivially, when a certain magnetic field component vanishes the corresponding magnetic length diverges, giving a vanishing contribution to $\mathcal{H}_{kin}$.

The Rashba term is obtained assuming the existence of an external electric field $\mathcal{E}_{so}$, in direction of the unitary vector $\boldsymbol{u}_\mathcal{E}$. It is proportional to the double product of vectors $\boldsymbol{\sigma}\cdot(\boldsymbol{\Pi}\times\boldsymbol{u}_\mathcal{E})$, where $\boldsymbol{\sigma}$ represents the vector of Pauli matrices for spin. If we assume an homogeneous electric field pointing in $\boldsymbol{x}$ direction the corresponding Hamiltonian contribution can be split, by analogy to the kinetic term, into non magnetic $\mathcal{H}_R^{(0)}$ and magnetic $\mathcal{H}_R^{(1)}$ terms as:

$$\mathcal{H}_R^{(0)} = \frac{\alpha}{\hbar}\left(p_z\,\sigma_y\tau_z - \cos\phi\,p_\phi\,\sigma_z - \frac{i\hbar}{2\rho}\sin\phi\,\sigma_z\right), \tag{4}$$

$$\mathcal{H}_R^{(1)} = \alpha\rho\left(\frac{\sin\phi}{l_x^2}\sigma_y\tau_z - \frac{\cos\phi}{l_y^2}\sigma_y - \frac{\cos\phi}{2l_z^2}\sigma_z\right). \tag{5}$$

As mentioned in Section 1 another natural choice for the Rashba term could be a radial field ($\boldsymbol{u}_\mathcal{E} = \boldsymbol{u}_\rho$) but, in agreement with reference [20], we have checked that this does not lead to the formation of any Majorana-like states. For a long-enough cylinder in absence of magnetic field one expects the first contribution to equation (4) dominate the others for large values of p_z, thus leading to the usual interpretation of the Rashba term as an effective magnetic field $\boldsymbol{B}_{so} \propto \alpha p_z \boldsymbol{y}$, in y direction and thus coupling with σ_y.

The Zeeman term for an external magnetic field along $\boldsymbol{n}$ reads

$$\mathcal{H}_Z = \Delta_B\,\boldsymbol{\sigma}\cdot\boldsymbol{n}. \tag{6}$$

Finally, the superconductor contribution $\mathcal{H}_S$ is:

$$\mathcal{H}_S = \Delta_0\tau_x, \tag{7}$$

where Δ_0 is the Cooper-pair breaking energy. The superconduction pairing term couples opposite isospin states and arises from a mean field approximation over electron interactions shielded by the atomic network.

Notice that the Zeeman effect allows the closing of the superconductor energy gap, shifting some quasiparticle states to zero energy while the Rashba spin-orbit term interaction introduces anti crossings in the system spectrum that separate the Majorana zero energy states from the others. The Rashba term arises from the self interaction between an electron (or hole) spin with its own motion due to the presence of a transverse electric field $\mathcal{E}_{so}$, perceived as an effective magnetic field in the rest frame of the quasiparticle. Spin-orbit effects in cylindrical shells similar to the ones considered here but without superconductivity have been studied in references [31,32].

The Rashba spin-orbit and Zeeman effects depend on the parameters α and Δ_B, respectively. Since we consider a nanowire made of an homogeneous material inside a constant magnetic field these parameters are assumed to be homogeneous. The potential, not included in the Hamiltonian, is taken as zero inside the nanowire and infinite outside. Therefore it is included into the calculations as a boundary condition. Summarizing, the Hamiltonian depends on the superconducting gap Δ_0, the Zeeman energy Δ_B and the Rashba coupling strength α, as well as on the direction of the magnetic field $\boldsymbol{n}$.

The explicit energy contributions from the orbital effects of the magnetic field are contained in the kinetic $\mathcal{H}_{kin}^{(1)}$ and $\mathcal{H}_R^{(1)}$ terms. Below we will also study the results when these contributions are omitted, finding in general that orbital effects are very important and cannot be neglected. The orbital terms increase with the cylinder radius due to contributions that are linear and quadratic in ρ and they contain the dependence on curvature of the model.

To obtain the energy spectrum the total Hamiltonian is diagonalized numerically using as a basis states characterized as:

$$|nms_\sigma s_\tau\rangle \qquad \begin{cases} n = 1, 2, \dots, \\ m = 0, \pm1, \pm2, \dots, \\ s_\sigma = \pm, \\ s_\tau = \pm, \end{cases} \tag{8}$$

where n is the quantum number associated with the infinite square well eigenstates (z direction), m is the L_z eigenvalue (angular momentum along z) while s_σ and s_τ are the spin and isospin quantum numbers. The numerical algorithm works in dimensionless units, defining energy and length units as:

$$E_U \equiv \frac{\hbar^2}{m^*\rho^2}, \tag{9}$$

$$L_U \equiv \rho. \tag{10}$$

More specifically, assuming a cylinder radius of $\rho = 50$ nm, and $m^* = 0.015m_e$ for InSb, one has $E_U = 2.03$ meV and $L_U = 50$ nm. From reference [22], typical values for the Rashba parameter and the superconducting gap are $\alpha \approx 20$ meV nm and $\Delta_0 \approx 0.25$ meV, which in scaled units are $\alpha \approx 0.2E_U L_U$ and $\Delta_0 \approx 0.12E_U$. We will present below the results in the generalized units, assuming an arbitrary m^* and ρ, since the conversion for each material and cylinder radius is just a trivial scaling.

3 Results on tilted fields

In reference [20] it was shown that the critical fields corresponding to transitions into the topological phase of the nanowire were strongly dependent on the external magnetic field orientation. Considering a nanowire whose dominant spin-orbit effective magnetic field $\boldsymbol{B}_{so}$ points along $\boldsymbol{y}$ (Fig. 1), if the external magnetic field $\boldsymbol{B}$ points also into this same direction then the Rashba $\boldsymbol{B}_{so}$ contribution and the Zeeman term commute and no anti crossings are induced in the spectrum. As a consequence, no spin less zero energy modes are observed since the Majorana conditions are not met. It was also shown in reference [20] that, due to the strong influence of the orbital effects, Majorana modes are neither possible with an external magnetic field along $\boldsymbol{x}$. Therefore, for the three main Cartesian orientations Majorana modes are found only when the magnetic field is pointing in the $\boldsymbol{z}$ direction, and for strong-enough values. We address in this section the study of the transition between these configurations and, particularly, the robustness of the Majoranas (or their lack of it) due to fluctuations in the magnetic field direction.

Figures 2a–2c show how the spectrum of a cylindrical nanowire changes when the magnetic field is tilted from the z-axis in the directions sketched in Figure 1, while its magnitude is maintained. Notice that Figure 2a proves that the Majorana modes are robust to a tilting of the magnetic field from $\boldsymbol{z}$ towards $\boldsymbol{x}$, up to almost 30° when the tilting is done within the $y = 0$ plane. On the contrary, Figure 2b shows that the Majorana modes break almost immediately if the tilting is done towards $\boldsymbol{y}$ in the $x = 0$ plane. Zero energy crossings are found in Figure 2b for $\theta \approx 15°$ and, when the magnetic field is further tilted, also around $\theta \approx 50°$, but this kind of crossings can be labeled as accidental since they only occur at specific points.

Majorana behavior is characterized by eigenvalues lying very close to zero for a continuous range of parameter values, protected from nearby states by a sizable energy gap much larger that their own energy. Accidental zero energy crossings, on the contrary, occur at specific values and in this sense they are weak against any small parameter fluctuation. Notice that Figure 2 shows that tilting directions towards $\boldsymbol{x}$ and $\boldsymbol{y}$ are not equivalent, in spite of being perpendicular between them and also with $\boldsymbol{z}$. As mentioned above, differences are due to the relative orientation with respect to the effective Rashba field $\boldsymbol{B}_{so}$, that in our case points in the $\boldsymbol{y}$ direction.

On the other hand, if the magnetic field is tilted away from $\boldsymbol{z}$ in the $x = y$ plane (Fig. 2c) the resulting spectrum has mixed features with respect to those of Figures 2a and 2b. The Majoranas break up for small angles but the resulting fermionic modes remain close to zero energy up to almost 40°. Therefore, cylinder Majoranas are robust to deviations of the external magnetic field from the cylinder axis only within the plane perpendicular to the spin-orbit effective magnetic field $\boldsymbol{B}_{so}$.

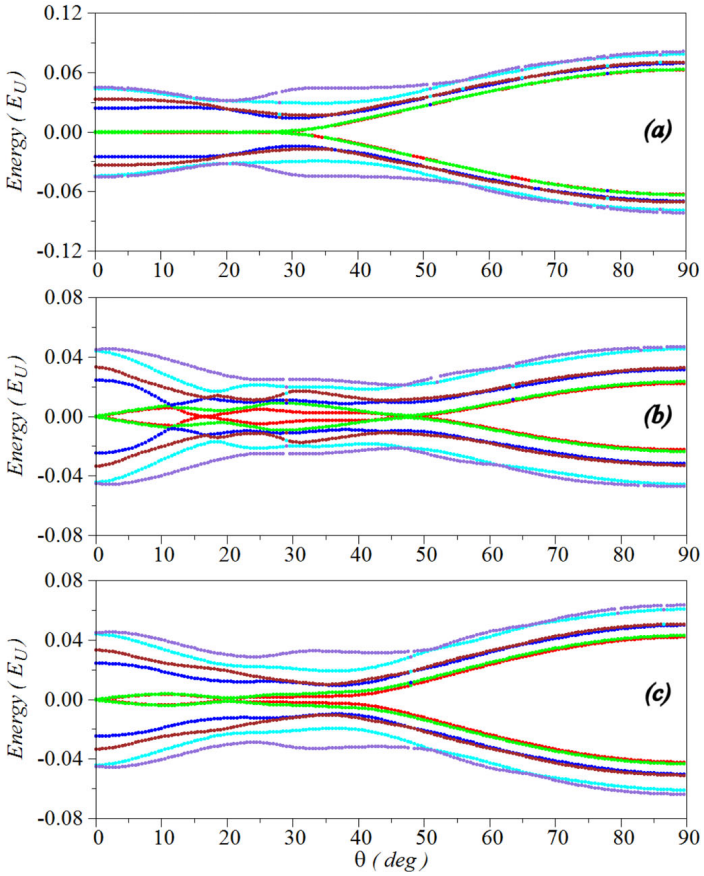

Fig. 2. Eigenenergies (including orbital effects) as a function of the magnetic tilting angle from the z axis, for different orientations: (a) $y = 0$ plane, (b) $x = 0$ plane, (c) $x = y$ plane. The parameters used are $\Delta_B = 0.2E_U$, $\Delta_0 = 0.12E_U$, $\alpha = 0.2E_U L_U$, $\mu = 0$ and $L_z = 30L_U$. The number of basis states are $N_n = 51$ and $N_m = 31$. Only the lowest 6 pairs of eigenvalues are displayed.

4 Dependence on nanowire characteristics

4.1 Spin-orbit coupling

Figure 3 shows a spectrum for a cylindrical nanowire with the same parameters used in Figure 2 as a function of the spin-orbit coupling strength α. The magnitude and the direction of the magnetic field are kept constant to $\Delta_B = 0.2E_U$ and $\boldsymbol{z}$, respectively. In principle, this change can be experimentally realized controlling the intensity of the transverse electrical field $\boldsymbol{\mathcal{E}}_{so}$. As observed in Figure 3, for zero spin-orbit the states lying closer to zero are two states of fermionic type at finite energies. Increasing the value of α those two states evolve into a Majorana pair

Eur. Phys. J. B (2014) 87: 84

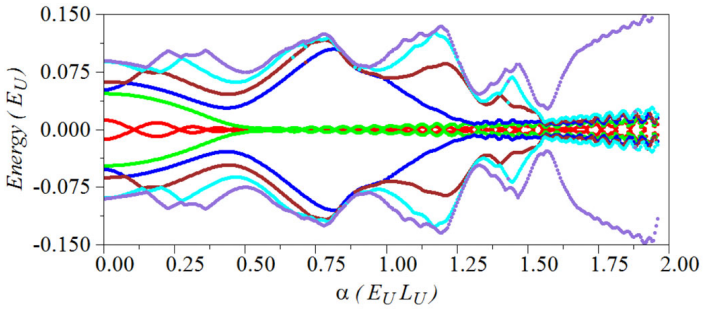

Fig. 3. Eigenenergies of a cylinder (considering the orbital effects) as a function of spin-orbit coupling. The rest of the parameters are the same of Figure 2, including the number of basis states and the number of displayed eigenvalues.

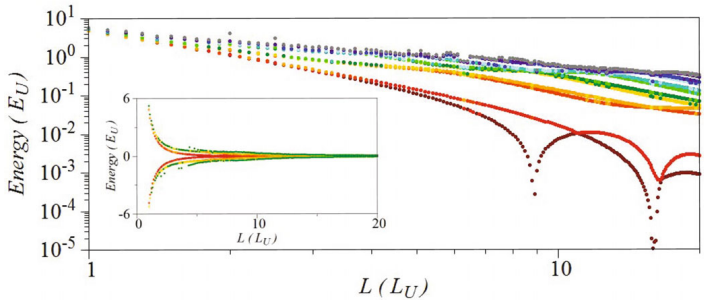

Fig. 4. Dependence of the spectrum of eigenergies of a cylinder with respect to its length. The rest of the parameters are the same of Figure 2. The main plot shows only positive energy eigenvalues in logarithmic scales while the inset contains both positive and negative eigenvalues in linear scales.

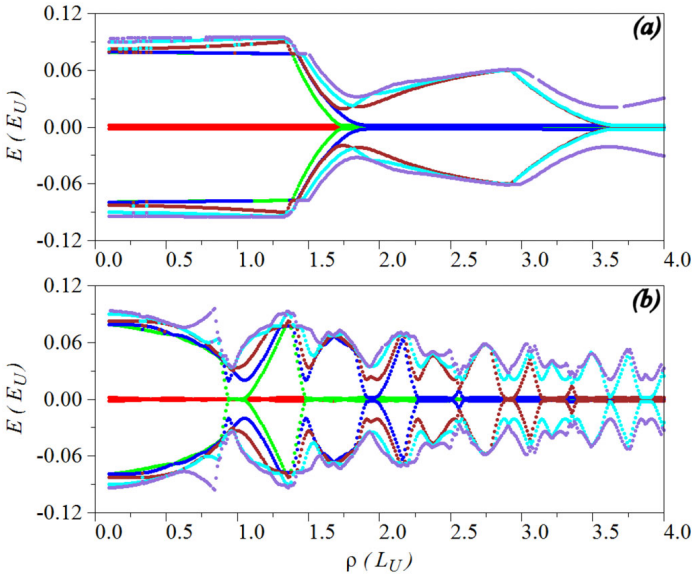

Fig. 5. Dependence of the spectrum of eigenergies of a cylinder with respect to its radius. The rest of the parameters are the same as in Figure 2. Panel (a) is the result obtained when neglecting the orbital contributions of the magnetic field $\mathcal{H}^{(1)}_{kin}$ and $\mathcal{H}^{(1)}_{R}$, while (b) is for the complete Hamiltonian. Note that the length unit L_U in this figure is taken as an arbitrary reference distance.

as their energy approaches zero. Note also that additional Majorana modes become activated sequentially, in more or less regular intervals of the coupling constant α. Each time a new Majorana mode arises, the protection (energy gap) diminishes for a short range of values, to increase again once the Majorana is fully formed.

Since the spin-orbit coupling is also affected by the orbital terms, when high values of α are achieved the spectrum of the modes near zero energy in Figure 3 becomes more and more oscillating, blurring away the Majorana character of these modes. Although the process of Majorana activation still works for the higher values of spin-orbit coupling, these states do not become Majorana-like due to their sizable energies that keep oscillating with increasing amplitudes. Figure 3 suggests an optimal range for the formation and coexistence of Majoranas when the amplitude of the energy oscillation around zero attains its minimum, with two pairs coexisting for $\alpha \approx 0.6 E_U L_U$.

4.2 Cylinder geometry

The length and radius of the nanowire are not tunable parameters in the same sense as the external magnetic and electric fields, but can be controlled by fabricating different versions of the nanowire with different dimensions. As can be seen in Figure 4 Majoranas are not possible for very short nanowires because both ends greatly interfere with each other creating a fermionic state. Qualitatively, for the particular choice of parameters in this figure the nanowire length must exceed at least six times its radius in order to be able to hold a Majorana state with energy lower than, roughly, $0.01 E_U$. When displayed in logarithmic scales, Figure 4 also shows that the energy of the states lying closer to zero oscillate as a function of the cylinder radius, similarly to the α dependence of Figure 3.

On the other hand, increasing the radius of the nanowire leads to a stacking of Majoranas (Fig. 5). A qualitatively similar coalescence is found for Shockley states at the surface of finite crystals [33], which is suggesting a generic behavior for edge states. A technical point in the analysis of a varying cylinder radius ρ is that this can no longer be identical to the length unit L_U. To avoid ambiguities, we take an arbitrary length as a reference L_U and measure all distances (including the varying cylinder radius in Fig. 5) with respect to this unit.

As shown in Figure 5a, if the orbital effects are disregarded, the zero point energy contribution of the angular momentum decreases as the radius becomes larger, allowing the activation of the Majorana modes, creating this way a stacking of zero modes at regular intervals of the radius. Each Majorana pair is associated with an angular momentum quantum number m. Since m and $-m$ eigenenergies are almost degenerate, two pairs are activated at around the same value of the radius. As they are not completely degenerate by the action of the transversal electric field, there is a slight difference in their activation value.

With orbital effects the spectrum becomes more involved (see Fig. 5b). First, the Majorana pairs are activated one by one as the value of the radius increases.

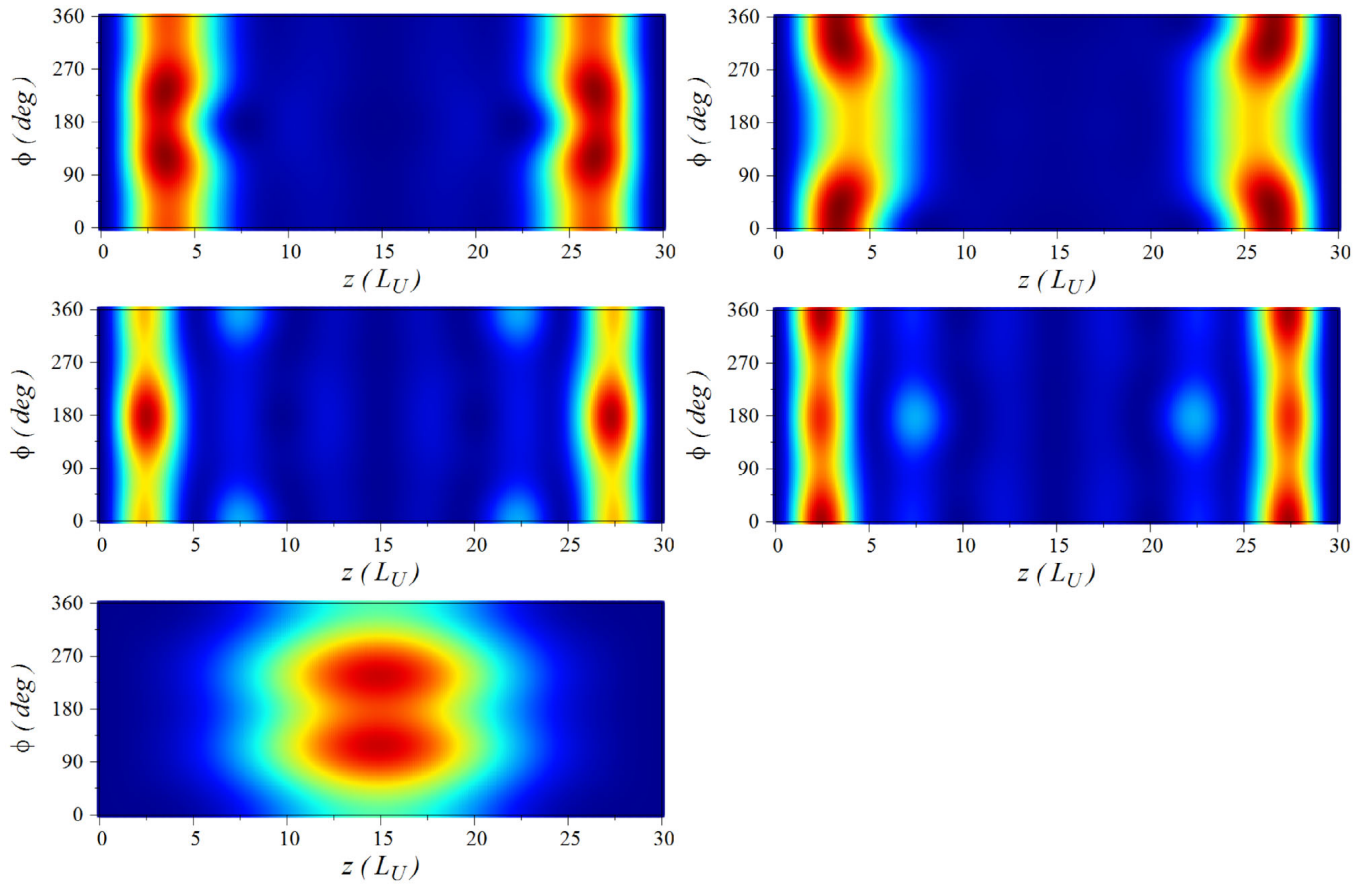

Fig. 6. Density distributions of the lower cylinder eigenmodes. The parameters used are $\Delta_B = 0.2E_U$, $\Delta_0 = 0.12E_U$, $\alpha = 0.2E_U L_U$, $\mu = 0$, $\rho = 3.2L_U$ and $L_z = 30L_U$. The densities of the first positive energy solutions are plotted. All of them are Majorana modes with the exception of the panel at the bottom that is a fermionic one.

Furthermore, each pair is destroyed shortly after its activation, developing into a fermion pair of states above the gap, and is re-formed again for larger values. This behavior is due to the increase with ρ of the orbital terms $\mathcal{H}^{(1)}_{kin}$ and $\mathcal{H}^{(1)}_{R}$. There is a competition between the different effects of the spin-orbit terms, some of them helping to create the Majorana and some of them trying to destroy the Majorana, with the former ones eventually wining for high values of the radius. Nevertheless, we stress the general tendency of Majorana mode stacking at zero energy for high values of the radius.

We finally discuss the spatial distribution of the probability densities associated with the Majorana-like states. A clear signature of Majorana character is a strong localization at the nanowire edges, with very small central overlaps. Figure 6 shows in a particular example that this is indeed observed, with a very clear difference between Majorana-like and fermionic modes. Figure 6 also shows that the above mentioned stacking is possible for high values of the radius because there is room for orthogonal wave functions, with almost non overlapping density distributions, to be formed on the same nanowire end. The higher the radius the larger the suitable region for the Majoranas to be formed, where more and more orthogonal zero energy wave functions can accommodate in complementary regions.

5 Conclusions

The diagonalization of the Hamiltonian for a two dimensional cylindrical shell has allowed us to discuss the eigenenergies and eigenstates of a finite nanowire. In particular, we have focussed on the Majorana state wave functions and the parameter configurations leading to their appearance. The resilience of the Majorana states to the tilting of the magnetic field, as far as 30° into the $\boldsymbol{\mathcal{E}}_{so}$ direction, has been shown; as well as the lack of it if one component points into the $\boldsymbol{B}_{so}$ direction. We have also learnt how a strong spin-orbit coupling is needed in order to have Majoranas but, at the same time, how orbital terms affect the role of the spin-orbit coupling. This means that for too high values of the spin-orbit coupling Majorana modes get blurred due to orbital effects.

Our main result is the stacking effect of Majorana modes for increasing nanowire radius and high enough values of the magnetic field. This is a novelty in comparison with one dimensional models, and it is an exclusive property of two dimensional models. It means that we can tune the number of localized Majorana modes on each nanowire end. Although not explored in this work, this is hinting interesting transport properties that could be useful to experimentally confirm the presence of Majoranas in nanowires and it will be matter of future work.

Work supported by MINECO Grant No. FIS2011-23526, the Conselleria d'Educació, Cultura i Universitats (CAIB) and FEDER.

References

1. A.Y. Kitaev, Phys. Usp. **44**, 131 (2001)
2. F. Wilczek, Nat. Phys. **5**, 614 (2009)
3. P.W. Brouwer, Science **336**, 989 (2012)
4. J.K. Pachos, *Introduction to topological Quantum Computation* (Cambridge University Press, Cambridge, 2012)
5. C. Nayak et al., Rev. Mod. Phys. **80**, 1083 (2008)
6. E. Majorana, Nuovo Cim. **14**, 171 (1937)
7. R.M. Lutchyn, J.D. Sau, S. Das Sarma, Phys. Rev. Lett. **105**, 077001 (2010)
8. Y. Oreg, G. Refael, F. von Oppen, Phys. Rev. Lett. **105**, 177002 (2010)
9. T.D. Stanescu, R.M. Lutchyn, S. Das Sarma, Phys. Rev. B **84**, 144522 (2011)
10. K. Flensberg, Phys. Rev. B **82**, 180516 (2010)
11. A.C. Potter, P.A. Lee, Phys. Rev. Lett. **105**, 227003 (2010)
12. A.C. Potter, P.A. Lee, Phys. Rev. B **83**, 094525 (2011)
13. S. Gangadharaiah et al., Phys. Rev. Lett. **107**, 036801 (2011)
14. R. Egger, A. Zazunov, A.L. Yeyati, Phys. Rev. Lett. **105**, 136403 (2010)
15. A. Zazunov, A.L. Yeyati, R. Egger, Phys. Rev. B **84**, 165440 (2011)
16. J. Klinovaja, S. Gangadharaiah, D. Loss, Phys. Rev. Lett. **108**, 196804 (2012)
17. J. Klinovaja, D. Loss, Phys. Rev. B **86**, 085408 (2012)
18. J.S. Lim et al. Phys. Rev. B **86**, 121103 (2012)
19. J.S. Lim, R. López, L. Serra, New J. Phys. **14**, 083020 (2012)
20. J.S. Lim, R. López, L. Serra, Europhys. Lett. **103**, 37004 (2013)
21. L. Serra, Phys. Rev. B **87**, 075440 (2013)
22. V. Mourik et al., Science **336**, 1003 (2012)
23. A. Das et al., Nat. Phys. **8**, 887 (2012)
24. H.O.H. Churchill et al., Phys. Rev. B **87**, 241401 (2013)
25. M.T. Denget al., Nano Lett. **12**, 6414 (2012)
26. A.D.K. Finck et al., Phys. Rev. Lett. **110**, 126406 (2013)
27. E. Prada, P. San-José, R. Aguado, Phys. Rev. B **86**, 180503(R) (2012)
28. J. Alicea, Rep. Prog. Phys. **75**, 076501 (2012)
29. N. Shaji et al., Appl. Phys. Lett. **90**, 042101 (2007)
30. O. Gül et al., Phys. Rev. B **89**, 045417 (2014)
31. M. Trushin, J. Schliemann, New J. Phys. **9**, 346 (2007)
32. A. Bringer, T. Schäpers, Phys. Rev. B **83**, 115305 (2011)
33. W. Shockley, Phys. Rev. **56**, 317 (1939)

Chapter 8

Charge and energy transport in a Majorana nanowire

Javier Osca, Rosa López and Jong Soo Lim
Draft version.

8.1 Objectives

In previous chapters we have been mainly focused on finding Majorana phase boundaries and in robustness considerations. These previous works help us locate in which regions of the parameter space it is possible to find Majorana modes for models that contain realistic physical effects. They were aimed to be a guide to obtain Majorana modes in the context of transport experiments. In this chapter we take the opposite approach. The Majorana transport properties are studied using an effective model to capture the Majorana most essential physics.

There is in the literature theoretical predictions for the DC conductance of Majorana nanowires [51,52]. However, the conductance is not the only transport property that can be measured in a Majorana nanowire. The Majorana AC response in the form of an admittance is also a quantity that can be measured. Furthermore, it is possible to measure not only charge but also the energy transport behavior of the Majorana modes.

In this chapter, the objective is to calculate the DC and AC electrical and energy currents of a Majorana nanowire connected to one or two reservoirs where each reservoir is connected to one side of the nanowire. The AC driving is considered to be applied in one of the reservoirs and finite size effects are also considered through the Majorana hybridization energy.

8.2 Methodology

In this chapter we use a combination of different mathematical techniques to carry out the charge and energy flow calculations. First, the nanowire is described with an effective model. The total Hamiltonian is composed as,

$$\mathcal{H} = \mathcal{H}_C + \mathcal{H}_M + \mathcal{H}_T \,, \tag{8.1}$$

where

$$\mathcal{H}_C = \sum_{\alpha,k,\sigma} \varepsilon_{\alpha k\sigma}(t) c^\dagger_{\alpha k\sigma} c_{\alpha k\sigma} \,, \tag{8.2}$$

describes the normal leads, $\varepsilon_{\alpha k\sigma}(t)$ is the energy of an electron of wavevector k and spin σ in the $\alpha = L, R$ reservoir and $c^\dagger_{\alpha k\sigma}$ and $c_{\alpha k\sigma}$ are the electron creation and annihilation operators, respectively. Note that $\varepsilon_{\alpha k\sigma}$ changes by the AC driving.

$$\mathcal{H}_M = \sum_{i\neq j} \frac{i}{2} \varepsilon_{M_{ij}} \eta_i \eta_j \,, \tag{8.3}$$

characterizes the coupled Majorana states, $\varepsilon_{M_{ij}}$ is the Majorana hybridization energy between the ones located at the i, j edges and η_i is the Majorana creation and annihilation operator at edge $i = \{1, 2\}$. Finally,

$$\mathcal{H}_T = \sum_k \int_0^L dx \, \left[t^*_k(x) c^\dagger_k \Psi(x) + H.c. \right] \,, \tag{8.4}$$

corresponds to the tunnel Hamiltonian between the normal lead and the Majorana state. $\Psi(x)$ is the Majorana field operator, $t_k(x)$ is the nanowire position dependent coupling amplitude and L is the nanowire length. Note that this model is general to any kind of Majorana nanowire device. We simply assume that the Majorana mode is present but no discussion is provided in this chapter about the mechanisms that make the Majorana mode possible, we refer the reader to previous chapters for that matter. Furthermore, note that this model implies an effective infinite superconductor gap because only transport through the Majorana mode is considered.

The Majorana field operator reads,

$$\Psi(x) = \frac{1}{2} \sum_\alpha f_\alpha(x) \eta_\alpha + f^*_\alpha(x) \eta^\dagger_\alpha \,, \tag{8.5}$$

where $f(x)$ is the Majorana wavefunction. Making the substitution of Eq. (8.5) into Eq. (8.4) gives,

$$\mathcal{H}_T = \sum_{\alpha,k,\sigma;\beta\in\{1,2\}} \left[V^*_{\alpha k\sigma\beta} c^\dagger_{\alpha k\sigma} \eta_\beta + V_{\alpha k\sigma,\beta} \eta_\beta c_{\alpha k\sigma} \right] \,, \tag{8.6}$$

where

$$V_{k,\beta} = \int_0^L dx \, t_k(x) f^*_\beta(x) \,. \tag{8.7}$$

The calculation of the time dependent current is posed as the calculation of the variation of the electron number in one of the contacts,

$$I_\alpha(t) = -e\langle \dot{n}_\alpha \rangle = -\frac{ie}{h}\langle [\mathcal{H}, n_\alpha] \rangle \,, \tag{8.8}$$

where e is the electron charge and n_α is the particle number at terminal α. When charge conservation applies $I_L = -I_R$, that it is not ensured in our description due to the presence of superconductivity but it must be enforced at the end by means of a self-consistent determination of the chemical potential at the nanowire. The resulting current expression can be split as follows,

$$I(\omega) = I_{DC} + I_{AC}(\omega) \,, \tag{8.9}$$

where I_{DC} is the stationary current and I_{AC} the time dependent one. From the currents we can calculate the DC linear conductance $G_o = dI/dV^{DC}$ and the admittance $g(\omega) = dI/dV^{AC}$. Note that the total voltage drop is $V = V^{DC} + V^{AC}(\omega)$.

The DC energy current calculation is very similar to the one done for charge. The calculation is posed as the calculation of the variation of energy in one of the contacts,

$$J_\alpha^{(DC)}(t) = -e\langle \dot{H}_\alpha \rangle \,, \tag{8.10}$$

where $\mathcal{H}_\alpha = \sum_{k,\sigma} \varepsilon_{\alpha k\sigma}(t) c^\dagger_{\alpha k\sigma} c_{\alpha k\sigma}$ is the energy at the reservoir α. On the other hand, the AC energy current in the reservoir of a Majorana capacitor circuit $J_C^{(AC)}(t)$ is calculated by energy conservation as suggested in Refs. [46,47],

$$J_C^{(AC)}(t) = -\left(J_M^{(AC)}(t) + \frac{J_T^{(AC)}(t)}{2} \right) \,, \tag{8.11}$$

where $J_M^{(AC)}(t) = \frac{\partial}{\partial t}\langle \mathcal{H}_M \rangle$ and $J_T^{(AC)}(t) = \frac{\partial}{\partial t}\langle \mathcal{H}_T \rangle$ are the time evolution of the mean energy in the Majorana nanowire and the tunnel region between the reservoir and the nanowire, respectively. From a theoretical point of view, the calculation of the AC energy currents can also be done from Eq. (8.10) but the resulting algebra is more straightforward carrying out the calculation from Eq. (8.11).

To calculate the DC and AC charge and energy currents we make use of the nonequilibrium (Keldysh) Green functions formalism. In this chapter we work in Nambu space because of the presence of superconductivity in the Majorana mode formulation. This means that the Green functions acquire a vectorial character to track the electron and hole degrees of freedom simultaneously.

8.3 Conclusions and remarks

In this chapter we have calculated the DC and AC charge and energy currents of a Majorana nanowire. In general, in a Majorana nanowire device inside a finite bias DC circuit there is no quasiparticle currents between terminals (assuming that the Majorana hybridization energy is small or zero). The reason is that the transport

through the Majorana channel is caused only by Andreev reflection. In this process an incident electron is reflected into a hole. Current conservation is achieved by the selfconsistent calculation of the chemical potential for the case that the Majorana device is floating. The current in the linear regime for each reservoir will be proportional to the quantum $2e^2/h$ and the voltage drop between the Fermi energy at that terminal and the nanowire. However, the conductance measured in the nanowire is dI/dV where V is the voltage drop between the two terminals. That leads to a quantum of conductance that deviates from the one presented above.

The AC response of this same kind of devices can be measured with the admittance calculated from the AC charge current. The most interesting case is the Majorana nanowire connecting one of its edges to a single reservoir. This reservoir contains the AC driving that produces a response in the nanowire. It is shown how the Majorana hybridization produces notable resonances in the real and imaginary parts of the admittance that are resilient to temperature effects. Furthermore, the linear admittance shows a peculiar behavior. The admittance acquires a constant term and the linear and quadratic ω dependent terms are proportional to remarkable fractional values. This particular behavior is caused again by the dominant role of the Andreev reflection in the Majorana transport process. In this sense, the admittance can be separated into two terms, one analogous to the quantum dot conductance and another that can be directly related to Andreev processes. The result is that we can not identify straightforwardly the linearized admittance to an equivalent RC circuit in the same way that can be done with a non-superconducting arbitrary device, like a quantum dot. Therefore the RC analogy in the presence of superconductivity must be taken with caution.

Finally, Majorana nanowires have proven to be very resilient against the flow of energy. The perfect particle-hole symmetry of the Majorana mode leads to zero stationary energy currents through the nanowire. Furthermore, a finite DC bias is needed in order to have a non vanishing response of the nanowire on top of an AC driving to break the electron-hole symmetry.

8.4 Draft

Charge and energy transport in a Majorana nanowire

Javier Osca,[1] Rosa López,[1] and Jong Soo Lim[2]

[1]*Institut de Física Interdisciplinària i de Sistemes Complexos IFISC (CSIC-UIB), E-07122 Palma de Mallorca, Spain*
[2]*School of Physics, Korea Institute for Advanced Study, Seoul 130-722, Korea*

The time dependent electrical and energy currents expressions are obtained for a topological Majorana circuit. In our setup, we consider one or two normal electrodes tunnel coupled to a Majorana nanowire. We employ a low-energy effective model for the Majorana nanowire that includes a finite overlap between the Majorana edge states along the wire. We consider the influence of an AC driving potential applied to the reservoir whereas the Majorana nanowire is kept to be grounded. Then, by means of the Keldysh-Green function formalism we derive the electrical and energy time dependent flows. We give a detailed analysis of both, the DC and AC current responses. Our main results for the AC transport report a singular behavior of the admittances for the electrical current signal when Majorana physics is present.

I. INTRODUCTION

Solid state devices have been revealed as new platforms to probe phenomena traditionally linked to the realm particle physics, like the occurrence of Dirac-like fermions[1–3]. Of particular relevance is the highly symmetric Dirac state in which particle and anti-particle weights are equally represented. Such uncommon state is named as Majorana fermion in honour to Ettore Majorana who in 1937 hypothesized its existence as a fundamental particle[4]. During decades the search of Majorana particles have been focused on the context of mutant neutrinos without success. However, few years ago Fu and Kane predicted theoretically their existence as localized electronic collective excitations at the interface between a topological insulator and a superconductor[5]. In this context, Majoranas are not fermions like neutrinos but chargeless, spinless, zero energy quasi-particles that are their own antiparticles.

The non-local nature of Majorana states combined together with their non-abelian interchange property makes them basic pillars for the development of robust topological quantum computation[6–9]. From a physical point of view, the importance of such exotic entities do not only resides in their topological properties but they also represent a new state of matter never seen before. The main obstacle towards their detection is that they are not influenced by electrical or magnetic fields. Experimental evidences of Majorana states have been reported by using (i) superconducting nanowires with strong spin-orbit interaction and magnetic fields[10–17] and (ii) a chain of iron atoms formed on the surface of a superconducting lead[18]. In both cases Majorana physics is measured as a zero-bias anomaly present in the nonlinear differential conductance.

The mentioned proposals to detect Majoranas in nanowires are grounded on DC transport measurements[10,17]. In this paper we face the question of probing Majorana physics differently. We propose to employ the time dependent response of Majorana states to AC fields. In general, time dependent fields have already been used for many purposes.

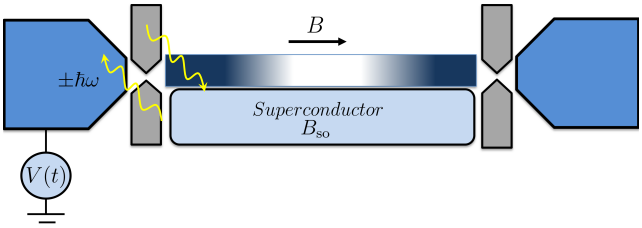

FIG. 1: Majorana nanowire circuit setup. A Majorana nanowire is tunnel barrier connected to metallic contacts. One of the contact is under the influence of an oscillatory electrical potential which drives charge and energy time dependent currents. Due to the presence of $V^{AC}(t)$ transport occurs by absorption or emission of energy quanta with energies $\hbar\omega$. The Majorana nanowire can be obtained, for example, by applying a magnetic field (B) and considering superconductivity and a Rashba field (B_{so}).

Instances are, charge qubit manipulation[19,20], controlled emission of electron-hole pairs[21], reconstruction of quantum states (tomography)[22,23] and leviton production[24], just to cite a few. For a slow AC driving, a second order expansion in the AC frequency yields a complex admittance usually characterized by two parameters, the capacitance C_q which provides spectroscopic information about the conductor and R_q that accounts for charge relaxation processes. Both quantities have been measured experimentally, in quantum capacitors,[25–29] carbon nanotubes,[30] superconducting josephson junctions,[31] and quantum dots[32].

The progress towards miniaturization and the new role of topology in the performance of new devices needs a profound understanding on how charge and energy flows response to electrical fields[33–35]. On the other hand, the cross-response of energy flow to an electrical signal lies in the field of thermoelectrical transport that for quantum systems is now an active area of research[36–42]. However, for topological materials its thermoelectrical response is, so far, a poor investigated issue[43–46].

Our objectives is to study the DC and AC response of the charge and energy currents in normal electrodes at-

tached to a Majorana nanowire. Then, either a static or a time-dependent electrical field generates a charge and energy current in the device. We focus our analysis of the admittance in the single terminal case. The considered setup is the topological analogue to the RC circuit by replacing the normal conductor (usually a quantum dot) by a Majorana nanowire. Our analytic results demonstrate that indeed, when superconductivity is present and for an ideal Majorana nanowire the RC circuit admittance has two contributions. Such admittance can be expanded in frequency up to second order in which the RC parameters appear. Then, the AC conductance is written as $g(\omega) = g_N(\omega) + g_S(\omega)$ where $g_N(\omega) = -i\omega C_q + \omega^2 C_q^2 R_q$ with $C_q = (1/2\pi)(e^2/2\Gamma)$, and $R_q = h/e^2$, that are the RC parameters for an normal quantum capacitor albeit for a factor two. Perfect Andreev processes add to the admittance a new term $g_S(\omega) = g_0 - i\omega C_S + \omega^2 C_S^2 R_S$. The first observation is that now C_S is a negative parameter. The sign of C_S reflects the fact that electrons are Andreev converted into holes, in which charge conservation is absent. Besides, the value for R_S is quite unusual. Adding both AC admittances, and since the currents that involve a Majorana mode are driven by Andreev processes, RC parameters for the full admittance are opposite in sign in comparison to the normal case, which is a remarkable finding.

Part of our results are also focused on the electrothermal energy admittance. It is known that for a normal RC circuit the energy current can be elapsed or delayed with respect to the AC signal depending on the conductor resonance positions. Besides, for interacting conductors, within a tunnel Hamiltonian formulation, the time-dependent energy flow needs a proper definition which includes the storage or accumulated energy at the tunnel barriers in order to keep causality[46,47]. For the topological RC circuit we derive the time-dependent energy current in the same spirit. Our results demonstrate that the AC energy formulation needs from a finite DC bias, otherwise such contribution vanishes due to electron hole symmetry.

The goal that we face consists of the calculation of the energy flux and charge flux in response to DC and AC electrical fields. For the time-dependent case, our transport formulation holds for arbitrary high frequencies, it is able to describe photon-assisted tunneling processes occurring in the energy-charge transport. Our only limitation is that we are restricted to the linear response regime, i.e., low AC driving amplitudes. For our calculations, we employ the nonequilibrium (Keldysh) Green's function formalism[48] which allows us to include the Majorana nanowire in a feasible way.

In Sec. II, we describe the theoretical model for a Majorana nanowire. We also derive both the stationary and time dependent energy and charge fluxes for a reservoir. From the previous results we obtain the electrical and electrothermal admittances. In Sec. III, we present our findings for DC and AC transport as a function of the quality of the Majorana state. Finally our conclusions are summarized in Sec. IV.

II. CHARGE AND ENERGY FORMULATION FOR A MAJORANA NANOWIRE

The aim of this work is to derive the electrical and energy currents for a circuit that contains a topological nanowire. For such purpose we consider a device comprised by one or two reservoirs tunnel coupled to different edges of a Majorana nanowire. Besides, we assume the influence of an AC potential applied directly to one of the reservoirs that oscillates in time. The Hamiltonian is formed by the three terms: $\mathcal{H}_C + \mathcal{H}_M + \mathcal{H}_T$ where

$$\mathcal{H}_C = \sum_{\alpha,k,\sigma} \varepsilon_{\alpha k\sigma}(t) c^\dagger_{\alpha k\sigma} c_{\alpha k\sigma}, \tag{1}$$

corresponds to the contact Hamiltonian composed by $\alpha = L, R$ electrodes [Left, Right]. Here, $\varepsilon_{\alpha k\sigma}(t) = \varepsilon_{\alpha k\sigma} + \mu_\alpha + eV_\alpha^{AC}(t)$ with $\mu_\alpha = E_F + eV_\alpha^{DC}$ as the chemical potential for the α-lead, $e > 0$ the unit charge, and $V_\alpha^{AC}(t)$ the electrical voltage modulation applied to the α-th electrode [see Fig. 1]. The operator $c^\dagger_{\alpha k\sigma}(c_{\alpha k\sigma})$ creates (annihilates) an electron with wavevector k and spin σ in the reservoir α. On the other hand, in a finite-length Majorana nanowire the two Majorana edge states have a finite overlap between their wave functions, which is quantified by the overlap integral $\varepsilon_{M_{ij}}$. The low-energy Hamiltonian of the Majorana nanowire is

$$\mathcal{H}_M = \sum_{i\neq j} \frac{i}{2} \varepsilon_{M_{ij}} \eta_i \eta_j = \frac{i}{4} \sum_{i,j} t_{ij} \eta_i \eta_j, \tag{2}$$

where $t_{11} = 0, \quad t_{22} = 0, \quad t_{12} = \varepsilon_M, \quad t_{21} = -\varepsilon_M$ and $\eta_i = \eta_i^\dagger$, $(i = \{1, 2\})$ are the two Majorana fermion operators which satisfy the Clifford algebra $\{\eta_i, \eta_j\} = 2\delta_{i,j}$. In addition, the Majorana operators can be written in terms of an ordinary fermion operator d which satisfies the usual fermionic commutation relations

$$\eta_1 = \frac{d + d^\dagger}{\sqrt{2}}, \quad \eta_2 = \frac{d - d^\dagger}{i\sqrt{2}}\,. \tag{3}$$

In terms of d operators the Majorana coupling term in Eq. (2) can be written as

$$\mathcal{H}_M = M_{12}(dd^\dagger - 1)\,, \tag{4}$$

which means that $M_{12(21)}$ is nothing but the energy splitting between empty $|0\rangle$ and filled ($|1\rangle = d^\dagger|0\rangle$) states. Finally, the tunneling between the lead α and each Majorana edge mode is,

$$\mathcal{H}_T = \sum_{\alpha,k,\sigma;\beta} \left[V^*_{\alpha k\sigma,\beta} c^\dagger_{\alpha k\sigma} \eta_\beta + V_{\alpha k\sigma,\beta} \eta_\beta c_{\alpha k\sigma} \right], \tag{5}$$

where $V_{\alpha k\sigma,\beta}$ is the tunneling amplitude which defines the tunneling rates between the reservoirs $\alpha = L, R$ and the Majoranas in the nanowire $\beta = 1, 2$.

Below, we use the Keldysh formalism for the calculation of nonequilibrium Green functions to derive the DC and AC transport for the energy and charge currents in terms of the Majorana nanowire Green functions.

A. DC charge current

1. General formulation of the charge current

We are interested in measuring the charge current at the α reservoir when DC and AC voltages are applied. We start with the calculation of the stationary charge flow. The charge current is the expectation value of the time derivative of the α-reservoir occupation operator

$$I_\alpha(t) = -e\langle \dot{n}_\alpha\rangle = -\frac{ie}{\hbar}\langle[\mathcal{H}, n_\alpha]\rangle\,, \tag{6}$$

where $n_\alpha = \sum_{k\in\alpha,\sigma} c^\dagger_{\alpha k\sigma}c_{\alpha k\sigma}$ denotes the α-reservoir quantum number operator. The current expression Eq. (6) is now expressed in terms of the lesser mixed lead-Majorana Green function $\mathcal{G}^<_{\alpha k\sigma,\beta}(t,t') = i\,\langle \eta_\beta(t')c_{\alpha k\sigma}(t)\rangle$ and the lesser Majorana-lead one $\mathcal{G}^<_{\beta,\alpha k\sigma}(t,t') = i\left\langle c^\dagger_{\alpha k\sigma}(t')\eta_\beta(t)\right\rangle$,

$$\begin{aligned} I_\alpha(t) \;=\; -\frac{e}{\hbar}\sum_{\beta,k\in\alpha,\sigma}\Big[&V_{\alpha k\sigma,\beta}(t)\mathcal{G}^<_{\alpha k\sigma,\beta}(t,t) \\ &-V^*_{\alpha k\sigma,\beta}(t)\mathcal{G}^<_{\beta,\alpha k\sigma}(t,t)\Big]\,. \end{aligned} \tag{7}$$

The current calculation can be simplified using the lead-Majorana and Majorana-lead equations of motion (EOM) and the Langreth rules dictated for swapping from a real time contour to a Keldysh complex time contour. In this manner the mixed Green functions are written as a function of the much simpler unperturbed green functions of the normal reservoir and the Majorana Green function,

$$\begin{aligned} \mathcal{G}^<_{\alpha k\sigma,\beta}(t,t') \;&=\; \frac{1}{\hbar}\sum_\gamma\int dt_1\; g^{e,r}_{\alpha k\sigma}(t,t_1)V^*_{\alpha k\sigma,\gamma}(t_1)\mathcal{G}^<_{\gamma,\beta}(t_1,t') \\ &+\; g^{e,<}_{\alpha k\sigma}(t,t_1)V^*_{\alpha k\sigma,\gamma}(t_1)\mathcal{G}^a_{\gamma,\beta}(t_1,t')\,, \\ \mathcal{G}^<_{\beta,\alpha k\sigma}(t,t') \;&=\; \frac{1}{\hbar}\sum_\gamma\int dt_1\; \mathcal{G}^r_{\beta,\gamma}(t,t_1)V_{\alpha k\sigma,\gamma}(t_1)g^{e,<}_{\alpha k\sigma}(t_1,t') \\ &+\; \mathcal{G}^<_{\beta,\gamma}(t,t_1)V_{\alpha k\sigma,\gamma}(t_1)g^{e,a}_{\alpha k\sigma}(t_1,t')\,, \end{aligned} \tag{8}$$

where $g^{e/h,r/a}_{\alpha k\sigma}(t_1,t_2)$ are the unperturbed reservoir retarded/advanced Green functions and $g^{e/h,<}_{\alpha k\sigma}(t_1,t_2)$ the lesser Green function both of them for the electron (hole) degrees of freedom [see appendix A]. On the other hand, $\mathcal{G}^{r/a}_{\beta,\gamma}(t_1,t_2)$ is the Majorana retarded (advanced) Green function and $\mathcal{G}^<_{\beta,\gamma}(t_1,t_2)$ is the lesser one. They are defined as $\mathcal{G}^<_{\beta,\gamma}(t_1,t_2) = -i\langle\eta_\gamma(t_2),\eta_\beta(t_1)\rangle$ and $\mathcal{G}^{r/a}_{\beta,\gamma}(t_1,t_2) = \mp i\theta(\pm t_1\mp t_2)\langle\{\eta_\beta(t_1),\eta_\gamma(t_2)\}\rangle$. The explicit expression for such Green functions can be found in the appendices A and B respectively.

Using the expressions of Eq. (8) we can write the charge current

$$\begin{aligned} &I_\alpha(t) = \\ &-\frac{e}{\hbar}\sum_{\beta,\gamma}\int\frac{dt_1}{\hbar}\Sigma^{e,r}_{0\alpha;\beta\gamma}(t,t_1)\mathcal{G}^<_{\gamma,\beta}(t_1,t)+\Sigma^{e,<}_{0\alpha;\beta\gamma}(t,t_1)\mathcal{G}^a_{\gamma,\beta}(t_1,t) \\ &-\mathcal{G}^r_{\beta,\gamma}(t,t_1)\Sigma^{e,<}_{0\alpha;\gamma\beta}(t_1,t) - \mathcal{G}^<_{\beta,\gamma}(t,t_1)\Sigma^{e,a}_{0\alpha;\gamma\beta}(t_1,t)\,. \end{aligned} \tag{9}$$

where the tunneling electron self-energies are defined as follows

$$\Sigma^{e,r/a}_{0\alpha;\beta\gamma}(t_1,t_2) = \sum_{k\in\alpha,\sigma} V_{\alpha k\sigma,\beta}(t_1)\mathrm{g}^{e,r/a}_{\alpha k\sigma}(t_1,t_2)V^*_{\alpha k\sigma,\gamma}(t_2)\,, \tag{10a}$$

$$\Sigma^{e,<}_{0\alpha;\beta\gamma}(t_1,t_2) = \sum_{k\in\alpha,\sigma} V_{\alpha k\sigma,\beta}(t_1)\mathrm{g}^{e,<}_{\alpha k\sigma}(t_1,t_2)V^*_{\alpha k\sigma,\gamma}(t_2)\,, \tag{10b}$$

and the hole ones

$$\Sigma^{h,r/a}_{0\alpha;\beta\gamma}(t_1,t_2) = \sum_{k\in\alpha,\sigma} V^*_{\alpha k\sigma,\beta}(t_1)\mathrm{g}^{h,r/a}_{\alpha k\sigma}(t_1,t_2)V_{\alpha k\sigma,\gamma}(t_2)\,, \tag{11a}$$

$$\Sigma^{h,<}_{0\alpha;\beta\gamma}(t_1,t_2) = \sum_{k\in\alpha,\sigma} V^*_{\alpha k\sigma,\beta}(t_1)\mathrm{g}^{h,<}_{\alpha k\sigma}(t_1,t_2)V_{\alpha k\sigma,\gamma}(t_2)\,. \tag{11b}$$

2. Stationary charge current

We consider first the stationary regime for the electrical current as a preliminary step of the time-dependent AC calculation, this implies to make $V^{AC}_\alpha(t) = 0$. In this sense, we are able to recover the Majorana quantum of conductance $(2e^2/h)$ for a topological NS junction reported in the literature[49,50] and the known values of the DC current further away of the linear regime[51,52].

In general, it is advantageous to switch to energy space, then the DC charge current expression Eq. (9) in matricial form is reduced to

$$I_\alpha = -\frac{2e}{h}\Re e\left\{\int d\varepsilon \mathrm{Tr}[\mathbf{\Sigma}^{e,r}_{0\alpha}(\varepsilon)\mathcal{G}^<_\eta(\varepsilon) + \mathbf{\Sigma}^{e,<}_{0\alpha}(\varepsilon)\mathcal{G}^a_\eta(\varepsilon)\right\}\,, \tag{12}$$

where the tunneling self-energy $\mathbf{\Sigma}^{<,r/a}_0(\varepsilon) = \mathbf{\Sigma}^{e,<,r/a}_0(\varepsilon) + \mathbf{\Sigma}^{h,<,r/a}_0(\varepsilon)$. In this expression,

$$\mathbf{\Sigma}^{e,r/a}_0(\varepsilon) = \sum_\alpha \mp i\mathbf{\Gamma}_\alpha(\varepsilon) + \mathbf{\Lambda}_\alpha(\varepsilon)\,, \tag{13}$$

and

$$\mathbf{\Sigma}^{h,r/a}_0(\varepsilon) = \sum_\alpha \mp i\mathbf{\Gamma}_\alpha(-\varepsilon) - \mathbf{\Lambda}_\alpha(-\varepsilon)\,. \tag{14}$$

They depend on the reservoir-Majorana nanowire coupling with matrix elements $[\mathbf{\Gamma}_\alpha(\varepsilon)]_{\gamma\beta} = \Gamma_{\alpha,\gamma\beta}(\varepsilon) = 2\pi\sum_{k\in\alpha} V_{\alpha k\sigma,\gamma}V^*_{\alpha k\sigma,\beta}\delta(\varepsilon-\varepsilon_{\alpha k\sigma})$ and on $[\mathbf{\Lambda}_\alpha(\varepsilon)]_{\gamma\beta} = \Lambda_{\alpha,\gamma\beta}(\varepsilon) = \sum_{k\in\alpha} V_{\alpha k\sigma,\gamma}V^*_{\alpha k\sigma,\beta}/(\varepsilon-\varepsilon_{\alpha k\sigma})$. For the lesser hopping self energy we have similar expressions,

$$\mathbf{\Sigma}_0^{e,<}(\varepsilon) = \sum_\alpha i f_e^\alpha(\varepsilon)\mathbf{\Gamma}_\alpha(\varepsilon)\,, \tag{15}$$

and

$$\mathbf{\Sigma}_0^{h,<}(\varepsilon) = \sum_\alpha i f_h^\alpha(-\varepsilon)\mathbf{\Gamma}_\alpha(-\varepsilon)\,, \tag{16}$$

that also depend on the Fermi function for electron $f(\varepsilon - V_\alpha^{DC}) = f_e^\alpha(\varepsilon)$ and hole degrees of freedom $f(\varepsilon+V_\alpha^{DC}) = f_h^\alpha(\varepsilon)$.

On the other hand, the full retarded(advanced) Majorana Green function reads

$$\mathcal{G}_\eta^{r/a}(\varepsilon) = \frac{2}{\varepsilon - i\mathbf{t} - 2\mathbf{\Sigma}_0^{r/a}(\varepsilon)}\,, \tag{17}$$

where $\mathbf{t}$ is the hybridization energy matrix with elements $t_{i,j} = \varepsilon_{M_{ij}}$ of $i \neq j$. Note that the Majorana Green function is given in matricial form $[\mathcal{G}_\eta^{<,r/a}]_{\gamma,\beta} = \mathcal{G}_{\gamma,\beta}^{<,r/a}$. Finally, the lesser Majorana Green function component takes the simple form

$$\mathcal{G}_\eta^<(\varepsilon) = \mathcal{G}_\eta^r(\varepsilon)\mathbf{\Sigma}_0^<(\varepsilon)\mathcal{G}_\eta^a(\varepsilon)\,. \tag{18}$$

Having in mind all these results the stationary DC current takes the form

$$I_\alpha = \frac{e}{h}\Im m\Big\{\int d\varepsilon \mathrm{Tr}\Big[f_e^\alpha(\varepsilon)\left(\mathcal{G}_\eta^r(\varepsilon) - \mathcal{G}_\eta^a(\varepsilon)\right)\mathbf{\Gamma}_\alpha(\varepsilon) + \mathcal{G}_\eta^<(\varepsilon)\mathbf{\Gamma}_\alpha(\varepsilon)\Big]\Big\}\,. \tag{19}$$

In spite of the familiar expression for the current notice that I_α is composed by electron and hole contributions and accounts Andreev tunneling events to transport charge. For a better understanding, let us insert explicitly Eqs. (17) and (18) in Eq. (19),

$$I_\alpha = -\frac{e}{h}\Big\{\int d\varepsilon \mathrm{Tr}\Big[\mathbf{\Gamma}_\alpha\mathcal{G}_\eta^r(\varepsilon)\sum_\beta \mathbf{\Gamma}_\beta\big(f_e^\beta(\varepsilon) + f_h^\beta(\varepsilon) - 2f_e^\alpha(\varepsilon)\big)\mathcal{G}_\eta^a(\varepsilon)\Big]\Big\}\,, \tag{20}$$

where we have applied the wide band limit approximation $\mathbf{\Gamma}_\alpha(\varepsilon) \approx \mathbf{\Gamma}_\alpha$.

In general, for an arbitrary bias configuration we have $I_L \neq -I_R$ that violates current conservation. To keep the current conservation law satisfied the chemical potentials in the reservoirs need to be symmetric $\mu_L = -\mu_R = eV/2$.

In such bias configuration, and for an ideal Majorana nanowire the charge current in the linear voltage regime simplifies to $I_L = -I_R = (2e/h)\mu_L = (2e^2/h)V/2$ that leads to a linear conductance $G_0 = dI_\alpha/dV = 1/2(2e^2/h)$ because V is the total measured voltage drop of the circuit.

3. *Stationary charge current in a many nanowire device*

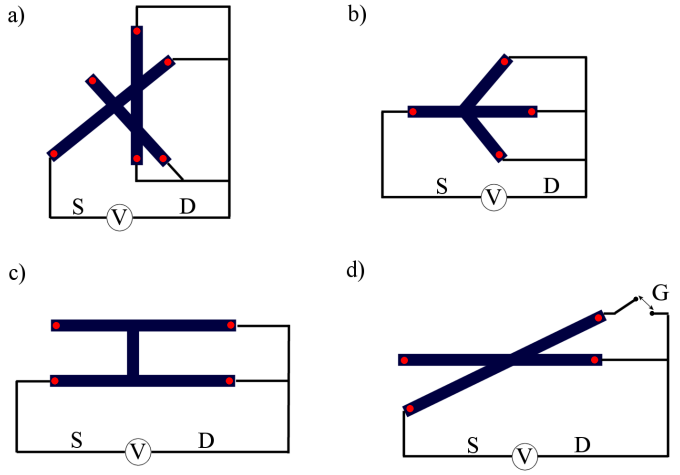

FIG. 2: Schematics of different many nanowire devices. Different Majorana nanowires (in blue) are interconnected in different ways to each other. Each Majorana (red dots) are attached to the nanowire edges and tunnel coupled to a source S or a drain D. Additionally in the device d) a gate G can be open or close to connect and disconnect a Majorana with the drain electrode.

We can extend our calculations of the stationary charge current to a whole family of many nanowire devices, provided that the hybridization energy between Majoranas is maintained close to zero. As shown in Fig. 2, we can define many Majorana devices made of N' nanowires with $2N'$ edges where each edge contains a Majorana state. At the same time, these Majoranas can be coupled to N reservoirs [$2N' > N$, not every Majorana needs to be coupled to a reservoir]. A specific description of the interaction between Majoranas would be needed for each particular device found in Fig. 2. Furthermore, these interactions will depend on the particular way in which the various Majorana nanowires are interconnected. However, if the Majoranas are well located on the edges the interaction between them is approximately zero. Therefore, the particularities of the unions between nanowires become irrelevant because Majoranas are edge states. On practical level, such devices will be modeled by a Hamiltonian with Eq. (1) contact and Eq. (5) tunneling energies where $\alpha = \{1, N\}$ and $\beta = \{1, 2N'\}$.

In this sense we can consider, for example, setups where $N-1$ Majorana states are tunnel coupled to a (*right side*) drain electrode, biased with $\mu_D = -eV_{SD}/N$

and the remaining edge state (*left side*) is contacted to a single terminal source biased by $\mu_S = ((N-1)/N)eV_{SD}$ where V_{SD} is the total potential drop between the source and the drain. Under these circumstances the source and drain voltage drop are determined selfconsistently making the current to be conserved through all the terminals $\sum_{i=1}^{i=N} I_i = 0$. Remarkably, this configuration leads to exotic Majorana conductances $G_0 = (2e^2/h)(N-1)/N$.

Additionally, in Fig. 2d we can see a nanowire arrangement similar to the ones proposed for braiding schemes[9,53,54]. In this arrangement opening or closing the gate G has the effect to change the Majorana conductance from $G_0 = e^2/h$ to $G_0 = 4/3(e^2/h)$.

B. DC energy current

The DC energy current calculation is very similar to the one done for charge. Energy current at the normal lead α is calculated as the energy change in the reservoir as follows

$$J_\alpha(t) = \langle \dot{H}_\alpha \rangle = \frac{i}{\hbar}\langle [\mathcal{H}, H_\alpha] \rangle \,, \tag{21}$$

where $H_\alpha = \sum_{k,\sigma} \varepsilon_{\alpha k\sigma}(t) c^\dagger_{\alpha k\sigma} c_{\alpha k\sigma}$ is the energy at the reservoir. In the same manner than in the charge calculation the resulting expression can be written in terms of the mixed Green functions

$$J_\alpha(t) = \frac{1}{\hbar}\sum_{\beta,k\in\alpha,\sigma} \varepsilon_{\alpha k\sigma}\left[V_{\alpha k\sigma,\beta}\mathcal{G}^<_{\alpha k\sigma,\beta}(t,t) - V^*_{\alpha k\sigma,\beta}\mathcal{G}^<_{\beta,\alpha k\sigma}(t,t)\right] . \tag{22}$$

We use here too the equation of motion for the mixed Green functions $\mathcal{G}^<_{\alpha k\sigma,\beta}(t,t)$ and $\mathcal{G}^<_{\beta,\alpha k\sigma}(t,t)$ and the Langreth rules to express the DC energy flow only in terms of the unperturbed reservoir and the Majorana Green functions. The matricial expression for the energy flow can be arranged to read

$$J_\alpha(t) = \frac{1}{\hbar}\int dt_1 Tr\left[\tilde{\Sigma}^{e,r}_{0\alpha}(t,t_1)\mathcal{G}^<_\eta(t_1,t) + \tilde{\Sigma}^{e,<}_{0\alpha}(t,t_1)\mathcal{G}^a_\eta(t_1,t) - \mathcal{G}^r_\eta(t,t_1)\tilde{\Sigma}^{e,<}_{0\alpha}(t_1,t) - \mathcal{G}^<_\eta(t,t_1)\tilde{\Sigma}^{e,a}_{0\alpha}(t_1,t)\right] , \tag{23}$$

where the matrix elements for $\tilde{\Sigma}^{e[<,r/a]}_{0\alpha}(t_1,t_2)$ are

$$\tilde{\Sigma}^{e[<,r/a]}_{0\alpha;\beta\gamma}(t_1,t_2) = \sum_{k\in\alpha,\sigma} \varepsilon_{\alpha k\sigma} V_{\alpha k\sigma,\beta}(t_1) \mathrm{g}^{e[<,r/a]}_{\alpha k\sigma}(t_1,t_2) V^*_{\alpha k\sigma,\gamma}(t_2) \,, \tag{24}$$

therefore the energy current expression reads

$$\begin{aligned} J_\alpha \;=\; & -\frac{1}{h}\Im m\Big\{ \int d\varepsilon\varepsilon \mathrm{Tr}\Big[f^\alpha_e(\varepsilon)\left(\mathcal{G}^r_\eta(\varepsilon) - \mathcal{G}^a_\eta(\varepsilon)\right)\mathbf{\Gamma}_\alpha(\varepsilon) \\ & +\; \mathcal{G}^<_\eta(\varepsilon)\mathbf{\Gamma}_\alpha(\varepsilon)\Big]\Big\} . \end{aligned} \tag{25}$$

Inserting Eqs. (17) and (18) in Eq. (25) and again under the wide limit approximation we arrive at

$$\begin{aligned} J_\alpha = \frac{1}{h}\Big\{ \int d\varepsilon\varepsilon \mathrm{Tr}\Big[& \mathbf{\Gamma}_\alpha \mathcal{G}^r_\eta(\varepsilon) \sum_\beta \mathbf{\Gamma}_\beta \big(f^\beta_e(\varepsilon) + f^\beta_h(\varepsilon) \\ & - 2f^\alpha_e(\varepsilon)\big)\mathcal{G}^a_\eta(\varepsilon)\Big]\Big\} . \end{aligned} \tag{26}$$

It is worthy to realize that the energy DC current vanishes identically due to the intrinsic particle-hole symmetry of the system. However this does not mean the the heat current is zero because the heat flow $Q_\alpha = J_\alpha - IV$ where $V = V_L - V_R$ is the total voltage drop. The only heat transfer in a truly Majorana device is due the Joule heating.

C. Time dependent AC charge current

We are now in position to compute the time dependent charge current for a Majorana nanowire. The calculation starts in the same way than the DC current calculation and the same steps are repeated until Eq. (9). However, the unperturbed electron(hole) lesser Green functions of the reservoir are now multiplied by $e^{-i\phi_\alpha(t_1,t_2)}$ where $\phi_\alpha(t_1,t_2) = \int_{t_2}^{t_1} dt' V^{AC}_\alpha(t')$. $V^{AC}_\alpha(t')$ is the AC driving potential at reservoir α. The electron(hole) self energies $\Sigma^{e/h,<}_0$ definitions [given by Eqs. (10b) and (11b)] depend on these Green functions, therefore they are also proportional to this term. We are interested in the linear response regime, for such purpose we expand the selfenergies $\Sigma^{e/h,<}_0$ at leading order in the AC driving intensity V^{AC}_α, then the electron and hole component read

$$\begin{aligned} \Sigma^{e/h,<}_{0\alpha;\beta\gamma}(t_1,t_2) \;&=\; e^{\mp i\phi_\alpha(t_1,t_2)}\Sigma^{e/h,<}_{0\alpha;\beta\gamma}(t_1,t_2)|_{\phi_\alpha(t_1,t_2)=0} \\ &\approx\; \Sigma^{e/h,<}_{0\alpha;\beta\gamma}(t_1,t_2)[1 \mp i\phi_\alpha(t_1,t_2)] \,, \end{aligned} \tag{27}$$

whereas $\Sigma^{e/h,r/a}_{0\alpha\beta\gamma}$ are time independent. The next step is the calculation of the time dependent Majorana Green functions for the retarded(advanced) and lesser components [see again appendix B]. Inserting the self-energies of Eqs. (10), (11) and (27) in the Majorana Green function expressions we obtain *(i)* that the retarded(advanced) Majorana Green function is kept as the stationary form whereas *(ii)* the lesser Green function becomes

$$\mathcal{G}_\eta^<(t,t') = i\sum_\gamma \Bigg(\int \frac{d\varepsilon_1}{2\pi} e^{-i\frac{\varepsilon_1}{\hbar}(t-t')} \mathcal{G}_\eta^r(\varepsilon_1)\mathbf{\Gamma}_\gamma (f_e^\gamma(\varepsilon_1) + f_h^\gamma(\varepsilon_1))\mathcal{G}_\eta^a(\varepsilon_1) - \int \frac{d\varepsilon_1}{2\pi}\int \frac{d\varepsilon_2}{2\pi}\; e^{-i\frac{\varepsilon_1}{\hbar}t} e^{-i\frac{\varepsilon_2}{\hbar}(t-t')} \mathcal{G}_\eta^r(\varepsilon_1+\varepsilon_2) eV_\alpha^{AC}(\varepsilon_1)\mathbf{\Gamma}_\gamma (F_e^\gamma(\varepsilon_1,\varepsilon_2) - F_h^\gamma(\varepsilon_1,\varepsilon_2))\mathcal{G}_\eta^a(\varepsilon_2)\Bigg), \quad (28)$$

where we have defined $F^\gamma(\varepsilon_1,\varepsilon_2) = [f^\gamma(\varepsilon_1+\varepsilon_2) - f^\gamma(\varepsilon_2)]/\varepsilon_1$.

Inserting now the time dependent Majorana Green functions such as Eq. (28) in the current expression [Eq. (9)] and after a tedious but simple algebra we arrive at

$$I_\alpha(t) = -\frac{e}{\hbar}\mathrm{Tr}\Bigg[\sum_\gamma \int_{-\infty}^{+\infty} \frac{d\varepsilon_1}{2\pi}\mathbf{\Gamma}_\alpha \mathcal{G}_\eta^r(\varepsilon_1)\mathbf{\Gamma}_\gamma (f_e^\gamma(\varepsilon) + f_h^\gamma(\varepsilon) - 2f_e^\alpha(\varepsilon))\mathcal{G}_\eta^a(\varepsilon_1) + i\sum_\gamma \int_{-\infty}^{+\infty}\frac{d\varepsilon_1}{2\pi}\int_{-\infty}^{+\infty}\frac{d\varepsilon_2}{2\pi} e^{-i\frac{\varepsilon_1}{\hbar}t} i\mathbf{\Gamma}_\gamma \mathcal{G}_\eta^r(\varepsilon_1+\varepsilon_2)\mathbf{\Gamma}_\alpha (F_e^\gamma(\varepsilon_1\varepsilon_2) - F_h^\gamma(\varepsilon_1,\varepsilon_2) - 2F_e^\alpha(\varepsilon_1,\varepsilon_2))\mathcal{G}_\eta^a(\varepsilon_2) eV_\alpha^{AC}(\varepsilon_1) - i\sum_\gamma \int_{-\infty}^{+\infty}\frac{d\varepsilon_1}{2\pi}\int_{-\infty}^{+\infty}\frac{d\varepsilon_2}{2\pi} e^{-i\frac{\varepsilon_1}{\hbar}t}\frac{\varepsilon_1}{2}\mathcal{G}_\eta^r(\varepsilon_1+\varepsilon_2)\mathbf{\Gamma}_\alpha F_e^\alpha(\varepsilon_1,\varepsilon_2)\mathcal{G}_\eta^a(\varepsilon_2) eV_\alpha^{AC}(\varepsilon_1)\Bigg]. \quad (29)$$

Some comments on Eq. (29) are in order. First of all, the first integral of Eq. (29) accounts for the DC current component already calculated above while the second and third integrals take into account the purely AC contribution. If we consider in Eq. (29) a change in the potential reservoir caused only by the AC modulation ($V_{DC} = 0$) then $F_e^\alpha(\varepsilon_1,\varepsilon_2) = F_h^\alpha(\varepsilon_1,\varepsilon_2) = F^\alpha(\varepsilon_1,\varepsilon_2)$, therefore the AC current spectrum reads,

$$I_\alpha(\varepsilon) = \frac{ie^2}{2h}\int_{-\infty}^{+\infty} d\varepsilon' \mathrm{Tr}\Bigg[\mathcal{G}_\eta^r(\varepsilon+\varepsilon')\mathbf{\Gamma}_\alpha \times \left(\varepsilon + 4i\sum_\gamma \mathbf{\Gamma}_\gamma\right)\mathcal{G}_\eta^a(\varepsilon')F^\alpha(\varepsilon,\varepsilon')V_\alpha^{AC}(\varepsilon)\Bigg]. \quad (30)$$

Finally, from Eq. (30) is straightforward to obtain the electrical AC admittance $g_\alpha(\varepsilon) = dI_\alpha/dV_\alpha^{AC}$,

$$g_\alpha(\varepsilon) = \frac{ie^2}{2h}\int_{-\infty}^{+\infty} d\varepsilon' \mathrm{Tr}\Bigg[\mathcal{G}_\eta^r(\varepsilon+\varepsilon')\mathbf{\Gamma}_\alpha \times \left(\varepsilon + 4i\sum_\gamma \mathbf{\Gamma}_\gamma\right)\mathcal{G}_\eta^a(\varepsilon')F^\alpha(\varepsilon,\varepsilon')\Bigg]. \quad (31)$$

In the following, we investigate the AC current signal for a quantum capacitor. In such a case we consider that a single terminal is tunnel coupled to the topological Majorana nanowire. This system then represents the minimal quantum capacitor circuit. In this case, Eq. (29) can be written as the sum of two contributions, $g(\omega) = g_N(\omega) + g_S(\omega)$,

$$g_N(\varepsilon) = \frac{ie^2}{2h}\varepsilon\int_{-\infty}^{+\infty} d\varepsilon' \mathrm{Tr}\big[\mathcal{G}_\eta^r(\varepsilon+\varepsilon')\mathbf{\Gamma}\mathcal{G}_\eta^a(\varepsilon')F_e(\varepsilon,\varepsilon')\big] \quad (32)$$

and

$$g_S(\varepsilon) = \frac{ie^2}{2h}2i\mathbf{\Gamma}\int_{-\infty}^{+\infty} d\varepsilon' \mathrm{Tr}\big[\mathcal{G}_\eta^r(\varepsilon+\varepsilon')\mathbf{\Gamma}\mathcal{G}_\eta^a(\varepsilon') \times [F_e(\varepsilon,\varepsilon') + F_h(\varepsilon,\varepsilon')]\big]. \quad (33)$$

Our first observation by comparing g_N and g_S is that g_N coincides with the expression for a normal RC setup albeit for a factor two caused by the Majorana statistics. The contribution $g_S(\varepsilon)$ contains the electron and hole Fermi factors as the F_e and F_h functions. This admittance reflects the fact that Andreev transport is present in the system which converts electrons into holes. Such conversion is reflected in the fact that now the admittance g_S has a relative phase compared with g_N of π [see details below].

Now for sufficiently slow AC signals we can perform an AC frequency expansion of both contributions for the electrical AC admittance $g_N(\omega)$, and $g_S(\omega)$ to determine the RC parameters. We perform such frequency expansion firstly for $g_N(\omega) \approx -i\omega C_q + \omega^2 C_q^2 R_q$, where

$C_q = \frac{1}{2\pi}\frac{e^2}{2\Gamma}$ and $R_q = \frac{h}{e^2}$. In normal conductors it is found that $R_q = h/2e^2$ exhibits an universal value[55–59] and $C_q = (1/2\pi)(e^2/\Gamma)$ in the particular case of a normal quantum dot. In those cases C_q has a physical sense as a quantum capacitance while R_q is related to charge relaxation resistance. Since the Majorana edge state has a Green function with a tunneling selfenergy that accounts for the electron and hole parts $\Gamma_e + \Gamma_h = 2\Gamma$, then the quantum capacitance reflects this fact as $C_q = \frac{1}{2\pi}\frac{e^2}{2\Gamma}$. This value is modified as long as the two Majorana edge states hybridize. For a finite overlap Majorana nanowire our results show $C_q = e^2\Gamma/(\pi\varepsilon_M^2)$. Therefore, the contribution of g_N to the capacitance offers a good indicator of the presence of a Majorana state having a fixed value for C_q.

We can now explore some limits from which R_q has simple form. In the zero temperature limit $R_q = h/e^2$. We have checked that indeed this value is kept independently if the two Majorana edge modes overlap or not. This result reflects the fact that the system is always coherent, either showing a non-local half-fermionic state at each nanowire edge or having a coherent electronic state broadly extended along the nanowire (for large values of ε_M). The total charge relaxation resistance is seen as the sum of two serial resistances of $h/2e^2$, each for electron and hole sectors. Then the total charge relaxation resistance becomes h/e^2 from the fact that the nanowire is superconductor.

The second contribution to the admittance is represented by Eq. (33) that shows an explicit dependence on the Andreev reflection processes. Due to the electron to hole conversion this admittance carries a global phase factor of π compared with g_N. This fact yields an unphysical negative capacitance when why try to make a comparison with a traditional RC system. The main reason is because we have Andreev processes that imply a Cooper pair outgoing supercurrent. If we try to do the RC analogy the obtained capacitance is then $C_S = -(1/2\pi)(e^2/\Gamma)$ which accounts the fact that electrons are converted into holes. Besides the R_S value takes a quite unusual value of $R_S = -\frac{5h}{12e^2}$ which has not a clear physical interpretation.

D. Time dependent energy current

Our purpose in this section is the derivation of the time dependent energy current for a Majorana nanowire in contact with a single reservoir in a capacitor setup. We evaluate the time derivative of each component of the Hamiltonian which is given by

$$\mathcal{Q}_X = \frac{d}{dt}\langle\mathcal{H}_X\rangle = \frac{i}{\hbar}\langle[\mathcal{H},\mathcal{H}_X]\rangle + \left\langle\frac{\partial\mathcal{H}_X}{\partial t}\right\rangle = \mathcal{J}_C(t) + P(t)\,, \tag{34}$$

where $\mathcal{Q}_X$ is the heat flow at the reservoir, $X = \{C, M, T\}$ is referred to C contact, M Majorana nanowire, and T tunneling term. Notice that in Eq. (34) the last term is the power $P(t) = I(t)V(t)$ supplied by an external source that must be equal to the heat dissipation far inside the reservoir. Besides, since the Hamiltonian operator $\mathcal{H}$ commutes with itself it is fulfilled

$$\frac{i}{\hbar}\langle[\mathcal{H},\mathcal{H}]\rangle = \mathcal{J}_C + \mathcal{J}_M + \mathcal{J}_T = 0\,, \tag{35}$$

where $\mathcal{J}_C$,$\mathcal{J}_M$ and $\mathcal{J}_T$ are the energy rates at the contact, the Majorana nanowire and at the interface between them.

As mentioned, our goal is to compute the flow of energy at the Majorana nanowire circuit that it is equal to the flow at the contact. For the stationary energy current above we did the calculation of the energy flow at the reservoir. However, a calculation of $\mathcal{J}_C$ is cumbersome in presence of an AC driving, therefore our strategy is to compute the energy change rates for the Majorana nanowire and tunnel barrier and then use Eq. (35) by energy conservation,

$$\mathcal{J}_C = -(\mathcal{J}_M + \mathcal{J}_T)\,. \tag{36}$$

Note than the AC driving lies in the reservoir therefore $\mathcal{H}_X$ with $X = T, M$ does not have any explicit dependence on time. Therefore, in these two cases $\mathcal{Q}_X = \mathcal{J}_X$ and we can make the approximation $d_t\langle\mathcal{H}_H\rangle = \partial_t\langle\mathcal{H}_H\rangle$ because the only time dependence is the explicit one from the time evolution operators. We start with the calculation from the time derivative of the lesser Majorana Green function

$$\mathcal{J}_M = \partial_t\langle\mathcal{H}_M\rangle \;= \frac{i}{4}\mathrm{Tr}\left[\mathbf{t}\partial_t\mathcal{G}^<_\eta(t,t)\right]\,. \tag{37}$$

Then, using Eq. (28) is easy to arrive at

$$\mathcal{J}_M(t) = \frac{ie}{4\hbar}\mathrm{Tr}\Bigg[\int\frac{d\varepsilon_1}{2\pi}\int\frac{d\varepsilon_2}{2\pi}e^{-i\frac{\varepsilon_1 t}{\hbar}}(i\mathbf{t}\varepsilon_1)\mathcal{G}^r_\eta(\varepsilon_1+\varepsilon_2) \times\left(F_e(\varepsilon_1,\varepsilon_2) - F_h(\varepsilon_1,\varepsilon_2)\right)\mathbf{\Gamma}\mathcal{G}^a_\eta(\varepsilon_2)V^{AC}(\varepsilon_1)\Bigg]\,. \tag{38}$$

Similarly, for the energy rate at the barrier we employ: $\mathcal{J}_T = \partial_t\langle\mathcal{H}_T\rangle$ where $\mathcal{H}_T$ is given by Eq. (5), which in terms of Green functions it reads as

$$\langle\mathcal{H}_T\rangle = -i\sum_{k,\sigma;\beta}\left[V_{k\sigma,\beta}\mathcal{G}^<_{k\sigma,\beta}(t,t) + V^*_{k\sigma,\beta}\mathcal{G}^<_{\beta,k\sigma}(t,t)\right]\,. \tag{39}$$

This now, it can be expressed in terms of Majorana Green functions by using the expressions of Eq. (8). In this manner the energy rate for the tunneling contribution becomes

$$\mathcal{J}_T(t) = \frac{ie}{2\hbar}\mathrm{Tr}\Bigg[\int_{-\infty}^{+\infty}\frac{\varepsilon_1}{2\pi}\int_{-\infty}^{+\infty}\frac{\varepsilon_2}{2\pi}e^{-i\frac{\varepsilon_1 t}{\hbar}}\varepsilon_1(\varepsilon_1+2\varepsilon_2-2i\mathbf{t}) \mathcal{G}^r_\eta(\varepsilon_1+\varepsilon_2)\mathbf{\Gamma}_\alpha\mathcal{G}^a_\eta(\varepsilon_2)F_e(\varepsilon_1,\varepsilon_2)V^{AC}(\varepsilon_1)\Big]\,. \tag{40}$$

Now using Eq. (36), (38) and (40) we can obtain the energy rate spectrum for the reservoir. However, neither $\mathcal{J}_C(\omega)$ nor $\mathcal{J}_M(\omega)$ have a well defined parity when the AC frequency is reversed, and therefore, within linear response theory, these two magnitudes do not represent physical quantities. Based on these observations, the reservoir and Majorana frequency dependent energy current expressions must be thus modified to exhibit a proper parity property when the AC frequency is reversed. We propose the expressions

$$\bar{\mathcal{J}}_C = \mathcal{J}_C(\omega) + \frac{1}{2}\mathcal{J}_T(\omega),\ \bar{\mathcal{J}}_M = \mathcal{J}_M(\omega) + \frac{1}{2}\mathcal{J}_T(\omega)\,, \quad (41)$$

that satisfy the parity property in close analogy as it has been done in quantum dot systems[46,47]. Remarkably, the choice of the factor $\frac{1}{2}\mathcal{J}_T(\omega)$ is unique in order to ensure a well defined parity property in both $\bar{\mathcal{J}}_C$, and $\bar{\mathcal{J}}_M$. Therefore, under the same considerations and approximations than in previous sections the contact energy flux reads,

$$\begin{aligned}\bar{\mathcal{J}}_C(t) \;=\; & -\frac{ie}{4\hbar}\mathrm{Tr}\Big[\int_{-\infty}^{+\infty}\frac{d\varepsilon_1}{2\pi}\int_{-\infty}^{+\infty}\frac{d\varepsilon_2}{2\pi}e^{-i\frac{\varepsilon_1 t}{\hbar}}\varepsilon_1(\varepsilon_1+2\varepsilon_2)\mathcal{G}^r_\eta(\varepsilon_1+\varepsilon_2)\mathbf{\Gamma}\mathcal{G}^a_\eta(\varepsilon_2)F_e(\varepsilon_1,\varepsilon_2)V^{AC}(\varepsilon)\\ & +\frac{ie}{4\hbar}\mathrm{Tr}\Big[\int_{-\infty}^{+\infty}\frac{d\varepsilon_1}{2\pi}\int_{-\infty}^{+\infty}\frac{d\varepsilon_2}{2\pi}e^{-i\frac{\varepsilon_1 t}{\hbar}}i\mathbf{t}\varepsilon_1\mathcal{G}^r_\eta(\varepsilon_1+\varepsilon_2)\mathbf{\Gamma}\mathcal{G}^a_\eta(\varepsilon_2)\left(F_e(\varepsilon_1,\varepsilon_2)+F_h(\varepsilon_1,\varepsilon_2)\right)V^{AC}(\varepsilon)\,. \quad (42)\end{aligned}$$

In the presence of a time dependent driving force, it is quite general to characterize the transport using the concept of admittance, and in this case the electrothermal admittance, defined as

$$m(\omega) = \frac{\bar{\mathcal{J}}_C(\omega)}{V_\alpha^{AC}(\omega)}. \quad (43)$$

We recall that $\bar{\mathcal{J}}_C(\omega)$ refers to the contact. Although the electrothermal admittance $m(\omega)$ is defined for the case of zero DC bias like the electrical one in general it is necessary the simultaneous application of an AC driving and a DC bias to obtain a non-zero electrothermal response of a Majorana capacitor. Therefore it is necessary to extend the definition of $m(\omega)$ to non-zero bias setups otherwise $m(\omega) = 0$ independently of the frequency ω and the hybridization value ε_M.

III. RESULTS

Our results are presented in this section where we investigate the DC and AC transport for the electrical and energy currents.

A. DC charge transport

We begin by analyzing the DC transport for the electrical and heat currents in a two terminal system in Fig. 3. We consider a symmetrically biased Majorana nanowire, i.e., $V_L = -V_R = V/2$. Firstly, we study the effect of the Majorana hybridization term $\varepsilon_M \neq 0$ in the I-V characteristic as shown in Fig. 3(a). The current becomes linear only for a small range of voltages [see Fig. 3(a) blue curve in comparison with the linearized current curve in black]. We observe that the electrical current is suppressed rapidly by increasing ε_M from zero because the Majorana state is destroyed and a fermionic state emerges at energies that are now not at zero energy. The effect of temperature is shown in Fig. 3(b). Temperature has a minor effect on the current in comparison with a finite Majorana hybridization. Nevertheless, starting with a good Majorana state with $\varepsilon_M = 0$ an enhancement of temperature tends to diminish globally the electrical current (see Fig. 3(b)) and the conductance diluting the Majorana signature.

B. DC heat transport

For the heat current versus the DC bias voltage we have a similar scenario than in the charge current as depicted in Fig. 3(c). The curve Q-V characteristic is quadratic by construction and it corresponds to the Joule heating. An enhancement of ε_M suppresses quite quickly the heat current due to the suppression of the electrical current. Finally, in Fig. 3(d) the heat current is shown for an ideal Majorana state and different temperature values. As previously, an increase of temperature leads to a reduced heat current due to a diminution of the electrical flow.

C. AC charge transport

Next, we focus on the behavior of the real and imaginary parts of the purely electrical admittance [shown in Figs. 4 and 5]. For simplicity we consider the single

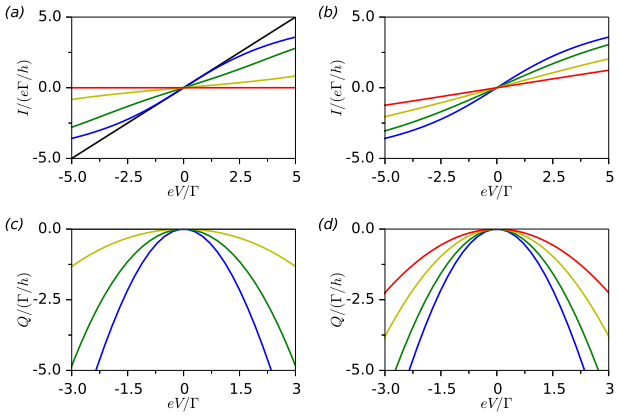

FIG. 3: a) Two terminal DC charge current $I/(e\Gamma/h)$ as function of the voltage bias eV/Γ for different Majorana hybridization energies $\varepsilon_M/\Gamma = 0.0, 0.2, 0.5, 100$ in blue, green, yellow and red respectively. It is also show in black the low temperature linearized current in the no hybridization scenario $I = (e^2/h)V$. b) The same as a) in the no hybridization scenario for different temperature regimes $k_BT/\Gamma = 0.0, 1.0, 2.5, 5.0$ in blue, green, yellow and red respectively. c) Two terminal DC heat current $Q/(\Gamma/h)$ as function of the voltage bias eV/Γ for different Majorana hybridization energies $\varepsilon_M/\Gamma = 0.0, 0.2, 0.5, 100$ in blue, green, yellow and red respectively. d) The same as c) in the no hybridization scenario for different temperature regimes $k_BT/\Gamma = 0.0, 1.0, 2.5, 5.0$ in blue, green, yellow and red respectively.

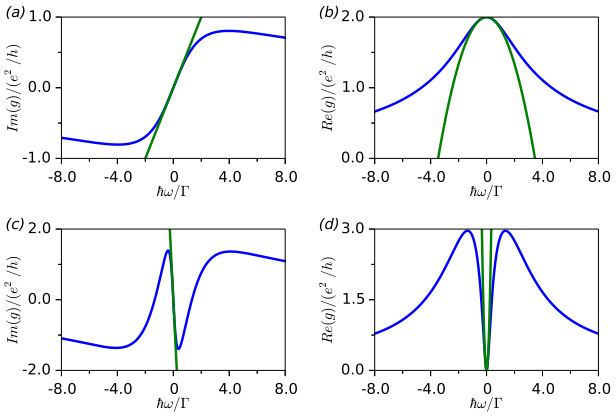

FIG. 4: a) Single terminal imaginary part of the electrical admittance $g(\omega)/(e^2/h)$ as function of the driving frequency $\hbar\omega/\Gamma$. The exact zero temperature admittance is plotted in blue while its linearized version $\Im m(g(\omega)) = -wC_T$ is plotted in green where the capacitance is $C_T = -(1/2\pi)(e^2/2\Gamma)$. b) Real part of the same admittances than in a). The exact zero temperature admittance is plotted in blue while its linearized version $\Re e(g(\omega)) = g_0 + w^2C_T^2R_T$ is plotted in green where the resistance is $R_T = -(h/e^2)(2/3)$ and the drain term is $g_0 = 2e^2/h$. c) and d) The same as a) and b) but with an hybridization energy $\varepsilon_M/\Gamma = 0.5$. In this case $C_T = e^2\Gamma/(\pi\varepsilon_M^2)$.

terminal case that can be viewed as a RC-circuit with a nanowire containing two Majorana edge mode [one at each side of the nanowire] but only one of the edges is connected to a reservoir. In Fig. 4 we illustrate the imaginary [Fig. 4(a)] and the real part [Fig. 4(b)] of the electrical admittance for the case where the nanowire hosts an ideal Majorana state $\varepsilon_M = 0$. We take the zero temperature limit that allows us to perform a simple discussion. The imaginary part of $g(\omega)$ has a positive slope. We have already discussed above the origin of Fig. 4(a) positive slope. The AC electrical admittance is indeed composed by two contributions g_N, and g_S which have a relative phase of π between them. The normal contribution $\Im m(g_N) = -i\omega\frac{1}{2\pi}\frac{e^2}{2\Gamma}$ is similar to a normal transmission conductance but it considers both channels, the electron and hole sectors with an effective broadening of 2Γ instead of Γ. However, due to the presence of Andreev electron-to-hole conversion the contribution for $\Im m(g_S) = i\omega\frac{1}{2\pi}\frac{e^2}{\Gamma}$ makes the overall AC admittance to exhibit a positive imaginary part as shown in Fig. 4(a). For the real part, depicted in Fig. 4(b) our results for the AC admittance reflect that there is a constant admittance term that does not vanish even when the AC frequency is zero. Such term $g_0 = 2e^2/h$ is due to the non-conserving charge transport caused by Andreev processes that produce an outgoing Cooper pair supercurrent. In this sense, the presence of superconductivity is implicitly considered in our Majorana description.

Remarkable is the fact that the charge relaxation resistance when the Majorana state is present reaches the value of $R_T = -\frac{2}{3}\frac{h}{e^2}$ that arises from $g = g_N + g_S = g_0 - i\omega C_T + \omega^2 C_T^2 R_T$. This value is extracted from the Green curve in Fig. 4(b) where a parabolic function fits the low frequency spectrum for $\Re e(g)$. As we know, $\Re e(g_N) = \omega^2 C_q^2 R_q + \cdots$ with $C_q = \frac{1}{2\pi}\frac{e^2}{2\Gamma}$, and $R_q = \frac{h}{e^2}$ and $\Re e(g_S) = g_0 + \omega^2 C_S^2 R_S$, with $C_S = -\frac{1}{2\pi}\frac{e^2}{\Gamma}$, and $R_S = -\frac{5h}{12e^2}$.

We observe that when the Majorana state is removed by allowing some degree of hybridization $\varepsilon_M \neq 0$ this scenario changes dramatically. This is showed in Fig. 4(c), and Fig. 4(d) for $\Im m(g)$, and $\Re e(g)$, respectively and when $\varepsilon_M/\Gamma = 0.5$. The slope for $\Im m(g)$ close to zero frequency now becomes negative and it depends on the value of ε_M, $C_T = \frac{e^2\Gamma}{\pi\varepsilon_M^2}$. Similarly, the curvature and sign of $\Re e(g)$ changes and becomes positive for a non ideal Majorana state. Notice that R_T does not match with the pure normal case since, even if the Majorana is not totally well formed, the superconductivity is still present. Finally, we discuss in Fig. 5 how the transition for the $\Im m(g)$, and $\Re e(g)$ occurs from an ideal Majorana towards a fermionic state when we increase the value of ε_M/Γ from 0 to 0.6. These results are reflected in Fig. 5(a) for the imaginary part of g. We can observe how the slope of such curve evolves from positive to negative values as long as ε_M grows. Besides, the curves develop some structure, a maximum and a minimum close to frequencies that match with the hybridization values $\hbar\omega \approx \pm\varepsilon_M$. Similar

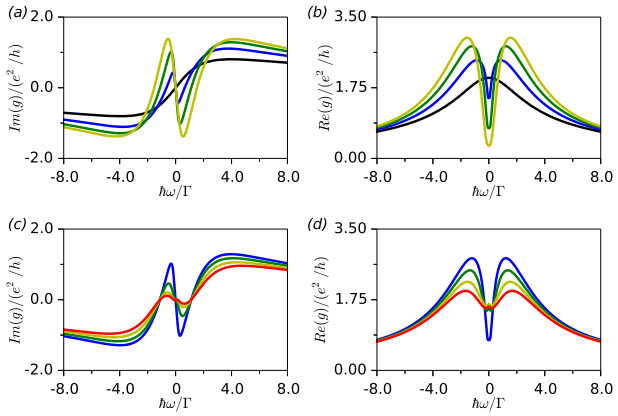

FIG. 5: a) Single terminal imaginary part of the electrical admittance $g(\omega)/(e^2/h)$ as function of the driving frequency $\hbar\omega/\Gamma$ for different Majorana hybridization energies $\varepsilon_M/\Gamma = 0.0, 0.2, 0.4, 0.6$ in black, blue, green and yellow respectively. b) Single terminal real part of the same admittances than in a). c) and d) The same as a) and b) but for different temperatures $k_BT/\Gamma = 0.05, 0.2, 0.4, 0.6$ in blue, green, yellow and red respectively and $\varepsilon_M/\Gamma = 0.4$.

features are also observed in Fig. 5(b) where the real part of the electrical admittance is plotted. At low, close to zero, frequencies and at $\varepsilon_M = 0$ the real part of the admittance exhibits a quadratic dependence with ω with a negative sign as we stated previously. Such behavior when ε_M increases, it is still quadratic, but it reverses its sign and two maxima appear that reflect the fact that Majorana physics are washed out. Finally, Figs. 5(c) and (d) show the dependence with temperature for a non ideal Majorana case for $\Im m(g)$ and $\Re e(g)$, for a finite hybridization energy ε_M. In these case, for both $\Im m(g)$ and $\Re e(g)$ the maxima and minima position that appear in the curves are not temperature dependent contrary to what happens with their value.

D. AC energy transport

The real and imaginary parts of the electrothermal admittance at finite DC bias are showed in Fig. 6. The imaginary part of the electrothermal admittance is plotted in Fig. 6(a) for various ε_M. Contrary to what happens with the electrical admittance, there is no change in the slope of the curves in $\Im m(m(\omega))$ when $\varepsilon_M = 0$ increases from zero to a finite value. Besides, for the real part, showed in Fig. 6(b) we have the same tendency for all curves independently on ε_M. Therefore we can conclude that there is no a clear indicator that the electrotermal admittance could be a good signature of the presence of a Majorana state. Roughly all curves are quite similar, for the real and imaginary parts of $m(\omega)$ independently on the value of the Majorana hybridization when we look at low frequencies. The temperature dependence for the electrothermal admittance is shown in the lower panel of Fig. 6. We observe that, for both, the imaginary and the real part of this admittance, the behavior of $m(\omega)$ is quite insensitive to a change in temperature [see Fig. 6(c), and (d)].

IV. CONCLUSIONS

In closing, we have investigated the electrical and energy current spectrum in the linear response regime for a Majorana nanowire that is coupled to one reservoir. Our results, valid for arbitrary AC frequencies, show that the energy reservoir current expression is zero unless a finite voltage bias is provided because of the symmetry of the particle and hole degrees of freedom. Additionally, our findings reflect the fact that the presence of the Majorana state affects strongly the shape of the electrical admittance in the quantum capacitor configuration. This admittance is formed by two contributions, g_N similar to a quantum dot admittance albeit by a doubling of the coupling that accounts transport events with two quasiparticle species, electrons and holes. And g_S that implies a Cooper pair outgoing flow. Both contributions, g_N, and g_S are dephased by a factor of π. Due to this fact, when Majorana physics is present the real and imaginary parts for the total admittance $g = g_N + g_S$ reverses its sign in comparison with a situation where the two edge Majorana state hybridize. Such change in sign for the low frequency region of g could serve as a good indicator for the presence of Majorana states.

V. ACKNOWLEDGEMENTS

We acknowledge Ll. Serra for critical reading and useful discussions. Work supported by MINECO Grant No. FIS2014-52564 and CAIB-Spain (Conselleria dEducaci, Cultura i Universitats) and FEDER. We hereby acknowledge the PhD grant provided by the University of the Balearic Islands.

Appendix A: Unperturbed reservoir Green functions

The EOM for the unperturbed reservoir Green function is

$$(i\hbar\partial_t - \varepsilon_{\alpha k\sigma})\tilde{g}^e_{\alpha k\sigma}(t,t') = \hbar\delta(t-t')\tau_z\,, \tag{A1}$$

where τ_z is the z-component Pauli matrix for the electron-hole space and $\tilde{g}^e_{\alpha k\sigma}(t,t')$ is the Keldysh matrix of the unperturbed Green function,

$$\tilde{g}^e_{\alpha k\sigma}(t,t') = \begin{pmatrix} g^{e,t}_{\alpha k\sigma}(t,t') & g^{<,t}_{\alpha k\sigma}(t,t') \\ g^{e,>}_{\alpha k\sigma}(t,t') & g^{e,t}_{\alpha k\sigma}(t,t') \end{pmatrix}. \tag{A2}$$

We consider the influence of a time dependent electrical signal $V^{AC}_\alpha(t)$ applied to an arbitrary α reservoir. In this

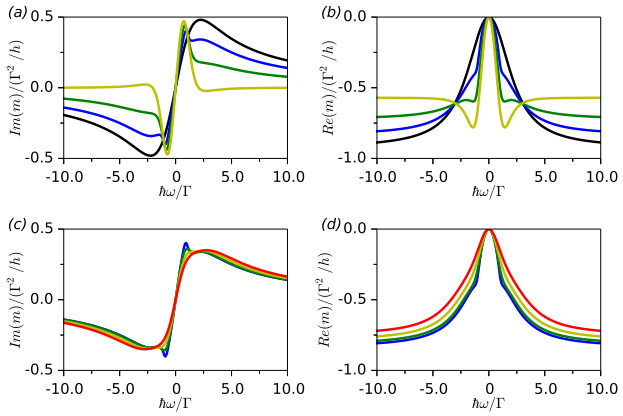

FIG. 6: a) Single terminal imaginary part of electrothermal admittance $m(\omega)/(\Gamma^2/h)$ in presence of a finite bias $eV/\Gamma = 1$ as function of the driving frequency $\hbar\omega/\Gamma$ for different Majorana hybridization energies $\varepsilon_M/\Gamma = 0.0, 0.5, 0.75, 1.0$ in black, blue, green and yellow respectively. b) Single terminal real part of the same admittances than in a). c) and d) The same as a) and b) but for different temperatures $k_BT/\Gamma = 0.05, 0.2, 0.4, 0.6$ in blue, green, yellow and red respectively and $\varepsilon_M/\Gamma = 0.5$.

manner, the unperturbed reservoir Green function for the electron and hole part acquires a time dependent phase $\phi_\alpha(t_1,t_2) = \int_{t_2}^{t_1}(dt'/\hbar)eV_\alpha^{AC}(t')$ taking the form,

$$g^{e,<}_{\alpha k\sigma}(t_1,t_2) = if(\varepsilon_{\alpha k\sigma} - V_\alpha)e^{-\frac{i}{\hbar}\varepsilon_{\alpha k\sigma}(t_1-t_2)}e^{-i\phi_\alpha(t_1,t_2)}\,, \tag{A3a}$$

$$g^{h,<}_{\alpha k\sigma}(t_1,t_2) = if(\varepsilon_{\alpha k\sigma} + V_\alpha)e^{\frac{i}{\hbar}\varepsilon_{\alpha k\sigma}(t_1-t_2)}e^{i\phi_\alpha(t_1,t_2)}\,, \tag{A3b}$$

$$g^{e,r/a}_{\alpha k\sigma}(t_1,t_2) = \mp i\theta(\pm(t_1-t_2))e^{-\frac{i}{\hbar}\varepsilon_{\alpha k\sigma}(t_1-t_2)}e^{-i\phi_\alpha(t_1,t_2)}\,, \tag{A3c}$$

$$g^{h,r/a}_{\alpha k\sigma}(t_1,t_2) = \mp i\theta(\pm(t_1-t_2))e^{\frac{i}{\hbar}\varepsilon_{\alpha k\sigma}(t_1-t_2)}e^{i\phi_\alpha(t_1,t_2)}\,, \tag{A3d}$$

where $f(\varepsilon - V_\alpha) = f_e^\alpha(\varepsilon)$ is the electron distribution function whereas $f^\alpha(\varepsilon + V_\alpha) = f_h^\alpha(\varepsilon)$ is the hole one. In the energy domain,

$$g^{e,r/a}_{\alpha k\sigma}(\varepsilon) = \frac{1}{\varepsilon - \varepsilon_{\alpha k\sigma} \pm 0^+}\,, \tag{A4}$$

and

$$g^{e,<}_{\alpha k\sigma}(\varepsilon) = 2i\pi f(\varepsilon_{\alpha k\sigma} - \mu_\alpha)\delta(\varepsilon - \varepsilon_{\alpha k\sigma})\,, \tag{A5}$$

where the same equations apply to the hole degree of freedom changing $\varepsilon_{\alpha k\sigma} \to -\varepsilon_{\alpha k\sigma}$

Appendix B: Majorana Green function

Here we explicitly calculate the Majorana Green function, lesser and retarded(advanced) components. They are needed for the current expression, see Eq. (9). The EOM for the causal Majorana Green function

$$i\hbar\partial_t\mathcal{G}^t_{\gamma,\beta}(t,t') = 2\hbar\delta_{\gamma,\beta}\delta(t,t') + i\sum_\mu t_{\gamma\mu}\mathcal{G}^t_{\mu\beta}(t,t') + \frac{2}{\hbar}\int dt_1\sum_\mu[\Sigma^e_{0\mu;\gamma\delta}(t,t_1) + \Sigma^h_{0\mu;\gamma\delta}(t,t_1)]\mathcal{G}^t_{\delta,\beta}(t_1,t') \tag{B1}$$

After applying the Langreth rules, the lesser, retarded(advanced) Majorana Green functions in a matrix form reads

$$\mathcal{G}^{r/a}_\eta(t,t') = \mathrm{g}^{r/a}_\eta(t,t') + \int\int\frac{dt_1}{\hbar}\frac{dt_2}{\hbar}\mathrm{g}^{r/a}_\eta(t,t_1)\mathbf{\Sigma}^{r/a}_0(t_1,t_2)\mathcal{G}^{r/a}_\eta(t_2,t')\,, \tag{B2}$$

$$\mathcal{G}^<_\eta(t,t') = \int\frac{dt_1}{\hbar}\int\frac{dt_2}{\hbar}\mathcal{G}^r_\eta(t,t_1)\mathbf{\Sigma}^<_0(t_1,t_2)\mathcal{G}^a_\eta(t_2,t')\,. \tag{B3}$$

Here $\mathbf{\Sigma}^{<,r/a}_0 = \mathbf{\Sigma}^{e,<,r/a}_0 + \mathbf{\Sigma}^{h,<,r/a}_0$ with elements given by $\mathbf{\Sigma}^{e/h,<,r/a}_0 = \sum_\alpha \mathbf{\Sigma}^{e/h,<,r/a}_{0\alpha;\gamma\delta}$. On the other hand, g_η is the unperturbed Majorana Green function that fulfills the EOM,

$$(i\hbar\partial_t - i\mathbf{t})\mathrm{g}_\eta = 2\hbar\delta(t,t')\tau_z\,, \tag{B4}$$

where τ_z is the z-component Pauli matrix for the electron-hole space.

Fourier transforming Eq. (B2) we obtain a simple energy dependent expression for the full retarded(advanced) Majorana Green function,

$$\mathcal{G}_\eta^{r/a}(\varepsilon) = \mathrm{g}_\eta^{r/a}(\varepsilon) + \mathrm{g}_\eta^{r/a}(\epsilon)\mathbf{\Sigma}_0^{r/a}(\varepsilon)\mathcal{G}_\eta^{r/a}(\varepsilon)\,, \qquad \text{(B5)}$$

that after these considerations reads

$$\mathcal{G}_\eta^{r/a}(\varepsilon) = \frac{2}{\varepsilon - i\mathbf{t} - 2\mathbf{\Sigma}_0^{r/a}(\varepsilon)}\,. \qquad \text{(B6)}$$

Besides, from Eq. (B3), the lesser Majorana Green function component takes the simple form

$$\mathcal{G}_\eta^{<}(\varepsilon) = \mathcal{G}_\eta^{r}(\varepsilon)\mathbf{\Sigma}_0^{<}(\varepsilon)\mathcal{G}_\eta^{a}(\varepsilon)\,. \qquad \text{(B7)}$$

[1] K. S. Novoselov, A. K. Geim, S.V. Mozorov, D. Jiang, Y. Zhang, S. V. Dubonos, I. V. Grigorieva, and A.A. Firsov, Science, **306**, 666 (2004).

[2] K. S. Novoselov, A. K. Geim, S.V. Mozorov, D. Jiang, I. V. Grigorieva, S. V. Dubonos, and A.A. Firsov, Nature(London), **438**, 197 (2005).

[3] A. H. Castro Neto, F. Guinea, N. M. R. Peres, K. S. Novoselov, and A. K. Geim, Rev. Mod. Phys. **81**, 109 (2009).

[4] E. Majorana, Nuovo Cim. **14**, 171, 1937

[5] L. Fu, and C. L. Kane, Phys. Rev. Lett. **100**, 096407 (2008).

[6] C. Nayak, S. H. Simon, A. Stern, M. Freedman, and S. Das Sarma, Rev. Mod. Phys. **80**, 1083 (2008).

[7] J. K. Pachos, Introduction to Topological Quantum Computation. Cambridge University Press (2012).

[8] S. R. Elliott, and M. Franz, Rev. Mod. Phys. **87**, 137163 (2015).

[9] J. Alicea, Y. Oreg, G. Refael, F. von Oppen, and M. P. A. Fisher, Nat Phys, **7**, 131136 (2011).

[10] V. Mourik, K. Zuo, S. Frolov, S. Plissard, E. Bakkers, and L. Kouwenhoven, Science, **336**, 10031007 (2012).

[11] H. O. H. Churchill, V. Fatemi, K. Grove-Rasmussen, M. T. Deng, P. Caroff, H. Q. Xu, and C. M. Marcus, Phys. Rev. B, **87**, 241401 (2013).

[12] M. T. Deng, C. L. Yu, G. Y. Huan, M. Larsson, and P. Caroff, Nano Lett., **12**, 6414 (2012).

[13] L. P. Rokhinson, X. Liu, and J. K. Furdyna, Nature Physics, **8**, 795 (2012).

[14] A. Das, Y. Ronen, Y. Most, Y. Oreg, M. Heiblum, and H. Shtrikman, Nature Physics, **8**, 887 (2012).

[15] A. D. K. Finck, D. J. Van Harlingen, P. K. Mohseni, K. Jung, and X. Li, Phys. Rev. Lett., **110**, 126406 (2013).

[16] J. D. Sau, S. Tewari, and S. Das Sarma, Phys. Rev. B, **85**, 064512 (2012).

[17] H. Zhang and et. al., ArXiv, **1603.04069v1** (2016).

[18] S. Nadj-Perge, I. K. Drozdov, J. Li, H. Chen, S. Jeon, J. Seo, A. H. MacDonald, B. A. Bernevig, and A. Yazdani, Science, **346**,6209, 602607 (2014).

[19] Büttiker, A. Prêtre, and H. Thomas, Phys. Lett. A **180**, 364 (1993).

[20] M. Büttiker, A. Prêtre, and H. Thomas, Phys. Rev. Lett. **70**, 4114 (1993).

[21] Y. Dovzhenko, J. Stehlik, K. D. Petersson, J. R. Petta, H. Lu, and A. C. Gossard Phys. Rev. B **84**, 161302(R) (2011). G. Cao, H-O. Li, T. Tu, L. Wang, C. Zhou, M. Xiao, G-C. Guo, H-W. Jiang, and G-P. Guo, Nat. Commun. **4**, 1401 (2013).

[22] W. Lu, J. Zhongqing, L. Pfeiffer, K. W. West and A. J. Rimberg, Nature **423,** 422 (2003).

[23] S. Gustavsson, R. Leturcq, T. Ihn, K. Ensslin and A. C. Gossard, J. Appl. Phys. **105**, 122401 (2009).

[24] T. Jullien, P. Roulleau, B. Roche, A. Cavanna, Y. Jin, and D. C. Glattli, Nature **514** 603, (2014).

[25] J. Gabelli, G. Fève, J.-M. Berroir, B. Plaçais, A. Cavanna, B. Etienne, Y. Jin, and D.C. Glattli, Science **313**, 49 (2006).

[26] J. Gabelli, G. Fève, T. Kontos, J.-M. Berroir, B. Plaçais, D.C. Glattli, B. Etienne, Y. Jin, and M. Büttiker, Phys. Rev. Lett. **98**, 166806 (2007).

[27] M. R.Delbecq, V. Schmitt, F. D.Parmentier, N. Roch, J.J. Viennot, G. Fève, B. Huard, C. Mora, A. Cottet, and T. Kontos, Phys. Rev. Lett. **107**, 256804 (2011).

[28] J. Gabelli, G. Fève, J.-M. Berroir, and B. Plaçais, Rep. Prog. Phys. **75**, 126504 (2012).

[29] M. Hashisaka, K. Washio, H. Kamata, K. Muraki, and T. Fujisawa, Phys. Rev. B **85**, 155424 (2012).

[30] S.J. Chorley, J. Wabnig, Z.V. Penfold-Fitch, K.D. Petersson, J. Frake, C.G. Smith, and M.R. Buitelaar, Phys. Rev. Lett. **108**, 036802 (2012).

[31] J. Basset, H. Bouchiat, and R. Deblock, Phys. Rev. B **85**, 085435 (2012).

[32] T. Frey, P.J. Leek, M. Beck, J. Faist, A. Wallraff, K. Ensslin, T. Ihn, and M. Büttiker, Phys. Rev. B **86**, 115303 (2012).

[33] S. Jezouin, F. D. Parmentier, A. Anthore, U. Gennser, A. Cavanna, Y. Jin, and F. Pierre, Science **342**, 601 (2013).

[34] C. W. Chang, D. Okawa, A. Majumdar, A. Zettl, Science, **314**, 1121 (2006).

[35] W. Lee, K. Kim, W. Jeong, L. A. Zotti, F. Pauly, J. C. Cuevas, and P. Reddy, Nature **498**, 209 (2013).

[36] R. Maynard, and E. Akkermans, Phys. Rev. B **32**, 5440 (1985).

[37] L. D. Hicks and M. S. Dresselhaus, Phys. Rev. B **47**, 16631 (1993).

[38] L. E., Bell, Science **321**, 1457 (2008).

[39] Y. Dubi and M. Di Ventra, Rev. Mod. Phys. **83**, 131 (2011).

[40] P. Rodgers, Nature Nanotech. **3**, 76 (2008).

[41] J.-P. Brantut, C. Grenier, J. Meineke, D. Stadler, S. Krinner, C. Kollath, T. Esslinger, and A. Georges, Science **342**, 713 (2013).

[42] Y. Kim, W. Jeong, K. Kim, W. Lee, and P. Reddy, Nature Nanotech. **10**, 1038 (2014).

[43] L. Arrachea, M. Moskalets, and L. Martin-Moreno, Phys. Rev. B **75**, 245420 (2007).

[44] M. Moskalets and M. Büttiker, Phys. Rev. B **80**, 081302(R) (2009).
[45] J. S. Lim, R. López, and D. Sánchez Phys. Rev. B **88,** 201304(R) (2013).
[46] M. F. Ludovico, J-S. Lim, M. Moskalets, L. Arrachea, and D. Sánchez Phys. Rev. B **89**, 161306(R) (2014).
[47] Guillem Rosello, Rosa Lopez, Jong Soo Lim, Phys. Rev. B 92, 115402 (2015)
[48] A.P. Jauho, N.S. Wingreen, and Y. Meir, Phys. Rev. B **50**, 5528 (1994).
[49] C.W.J. Beenakker, Annu. Rev. Con. Mat. Phys. **4**, 113 (2013)
[50] M. Wimmer, A.R. Akhmerov, J.P. Dahlhaus, C.W.J. Beenakker, New J. Phys. 13, 053016 (2011)
[51] Jong Soo Lim, Rosa Lopez, Llorens Serra, New J. Phys. 14, 083020 (2012)
[52] Jascha Ulrich, Fabian Hassler, Phys. Rev. B 92, 075443 (2015)
[53] Cssio Sozinho Amorim, Kazuto Ebihara, Ai Yamakage, Yukio Tanaka, Masatoshi Sato, Phys. Rev. B 91, 174305 (2015).
[54] Fabio L. Pedrocchi, David P. DiVincenzo, Phys. Rev. Lett. 115, 120402 (2015)
[55] M. Büttiker and T. Christien in *Mesoscopic Electron Transport*, edited by L. Kouwenhoven, G. Schön, and L. Sohn, NATO ASI Series E, Kluwer Ac. Publ., Dordrecht (1996).
[56] Y. Fu and S.C. Dudley, Phys. Rev. Lett. **70**, 65 (1993).
[57] T. Christen and M. Büttiker Phys. Rev. Lett. **77**, 143 (1996).
[58] T. Christen and M. Büttiker Phys. Rev. B **53**, 2064 (1996).
[59] A. Prêtre, H. Thomas, and M. Büttiker Phys. Rev. B **54**, 8130 (1996).

Chapter 9

Outlook

The study of Majorana devices is mainly motivated by their potential applications in quantum computation technologies. At present Majorana modes have been theoretically predicted and studied but there is no widespread consensus yet on their experimental discovery. Current experiments in Majorana nanowires are aimed at demonstrating the existence of Majorana modes through the detection of their conductance signature.

It is the opinion of the author of this thesis that the scientific community is focused in finding a *silver bullet*. That is, a single irrefutable evidence of the Majorana phenomena. The objective seems to be to find out a single experiment with a single measurement that provides us with a definite answer. Although this would be indeed very convenient, it is this author's opinion that, most likely, an accumulation of many circumstantial evidences could be the *silver bullet* we are searching for. This thesis has been developed with the aim to be useful in that direction.

In this work we have made different theoretical predictions of the Majorana mode behavior. First, we started questioning ourselves about the robustness of the Majorana modes away from ideal theoretical conditions. These ideal conditions are a 1d closed nanowire inside an external magnetic field perfectly oriented in the nanowire longitudinal direction. We have studied how this robustness can be affected by the presence of a junction in an open nanowire and by the tilt of the magnetic field away from the longitudinal axis. In particular we have uncovered the projection rule for 1d nanowires that is also fulfilled approximately in quasi-1d planar nanowires. This is a mathematical relation between the transverse component of the magnetic field and the proximity induced superconductivity that limits the range of parameters where it is possible to find a Majorana mode. Furthermore, in quasi-1d nanowires the possibility of electronic transverse motion allows kinetic orbital effects in presence of components of the magnetic field perpendicular to the nanowire surface. It is also shown how this effects lead to a characteristic phase diagram where the phase boundaries depend on the magnetic field strength and orientation.

These considerations on robustness have led to a rather detailed knowledge about the Majorana phase dependence on the nanowire materials, the proximity induced

superconductivity and, most notoriously, the external magnetic field configuration. Our main idea has been to clarify the location of the phase boundaries with the aim to apply this knowledge to transport problems. Experiments showing the zero bias peak in the conductance in the predicted range of values and for no other configurations would be a strong point in favor of the Majorana existence.

Next, we thought about the possibility of extending the range of measurements in the transport problems. Current experiments measure the mentioned peak in conductance. This is measured probing the said conductance for different DC voltage biases. However, the Majorana admittance in presence of an AC driving calculated in this thesis has some particular features of its own. Furthermore, the Majorana hybridization in a finite nanowire creates notable resonances in the admittance if we use the nanowire as a capacitor. Finally, we go beyond the transport problems focusing on the absorption spectrum of a Majorana nanowire as an alternative but complementary method of Majorana measurement. We show how the Majoranas leave a signature in the absorption spectrum when the light is polarized in the transverse direction of the nanowire.

To state that these behaviors are individually unique of the Majorana modes would be a slight overstatement because, on an scientific basis, this would require a specific comparison between each of the reported behaviors and all the possible alternative explanations and this is out of the scope of this thesis. Nevertheless, if for example a zero bias peak consistent with the reported Majorana physics is found in a planar nanowire only in the proper regions of its phase diagram; and at the same time this nanowire has the proper Majorana AC response and optical absorption profile then we think that it would be difficult and a tremendous coincidence to find out an alternative explanation to all these evidences simultaneously. As a conclusion, we have increased the available knowledge on Majorana modes with the aim to help in their detection and their later practical use.

However, this is an ongoing work that will not end with this thesis. For example, in Chap. 5 the local currents of a Majorana mode were calculated with the aim to find out the characteristic features of these currents. It was already stated in Chap. 5 the need to study the local currents in open nanowires for different nanowire geometries. It is also important to clarify the role of the electronic orbital motion in these geometries. On the other hand, an expanded knowledge is required about new Majorana devices that have been proposed, some of them using semiconductor technology while others use a different physical basis.

Erratum

Pag. 26. Eq. (1): It should be $\hbar$ instead of h

Pag. 41. Eq. (1): It should be $\hbar$ instead of h

Pag. 63. Eq. (20): The exponentials should have an additional s_τ, that is $e^{\pm i s_\tau (y - s_\tau y_c) x / l_z^2}$. The gauge center must be counted as a global phase change for the eigenstate.

Curriculum Vitae

Academic formation
Master in Physics of Complex Systems (2013)
Master in Physics (2012)
Degree in Physics (Licenciatura) (2011)
Computer Engineering (2005)
Computer Systems Technical Engineering (2002)

Articles published
Quasi-particle current in planar Majorana nanowires
Javier Osca and Llorenç Serra
J. Phys. Conf. Ser. **647** 012063
Published 13 October 2015

Electromagnetic absorption of quasi-1d Majorana nanowires
Javier Osca and Llorenç Serra
Phys. Status Solidi C **12**, No 12, 1409-1411
Published 31 July 2015

Majorana states and magnetic orbital motion in planar hybrid nanowires
Javier Osca and Llorenç Serra
Phys. Rev. B **91**, 235417
Published 12 June 2015

Electromagnetic absorption of semiconductor 2d Majorana nanowires
Daniel Ruiz, Javier Osca and Llorenç Serra
J. Phys. Condens. Matter **27** 125302
Published 10 March 2015

Effects of tilting the magnetic field in one-dimensional Majorana nanowires
Javier Osca, Daniel Ruiz and Llorenç Serra
Phys. Rev. B **89**, 245405
Published 5 June 2014

Majorana mode stacking, robustness and size effect in cylindrical nanowires
Javier Osca, Rosa López and Llorenç Serra
Eur. Phys. J. B **87**, 84
Published 9 April 2014

Majorana modes in smooth normal-superconductor nanowire junctions
Javier Osca and Llorenç Serra
Phys. Rev. B **88**, 144512
Published 22 October 2013

Articles in preparation
Charge and energy transport in a Majorana nanowire
Javier Osca, Rosa López and Jong Soo Lim

Grants received
UIB Doctoral grant (May 2013 -September 2016)
UIB Colaboration grant (June-August 2012)

Stays at research centers
Dahlem Center for Complex Quantum Systems
Berlin, Germany. 4-22 April (2016)

Talks
Local currents in quasi-1d Majorana nanowires
Nonequilibrium condensed matter and biological systems
Madrid, 10 March (2016)

Living on the edge, Majoranas in nanowires
IFISC Seminar
Palma de Mallorca, 25 March (2015)

Posters
Majorana states in presence of orbital motion in planar hybrid nanowires
Javier Osca and Llorenç Serra
EDISON 19
Salamanca, Spain (2015)

Optical absorption of 2d Majorana nanowires
Javier Osca, Daniel Ruiz and Llorenç Serra
EDISON 19
Salamanca, Spain (2015)

Optical absorption of 2d Majorana nanowires
Javier Osca, Daniel Ruiz and Llorenç Serra
Quantum Thermodynamics II
Palma de Mallorca, Spain (2015)

Majorana modes in smooth normal-superconductor nanowire junctions
Javier Osca and Llorenç Serra
GEFENOL IV
Palma de Mallorca, Spain (2014)

Majorana modes in smooth normal-superconductor nanowire junctions
Javier Osca and Llorenç Serra
Frontiers 2014
San Sebastián, Spain (2014)

Majorana modes in smooth normal-superconductor nanowire junctions
Javier Osca and Llorenç Serra
Spin Qubit 2
Konstanz, Germany (2014)

Effects of tilting the magnetic field in one dimensional Majorana nanowires
Javier Osca and Llorenç Serra
NGSCES 2014
Niza, France (2014)

Other conferences attended
GEFENOL III
Palma de Mallorca, Spain (2013)

IFISC Conferences on Modern Optics
Palma de Mallorca, Spain (2010)

Extra courses
Topology in Condensed Matter: Tying Quantum Knots
Edx Course. 5 February-14 May (2015)
Online course